

## Material characterisation of existing masonry

### A strategy to determine strength, stiffness and toughness properties for structural analysis

Jafari, S.

**DOI**

[10.4233/uuid:3bcbbc72-0212-44e9-ac86-2fdc54ec5987](https://doi.org/10.4233/uuid:3bcbbc72-0212-44e9-ac86-2fdc54ec5987)

**Publication date**

2021

**Document Version**

Final published version

**Citation (APA)**

Jafari, S. (2021). *Material characterisation of existing masonry: A strategy to determine strength, stiffness and toughness properties for structural analysis*. [Dissertation (TU Delft), Delft University of Technology]. <https://doi.org/10.4233/uuid:3bcbbc72-0212-44e9-ac86-2fdc54ec5987>

**Important note**

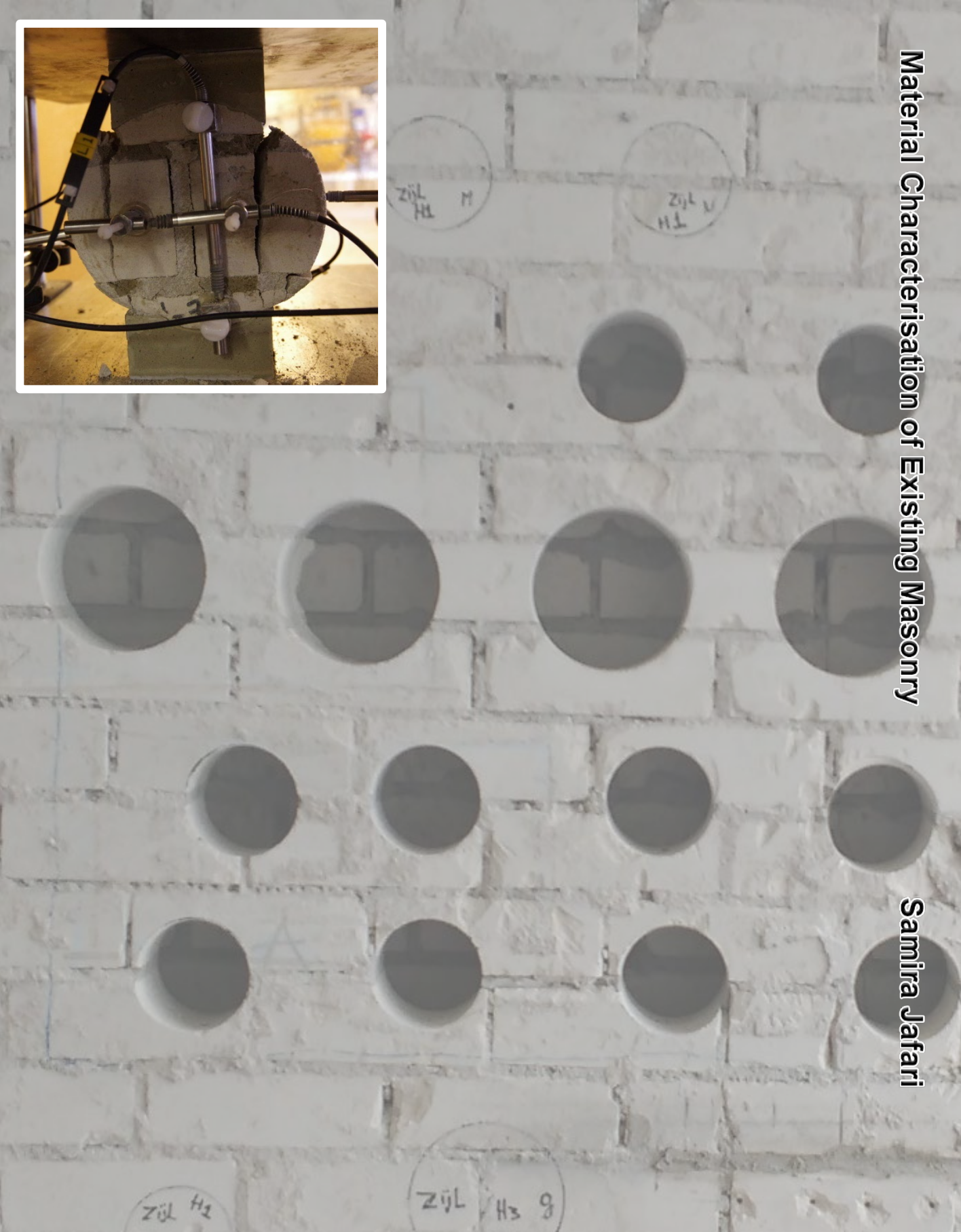
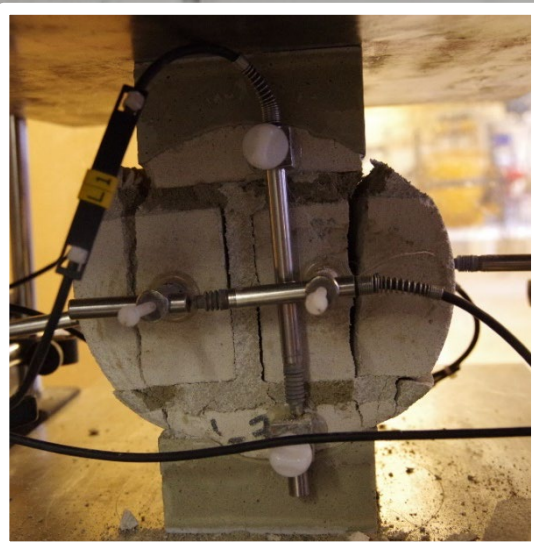
To cite this publication, please use the final published version (if applicable).  
Please check the document version above.

**Copyright**

Other than for strictly personal use, it is not permitted to download, forward or distribute the text or part of it, without the consent of the author(s) and/or copyright holder(s), unless the work is under an open content license such as Creative Commons.

**Takedown policy**

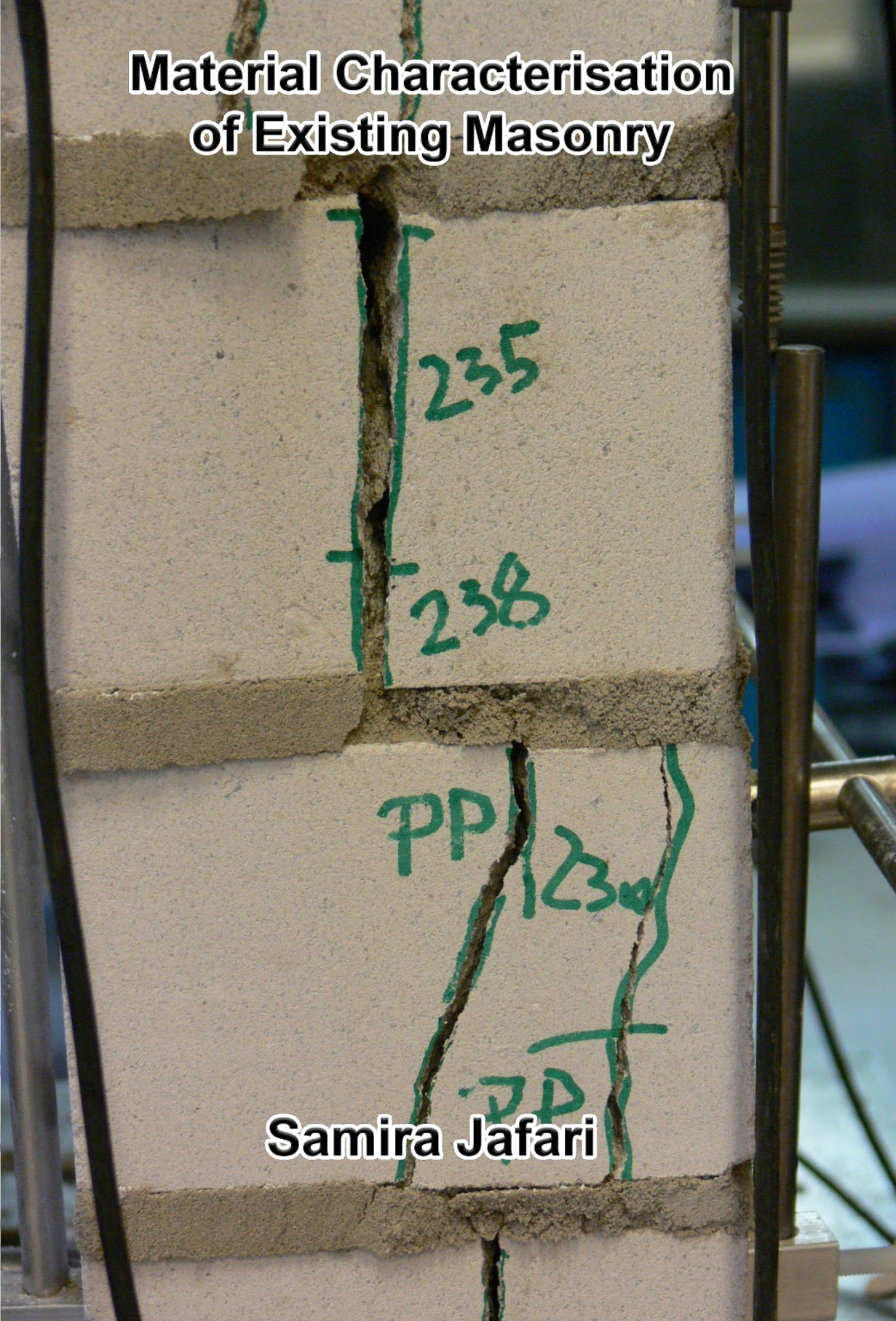
Please contact us and provide details if you believe this document breaches copyrights.  
We will remove access to the work immediately and investigate your claim.



Material Characterisation of Existing Masonry

Samira Jafari

# Material Characterisation of Existing Masonry



Samira Jafari

# **MATERIAL CHARACTERISATION OF EXISTING MASONRY:**

A STRATEGY TO DETERMINE STRENGTH, STIFFNESS AND  
TOUGHNESS PROPERTIES FOR STRUCTURAL ANALYSIS



# **MATERIAL CHARACTERISATION OF EXISTING MASONRY:**

A STRATEGY TO DETERMINE STRENGTH, STIFFNESS AND  
TOUGHNESS PROPERTIES FOR STRUCTURAL ANALYSIS

## **Dissertation**

for the purpose of obtaining the degree of doctor  
at Delft University of Technology,  
by the authority of the Rector Magnificus prof.dr.ir. T.H.J.J. van der Hagen,  
chair of the Board for Doctorates,  
to be defended publicly on  
Friday 24 September 2021 at 10:00 o'clock

by

**Samira JAFARI**

Master of Science in Civil Engineering,  
Iran University of Science and Technology, Iran  
born in Tehran, Iran

This dissertation has been approved by the promotor.

Composition of the doctoral committee:

Rector Magnificus	chairperson
Prof. dr. ir. J.G. Rots	Delft University of Technology, promotor
Dr. R. Esposito	Delft University of Technology, supervisor

Independent members:

Dr.ir. R. van der Pluijm	Wienerberger, Netherlands
Ass.prof.dr.ir.-arch E. Verstrynge	Katholieke Universiteit Leuven, Belgium
Prof.ing. C. Mazzotti	Università di Bologna, Italy
Prof.dr. P.B Lourenço	University of Minho, Portugal
Prof.dr.ir. H.E.J.G. Schlangen	Delft University of Technology
Prof.dr. A. Scarpas	Delft University of Technology & Khalifa University, United Arab Emirates



This research was funded by Nederlandse Aardolie Maatschappij (NAM), under contract numbers UI46268 “Physical testing and modelling – Masonry structures Groningen” (contract holders Jan van Elk and Jeroen Uilenreef) and UI63654 “Testing program 2016 for Structural Upgrading of URM Structures” (contract holders Dick den Hertog and Reza Sarkhosh), which is gratefully acknowledged.

Keywords:

Dutch Unreinforced Masonry, Material Characterisation, Experiments, Compression, Bending, Shear, Clay Brick Masonry, Calcium Silicate Element Masonry, Toughness, Orthotropic Behaviour, Core Testing Methods, Statistical Analysis, Correlation Study

Printed by: Ipskamp Printing, The Netherlands.

Cover design: Samira Jafari  
Cover photo credit: Samira Jafari, Edwin Meulman

Copyright © 2021 by S. Jafari. All rights reserved.

ISBN 978-94-6421-457-4

An electronic version of this dissertation is available at  
<http://repository.tudelft.nl/>.

*If your knowledge of fire has been turned to certainty by words alone, then seek to be cooked by the fire itself. Do not abide in borrowed certainty. There is no real certainty until you burn; if you wish for this, sit down in the fire.*

*Rumi*





# SUMMARY

Understanding the behaviour of unreinforced masonry (URM) structures requires in-depth insight into the mechanical properties of its constituents and their interaction under compression, tension, and shear loading. As a result, a complete picture of masonry characteristics, accounting for its full nonlinear response and its statistical distribution, has long been of scientific research interest worldwide. This has become a necessity for the Netherlands in recent years because of the induced seismicity affecting the vulnerable masonry building stock in the province of Groningen.

The more rigorously the mechanical properties are determined, the more they engender confidence in the reliability of structural analyses. This calls for an interdisciplinary approach, whereby experimental research focuses on meeting the demands of structural analysts and numerical modellers. As a result, laboratory and in-situ testing campaigns can provide input parameters and a basis for the validation and calibration of the various models to be used in deterministic or probabilistic settings. Nevertheless, a thorough characterisation of the material properties of existing unreinforced masonry structures is widely acknowledged as a challenging task, given the quasi-brittle nature of masonry, a very diverse range of masonry types, a lack of reliable in-situ semi-invasive testing methods, and a large number of tests required to be carried out.

To this end, both invasive and semi-invasive testing methods are adopted in this thesis. The former refers to tests on medium-sized samples, which follow the guidelines of the European standards for the selection of each sample's size. The latter points to a novel testing method, whereby small-diameter cores are extracted perpendicular to the wall surface. In this thesis, the studied masonry types are either laboratory-made, replicating the five most typical Dutch masonry types, or field-extracted, from nineteen different URM dwellings and schools in the Groningen region, built between 1910 and 2010. The typical masonry types include clay brick masonry, calcium-silicate brick masonry and calcium-silicate element masonry.

By performing 218 invasive tests on laboratory-made replicated masonry specimens, this thesis provides comprehensive insight into the behaviour of five masonry types and its constituents. It covers several aspects that have been addressed only partially in the literature: 1) investigating the response of masonry under different stress states, i.e. compression, bending, and shear; 2) analysing the complete nonlinear behaviour not only in the pre-peak but also in the post-peak regime; and 3) exploring the orthotropic response under compression and bending loads. Moreover, this lab-testing campaign has studied the influence of brick type, number of wythes, and joint thickness on the response of masonry.

By performing 478 invasive tests on field-extracted masonry specimens, this thesis offers a regional dataset of material properties. This dataset, along with previously available data from the literature, has been transferred into material properties table that have been incorporated into the Dutch standard for the

assessment of existing URM buildings subjected to induced earthquakes. Moreover, this research provides new insights into the inter-building variability of material properties and their statistical distribution.

This thesis also investigates the suitability of a novel semi-invasive testing method, whereby 167 small-diameter cores were subjected to compression as well as shear-sliding load. To this end, a comparative study was conducted, in which the material properties obtained from tests on cores, namely strength, stiffness, and toughness, are correlated with those found from tests on companion specimens. Promising conclusions are drawn, indicating that this testing method can be regarded as a reliable and practical alternative to conventional flat-jack based in-situ testing methods.

Considering the comprehensive dataset established and the study of different testing methods, this thesis ultimately formulates a strategy to characterise the material properties for assessment of existing URM structures. To this end, this research investigated the presence of relationships between different material properties, thus offering recommendations to indirectly derive elastic and toughness properties as a function of easy-to-obtain properties, i.e. strength found from testing cores and bond wrench tests. Moreover, this study introduced improved constitutive functions for compression, bending, and shear loading. Therefore, following this strategy, an acceptable level of knowledge on material properties can be gained, while intrusiveness and damage due to sampling remain limited.

# SAMENVATTING

Om het gedrag van ongewapende metselwerkconstructies (afgekort als URM, Un-Reinforced Masonry) te begrijpen, is diepgaand inzicht nodig in de mechanische eigenschappen van de samenstellende delen en hun interactie voor belasting op trek, druk en afschuiving. Om deze reden is het verkrijgen van een compleet beeld van de metselwerk karakteristieken, inclusief het volledige niet-lineaire gedrag en de statistische verdeling, al lange tijd een wereldwijd wetenschappelijk onderzoeksbelang. In Nederland is het de laatste jaren een noodzaak geworden vanwege de geïnduceerde seismiciteit die de kwetsbare metselwerkconstructies in de provincie Groningen aantast.

Hoe beter de mechanische eigenschappen worden bepaald, des te meer dragen ze bij aan de betrouwbaarheid van constructieve analyses. Dit vraagt om een interdisciplinaire aanpak, waarbij experimenteel onderzoek zich richt op de vragen van constructeurs en numerieke modelleers. Op deze wijze leveren laboratorium- en in-situ-testcampagnes inputparameters als een basis voor de validatie en kalibratie van modellen die in zowel deterministische als probabilistische context. Niettemin wordt een grondige karakterisering van de materiaaleigenschappen van bestaande ongewapende metselwerkconstructies doorgaans als een uitdagende taak gezien, vanwege zowel de quasi-brosse aard van metselwerk, het brede scala aan metselwerktypen, het gebrek aan betrouwbare in-situ semi-invasieve testmethoden en het grote aantal proeven dat moet worden uitgevoerd.

Daartoe worden in dit proefschrift zowel invasieve als semi-invasieve testmethoden toegepast. De eerste betreffen proeven met een focus op middelgrote monsters, volgens richtlijnen van de Europese normen voor de selectie van de grootte van elk monster. De tweede betreffen een nieuwe testmethode, waarbij cilinder-vormige kernen met een kleine diameter loodrecht op het wandoppervlak worden geëxtraheerd. In dit proefschrift zijn de bestudeerde metselwerktypen ofwel in het laboratorium gemaakt, als replica's van de vijf meest kenmerkende Nederlandse metselwerktypen, ofwel uit het veld geëxtraheerd en naar de testlocatie afgevoerd, vanuit negentien verschillende URM-woningen en -scholen in de regio van Groningen gebouwd tussen 1910 en 2010. De kenmerkende metselwerktypen omvatten baksteenmetselwerk, kalkzandsteenmetselwerk en metselwerk van grote kalkzandsteenelementen.

Door het uitvoeren van 218 invasieve proeven op in het laboratorium gemaakte gerepliceerde metselwerkproefstukken, biedt dit proefschrift uitgebreid inzicht in het gedrag van vijf soorten metselwerk en zijn bestanddelen. Het omvat verschillende aspecten die slechts gedeeltelijk in de literatuur zijn behandeld: 1) onderzoek naar de respons van metselwerk onder verschillende spanningstoestanden, waaronder druk, buiging en afschuiving; 2) het analyseren van het volledige niet-lineaire gedrag, niet alleen het gedrag voor en tot de piek, maar ook het na-piek softening gedrag; en 3) het onderzoeken van het orthotrope gedrag van metselwerk onder druk- en buigbelastingen. Naast deze studies, heeft deze laboratoriumtestcampagne de invloed van het steentype, het aantal lagen

(halfsteens en steens) en devoegdikte op het gedrag van metselwerk verder bestudeerd.

Door het uitvoeren van 478 invasieve proeven op in het veld gewonnen metselwerkproefstukken, biedt dit proefschrift een regionale dataset van materiaaleigenschappen. Deze dataset is, samen met eerder beschikbare data uit de literatuur, omgezet naar een tabel met materiaaleigenschappen die is opgenomen in de Nederlandse norm voor de beoordeling van bestaande URM-gebouwen die onderhevig zijn aan geïnduceerde aardbevingen. Bovendien levert dit onderzoek nieuwe inzichten op in de inter-gebouwvariabiliteit van materiaaleigenschappen en hun statistische verdeling.

Dit proefschrift onderzoekt ook de geschiktheid van een nieuwe semi-invasieve testmethode, waarbij 167 kernen met een kleine diameter werden onderworpen aan zowel druk als schuifbelasting. Een vergelijkend onderzoek is uitgevoerd, waarin de materiaaleigenschappen die verkregen zijn vanuit proeven op kernen, namelijk sterkte, stijfheid en taaigheid, worden gecorreleerd met de eigenschappen die gevonden zijn op traditionele monsters. Veelbelovende conclusies worden getrokken die erop wijzen dat deze kerntestmethode kan worden beschouwd als een betrouwbaar en praktisch alternatief voor conventionele in-situ methoden op basis van flat-jack testen.

Gezien de omvangrijke dataset die is opgesteld en de studie van verschillende testmethoden, formuleert dit proefschrift uiteindelijk een strategie om de materiaaleigenschappen te karakteriseren voor de beoordeling van bestaande URM-constructies. Daartoe is de aanwezigheid van relaties tussen verschillende materiaaleigenschappen onderzocht, waarbij aanbevelingen worden gedaan om de elastische en taaigheidseigenschappen indirect te ontlenen aan eenvoudiger te verkrijgen eigenschappen, namelijk de sterkte op basis van kernproeven en hefboomproeven (bond wrench). Daarnaast introduceert deze studie verbeterde constitutieve spannings-rek functies voor druk, buiging en afschuiving. Door deze strategie te volgen, kan een acceptabel kennisniveau over materiaaleigenschappen worden verkregen, terwijl intrusiviteit en schade door bemonstering beperkt blijven.

# SYMBOLS AND ABBREVIATIONS

The frequently used variables in this thesis are listed herein. The description of each symbol is given.

## Roman Symbols

$A_{core}$ $A_{cap}$	Maximum horizontal cross-sectional area of the core and of the cap
$D$	core diameter
$d_1$ $d_2$ $d_3$	Distance between the inner load bearings, outer load bearings, and outer and inner load bearings in the bending set-up
$e_1$ $e_2$	the distance from the applied load to the tension face of the specimen tested using bond wrench set-up and the distance from the centre of gravity of the clamp to the tension face of the specimen
$E_2$ $E_{2,h}$	Vertical and horizontal Young's modulus of masonry evaluated at 1/3 of the maximum stress
$E_3$ $E_{3,h}$	Vertical and horizontal Young's modulus of masonry evaluated between 1/10 and 1/3 of the vertical and horizontal maximum stress
$E_{3,fd}$	Elastic modulus of masonry evaluated using the force-deflection curve in the elastic range, between 1/10 and 1/3 of the maximum force
$E_{3,mc}$	Elastic modulus of masonry evaluated using the moment-curvature curve in the elastic range, between 1/10 and 1/3 of the maximum force
$E_{3m}$ $E_{3b}$	Young's modulus of mortar and unit evaluated between 10% and 30% of the maximum load
$E_{3b-1}$ $E_{3b-3}$	Young's modulus of unit evaluated from out-of-plane bending and in-plane bending test between 10% and 30% of the maximum load
$E_{3,fd}$	Elastic modulus of masonry evaluated using the force-deflection curve in the elastic range, between 1/10 and 1/3 of the maximum force
$E_{3,mc}$	Elastic modulus of masonry evaluated using the moment-curvature curve in the elastic range, between 1/10 and 1/3 of the maximum force
$E_{3m}$ $E_{3b}$	Young's modulus of mortar and unit evaluated between 10% and 30% of the maximum load
$E_{3b-1}$ $E_{3b-3}$	Young's modulus of unit evaluated from out-of-plane bending and in-plane bending test between 10% and 30% of the maximum load

$f_{bm}$ $f_{bb1}$ $f_{bb3}$	Flexural strength of mortar, in-plane flexural strength of unit, and out-of-plane flexural strength of unit
$f_m$ $f'_b$ $f_b$	Compressive strength of mortar, unit, and unit normalised compressive strength
$f_{tm}$ $f_{tb}$	Tensile strength of mortar and unit
$f'_k$	Characteristic compressive strength of masonry
$f'_m$ $f_{m,h}$	Vertical and horizontal compressive strength of masonry
$f_w$	Bond strength
$f_{x1}$ $f_{x2}$ $f_{x3}$	Flexural strength evaluated from vertical out-of-plane bending, horizontal out-of-plane bending, and in-plane bending tests
$f_{t1}$ $f_{t2}$ $f_{t3}$	Tensile strength indirectly evaluated from vertical out-of-plane bending, horizontal out-of-plane bending, and in-plane bending tests
$f_{v,core}$ $f_{p,core}$	Tangential shear strength and the corresponding normal stress associated with the maximum vertical load from shear-sliding test on core
$f_v$ $f_p$	Shear strength and normal pre-compression stress from shear-compression test on triplets
$F_h$	Horizontal pre-compression load from shear-compression test on triplets
$G_{fx1}$ $G_{fx2}$ $G_{fx3}$	Fracture energy under vertical out-of-plane bending, horizontal out-of-plane bending, and in-plane bending
$G_{f-c}$ $G_{f-c,h}$	Compressive fracture energy of masonry under vertical and horizontal loading
$G_{fw}$	Fracture energy of a joint from bond wrench test
$G_{f-cp}$	Predicted compressive fracture energy of masonry
$G_m$ $G_{m,core}$	Shear modulus calculated between 10% and 30% of the maximum load from test on triplet and test on core
$G_{f-I}$ $G_{f-II}$	Mode-I and mode-II fracture energy
$G_{f-tm}$	Tensile fracture energy of mortar
$G_3$	Mortar shear modulus evaluated between 10% and 30% of the maximum load
$h_u$ $l_u$ $t_u$	Unit height, length, and thickness
$h_m$ $l_m$ $t_m$	Wallet height, length, and thickness
$I_u$ $I_m$	Moment of inertia of unit and of wallet along the cross-section
$k_k$	Ratio between the elastic modulus and characteristic compressive strength of masonry
$k_m$	Ratio between the Young's modulus and the mean values of compressive strength
$l_j$ $w_j$	Mean length of the bed joint and mean width of the bed joint
$M_{el}$	Bending moment in the linear elastic stage between 10% and 30% of the maximum bending moment

$m$	Self-weight of wallet
$VF_b$	Volume fraction of unit in a masonry wallet
$VR_{mh}$	Volume ratio of bed joint to mortar in a masonry wallet
$v_p$ $u_p$	Plastic sliding displacement and the corresponding plastic normal displacement

### Greek Symbols

$\delta_{peak}$	Shear sliding corresponds with maximum load
$\delta^*$	Shape factor to normalise the unit compressive strength
$\varepsilon_p$ $\varepsilon_{p,h}$	Strain corresponding to vertical and horizontal compressive strength
$\varepsilon_{pp}$	Predicted peak strain under compressive load
$\varepsilon_u^*$	Ultimate compressive strain
$K_{el}$	Curvature corresponds with the bending moment in the linear elastic stage between 10% and 30% of the maximum bending moment
$\mu$ $\mu_{core}$	Initial friction coefficient obtained from test on triplet and from test on core
$\nu$ $\nu_h$	Poisson's ratio under vertical and horizontal loading
$v_{el}$	Deflection in the linear elastic stage within 10% and 30% of the maximum force
$\sigma_u$	Confining compressive stress at which the dilatancy becomes zero
$\chi_i$	Nearest distance between the bending crack and the outer bearings
$\psi$	Dilatancy
$\Psi_0$	Dilatancy at zero normal confining stress and shear-sliding

### Abbreviations

ADB	Adobe Masonry
CON	Conventional Concrete Masonry
CSB	Calcium Silicate Brick Masonry
CSER	Compressed-Stabilized Earth Masonry
FEM	Finite Element
GEO	Geopolymer Masonry
HPT	Helix Pull-out Test
LVDT	Linear Variable Differential Transformers
MSE	Mean Squared Error
NLKA	Nonlinear Kinematic Analysis
NLPO	Nonlinear Push-Over Method
NLTH	Nonlinear Time History Method
NZSEE	New Zealand Society for Earthquake engineering
PPT	Pin Penetrometer Test

SLaMA

Simple Lateral Mechanism Analysis

URM

Un-Reinforced Masonry



# CONTENTS

<b>Summary</b>	<b>vii</b>
<b>Samenvatting</b>	<b>ix</b>
<b>Symbols and abbreviations</b>	<b>xi</b>
<b>1 Introduction</b>	<b>1</b>
1.1 Background	1
1.2 Overview of masonry response	3
1.3 Overview of conventional testing methods	6
1.4 Challenges of material characterisation for existing masonry structures	10
1.5 Research questions	12
1.6 Research scope, methodology and contributions	12
1.7 Thesis outline	14
<b>2 Comprehensive characterisation of nonlinear response of laboratory-made masonry: Compression, bending and shear behaviour</b>	<b>17</b>
2.1 Experimental programme on laboratory-made specimens	18
2.2 Compression and flexural properties of mortar joint	21
2.3 Compression and flexural properties of unit	23
2.4 Nonlinear compressive behaviour	27
2.4.1 State-of-the-art: Compression response	27
2.4.2 Testing procedure and data elaboration	29
2.4.3 Overall response	31
2.4.4 Compressive strength	36
2.4.5 Young's modulus	38
2.4.6 Compressive fracture energy	39
2.5 Nonlinear bending behaviour	40
2.5.1 State-of-the-art: Bending response	40
2.5.2 Testing procedure and data elaboration	43
2.5.3 Overall response	47
2.5.4 Flexural strength	54
2.5.5 Young's modulus	56
2.5.6 Fracture energy in bending	56
2.5.7 Uniaxial tensile strength	58
2.6 Nonlinear shear-sliding behaviour along the interface	59
2.6.1 State-of-the-art: Shear response	59
2.6.2 Testing procedure and data elaboration	61
2.6.3 Overall response	62
2.6.4 Cohesion and friction coefficient	65
2.6.5 Residual friction coefficient	66
2.6.6 Shear modulus of the mortar joint	67
2.6.7 Cohesion softening and mode-II fracture energy	68
2.6.8 Dilatancy	68
2.7 Concluding remarks	70

<b>3 Material properties of Dutch masonry buildings built between 1912 and 2010: Laboratory and in-situ tests</b>	<b>73</b>
3.1 Overview of testing programme on field-extracted Samples	74
3.2 Comparison between the results of laboratory and in-situ testing methods	82
3.3 Nonlinear behaviour of field-extracted masonry	88
3.3.1 Compressive response	88
3.3.2 Bending response	91
3.3.3 Shear response	93
3.4 Inter-building distribution of material properties	95
3.4.1 Overall results of all masonry types	96
3.4.2 Subdivision of material properties	99
3.5 Dataset of material properties of Dutch masonry	111
3.6 Concluding remarks	114
<b>4 Core testing method to assess nonlinear compression behaviour of brick masonry</b>	<b>117</b>
4.1 State-of-the-art	118
4.2 Material and methods	120
4.2.1 Testing set-ups and procedures	122
4.2.2 Specimen geometries	123
4.3 Global behaviour	125
4.3.1 General response	125
4.3.2 Response of each masonry object	128
4.4 Correlation study	134
4.5 Concluding remarks	137
<b>5 Core testing method to assess nonlinear shear sliding behaviour of the brick-mortar interface</b>	<b>139</b>
5.1 State-of-the-art	140
5.2 Materials and methods	143
5.2.1 Testing procedure	144
5.2.2 Elaboration of experimental results	146
5.3 Global behaviour	151
5.4 Cohesion and friction coefficient	155
5.5 Plastic shear modulus of the mortar joint	156
5.6 Fracture energy for shear-sliding cracking	157
5.7 Dilatant behaviour	161
5.8 Concluding remarks	163
<b>6 Strategy for the material characterisation of existing structures: Correlation and constitutive laws</b>	<b>167</b>
6.1 Prediction of material properties	168
6.1.1 Mortar properties	170
6.1.2 Unit properties	171
6.1.3 Masonry compressive strength	173
6.1.4 Masonry Young's modulus	174
6.1.5 Strain corresponding to masonry compressive strength	177
6.1.6 Compressive fracture energy of masonry	178
6.1.7 Bond strength	179
6.1.8 Cohesion	181

---

6.1.9	Tensile fracture energy of mortar, units, and masonry	184
6.1.10	Shear fracture energy	185
6.1.11	Orthotropic behaviour of masonry under compression and bending loads	186
6.2	Prediction of stress-strain relationship	189
6.2.1	Compression	189
6.2.2	Bending	196
6.2.3	Shear	200
6.3	Concluding remarks	203
<b>7</b>	<b>Conclusions</b>	<b>207</b>
7.1	Summary of main research findings	208
7.2	Recommendations for future research	217
<b>A</b>	<b>Material testing</b>	<b>219</b>
<b>B</b>	<b>Influence of triplets' geometry on shear properties</b>	<b>229</b>
	<b>Bibliography</b>	<b>231</b>
	<b>List of Publications</b>	<b>247</b>
	<b>Curriculum Vitae</b>	<b>249</b>
	<b>Acknowledgments</b>	<b>251</b>



## INTRODUCTION

---

### 1.1 BACKGROUND

Over the last decade, the Netherlands has been confronted with frequent earthquakes induced by gas exploitation from shallow deposits in the Groningen region. Since 1963, underground resources have been continuously extracted from the Groningen gas field, which is the largest natural gas reservoir in Europe. However, at the time when extraction began, no one would have believed that approximately 50 years later the country would face a serious problem as a result of constant human intervention in the environment. The first recorded earthquake in the Groningen field dates back to 1991 and had a magnitude of  $M < 2.5$ . Since then, the frequency and magnitude of the earthquakes have steadily increased, causing damage as well as safety issues. Damage relates to cracks have been observed as a consequence of the repeated light earthquakes, while safety relates to the possibility of local or global collapse given the potential for a strong future earthquake to happen. These consequences of induced seismicity have a strong social and psychological impact on local residents; hence, the situation has been characterised as a ‘crisis’ (e.g., van der Voort & Vanclay, 2015; Schmidt et al., 2018). Although the Minister of Economic Affairs has recently firmly decided to reduce gas exploration, thereby reducing the seismic hazard, there is still a need for solid seismic assessment of the building structures both for the lower damage state and for the near collapse state.

In the Netherlands, like many other parts of the world, unreinforced masonry (URM) buildings, especially those made of regular units of bricks, are identified as the most seismically vulnerable structures. For the province of Groningen, which is mainly a rural area and only partly urban, the percentage of unreinforced masonry building structures is higher than average, with estimates up to 77% (Crowley et al., 2020). The building stock in the Groningen region expanded over a long period, and over time the construction details as well as the materials used underwent significant changes, Figure 1.1. Older, pre-war buildings mainly consist of double-wythe brick masonry walls (‘steensmuren’) with timber floors, while beginning in 1945 cavity walls (‘spouwmuren’) entered the scene, and timber floors were gradually replaced by concrete floors. The cavity walls often consist of a non-load-bearing outer leaf of single-wythe clay brick masonry and a load-bearing inner leaf of single-wythe calcium-silicate masonry; the latter was initially made of brick, but since the ‘70s it has gradually been replaced by larger block and element formats. Overall, this building style can be characterised as very slender with large window openings and a lack of seismic detailing. In fact, the buildings have never been designed to withstand earthquake loads. Apart from this, unreinforced masonry is

generally vulnerable to seismic loading. This is because the material is inherently quasi-brittle. It behaves highly nonlinearly with poor characteristics in tension and shear, leading to mode-I type cracks and mode-II type slip and shear failures, and crushing and splitting in compression. Such material characteristics make URM structural components prone to in-plane and out-of-plane failure, thus threatening human life as well as world cultural heritage (D'Ayala & Speranza, 2003; de Felice, 2011).

In efforts to mitigate dwelling vulnerability, the nonlinear response of the URM structures should be accurately assessed. Prior to making any decisions regarding strengthening and rehabilitation techniques, the nonlinear response of masonry from the formation of light damage up to the condition of near collapse needs to be determined. To this end, guidelines such as the Dutch standard NPR 9998 (NEN 2018) offer a range of analysis methods, including Nonlinear Push-Over Methods (NLPO) and Nonlinear Time History Methods (NLTH), which consider nonlinear masonry behaviour in a quasi-static and dynamic fashion, respectively. These methods can be employed in combination with different representations of masonry, among which the most common are continuum damage models and structural-component based models. The former subdivide piers and spandrels into small elements driven by constitutive models at the materials scale, while the latter treat piers and spandrels as single components with structural properties. In addition, analytically based NLPO methods exist, like the Simple Lateral Mechanism Analysis (SLaMA) for in-plane and Nonlinear Kinematic Analysis (NLKA) for out-of-plane behaviour, for example, NPR 9998 (NEN 2018). Furthermore, a new trend in research, not yet adopted in engineering practice, focuses on the development of multiscale approaches in which structural response is obtained by upscaling detailed brick-to-brick models at the constituent level (e.g., Silva et al., 2020). In the end, all methods require inputs regarding the material properties of masonry or of its constituents. The structural and analytical models require stiffness and strength properties, while the continuum damage and the detailed brick-to-brick models require complete stress-strain laws including hardening and softening regimes, that is, a characterisation of toughness in addition to strength and stiffness. Moreover, these complete stress-strain laws should be available for tension, shear, compression and multi-axial combinations thereof, including orthotropic effects induced by the bond pattern of the masonry.

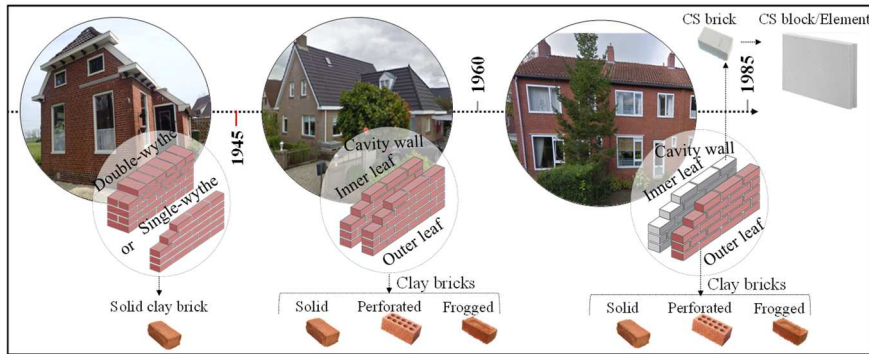


**Figure 1.1:** Correlation between different building typologies and construction materials in the Netherlands.

A complete picture of masonry characteristics, accounting for its full nonlinear response and its statistical distribution, has long been of scientific research interest worldwide, and it has become a necessity for the Netherlands in recent years. The absence of well-defined material parameters brings a set of tacit assumptions into the modelling process, thus reducing confidence in the reliability of the structural analysis. Hence, the more rigorously the input parameters can be determined, the more they can engender confidence in the reliability of the prediction models. This calls for an interdisciplinary approach, whereby experimental research is focused on meeting the demands of model developers. As a result, laboratory testing and in-situ testing campaigns are needed to provide a basis for the validation and calibration of the various models to be used in deterministic or probabilistic settings.

Although this research provides a context for the Groningen seismic case and was evolved together with large-scale tests on structural components and buildings (Messali & Rots, 2018; Damiola et al., 2018; Esposito et al., 2019; Messali et al., 2020), the characterisation of masonry material is also of relevance for other challenges. In this framework, forecasts of damage to URM structures due to subsidence in soft soil deltas or of settlement damage due to tunnelling or other subsurface building activities are long-standing problems not only in the Netherlands, but also in other countries (e.g., Burd et al., 2000; Can et al., 2012; Giardina et al., 2015; Peduto et al., 2019). Recently, the collapse of quay walls in Amsterdam highlighted once again the importance of material characterisation for preserving cities' masonry infrastructure (e.g., Korff et al., 2021).

## 1.2 OVERVIEW OF MASONRY RESPONSE

Within the framework of analysing the masonry response, we need to first provide a clear picture of the set of input masonry properties that are of interest to research and engineering communities. Concerning the structural assessment of URM buildings, the complete response of masonry, associated with all the possible local material failures, namely pure crushing, tensile cracking, debonding, shearing along the brick-mortar interface, or any combination of these, is essential. Accordingly, compression, bending, and shear tests can be performed to account for all the local

in-plane and out-of-plane failures of masonry. This section focuses on the behaviour itself and the parameters describing the behaviour. The performance and limitations of conventional laboratory and in-situ testing methods will be discussed in Section 1.3.

To date, several different structural representations of masonry are available for use in the numerical and analytical assessment methods mentioned above, each calling for a distinct level of refinement regarding the material input. This study focuses on three types of representations: continuum representations, detailed brick-to-brick models and structural component-based models. For a more comprehensive overview of masonry representations, the reader is referred to D'Altri et al. (2019b). These sets of models' input parameters, organised into three categories, are listed in Table 1.1.

The first class, continuum representations, relates to smeared crack/crush models (e.g., Gambarotta & Lagomarsino, 1997; Lourenço et al., 1998; Pelà et al., 2011). Here, masonry is treated as a homogenous continuum material, where the different mechanical responses of constituents, such as brick, mortar, and interfaces, are not considered. These types of models are built upon the formulation of stress-strain relationships under compression and tension loading. As specified in Table 1.1, the material properties are defined at the masonry level, in terms of stiffness (i.e. Young's modulus and Poisson's ratio), strength (i.e. tensile and compressive strength), and toughness (fracture energy and shape of the softening branch). Considering that the brick arrangement is responsible for the orthotropic behaviour of the masonry material, continuum damage models often adopt an orthotropic formulation. Consequently, the mechanical properties should be defined at least along the two principal directions, that is, loading perpendicular and parallel to the bed joints. For the sake of simplicity, these will be denoted as vertical and horizontal properties, although formally the direction of bed joints can also be non-horizontal.

The second class, detailed brick-to-brick representation, treats masonry as an assembly of individual constituents, namely bricks, mortar joints, and brick-mortar interfaces. Within this class, we can distinguish between the discrete model and the homogenisation-based model. The former adopts the finite element method to directly discretise masonry with continuum elements for bricks and mortar joints, and interface elements for the brick-mortar interface (e.g., Lotfi & Shing, 1991; Lourenço & Rots, 1997; Milani, 2008; D'Altri et al., 2019a). The latter uses computational or analytical homogenisation approaches (e.g., Massart et al., 2007; Sacco, 2009) to derive the response at the masonry level based on the mechanical behaviour of the constituents. In both approaches, the input parameters are no longer described at the level of the masonry as a whole, but at the constituent level. Properties related to cracking and crushing failure of the constituents are generally associated with bricks and mortar elements, while properties related to shear-sliding and debonding failure are coupled to the brick-mortar interface. This allows considering not only tensile and shear failure at the interface, but also dilatancy effects associated with the uplift upon shearing.



The third class of representations relates to structural component-based models, either analytical or numerical (e.g., for SLaMA see Gentile et al., 2019; for Equivalent frame models see Lagomarsino et al., 2013; and for Rigid body spring mass model see Silva et al., 2017). Here, besides compression and shear properties, knowledge of the bending properties of masonry under both in-plane and out-of-plane bending loads is highly relevant. The bending properties can be interpreted as indirect tension, while the abovementioned properties for the continuum and the detailed brick-to-brick representations relate to direct tension. There is a correlation between the two, related to the theory of fracture mechanics. Three bending properties can be determined: out-of-plane vertical bending (the moment vector in the plane of the wall and parallel to the bed joints), out-of-plane horizontal bending (the moment vector in the plane of the wall and perpendicular to the bed joints) and in-plane bending (the moment vector orthogonal to the plane of the wall). Again, both strength and toughness parameters can be defined, the first for analytical as well as numerical models, and the second for numerical models only.

**Table 1.1:**

Overview of input parameters required by the three classes of models.

Model parameters	Continuum damage models	Detailed brick-to-brick models	Structural component-based models
<b><i>Masonry properties</i></b>			
Young's modulus	■		■
Poisson's ratio			
Compressive strength			
Tensile strength			
Bending strength			■
Fracture energy in compression	■		
Fracture energy in tension			
<b><i>Brick and mortar properties</i></b>			
Young's modulus		■	
Compressive strength			
Tensile strength			
Fracture energy in compression			
Fracture energy in tension			
<b><i>Brick-mortar interface properties</i></b>			
Tensile strength		■	
Cohesion/ Initial shear strength			
Initial friction coefficient			
Residual friction coefficient			
Dilatancy			
Fracture energy in tension			
Fracture energy in shear			

### 1.3 OVERVIEW OF CONVENTIONAL TESTING METHODS

In order to characterise the nonlinear response of masonry and its constituents, a large variety of laboratory and in-situ testing methods have been developed in the literature. Table 1.2 provides a list of model parameters and indicates the possibility of determining each one, either by means of conventional laboratory tests on medium-sized portions of masonry and masonry constituents or by using in-situ testing methods. By means of displacement-controlled testing set-ups, which are not mandatory by standards, the former test often allows for capturing the complete nonlinear behaviour and thus the full range of mechanical properties. Nevertheless, the applicability of conventional laboratory tests to existing buildings is often limited due to the invasive extraction of medium-sized samples. To overcome this limitation, in-situ testing methods with limited invasiveness to the building are often adopted, although they provide less information.

**Table 1.2:**

Overview of laboratory and in-situ tests to obtain the model input parameters.

Model parameters	Uniaxial comp. loading			Uniaxial tensile loading			Bending load			Bond wrench test			Shear-comp. loading			
	Lab	situ	In-	Lab	situ	In-	Lab	situ	In-	Lab	situ	In-	Lab	situ	In-	
<b><i>Masonry properties</i></b>																
Young's modulus	■						■									
Poisson's ratio	■															
Compressive strength	■															
Tensile strength				■						■ *						
Bending strength							■									
Fracture energy in comp.	■															
Fracture energy in tension				■												
Fracture energy in bending							■									
<b><i>Brick and mortar properties</i></b>																
Young's modulus	■						■									
Compressive strength	■															
Tensile strength				■						■ *						
Fracture energy in comp.	■															
Fracture energy in tension				■												
<b><i>Brick-mortar interface properties</i></b>																
Tensile strength				■						■ *			■ *			
Cohesion													■			
Initial friction coefficient													■			
Residual friction coefficient													■			
Dilatancy													■			
Mode I fracture energy				■						■ *			■			
Mode II fracture energy													■			

\*Indirect evaluation of tensile properties using the outcomes of vertical out-of-plane bending or bond wrench tests.

A medium-sized masonry sample, comprising a minimum of two bricks in length and five brick courses in height, can be subjected to uniaxial compressive load either in the laboratory using a hydraulic press or in-situ by means of two flat-jacks inserted in the bed joints, Figure 1.2a,b. These tests can be performed following the outlines of the European standard EN 1052-1(CEN 1998) and the American standard ASTM C1197-14(2014), respectively. Despite the invasive sampling procedure, which is costly and not always practical, laboratory tests allow for capturing the full nonlinear compression behaviour of masonry, thus not only providing insights into its strength and stiffness, but also into its toughness. To minimise the extent of damage due to sampling, the double flat-jack test was introduced as an in-situ testing method to evaluate the elastic properties as well as the compressive strength of masonry. However, previous studies have raised doubt regarding the accuracy of the strength measurement, particularly in low-rise buildings with low stress acting on the wall (e.g., Binda & Tiraboschi, 1999). It turned out that when pressure in the flat-jacks exceeded the overburden, the test was often interrupted due to the undesired failure of the contrast portion. Accordingly, the range of applicability of this testing method is often limited to walls with a high value of overburden. In addition, the findings of previous studies have shown that the testing results can vary widely when the compressive stress field is not well distributed, due to the poor quality of either the masonry or the cutting operation (e.g., Noland et al., 1988; Binda & Tiraboschi, 1999; Cescatti et al., 2016). Taking into account the orthotropic behaviour of masonry, knowledge of its horizontal compression response can currently be gained only with laboratory tests, Figure 1.2c. Similar to masonry, direct insights into the compression properties of masonry constituents can be gained using laboratory tests on extracted pieces, such as compression tests on bricks (NEN 772-1:2011) and double-punch tests on mortar (DIN 18555-9:1999). Apart from laboratory tests, non-invasive in-situ testing techniques are often used to provide an indication of the quality and homogeneity of brick and mortar. Past research into non-invasive in-situ testing methods has focused primarily on the indirect estimation of compressive strength. In this context, the New Zealand Society for Earthquake Engineering (NZSEE 2017) gives an indication of the compressive strength of mortar and brick as a function of surface hardness determined from a simple scratch test.

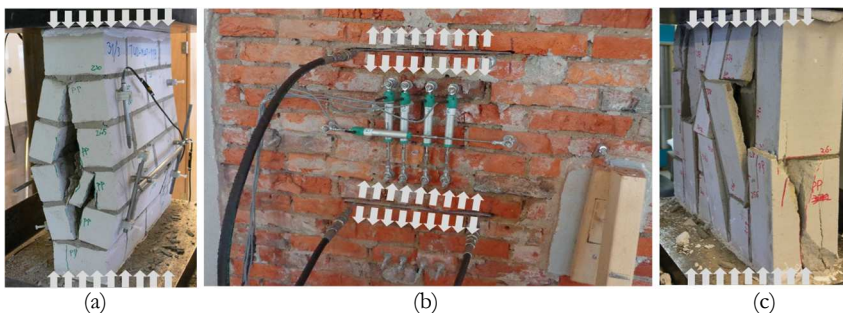


**Figure 1.2:** Compression tests on masonry: (a) vertical compression test on extracted wallet; (b) in-situ double-flat jack test, photo is taken from EUcentre (2015); (c) horizontal compression test on extracted wallet.

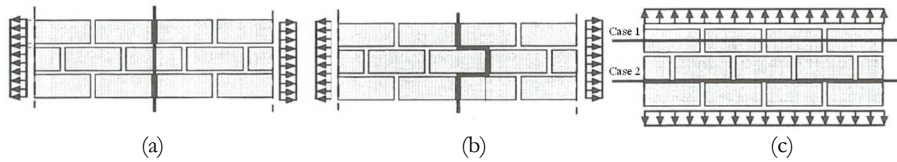


**Figure 1.3:** Tensile tests on masonry wallets: tensile stress parallel to the bed joints with the formation of (a) a splitting crack; (b) a step-wise crack; (c) tensile stress perpendicular to the bed joint with debonding along the interface, extracted from Schubert, 1994.

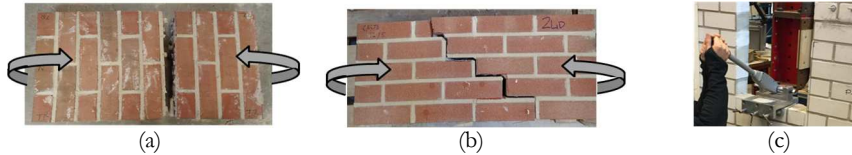


**Figure 1.4:** Bending tests on wallets with (a) moment vector parallel to the bed joints and (b) moment vector perpendicular to the bed joints; (c) bond wrench test.

An understanding of the tensile response of masonry as well as its constituents can only be gained through laboratory tests. To date, there have been few studies that have conducted direct tensile tests on masonry wallets with loading directions parallel and perpendicular to the bed joints (e.g., Backes, 1985; Schubert, 1994). For the tensile stress parallel to the bed joints, the failure is governed by either a splitting crack running almost vertically through the wallet, or a step-wise crack passing through multiple head and bed joints, as illustrated in Figure 1.3a,b. Accordingly, for a better understanding of the failure mechanism, a distinction should be made between the properties of bed joints and head joints, as the latter are often not fully mortared. For the tensile stress perpendicular to the bed joints, two types of failure often occur: debonding along the interface or tensile failure of the brick, Figure 1.3c. Consequently, the tensile strength of masonry can be equated with either tensile bond strength or unit tensile strength. Accordingly, instead of the tensile loading of wallets, previous studies have adopted couplet specimens, thus dealing with a single joint (e.g., van der Pluijm, 1999). Similar to masonry couplets, brick and mortar prisms with a central notch can be subjected to uniaxial tensile loading. Nevertheless, the uniaxial tensile testing method has not gained much in popularity due to the number of complexities involved throughout the testing process, including the preparation of the samples as well as the testing set-up. Moreover, the effect of boundary conditions on the post-peak response has not been clearly demonstrated (e.g., van der Pluijm, 1999). To overcome such limitations, bending tests have often been adopted in the literature, although these provide only an indirect estimation of tensile strength.

The bending response of masonry can be obtained in the laboratory by performing out-of-plane bending tests on wallets along two directions, with moment vectors parallel as well as perpendicular to the bed joints, Figure 1.4a,b. For testing purposes, the outlines of the European standard EN 1052-2(CEN 2016) can be followed. Accordingly, using a displacement-controlled testing set-up, insights can be gained into the flexural strength, Young's modulus, and often the fracture energy. Note that although fracture energy in bending is not used as an input parameter, it could be associated with fracture energy in tension. To determine

the flexural strength of brick as well as of mortar, researchers have often performed three-point bending tests on extracted samples. As mentioned above, these values can be translated into the tensile properties. Apart from the bending test, the bond wrench test can provide information on flexural bond properties at the brick-mortar interface that can be used to indirectly estimate the tensile properties, Figure 1.4c. This test has the advantage of simplicity and of causing limited damage to the structures; thus it can be used in both laboratory and in-situ applications. The test is mainly designed to evaluate flexural bond strength, but with a set-up adopting a crack-mouth opening control across the mortar joint, Gaggero (2019) was recently able to record the complete nonlinear response as well as evaluate the associated fracture energy.

Knowledge on the shear-sliding behaviour along the masonry brick-mortar interface can be gained from laboratory shear-compression tests, or from an in-situ test known as the 'shove test' or 'push test', Figure 1.5a,b. Of the different standardised testing methods, the shear-compression test on triplets prescribed by the European standard EN 1052-3(CEN 2002) is the most commonly adopted method. By means of displacement-controlled equipment, both pre- and post-peak shear properties can be determined, thus providing information on cohesion, the initial and residual friction coefficients, dilatancy, and mode-II fracture energy. However, the invasive extraction of multiple samples, comprising one brick in length and three courses of bricks in height, is the major drawback in terms of the practical application of this method. As an alternative, American standard ASTM C1531(2016) introduced the application of an in-situ shove test, which involves a minimum disturbance to the wall integrity. This testing method often succeeds the double flat-jack tests. The only modification is that the tested brick is isolated from the two lateral sides and is pushed using a hydraulic jack. Unlike tests on triplets, the shove test allows for determining only the values of the residual friction coefficient and cohesion, assuming that the values of the initial and the residual friction coefficients are equivalent. To perform a shove test, specialised technical experts should continuously monitor the deformations in the masonry wall using accurate instrumentation. This should be done to prevent the unwanted cracking of the contrast portion of the wall, which could introduce uncertainty regarding the reliability of the test results (Binda & Tiraboschi, 1999; Cescatti et al., 2016). As the wall integrity is to some extent disturbed, the objective interpretation of the factual normal stress acting on the tested brick due to the contribution of both flat-jacks and overburden is seldom possible. It is worth mentioning that apart from the aforementioned testing methods, diagonal compression tests can be performed on a large portion of masonry (not less than  $1.2 \times 1.2$  m), either in the laboratory, Figure 1.5c, following the outlines of ASTM E519/519M(2015), or in-situ, while the wallet is disjointed from the rest of the wall on three sides. Nevertheless, the interpretation of the results of these tests remains controversial, as the stress state at the centre of the wallet is not a pure shear stress. Additionally, the diagonal compression test aims mainly to retrieve information on the tensile strength of masonry as a homogenous material, rather than on shear properties at the brick-mortar interface.

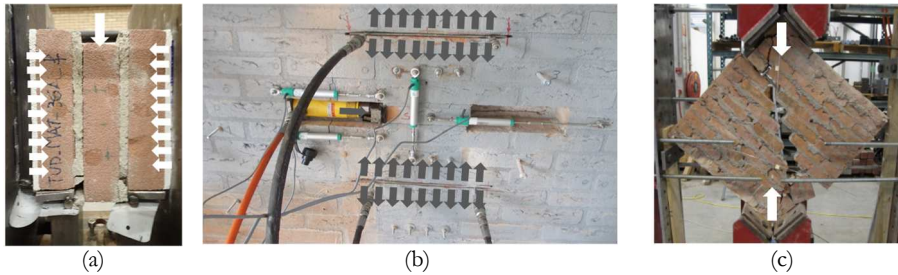


**Figure 1.5:** (a) Shear-compression test on triplet; (b) in-situ shove test, photo is taken from EUcentre (2015); (c) diagonal compression test on wallet, photo is taken from Vermeltfoort (2015).

## 1.4 CHALLENGES OF MATERIAL CHARACTERISATION FOR EXISTING MASONRY STRUCTURES

Why does it remain difficult to provide a complete overview of the material properties of existing masonry structures? The main hindrances to a comprehensive experimental characterisation of masonry are the quasi-brittle nature of masonry, the existence of many diverse masonry types, the lack of a reliable in-situ semi-invasive testing method, and the ambiguity in providing an acceptable level of knowledge on material properties with a minimum disturbance to the wall integrity. Each of these aspects will be further elaborated on in this section, thereby identifying the research gaps.

The majority of past experimental research has paid little attention to the characterisation of toughness. From the phenomenological point of view, a complete description of the masonry response is required. However, due to the quasi-brittle nature of masonry, it is often impossible to capture the softening branch, particularly under tensile loading. Accordingly, despite its importance, there remains a paucity of experimental evidence on toughness, which can be quantified in terms of fracture energy. Insights into the values of fracture energy are highly appreciated, when numerical analyses account for the material nonlinearity.

Several countries, such as the Netherlands, suffer from the lack of a comprehensive database containing the properties of the most common masonry types. Generally, when invasive tests on existing structures are not possible (e.g., in the case of heritage structures), practitioners look for a benchmark of material properties. Besides knowledge on material properties, insight into the statistical distribution function for each property is of relevance. Accordingly, it can be expected that building codes and national regulations in countries with relatively high seismicity should provide or regularly expand a benchmark of the material properties. To this end, countries such as Turkey (e.g., Ispir et al., 2009), and New Zealand (e.g., Almesfer et al., 2014; Lumantarna et al., 2014a; Lumantarna et al., 2014b) have adopted an extensive experimental approach, including in-situ tests as well as laboratory tests on field-extracted samples. In this context, a large number of buildings were selected for testing purposes. As expected, the local material availability and construction techniques caused considerable variation not only in the physical but also in the mechanical characteristics of masonry. Accordingly, the

database of material properties ascertained in one specific region cannot be easily generalised/extrapolated to other regions with a different context.

There is a paucity of evidence on the potential for semi-invasive in-situ testing methods to provide insight into toughness properties. As reported in Chapter 3, no good correspondence has been found between the material properties obtained from laboratory tests and those obtained from conventional in-situ tests. Although a comprehensive overview of material properties can be obtained using laboratory testing methods, the opportunity to extract a complete series of samples is not offered for each building. Accordingly, these limitations have given rise to the development of novel methodologies. As the sampling of small-diameter cores causes limited damage to building functionality, the core testing method has gained renewed interest in recent years (e.g., Sassoni & Mazzotti, 2013; Mazzotti et al., 2014; Pelà et al., 2016b; Pelà et al., 2016a). However, this method has been mainly used to characterise the pre-peak properties and not the post-peak softening response. In addition, although this testing method was introduced for the characterisation of existing structures, previous studies have mainly focused on laboratory-made samples. Therefore, the wide variation in testing results for existing structures, often caused by the influence of aged materials and workmanship, was deliberately overlooked.

Considering the substantial number of input parameters required by the models and the difficulties of determining these parameters with a limited number of tests, the study of the correlation between material properties is of relevance; yet, this has not been systematically carried out in the literature. Providing detailed knowledge on masonry material properties is a laborious task, and not always practical. In return, exploring the possible correlation between the material properties is of prognostic interest, as it could reduce the number of necessary tests. Eurocode 8(CEN 2008) gave an indication of the number of tests under three different levels of in-situ inspection: limited, extended, and comprehensive in-situ inspection. Each of these inspection levels corresponds to a different knowledge level as well as a confidence factor to reduce the mean values of material properties to be used as input for structural analyses. As expected, the lower the number of tests, the more limited the knowledge level, and, thus, the higher the safety factor to be considered in structural analyses. Nevertheless, the available design codes and standards do not touch upon on a guideline to reduce the number of types of tests, while simultaneously maintaining the level of knowledge on material properties. This may be possible only by establishing correlations between material properties obtained by different types of tests.

In short, the existing literature on the behaviour of masonry at the material scale lacks an integrative approach that could guide practitioners through the decision-making process by prioritising particular types of tests and optimising the identification of input parameters for structural assessment.

## 1.5 RESEARCH QUESTIONS

The main objective of this study is to provide input parameters with a distinct level of refinement for use in the numerical and analytical assessment methods for existing URM structures. To this end, the study follows an experimental approach, an indispensable tool for understanding masonry behaviour, aiming to provide answers to the following sub-questions:

- How can the complete nonlinear compression, bending, and shear behaviour of masonry and its constituents be experimentally characterised, with particular attention to toughness properties?
- How can a comprehensive database of material properties for typical Dutch masonry be provided, supporting the formulation of provisions in assessment codes?
- How can the compression and shear properties of existing masonry be characterised by adopting a semi-invasive testing method compatible with in-situ investigations?
- How can a comprehensive level of knowledge on material properties for structural analysis be provided in a cost-effective manner?

## 1.6 RESEARCH SCOPE, METHODOLOGY AND CONTRIBUTIONS

To develop an integrative approach that prioritises the type of tests and optimises the identification of input parameters, this thesis aims to formulate a strategy for the material characterisation to be incorporated in the structural assessment of existing URM structures. To this end, the current research adopts both laboratory-made and field-extracted samples. As expected, extracting a complete set of samples from existing buildings is almost impossible; for example, the complete characterisation of masonry with nominal brick dimensions of  $210 \times 71 \times 100$  mm requires the extraction of samples for approximately  $11 \text{ m}^2$ , which correspond to a wall with dimensions of  $4 \times 2.7$  m. In return, replicating masonry allows for carrying out a complete study of the material response independent of the sample size. As a result, for the five most typical masonry types, the entire set of specimens required to characterise the compression, bending, and shear behaviour of masonry was replicated in the laboratory at Delft University of Technology. In addition to the laboratory-made samples, this research further benefited from performing tests on field-extracted samples. In this context, sixteen different Dutch URM dwellings built between 1910 and 2010, including both residential buildings and schools, were selected for the purpose of testing. Following the outlines of ASTM C1532(2005), samples were extracted and packed and then transported to the laboratory. It is worth mentioning that the insights gained from tests on field-extracted samples and laboratory-made specimens are complementary and support the broader conclusions.



Taking into account the extent of the invasiveness caused by the sampling, the laboratory testing methods adopted in this research are classified as invasive or semi-invasive. The former refers to tests on medium-sized samples, whereby the guidelines of the European standards were followed for the selection of each sample's size. The latter points to tests on small-diameter cores extracted from walls to fully characterise the nonlinear compression and shear-sliding behaviour of brick masonry.

The most significant contributions of this thesis are as follows:

- It provides improved insights into the strength, stiffness, and toughness of different masonry types under compressive, bending, and shear loading as well as investigates the orthotropic behaviour of masonry. By means of well-designed displacement-controlled or crack-controlled testing set-ups, the complete nonlinear response of the five most typical Dutch masonry types is provided and synthesised in terms of constitutive laws. This information, collected from tests on laboratory-made masonry specimens, provides the groundwork for the development and validation of models for structural analyses.
- It provides a comprehensive database of material properties for typical Dutch masonry, accounting for divisions based on masonry types and year of construction, and it introduces a statistical distribution function for each property. These results, obtained from tests on field-extracted masonry samples, can be applied not only towards the assessment of URM buildings in the Netherlands, but also toward the same masonry in other countries using similar construction methods. In addition, the knowledge provided on the statistical distribution of material properties can provide a further step towards the probabilistic analysis of existing masonry structures accounting for the variability of material properties.
- It investigates the potential of semi-invasive core testing methods to evaluate not only strength and stiffness, but also toughness for seven masonry types under compression and shear-sliding load. Considering the relatively large dataset obtained from tests on different masonry types, including both laboratory-made and field-extracted specimens, the core testing method can be regarded as a reliable alternative to the conventional in-situ testing methods.
- It explores the presence of statistical relationships between different material properties to minimise the burden associated with performing complex and invasive experimental studies. This is achieved in light of the rich database established from tests on field-extracted and laboratory-made masonry specimens. Intriguing trends are observed between different material properties, which in some instances are supported by data from the literature. Accordingly, recommendations are put forward to indirectly derive elastic and toughness properties as a function of strength properties. Therefore, a complete picture of material properties can be obtained, while minimising the number of experiments and the extent of their invasiveness.

## 1.7 THESIS OUTLINE

Figure 1.6 presents the thesis outline, highlighting two main streams: a comprehensive characterisation of masonry behaviour, including Chapter 2 and Chapter 3, and the development of semi-invasive testing methods for material tests in existing structures, which includes Chapter 4 and Chapter 5. The knowledge from both streams are used in Chapter 6 to formulate a strategy. The synopsis of each chapter is as follows:

**Chapter 2** and **Chapter 3** provide a comprehensive characterisation of masonry and its constituents for laboratory-made and field-extracted masonry specimens subjected to compression, bending, and shear loading. The testing procedure and the data analysis, which includes the full representation of stress-displacement curves in combination with crack evolution, are extensively discussed in **Chapter 2** for the five laboratory-made masonry types. **Chapter 3** focuses the attention on the variability of material properties and the importance of statistical analysis by analysing the experimental results from field-extracted specimens typical of the Netherlands. Moreover, **Chapter 3** highlights the importance of developing a suitable in-situ testing method, as no good agreement was found between the results of the laboratory tests and one of the conventional in-situ testing methods.

Due to the lack of accuracy of conventional in-situ testing methods and their limitations in providing a comprehensive characterisation, **Chapter 4** and **Chapter 5** investigate the potential of tests on small-diameter cores to provide the complete nonlinear behaviour of masonry under compression and shear-sliding load, respectively. The applicability of the core testing method is investigated for seven masonry types, including both laboratory-made and field-extracted masonry types. The suitability of the testing methods is validated by comparison with the results of laboratory tests on medium-sized specimens.

**Chapter 6** explores the possible relationships between different material properties and compares them with data from the literature, thus leading to intriguing conclusions. Moreover, this chapter formulates constitutive models under compression, bending, and shear loading, which are calibrated for five different masonry types.

**Chapter 7** summarises the major findings of the research and gives recommendations.

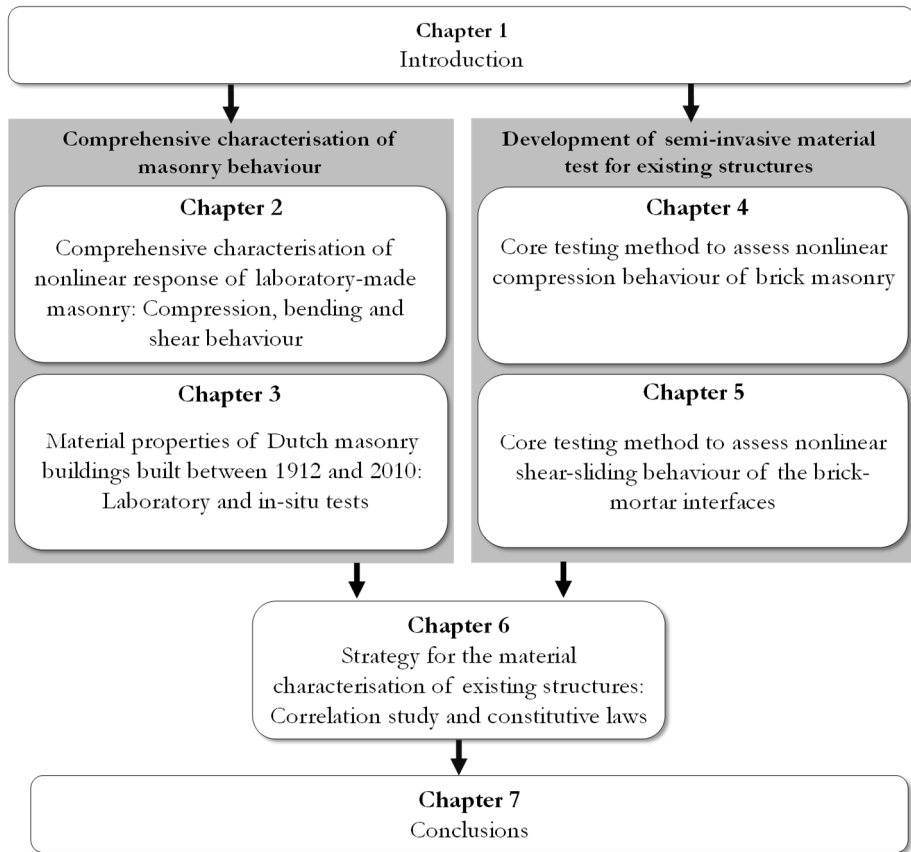


**Figure 1.6:** Thesis outline.



# COMPREHENSIVE CHARACTERISATION OF NONLINEAR RESPONSE OF LABORATORY-MADE MASONRY: COMPRESSION, BENDING AND SHEAR BEHAVIOUR

---

This chapter takes a systematic experimental approach, providing comprehensive insight into the behaviour of the five most common Dutch masonry types. It is deemed to be comprehensive because it covers several aspects that are limited in the literature: 1) investigating the response of masonry under different stress states, i.e. compression, bending, and shear; 2) analysing the complete nonlinear behaviour, not only in the pre-peak phase, but also beyond that; and 3) exploring the orthotropic response under compression and bending load. To this end, the complete series of specimens required to characterise the compression, bending, and shear response of masonry were built in the laboratory, as briefed upon in Section 2.1. In fact, the replication of masonry specimens in the laboratory is a gateway to reducing the variability and uncertainty in masonry response that arises from performing tests on statistically and geometrically non-representative samples. The mechanical properties of the masonry constituents, i.e. mortar and unit, adopted for the specimen replication, are presented in Section 2.2 and Section 2.3, respectively. Thereafter, the nonlinear behaviour of the five laboratory-made masonry types is exhaustively discussed under compression loading in Section 2.4, under out-of-plane and in-plane bending loads in Section 2.5, and under shear-compression loading in Section 2.6. For each distinct behaviour, a review of state-of-the-art is presented. Subsequently, the testing procedures and the data elaboration are explained, while the supporting appendices include a full description of the testing set-ups, measuring systems, and specimen preparation. Moreover, the overall responses of masonry in terms of stress-strain or stress-sliding developments in combination with crack growth are discussed in full. By contributing to the pool of experimental data, this research also allows for the investigation of the influence of brick types, number of wythes, and joint thickness on the response of masonry in terms of strength, stiffness, and toughness. Finally, Section 2.7 presents the main findings of the present work. The results of this chapter are complementary to Chapter 3, where tests on field-extracted samples are discussed.

## 2.1 EXPERIMENTAL PROGRAMME ON LABORATORY-MADE SPECIMENS

Unreinforced masonry (URM) structures can experience a broad range of local and global failures. As long as there is no trace of lateral loading, masonry can withstand considerable gravity loads; however, its vulnerability to lateral loads such as wind and earthquakes is well-known. At the local scale, the failure of masonry can be observed as pure crushing, tensile cracking, debonding along interfaces, shearing, or any combination of these. At the structural scale, the failure can be attributed to crushing, in-plane shear failure, and out-of-plane failure mechanisms, causing an imminent threat to public safety. Thus, to fully understand the response of masonry functioning as a holistic system, gaining sound knowledge of the nonlinear behaviour of masonry at the component- and material-scale is indispensable. Insights into the nonlinear response of masonry at the material-scale can be gained by means of an extensive experimental approach, whereby medium-sized masonry specimens are tested under compression, bending, and shear loading in an aim to obtain a comprehensive picture of the properties in terms of stiffness, strength, and toughness.

This section gives an overview of the experimental programme, which aims at providing a coherent framework for fully understanding the nonlinear behaviour of unreinforced masonry. The study focuses on the most common Dutch masonry types present in the Groningen region, where structures are vulnerable to induced seismicity events. In particular, the two main typologies of low-rise masonry buildings were identified as detached houses built before 1945, and terraced houses constructed after 1945 (Arup, 2013). The detached houses are low-rise buildings, in which the load-bearing walls were made of single- or double-wythe clay brick masonry. The terraced house typology is often known as masonry with a cavity wall system of a very limited thickness, in which calcium silicate (CS) masonry and clay brick masonry are used for the inner and outer leaves, respectively. Since the 1980s, with the demand for accelerating the construction process and subsequently reducing the construction costs, the dimensions of masonry units underwent some changes. Accordingly, in the Netherlands, the inner leaf of the cavity wall was often constructed with large blocks or CS elements with a thin mortar layer instead of using CS bricks with conventional mortar joints. In the end, the most common masonry types identified during the construction period and taken as reference were single-wythe CS brick masonry, single-wythe perforated clay brick masonry, single-wythe solid clay brick masonry, double-wythe solid clay brick masonry, and single-wythe CS element masonry with a thin layer mortar joint.

Despite the effort made to acquire standard size samples extracted from existing buildings, as will be presented in Chapter 3, a comprehensive characterisation of the material response of the field-extracted samples was not possible, thus emphasising the need for the structured replication of the masonry and the use of laboratory-made specimens. Generally, the accuracy of results obtained from tests on field-extracted masonry are questionable, as the integrity of the samples could be affected during the process of cutting, handling, and transporting them. Moreover, extracting a complete set of samples from existing buildings was almost

impossible, particularly in terms of the mechanical characteristics of double-wythe and CS element masonry. Accordingly, instead of performing tests on statistically and geometrically non-representative samples, tests on laboratory-made specimens were deemed an acceptable alternative. Therefore, the five most representative masonry types in the Netherlands were replicated in the laboratory, thus enhancing the availability and integrity of the experimental results.

Table 2.1 presents an overview of the characteristics of the replicated masonry types, including bonding pattern, joint thickness, unit size, and construction period. The replicated masonry types can be divided into two categories: brick masonry with a conventional joint of 10 mm, and element masonry with a thin, 2–4 mm layer of mortar. The units adopted in the former category were solid CS bricks and clay bricks, either solid or perforated, Figure 2.1. Along the wythe, specimens were either single-wythe (100 mm in thickness) with a ‘running’ bond pattern, Figure 2.2a, or double-wythe (210 mm in thickness) with a ‘Dutch cross bond’ pattern, Figure 2.2b. It should be underlined that the single- and double-wythe solid clay masonry specimens were both constructed using the same materials. The CS elements, Figure 2.1d, had a size of roughly 897×643×100 mm and were assembled using a very thin mortar layer (2–3 mm). To facilitate the construction process, each element was produced with a tongue and groove connection on the side. The use of a crane to assemble the construction was inevitable, due to the significant weight of each element (approximately 100 kg). To this end, two holes were present on the top side of each element, providing a support for the crane hook. Eventually, plastic tools designed for this purpose filled these holes. Since the production process of CS element masonry has become partially standardised, their mechanical properties can be studied by performing tests on replicated masonry. Due to the large size of the double-wythe solid clay brick masonry and CS element masonry, the handling and testing of the wallets was quite challenging.

**Table 2.1:**

Overview of the masonry types constructed in the laboratory.

Code	Masonry	Thickness in wythe	Bond pattern	Joint	Unit size	Const. period
				mm	( $l_u \times h_u \times t_u$ ) mm <sup>3</sup>	
MAT-1	CS brick	Single	Running bond	10	210×70×100	2015 – Apr.
MAT-2	Perforated clay brick	Single	Running bond	10	210×50×100	2015 – Apr.
MAT-3	Solid clay brick	Single	Running bond	10	210×50×100	2016 – Sep.
MAT-4	Solid clay brick	Double	Dutch cross bond	10	210×50×100	2016 – Sep.
MAT-5	CS element	Single	Running bond	2-4	897×643×100	2016 – Sep.



**Figure 2.1:** Units used for the construction of masonry samples: (a) CS brick; (b) perforated clay brick; (c) solid clay brick; (d) CS element.

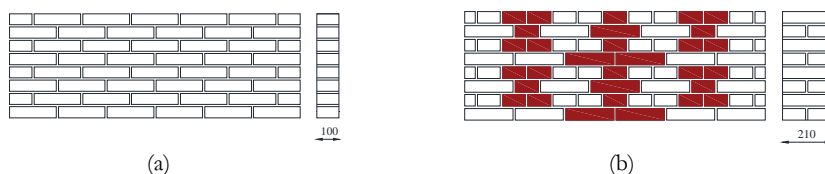


**Figure 2.2:** Adopted bond patterns: (a) running bond pattern for single-wythe specimens; (b) Dutch cross bond pattern for double-wythe specimens (dimensions are in mm).

Aiming to minimise the variation in material properties for each masonry type, the units and mortar were selected from the same production batch and specimens were built by qualified bricklayers, who followed predefined construction protocols. Table 2.2 gives the number and dimensions of the entire set of specimens adopted to characterise the compression, bending, and shear behaviour of masonry following the guidelines of the European standards. Compression and out-of-plane bending behaviour of masonry were investigated along two loading directions, as masonry is well acknowledged as an orthotropic material. Previous experimental studies have shown that masonry exhibits distinct material properties as the loading direction is changed with respect to the joint orientations (e.g., see Page, 1981). The brick-mortar interface, the so-called ‘plane of weakness’, is the major source of anisotropy in masonry, as the bond quality of the vertical head-joints is not the same as the horizontal bed-joints. In fact, the self-weight applied from upper masonry portion facilitates the bond developments along the bed-joints. As a result, not only the masonry properties, but also the failure mechanisms, are influenced considerably by the change in loading direction.

The construction of specimens occurred in different phases, and this chapter focuses on two different construction periods: April 2015 and September 2016. In fact, tests on masonry at the material-level were part of a larger experimental campaign, which investigated the behaviour of masonry at the component-level (Damiola et al., 2018; Messali & Rots, 2018; Messali et al., 2020) as well as the structural-level (Esposito et al., 2017; Esposito et al., 2019). Detailed information regarding the testing programme, construction of the specimens, and the testing results can be found in the supporting reports/papers on Structural Response to Earthquakes (2020).

**Table 2.2:**

Overview of the number and dimensions of the constructed specimens.

Type of test		No. sample	Dimensions-mm <sup>3</sup>		
			Brick masonry Single-wythe	Brick masonry Double-wythe	CS element Single-wythe
Compression	Vertical	6	430×475×100	540×650×210	1283×1290×100
	Horizontal	6	430×475×100	540×650×210	1283×1290×100
Bending	Out-of-plane_Vertical	5	430×600×100	760×900×210	1350×1950×100
	Out-of-plane_Horizontal	5	880×300×100	1200×650×210	2300×1300×100
	In-plane_Horizontal	5	880×300×100	1400×350×210	2300×650×100
	Bond wrench	10	210×80×100	210×80×100	120×220×100
Shear-compression test		9	210×180×100	210×180×100	300×300×100



## 2.2 COMPRESSION AND FLEXURAL PROPERTIES OF MORTAR JOINTS

To control the consistency of the mortar, a flow table test (slump test) was conducted after the preparation of each batch. The test was performed in agreement with standard EN 1015-3(CEN 1999), and the mean measured diameter of the mortar indicates the mortar consistency or workability. For the different masonry types, the diameter of the mortar varied between 174 and 188 mm, Table 2.3.

To characterise the mechanical properties of the pre-mixed general-purpose mortar, compression and three-point bending tests were conducted. During each day of construction, at least three mortar prisms were collected and cast in moulds. Following the guidelines of standard EN 1015-11(CEN 1999), the prisms were tested at least 28 days after casting. The flexural strength of mortar,  $f_{bm}$ , was determined using a three-point bending test, Figure 2.3a. Brittle failure was reported, as a vertical crack often formed in the middle of the bar. The compressive strength of mortar,  $f_m$ , was obtained from compression tests on the broken pieces with a length of at least 40 mm obtained from the flexural test. The typical crack pattern of the mortar under compressive loading is shown in Figure 2.3b. Due to the confinement effect of the loading plates, the inner part of the cubic mortar generally remained uncracked. However, cone-shaped cracks developed along the edges of the specimen. More information regarding the testing set-up and the loading procedure can be found in Appendix A.1.

An overview of the mechanical properties of mortar is presented in Table 2.3. To replicate brick masonry, commercial pre-mixed mortar was used; the cement:lime:sand ratio is listed in Table 2.3. Given that the mortar properties were evaluated as an average of the strength obtained from different casting days, a one-way analysis of variance (ANOVA) was performed to assess the presence of any statistically significant differences between them. To this end, SPSS software version 14.0 was used. The P-values for both the flexural and compressive strength of each mortar type are listed in Table 2.3. A P-value higher than 0.05 means that no statistical differences exist in the strength of the mortar bars collected on different casting days. A P-value higher than 0.05 was only found for the flexural strength of the mortar used for the construction of MAT-3/MAT-4 specimens, meaning that the mortar bars came from a population with equal means. By contrast, for compressive strength all masonry types resulted in P-values less than 0.05, thus indicating the intrinsic variability of mortar properties in spite of all the attempts to select mortars from the same manufacturing batch and to control the mixing process.

Using a box plot, the visual representations of the statistical distribution of flexural and compressive strength of mortar are presented in Figure 2.4. The central mark indicates the median, while the bottom and top edges of the box refer to the first quartile and third quartile, respectively. The whiskers show the minimum and maximum data, and the outliers are plotted individually using a plus marker. Note that the outliers are taken into account in the calculation of the mean values. As mentioned earlier, the mortar properties were selected to resemble the masonry type

constructed in the Netherlands during the specific construction periods. Accordingly, the older the masonry type, the lower the mortar strength. As a result, the lowest values of strength belonged to the mortar used to reproduce clay masonry types constructed before 1945, i.e. the MAT-3 and MAT-4 specimens. By contrast, the highest values of flexural strength and compressive strength belonged to the CS element masonry with a thin mortar layer, which has been a popular construction practice since the mid-1980s (Vermeltfoort & Van Schijndel, 2013).

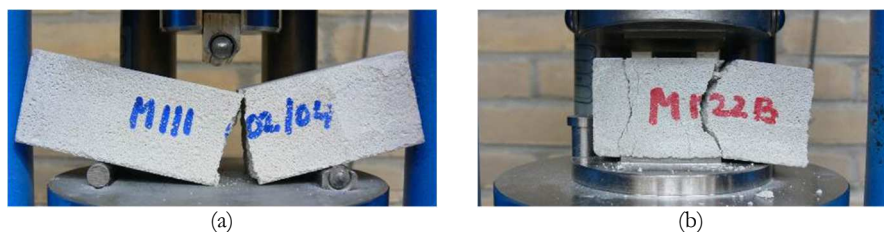


**Figure 2.3:** Tests on mortar specimens: (a) three-point bending test; (b) compression test.

**Table 2.3:**

Overview of the mortar properties adopted for the construction of laboratory-made masonry specimens.

Masonry type	Mortar proportion* C:L:Sa	Flow mm	Flexural strength				Compressive strength			
			No. test	$f_{mb}$ MPa	C.o.V.	P-value	No. test	$f_m$ MPa	C.o.V.	P-value
MAT-1	1:0:3	174	31	2.79	0.08	0.017	65	6.59	0.10	0.000
MAT-2	1:0.4:1.25	177	23	2.43	0.13	0.008	48	6.11	0.09	0.000
MAT-3/4	1:2:9	188	50	1.40	0.12	0.075	108	3.81	0.09	0.000
MAT-5	Thin layer	185	17	4.66	0.22	0.004	36	16.10	0.09	0.000

\*Cement to lime to sand ratio.

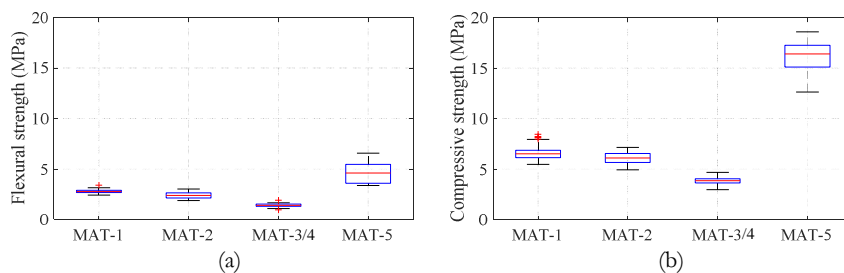


**Figure 2.4:** Overview of mortar strength: (a) flexural strength; (b) compressive strength. The whiskers show the minimum and maximum data, and the outliers are plotted individually using a plus marker. The outliers were taken into account in the calculation of the mean values as there was no compelling reason to exclude them.

### 2.3 COMPRESSION AND FLEXURAL PROPERTIES OF UNIT

Compression tests on individual bricks as well as on stack-bond prisms were performed to determine the compressive strength and elastic modulus of the bricks, respectively. The compressive strength of the bricks was measured according to the provisions of EN 772-1(CEN 2011). Nevertheless, due to the small height of the bricks as well as the limitations of the available equipment, no useful insight into the Young's modulus was provided. To overcome this limit, an alternative test proposed by Vermeltfoort (2005), who suggested adopting a stack-bond prism with a height-to-thickness ratio between 4 and 5, was applied. To build the stack-bond prism, a thin layer of high strength adhesive, Sikadur 30, was applied to each bed face of bricks.

The out-of-plane flexural properties of the bricks were determined from three-point bending tests. Following the guidelines of standard NEN 6790(2005), a unit was subjected to three-point bending loads, being the applied load parallel to the bed faces (out-of-plane bending). Note that a detailed report of the test procedure is given in Appendix A.2.

The typical failure of the bricks under compression and bending loads is shown in Figure 2.5. Under compression loading, the final crack pattern of the individual bricks was characterised by vertical cracks along the edges, Figure 2.5a. However, the inner part of the bricks remained mainly uncracked due to the confinement effect of the loading plates. In contrast, along the thickness of the stack-bond prisms, inclined or vertical splitting cracks formed in the vicinity of the loading plates, developing further toward the centre. Along the thickness, the failure mode of the CS brick prisms was dominated by v-shaped cracks, while a vertical tensile crack developed up to the mid-height of the clay prisms. Under out-of-plane bending load, the ultimate failure of the bricks, regardless of the brick type, was often associated with a splitting vertical crack that formed along the axis of symmetry.

The large size of the CS element allowed for investigating the possible effect of size on the compression properties. The compression properties of the CS elements were obtained from tests on full-scale elements as well as tests on representative cut portions, Figure 2.6. Representative cut portions, either rectangular specimens with a height-to-thickness ratio of 4.5 (225×450×100 mm) or small cubes (100×100×100 mm), were cut from each single element. The cubic specimens were adopted following the outlines of standard EN 771-2(CEN 2011+A1:2015) and the rectangular specimens were sawn-cut with the aim of evaluating the Young's modulus.

To investigate the bending behaviour of CS element masonry, both three-point in-plane and out-of-plane bending tests were performed. The former test was performed on full-scale elements, and the latter on representative portions (200×100×100 mm) sawn-cut from each single element following standard EN 771-2(CEN 2011+A1:2015), as seen in Figure 2.7.

The typical final crack patterns of the CS elements under compression and bending loads are presented in Figure 2.6 and Figure 2.7, respectively. As mentioned earlier, both sawn-cut portions and the full-scale CS elements were subjected to compression and bending loads. Under compression loading, the influence of the unit size on the final crack pattern is obvious. The smaller the specimen, the more ductile the behaviour, and the more localised cracks were observed. The full-scale element showed a very brittle failure. In both the out-of-plane and in-plane bending tests, a brittle failure was observed, in which a tensile crack developed beneath the loading point.

A summary of the compression properties of the bricks and CS element is given in Table 2.4. Assuming a uniform stress distribution during the compression test, the unit compressive strength,  $f_b^*$ , was calculated as a ratio of maximum compressive force to the loading cross-sectional area. Following Annex A of the standard EN772-1(CEN 2011), the compressive strength of the unit was normalised using a shape factor,  $\delta^*$ . Hence, Table 2.4 also reports the normalised values of the unit compressive strength,  $f_b$ . The elastic modulus of the unit,  $E_{3b}$ , was calculated in the linear phase of the stress-strain diagram between 10% and 30% of the maximum compressive load.

Table 2.5 lists a summary of the bending properties of the bricks and CS element. Assuming a linear stress distribution over the height of the cross-section, the out-of-plane flexural strength,  $f_{bb1}$ , and in-plane flexural strength of the unit,  $f_{bb3}$ , were determined as:

$$f_{bb1} = \frac{3 F_{\max,b} d_1}{2 h_u t_u^2} \quad (2.1)$$

$$f_{bb3} = \frac{3 F_{\max,b} d_1}{2 t_u h_u^2} \quad (2.2)$$

where  $F_{\max,b}$  is the maximum bending load,  $d_1$  is the distance between the supports,  $h_u$  is the height of the unit, and  $t_u$  is the thickness of the unit. The Young's modulus of the masonry units from bending test,  $E_{3b}$ , was evaluated as follows:

$$E_{3b} = \frac{F_{el} d_1^3}{48 v_{el} I_u} \quad (2.3)$$

where  $F_{el}$  and  $v_{el}$  are the load and vertical displacement in the linear elastic stage within 10% and 30% of the maximum stress, respectively, and  $I_u$  is the moment of inertia of the unit along the cross-section.

The statistical distribution of the normalised compressive strength and out-of-plane flexural strength is presented in Figure 2.8. The lowest normalised compressive strength belonged to the CS bricks, and the highest was found for the solid clay bricks. Concerning the CS elements, a higher compressive strength was found by decreasing the height to thickness ratio, see Table 2.5. However, similar values of normalised compressive strength were found as the shape factor was applied for the specimens with a height-to-thickness ratio greater than 1. Regarding

the out-of-plane flexural test, the highest and the lowest strength are attributed to solid clay and CS bricks, respectively. For the CS element masonry, the in-plane flexural strength was found to be two times higher than the out-of-plane flexural strength. Such a difference can be attributed to tests on specimens with different height to thickness ratio and/or orthotropic behaviour due to manufacturing process.

In this study, the Young’s modulus was determined from both compression and bending tests. For all the studied units, both testing methods provided comparable values of the elastic modulus, with the exception of solid clay bricks. For this unit type, the elastic modulus in bending is 1.6 times higher than that obtained from the compression tests. At this moment, no clear answer can be suggested for such deviation; however, the accuracy of the data can be improved by performing further tests.



**Figure 2.5:** Typical failure of CS bricks and clay bricks: (a)–(b) single bricks under compression load; (c)–(d) stack-bond prism in compression; (e)–(f) single bricks under out-of-plane bending loads.

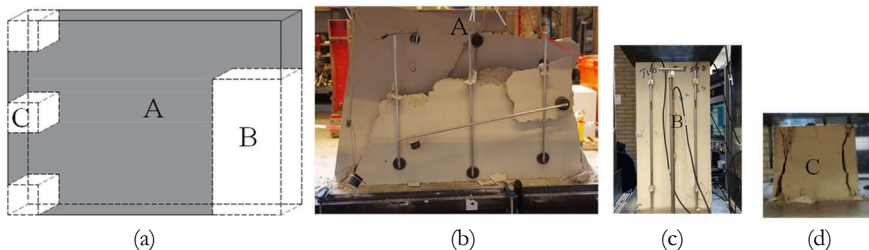


**Figure 2.6:** CS element under compression loading: (a) overview of adopted specimens; typical crack patterns from tests on (b) full-scale element, (c) rectangular prism, and (d) cubic specimen.

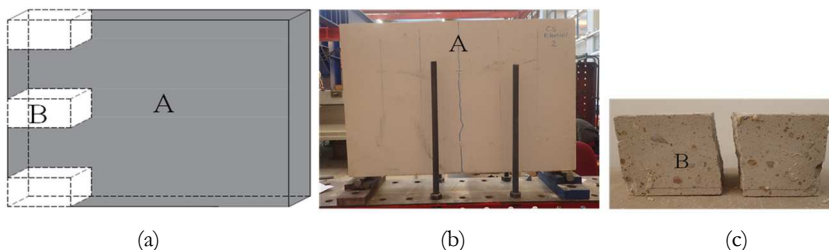


**Figure 2.7:** CS element under bending loading: (a) overview of adopted specimens; final crack patterns from (b) in-plane tests on full-scale element (c) out-of-plane test on rectangular prism.

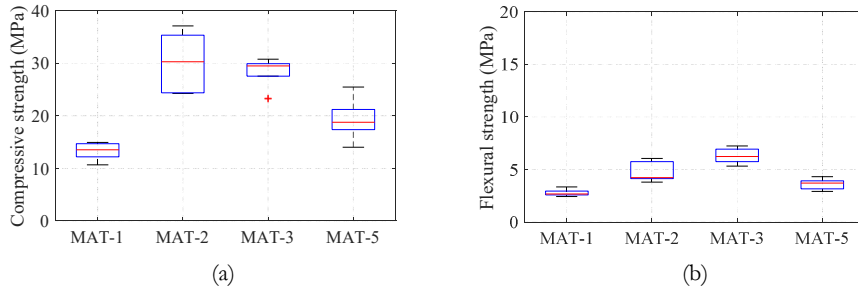


**Figure 2.8:** Overview of mechanical properties of units: (a) normalised compressive strength; (b) out-of-plane flexural strength.

**Table 2.4:**

Overview of the compression properties of units.

Masonry types	No. test	Compression test			
		$f_b^*$ MPa	$f_b$ MPa	$\delta$ -	$E_{3b}$ MPa
<b>CS brick (MAT-1)</b>					
Single brick	6	18.76 (0.13)	13.26 (0.13)	0.71 (-)	-
Stack-bond prism with h/t=5	5	-	-	-	8874 (0.14)
<b>Perforated clay brick (MAT-2)</b>					
Single brick	6	39.57 (0.13)	29.68 (0.13)	0.75 (-)	-
Pile of bricks with h/t = 4	6	-	-	-	6313 (0.15)
<b>Solid clay brick (MAT-3 &amp; MAT-4)</b>					
Single brick	9	39.12 (0.10)	28.31 (0.10)	0.72 (-)	-
Pile of bricks with h/t=4	2	-	-	-	6907 (0.04)
<b>CS element masonry (MAT-5)</b>					
Cut portions with h/t = 1	18	19.45 (0.16)	19.45 (0.16)	1.00 (-)	-
Cut portions with h/t=5	6	15.96 (0.08)	19.15 (0.08)	1.20 (-)	8603 (0.11)
Full-scale with h/t=9	1	14.21 (-)	20.61 (-)	1.45 (-)	7630 (-)

**Table 2.5:**

Overview of the bending properties of units.

Masonry types	Density	No. test	Bending test			
			$f_{bb1}$ MPa	$E_{3b-1}$ MPa	$f_{bb3}$ MPa	$E_{3b-3}$ MPa
<b>CS brick (MAT-1)</b>						
Single brick		11	2.79 (0.11)	9598 (0.31)	-	-
<b>Perforated clay brick (MAT-2)</b>						
Single brick		7	4.78 (0.20)	6676 (0.66)	-	-
<b>Solid clay brick (MAT-3 &amp; MAT-4)</b>						
Single brick		9	6.31 (0.11)	11451 (0.17)	-	-
<b>CS element masonry (MAT-5)</b>						
Cut portions		18	3.64 (0.13)	8613 (0.24)	-	-
Full-scale		4	-	-	1.78 (0.02)	9136 (0.27)

## 2.4 NONLINEAR COMPRESSIVE BEHAVIOUR

This section first discusses the current state-of-the-art of masonry under compressive loads. Second, it details the testing procedure and data elaboration. Third, the overall response of masonry is discussed in terms of stress-strain curves in combination with crack growth. Eventually, the compression properties of the laboratory-made masonry are analysed in terms of compressive strength, Young's modulus, and compressive fracture energy.

### 2.4.1 State-of-the-art: Compression response

Research into the characterisation of the uniaxial compressive response of masonry, in terms of Young's modulus and compressive strength, has a long history, though compressive fracture energy has received limited attention. So far, a substantial amount of experimental research on a large variety of masonry types has been performed, in which the stress-strain relationships and failure patterns have been extensively discussed (e.g., Vermeltoort, 2005). However, the existing pool of experimental studies has made only a small contribution to improving the extent of knowledge on the post-peak characteristics of masonry. The lack of insight into the degradation response of masonry, quantified by means of compressive fracture energy, is often associated with the limitations of the load-controlled testing set-up or the lack of an accurate measuring system in the post-peak regime due to extensive localised damage. Accordingly, only a few studies provided insights into the softening degradation response of masonry under compression loading (e.g., Augenti & Parisi, 2010; Segura et al., 2018).

Previous studies on the compression response of masonry have mostly adopted the stack-bond prism, due to its simple construction and handling, rather than relatively large wallets resembling the actual bond pattern. Following international standards, two types of specimens with different geometries and morphologies can be adopted: the wallet with running bond, as recommended by the European standard EN 1052-1(CEN 1998) and the stack-bond prism, as suggested in the American standard ASTM C1314(2018). Nevertheless, limited studies have attempted to compare the differences between the compression responses of these two specimens. In this context, Segura et al. (2018) performed compression tests on one masonry type, built using mortar with a compressive strength of less than 2 MPa. An acceptable correspondence was reported between the compression properties of the prisms and of the wallets in terms of compressive strength and corresponding strain, as well as the Young's modulus. This conclusion was in line with the observations of Gumaste et al. (2007), who investigated the compressive strength of prisms and wallets for six different clay brick masonry types. However, for masonry with a compressive strength higher than 5 MPa and lower than 12 MPa, a large difference of up to 50% between the compressive strength of the prisms and of the wallets was reported. Besides spotting the differences in the mechanical properties of the two types of samples, inconsistency in their failure patterns was also revealed. As reported by Segura et al. (2018) and Gumaste et al. (2007), the failure of the prisms was mainly governed by the formation of splitting cracks along the extremities, while in the central part it was rather uncracked. Nevertheless, the

failure of masonry is not always limited to the formation of tensile cracking in bricks. An intricate cracking pattern, including the formation of mixed shearing, debonding, and tensile cracks, can be expected as the dimensions and morphology of the tested samples are closer to reality (e.g., Vermeltfoort, 2005; Gumaste et al., 2007). In light of such findings in the literature, instead of a stack-bond prism, this research adopts wallets, thus incorporating the influence of vertical head joints on the compression response of masonry.

Thus far, several researchers have investigated the nonlinear response of masonry under both monotonic and cyclic uniaxial compression loading. Generally, no significant difference was reported between the compressive strength and the Young's modulus of the monotonically and the cyclically loaded clay brick masonry samples (e.g., Dhanasekar et al., 1997; Ispir & Ilki, 2013; Segura et al., 2018). However, Dhanasekar et al. (1997) found a different trend between the response of shell-bedded and full-bedded concrete masonry tested under monotonic and cyclic compression loading. Owing to the cyclic loading sequence, only the compressive strength of the full-bedded concrete masonry decreased by up to 20%. Naraine and Sinha (1989) showed that the envelope curves of cyclically loaded specimens conformed relatively well to the response of the monotonically loaded samples, although irreversible strains were reported in each cycle.

In an investigation into the orthotropic behaviour of masonry, previous studies often performed compression tests along the two orthogonal directions. In this context, the compression load was applied either perpendicular to the bed-joints, known as the 'vertical configuration' or parallel to the bed-joints, known as the 'horizontal configuration'. In addition, some researchers, such as Dhanasekar et al. (1997) and Facconi (2012) performed compression tests on the inclined wallets, in which the angles between the loading directions and the bed-joints were  $45^\circ$  and  $22.5^\circ$ . As reported by Facconi (2012), the highest value of compressive strength was attributed to the vertical loading direction, while the lowest was found for a wallet tested under an inclination angle of  $22.5^\circ$ . The failure of the latter specimens was mainly governed due to the formation of shearing cracks, rather than the splitting of bricks. Naraine and Sinha (1989) found higher compressive strength under horizontal loading rather than the vertical loading; a ratio of 1.1 was reported. Despite the importance of the orthotropic behaviour of masonry, there remains a paucity of evidence on its influence on the Young's modulus and compressive fracture energy.

Considering these gaps in the literature, the outline of this chapter is as follows: investigating the possible influence of the loading scheme (i.e. monotonic and cyclic), and the loading configuration (loading parallel and perpendicular to the bed joints) on the compression response of wallets. In general, particular attention is given to the complete characterisation of the nonlinear behaviour of masonry, including the estimation of the compressive fracture energy.



## 2.4.2 Testing procedure and data elaboration

To provide a refined mechanical characterisation of masonry, monotonic and cyclic compression tests along the two orthogonal directions were performed on relatively large wallets, representing the true bonding pattern. For each masonry type, twelve equivalent wallets were built. Standard EN 1052-1(CEN 1998) was used as a guideline when deciding on the size of wallets, curing, and loading rate. To investigate the orthotropic behaviour of masonry, of twelve wallets, six were subjected to vertical loading, and the other six to horizontal compression loading. Vertical and horizontal compression loading refer to a configuration in which the axial load is applied perpendicular and parallel to the bed joints, respectively. To avoid the possible influence of size on the orthotropic behaviour, square-shape wallets were built. For more information regarding the wallets' dimensions, see Table 2.2. To monitor the compression response beyond the collapse load, a displacement-controlled set-up was administered. The specification of the testing set-up, measuring system, and loading scheme can be found in Appendix A.3. Each wallet was equipped with vertical and horizontal Linear Variable Differential Transformers (LVDTs) to record axial and transversal deformations. For each masonry type, the LVDT lengths are presented in Appendix A.3. The length of the LVDTs was generally higher than the one prescribed by standard EN 1052-1(CEN 1998), aiming for a realistic estimation of the compressive fracture energy. In general, no rotation or buckling of the vertical LVDTs in the pre-peak phase was reported. On the contrary, large out-of-plane or in-plane post-peak deformations often caused the rotation and detachment of the LVDTs; thus, the corresponding readings of such LVDTs were not considered. In return, to obtain the stress-strain relationship in the post-peak phase, the readings from the hydraulic jack were used. The vertical displacement of the jack had the same trend as of the LVDTs, Figure 2.9a. Accordingly, to obtain the full stress-strain relationship, the LVDT readings were used in the pre-peak phase, and in the post-peak phase the jack's readings were used, applying a scalar factor that allowed for obtaining the same peak displacement.

In this study, the compressive behaviour of masonry is characterised in terms of compressive strength and corresponding peak strain, Young's modulus, Poisson's ratio, and compressive fracture energy. The compressive strength of masonry in the vertical,  $f_m$ , and horizontal,  $f_{m,h}$ , directions was determined as a ratio between the failure load and the loaded cross-sectional area of the individual specimens. The peak strain,  $\epsilon_p$ , was the strain corresponding to the peak load. The Young's modulus was evaluated in line with the recommendations of both EN 1052-1(CEN 1998) and ASTM E111(2017). Following the former standard, the Young's modulus was evaluated at 1/3 of the maximum stress,  $E_2$ . However, a closer look into the initial start-up of the stress-strain curve revealed that the estimation of the elastic modulus could be affected by the gradual contact between the loading plates and the specimen. Hence, the prescriptions of ASTM E111(2017) were followed, in which the chord modulus was determined between 1/10 and 1/3 of the maximum stress,  $E_3$ , Figure 2.9b. Poisson's ratio was evaluated as a ratio of the longitudinal to the axial strain in the linear phase, between 1/10 and 1/3 of the maximum stress. To describe the gradual post-peak softening, the concept of compressive fracture

energy, introduced by van Mier (1984) for concrete and further extended for masonry by Lourenço (1997b), was adopted. The compressive fracture energy,  $G_{f-c}$ , was calculated as the area underneath the stress-axial displacement curve, from zero to ultimate displacement. Generally, the compression test was terminated at a stress corresponding to 20% of the peak load. Hence, the ultimate strain was approximated assuming that after the attainment of  $0.5f_m$  the stress-strain curve followed a linear trend, having a slope ascertained from a linear regression between  $0.5f_m$  and  $0.3f_m$ , Figure 2.10.

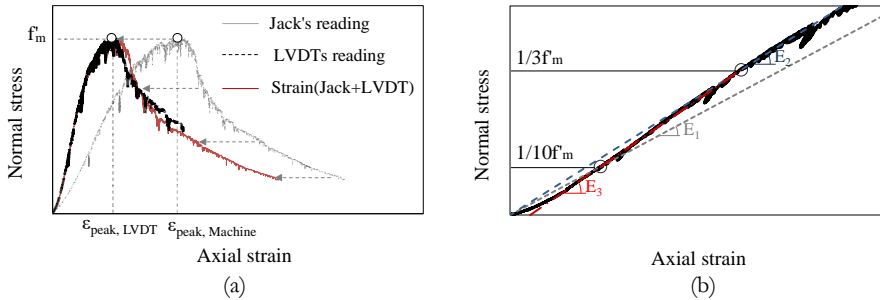


**Figure 2.9:** (a) Capturing the full response under compression loading using LVDT readings in the pre-peak and jack readings in the post-peak phase; (b) evaluation of the Young's modulus under compressive load.

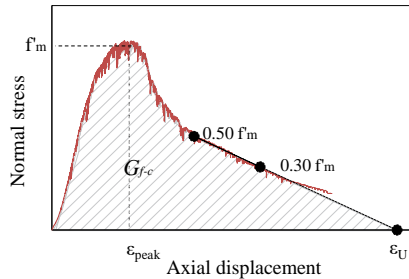


**Figure 2.10:** Estimation of compressive fracture energy.

**Table 2.6:**

Summary of the compression properties of masonry subject to vertical compression loading. Coefficient of variation in parentheses.

Masonry type	Vertical Compression Test						
	No. test	$f_m$ MPa	$E_2$ MPa	$E_3$ MPa	$\epsilon_p$ ‰	$G_{f-c}$ N/mm	$\nu$ -
MAT-1	5	5.93 (9%)	3103 (10%)	2749 (10%)	9.53 (9%)	34.31 (14%)	0.11 (20%)
MAT-2	6	14.73 (7%)	7810 (15%)	8291 (13%)	2.69 (20%)	31.65 (15%)	0.10 (45%)
MAT-3	6	14.02 (4%)	4640 (25%)	5019 (32%)	4.26 (10%)	33.77 (10%)	0.18 (34%)
MAT-4	6	10.67 (12%)	2737 (22%)	3035 (14%)	4.06 (13%)	35.68 (15%)	0.22 (12%)
MAT-5	6	13.93 (7%)	8557 (19%)	8382 (14%)	2.01 (19%)	20.43 (26%)	0.40 (87%)

**Table 2.7:**

Summary of the compression properties of masonry subject to horizontal compression loading. Coefficient of variation in parentheses.

Masonry type	No. test	Horizontal Compression Test					
		$f_{m,b}$ MPa	$E_{2,b}$ MPa	$E_{3,b}$ MPa	$\varepsilon_{p,b}$ ‰	$G_{f-c,b}$ N/mm	$\nu_h$ -
MAT-1	6	7.56 (2%)	2208 (30%)	2079 (30%)	7.99 (20%)	41.94 (12%)	0.37 (32%)
MAT-2	6	7.52 (8%)	4942 (9%)	4570 (15%)	3.71 (42%)	22.16 (17%)	1.05 (52%)
MAT-3	6	13.11 (18%)	3315 (19%)	3193 (21%)	5.88 (18%)	38.14 (22%)	0.80 (80%)
MAT-4	6	9.15 (10%)	3873 (14%)	3719 (18%)	4.55 (25%)	30.07 (14%)	1.49 (0.65%)
MAT-5	6	9.42 (17%)	8416 (20%)	7701 (17%)	1.59 (25%)	12.79 (34%)	-

### 2.4.3 Overall response

This section discusses the nonlinear compressive response of masonry in terms of stress-strain developments in combination with crack growth. In Figure 2.11–Figure 2.15 the response of each monotonically loaded specimen and the envelope curve of each cyclically loaded specimen are presented in grey, while the mean stress-strain curves are shown in black. Following the approach proposed by Augenti and Parisi (2010), the mean stress-strain curve is obtained by considering pre-defined increments of axial strain and calculating the corresponding average stress and lateral strain. In this study, an increment of axial strain equal to  $1.5E-05 \pm 1\%$  was chosen. The axial and the lateral strains are referred to as the strains measured parallel and perpendicular to the loading direction, respectively.

The analysis of the stress-strain curves, accounting for the two loading directions, was carried out over three phases: initial linear phase, pre-peak nonlinear phase, and post-peak softening phase. In the linear phase, often no cracks appeared on the wallets' surface. In the nonlinear pre-peak phase, distributed cracks due to incompatibility between the properties of the masonry constituents gradually formed. Towards the peak load, the rate of the crack propagations drastically accelerated, cracks became wider and deeper, and thus stiffness reduced. In the post-peak phase, a softening branch was recorded, indicating a gradual decrease in the mechanical resistance of brick masonry. However, the post-peak response of the CS element wallets was not captured due to the brittle failure.

Under vertical and horizontal loading configurations, the onset of damage in *single-rythe CS brick masonry* was characterised by debonding cracks formed in line with the loading direction, Figure 2.11. Moreover, in the case of horizontally loaded wallets, debonding cracks developed at the joints parallel to the loading direction. By further increasing the compressive load, the length and the number of cracks increased. In the vertical loading direction, diffused cracks formed in the central part of the wallets, while under horizontal loading, the damage was mainly concentrated in the bottom or upper part of the wallets. In the post-peak phase, a different failure mechanism was observed under the two loading directions. In the case of the vertical configuration, along the width of the wallet a deep out-of-plane

splitting of bricks and mortar was observed, dividing the wallets into two parts, Figure 2.11a. Under horizontal loading, substantial damage in the form of splitting cracks and the delamination of bricks was observed along the length of the wallets, while in-plane ‘V-shaped’ cracks formed along the thickness, Figure 2.11b.

Under vertical and horizontal loading, the pre-peak cracks in *single-nythe perforated clay brick masonry* mainly developed in the bricks, being parallel to the loading direction, Figure 2.12. In the nonlinear pre-peak phase, vertical cracks also developed along the width of the wallets. Under vertical loading, multiple cracks occurred simultaneously, while under horizontal loading, a localised crack often developed, crossing the brick holes. In general, formations of the splitting cracks in the perforated masonry were accompanied by an explosive sound. In the post-peak phase, the surface of the wallets was significantly affected by multiple splitting cracks as well as spalling of the brick surface. Along the thickness, in-plane branching cracks under vertical loading and out-of-plane splitting and bursting of the bricks under horizontal loading were observed.

Under vertical and horizontal compression loading, *single-nythe solid clay brick masonry* wallets showed splitting cracks starting in the bricks, while no or limited debonding cracks were reported, Figure 2.13. In the case of vertical compression tests, the cracks mainly occurred in the central part of the specimens. By contrast, for the horizontal configuration, the damage was concentrated at the top or bottom of the specimens, where half bricks were located, and the spalling of bricks from the surface was observed. In the post-peak phase, the specimens tested under the two configurations showed different behaviour. In the case of vertical loading, the vertical cracks mainly occurred along the thickness of the wallets, by splitting it in two parts. Under horizontal loading, splitting cracks developed throughout the whole height of the wallet. This behaviour was different from the other brick masonry types, in which the damage was mainly characterised by debonding along the interface.

The development of cracks in *double-nythe solid clay brick masonry* tested under vertical and horizontal compression loading is presented in Figure 2.14. Under the vertical configuration, vertical splitting cracks started in the bricks in the top and bottom parts of the specimens. Under the horizontal configuration, cracks started at the brick-mortar interface parallel to the loading direction, and later developed in the bricks, causing spalling of the external surface. In the post-peak phase, the vertical cracks mainly developed through the length of the specimen, by splitting it in several parts. Under the vertical loading configuration, splitting cracks in the bricks and interface debonding in subsequent layers resulted in the formation of a diagonal shearing crack. Under horizontal loading, the debonding and splitting cracks occurred in a distributed manner over the length of the specimen. In the thickness, ‘V-shaped’ in-plane splitting cracks and out-of-plane movements due to a buckling mechanism were observed under vertical and horizontal loading, respectively.

Figure 2.15 shows the crack pattern in *single-wythe CS element masonry* tested under vertical and horizontal compression loading. Under both loading directions, limited cracks appeared on the wallet surface until the peak load was reached. For both vertical and horizontal compression tests, localised cracks were formed, resulting in one side being more damaged than the other side. In the case of the vertical configuration, the first cracks appeared in the middle bed joint. As the load was increased, the cracks mainly accumulated in the unit, causing spalling and delamination. When maximum stress was reached, localised vertical cracks developed on the side joints, as well as along the thickness, thus causing a brittle failure. In the case of the horizontal compression test, cracking and spalling started around the middle head joint, orthogonal to the applied load. With continued deformations, the damage was concentrated in the bed joints, where smaller units were located. Along the width of the wallets, in-plane branching cracks occurred. Beyond the peak load, a brittle failure occurred, and no post-peak softening behaviour was observed.

In line with the objectives of the testing programme, the following observations were made:

- No difference in the response and the cracking pattern of the monotonically and cyclically loaded specimens was noticed.
- Different crack patterns were observed as the loading configuration changed. Under vertical loading, vertical splitting cracks developed and often caused local failure of wallets. Under horizontal loading, debonding cracks along the interface often developed, thus forming a series of detached columns of bricks.
- No significant difference in the behaviour of single- and double-wythe wallets was noticed in terms of the stress-strain relationship and the crack pattern.
- CS element masonry with a thin mortar layer showed a stiffer pre-peak branch than the one for conventional brick masonry. Moreover, the crack pattern of the CS element masonry differed significantly from that of the brick masonry types.

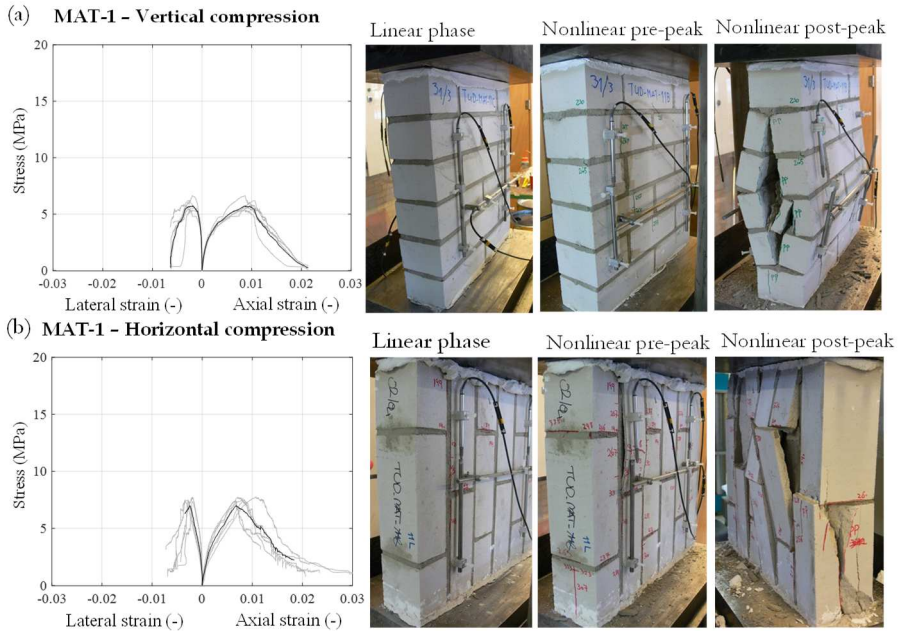


**Figure 2.11:** Stress-strain relationship and crack pattern of MAT-1 single-wythe CS brick masonry under: (a) vertical loading configuration; (b) horizontal loading configuration.

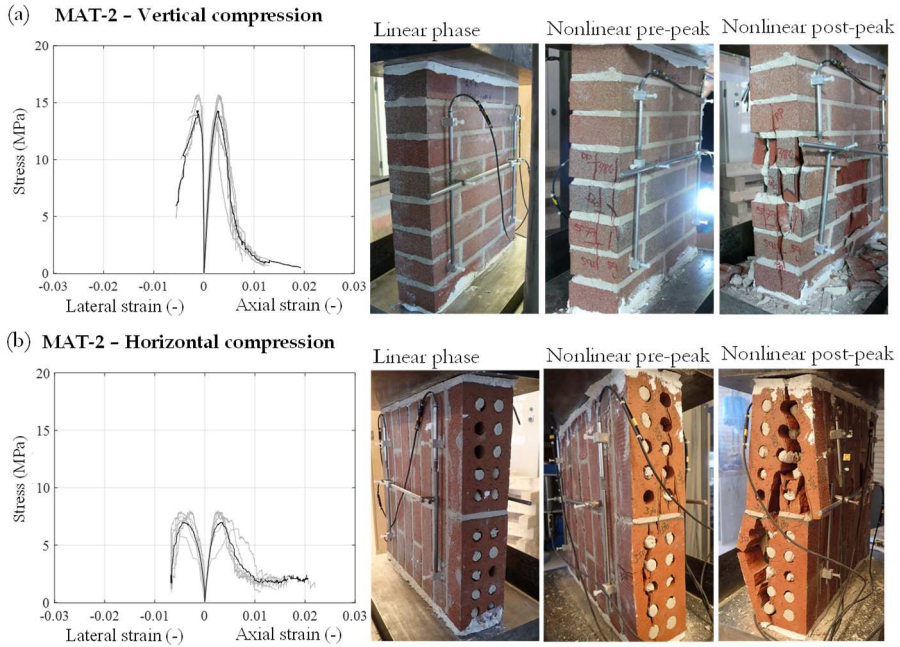


**Figure 2.12:** Stress-strain relationship and crack pattern of MAT-2 single-wythe perforated clay brick masonry under: (a) vertical loading configuration; (b) horizontal loading configuration.

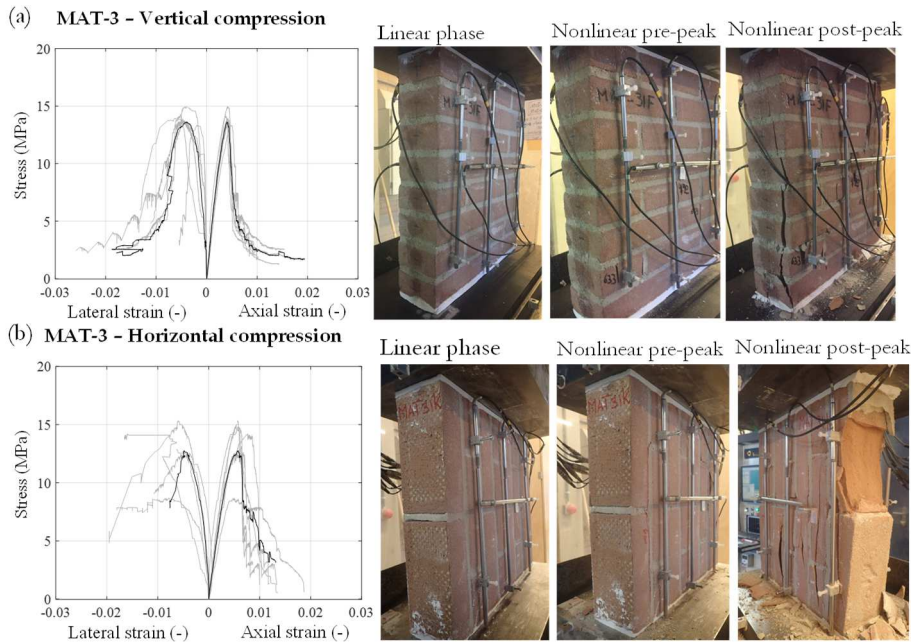


**Figure 2.13:** Stress-strain relationship and crack pattern of MAT-3 single-wythe solid clay brick masonry under: (a) vertical loading configuration; (b) horizontal loading configuration.

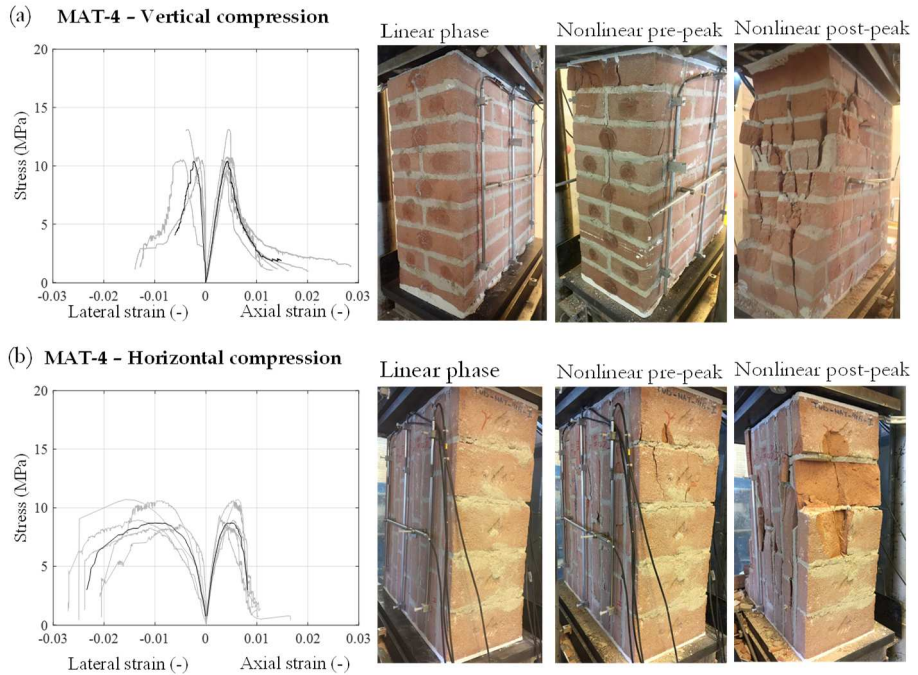


**Figure 2.14:** Stress-strain relationship and crack pattern of MAT-4 double-wythe solid clay brick masonry under: (a) vertical loading configuration; (b) horizontal loading configuration.

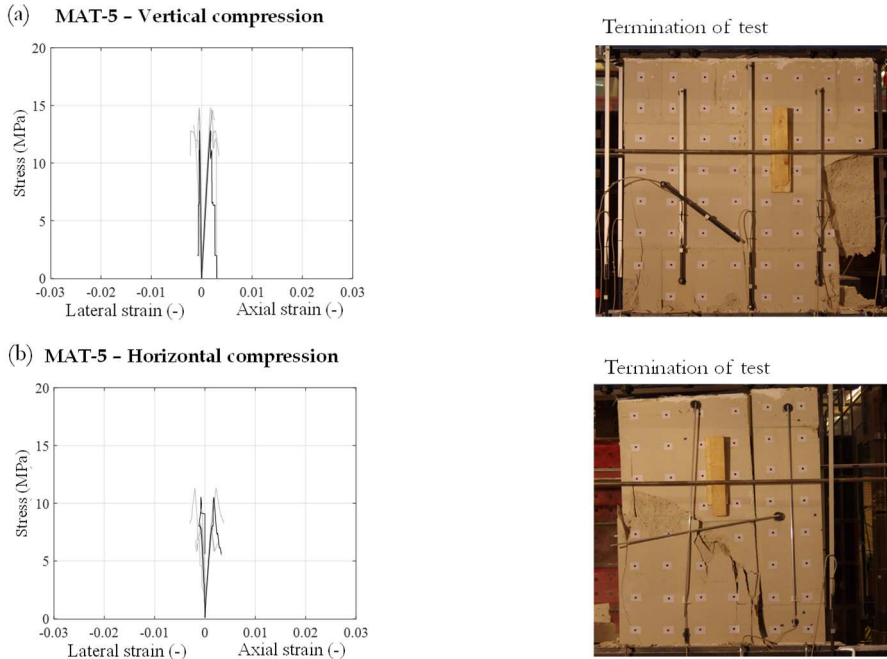


**Figure 2.15:** Stress-strain relationship and crack pattern of MAT-5 single-wythe CS element masonry under: (a) vertical loading configuration; (b) horizontal loading configuration.

## 2.4.4 Compressive strength

Tests on five different masonry types provide a basis, albeit limited, for analysing the possible influence of mortar compressive strength, unit compressive strength, masonry size, and mortar thickness on the compressive strength of masonry wallets loaded along the two orthogonal directions. An overview of the compressive strength of the mortar and of the units is shown in Figure 2.16a, and the compressive strength of the five masonry types under vertical and horizontal configurations is shown in Figure 2.16b.

The influence of mortar compressive strength on the compressive strength of the masonry wallets can be investigated by comparing the results of the MAT-2 perforated clay brick masonry and those of the MAT-3 solid clay brick, both constructed using bricks with similar values of compressive strength and Young's modulus, Figure 2.16. Despite a considerable difference in the mortar compressive strength of both masonry types, comparable values of compressive strength under the vertical loading configuration were found. However, in the horizontal loading direction, MAT-3 solid clay brick masonry showed a strength almost two times higher than that shown by MAT-2 perforated clay brick masonry. Such a difference can be explained by the physical characteristics of the perforated clay brick masonry, leading to the formation of splitting cracks in the vicinity of the holes, as mentioned in Section 2.4.3. Accordingly, under both vertical and horizontal loading, the contribution of the mortar compressive strength on the compressive strength of



masonry is not as significant as that of the brick. Moreover, the comparison revealed that the importance of the surface characteristics of the bricks is more prominent under the horizontal loading configuration.

The compressive strength of the MAT-1 CS brick masonry and of the MAT-2 perforated clay brick masonry can be compared with respect to the brick compressive strength, as they both had mortar with similar compressive strength values. Under vertical compression loading, MAT-2 perforated clay brick masonry with stronger bricks than the MAT-1 CS brick masonry showed a compressive strength value that was approximately 1.4 times higher. Nonetheless, under horizontal loading, both masonry types showed the same values of compressive strength. Accordingly, it can be concluded that the compressive strength of the brick plays an important role under vertical compression loading. This finding supports the conclusion reached in the previous paragraph.

There was a difference between the compressive strength of the MAT-4 double-wythe and MAT-3 single-wythe solid clay brick masonry, constructed using the same brick and mortar. As single- and double-wythe wallets had different height to thickness ratios, an attempt was made to correct the values of the masonry compressive strength, by applying a correction factor suggested in the Indian standard (IS:1905-1987). By doing so, the difference between the two values even increased by 54%. At this moment, the rationale behind such a difference is not evident; thus, further experimental and numerical investigations are suggested to study the size effect and the possible influence of the collar joints on the stress distribution.

Unlike brick masonry types, the compressive strength of MAT-5 CS element masonry did not lie between the compressive strengths of its constituents and was indeed much lower. It can be expected that by reducing the joint thickness, CS element masonry would behave more as a homogeneous continuum rather than an ordered discontinuum.

In conclusion, apart from the decisive role of the unit and mortar compressive strength on the compressive strength of masonry, the influence of the masonry size and the joint thickness should not be overlooked.

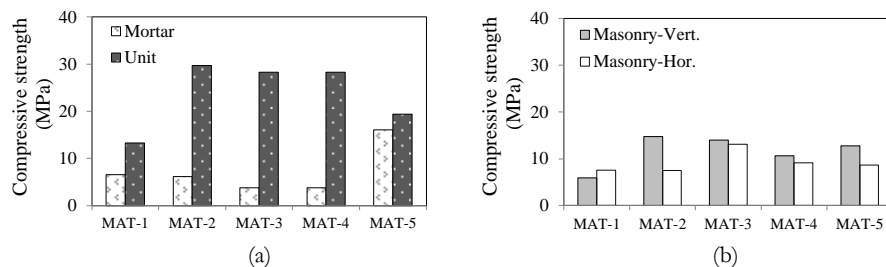


**Figure 2.16:** Overview of the compressive strength of the five laboratory-made masonry types: (a) mortar and units; (b) masonry wallets under vertical and horizontal loading configurations.

### 2.4.5 Young's modulus

This section analyses the influence of the unit and mortar properties on the Young's modulus of the five different masonry types. An overview of the Young's modulus of the five different types of the laboratory-made masonry and its constituents is shown in Figure 2.17. Although the mortar deformation under compressive load was not measured, its stiffness was estimated to be 200 times the mortar compressive strength (Kaushik et al., 2007), Figure 2.17a. Under both compressive loading directions, the highest and lowest values of the Young's modulus were found for the MAT-5 CS element masonry and MAT-1 CS brick masonry, respectively.

The Young's modulus of the MAT-2 perforated clay brick masonry and MAT-3 solid clay brick masonry can be compared to investigate the influence of mortar stiffness, as both masonry types were built with bricks having similar values of compressive strength and Young's modulus. Higher values for the Young's modulus were found for the MAT-2 perforated clay brick masonry than that for the MAT-3 solid clay brick masonry. Accordingly, it can be concluded that masonry with stiffer mortar resulted in stiffer masonry; this conclusion was valid under both loading directions.

The influence of brick stiffness on the Young's modulus of masonry can be investigated by comparing MAT-1 CS brick masonry and MAT-2 perforated clay masonry, as they both had mortar with similar characteristics. Under both vertical and horizontal loading configurations, MAT-2 perforated clay brick masonry with stronger and even less-stiff bricks showed higher values of the Young's modulus than did the MAT-1 CS brick masonry. Accordingly, it can be concluded that increasing the stiffness of the masonry constituents did not necessarily result in stiffer masonry.

A comparison between the results of the MAT-4 double-wythe and MAT-3 single-wythe wallets can be used for investigating the influence of the size and number of wythes on the Young's modulus. Under the vertical loading configuration, the Young's modulus of the MAT-4 double-wythe wallets was lower than that of the MAT-3 single-wythe wallet. This observation is in line with the findings of Gumaste et al. (2007). However, in the horizontal loading direction, a different trend was observed, as the Young's modulus of the double-wythe wallets was higher than that of the single-wythe masonry. At this moment, no explanation can be offered for such an observation. As for the compressive strength, further experimental and numerical investigations are suggested.

The stiffness of the MAT-5 CS element masonry with a thin layer of joint was slightly affected by the loading direction. In addition, it was noticed that the Young's modulus of masonry wallets closely corresponded with the Young's modulus of the units rather than that of the mortar. This observation implies that the mortar contributes little to the stiffness of masonry with large elements and a thin layer of joint. Unlike CS element masonry, the stiffness of the brick masonry often falls between the stiffness of its constituents.

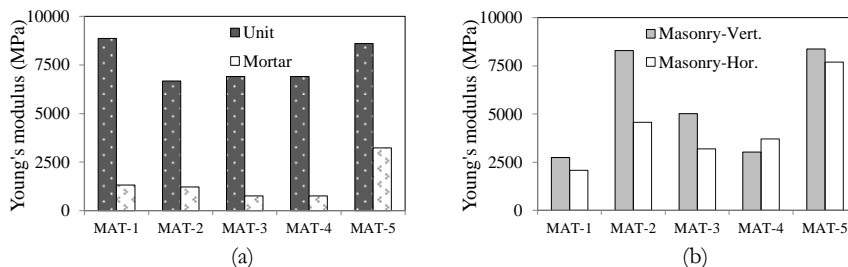


**Figure 2.17:** Overview of the Young's modulus of the five laboratory-made masonry types: (a) mortar and units; (b) masonry wallets under vertical and horizontal loading configurations.

## 2.4.6 Compressive fracture energy

Characterising the compressive fracture energy, barely investigated in literature, becomes crucially important within the framework of the nonlinear assessment of existing masonry structures. The importance of the compressive fracture energy for the numerical and analytical modelling of masonry buildings becomes highly relevant when considering that under in-plane excitations the collapse of slender piers, present in building facades, is frequently attributed to the rocking mechanism, which is governed by compression failure.

An overview of the vertical and horizontal compressive fracture energy of the analysed masonry types is presented in Figure 2.18. As discussed in Section 2.2 and Section 2.3, the compressive fracture energy of the masonry constituents was not measured. Generally, the compressive fracture energy of wallets was found to be higher under vertical loading than horizontal loading, except for the MAT-3 singlewythe solid clay masonry.

Under vertical loading, not much difference was noticed between the compressive fracture energy of the different brick masonry types, while larger differences were observed under the horizontal configuration. Although MAT-1 CS brick masonry had the lowest strength and stiffness, no significant difference was observed in terms of its vertical compressive fracture energy with respect to the other brick masonry types.

The lowest values of both vertical and horizontal compressive fracture energy were found for MAT-5 CS element masonry with a thin layer of joint, showing a brittle failure. This could be explained by the fact that the CS element masonry wallets were made of fewer joints than wallets with conventional joints, thus exhibiting much stiffer behaviour.

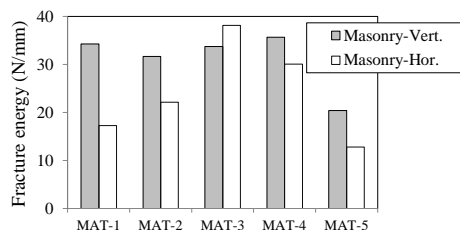


**Figure 2.18:** Overview of the compressive fracture energy of the five laboratory-made masonry wallets under vertical and horizontal loading configurations.

## 2.5 NONLINEAR BENDING BEHAVIOUR

This section first discusses the current state-of-the-art of masonry under bending load. Second, the testing procedure and data elaboration are detailed. Third, the overall response of masonry is discussed in terms of flexural stress-deflection and moment-curvature curves. Moreover, the typical ultimate crack patterns for out-of-plane, in-plane, and bond wrench tests are discussed. Eventually, the bending properties of the laboratory-made masonry are characterised in terms of flexural strength, flexural bond strength, Young's modulus, fracture energy in bending, and uniaxial tensile strength.

### 2.5.1 State-of-the-art: Bending response

Experimental insight into the bending behaviour of masonry is of great interest, as it can be used for the validation of analytical models as well as for providing indirect access to the tensile properties of masonry. Knowledge about the bending behaviour of masonry is of considerable relevance, as unreinforced masonry walls are often vulnerable to in-plane and out-of-plane bending loads. In this context, codes of practice and the literature have proposed analytical models for linear analysis under service load or for ultimate limit state design, aiming to prevent the collapse of walls. The development and verification of analytical models, often resting on principles of mechanics and statistical approaches, can be made in view of experimental test data on masonry at the component- and material-scale (e.g., see van der Pluijm, 1999; Vaculik, 2012; Vaculik & Griffith, 2017). Apart from analytical models, a bending test can indirectly provide insight into the tensile properties, which are required for the nonlinear structural assessment. Due to the number of complexities involved during the tensile test (van der Pluijm, 1999), such as the preparation of samples as well as the testing set-up, and the unknown effect of boundary conditions on the post-peak response, the direct tensile test was never widely adopted among the masonry research community. In turn, flexural bending tests and simple bond wrench testing methods gained in popularity, eventually becoming a part of the European standards for the testing of masonry.

The four-point bending test arrangement, standardised in EN 1052-2(CEN 2016), became popular as the masonry portion between the two inner loads experiences a pure bending moment without significant axial or shear forces, while the bond wrench testing method, described in EN 1052-5(CEN 2013), gained popularity owing to its simplicity and versatility. To perform a bending test, the dimensions of the samples should be large enough to allow the testing of multiple joints at the same time, while the failure is governed by the weakest joint. Following standard EN 1052-2(CEN 2016) the bending tests can be performed along the two orthogonal bending directions: the moment vector parallel to the bed joints ( $\theta=0^\circ$ ), and the moment vector perpendicular to the bed joints ( $\theta=90^\circ$ ). Throughout this chapter, these tests are denoted as vertical bending and horizontal bending, respectively. The relatively large size of the wallet is the main hindrance to the wide application of this method. As an alternative to laborious four-point out-of-plane bending tests, a simple bond wrench test on couplets was introduced to gain information on the quality of the developed bond along the brick-mortar interface

by determining the flexural bond strength, which can provide an indirect estimate of the masonry tensile strength. However, this testing method often suffers from a large dispersion of the testing results (Lawrence & Page, 1994).

Previous studies on the bending behaviour of masonry often only dealt with strength characterisation, since the brittle failure presented an obstacle to capturing the degradation response. Numerous studies have attempted to understand the resistance mechanism of masonry under lateral out-of-plane loading along the two orthogonal bending directions: the moment vector parallel to the bed joints ( $\theta=0^\circ$ ), and the moment vector perpendicular to the bed joints ( $\theta=90^\circ$ ). However, van der Pluijm (1999) and Willis (2004) broadened the scope of their research by bending wallets in more directions, in order to investigate the pre-peak behaviour of brick masonry extensively. To the author's knowledge, a limited number of studies were able to characterise the post-peak behaviour of masonry under out-of-plane and in-plane bending loads. To capture the post-peak response of masonry under in-plane bending load, three-point bending tests were often conducted on wallets, in which the opening of a notch in the middle of wallets was controlled, (e.g., see Guinea et al., 2000 and Chaimoon & Attard, 2009).

A large body of previous experimental studies investigated the influence of the mechanical properties of mortar, the physical characteristics of bricks, wallet size, and the level of pre-compression stress on the bending behaviour of masonry. To this end, either four-point out-of-plane bending tests on wallets or multiple bond wrench tests on a single joint were conducted. However, as mentioned earlier, a significant amount of research attention was focused on the characterisation of flexural strength.

Previous studies have found that mortar strength has a significant influence on the flexural strength of masonry. Jiao et al. (2019) found that an increase in the mortar strength of alkali-activated slag concrete hollow blocks with a thin joint resulted in higher values of vertical as well as horizontal flexural strength. The experimental results indicated an increasing linear trend between the mortar compressive strength and the flexural strength of the wallets. However, Jiao et al. (2019) noticed that an increase in mortar strength had a greater influence on the vertical flexural strength, as less difference existed between the vertical and horizontal flexural strength. Apart from the mechanical properties of mortar, joint thickness influences the flexural strength of masonry. Schubert (1994) reported higher values of flexural strength for masonry with a thin layer of mortar joint than for masonry with conventional joints.

Several researchers reported on the effects of the surface characteristics of bricks on the flexural strength of masonry. Keeping the mortar composition constant, Sarangapani et al. (2005) concluded that an increase in the area of the frog in bricks caused an enhancement in the bond strength. Khalaf (2005) found lower values of bond strength for perforated masonry than for solid wire cut bricks, as the presence of holes in the perforated clay brick reduces the bonding area. In addition, Singh and Munjal (2017) found higher values of bond strength for burnt clay brick masonry than for concrete brick masonry.

Previous studies found that the vertical flexural strength of masonry is dependent upon the unit size as well as the wallet size. Baker and Franken (1976) concluded that the vertical out-of-plane flexural strength of masonry could be significantly influenced by the wallet size. In this context, Barros and Lourenço (2000) found that an increase in the height of aerated concrete block masonry with thin layer mortar joint caused a reduction in the vertical flexural strength of masonry.

All the above-mentioned studies were performed on wallets with zero pre-compression stress; however, Gourav and Reddy (2018) performed out-of-plane bending tests on wallets with and without pre-compression to understand the vertical and horizontal out-of-plane flexural behaviour of fly ash-lime-gypsum brick masonry. Gourav and Reddy (2018) found that by increasing the pre-compression stress, both the vertical and horizontal flexural strength of the masonry wallet increased. They reported a linear relationship between the flexural strength and pre-compression stress. Similar to previous studies, at zero pre-compression stress, the horizontal flexural strength was found to be higher than the vertical flexural strength. This trend was still valid for a pre-compression stress lower than approximately 0.30 MPa. However, beyond this level, an inverse trend was found, with the vertical flexural strength higher than the horizontal flexural strength, see Figure 2.19.

Despite the valuable contributions of the previous studies for understanding the bending behaviour of masonry, little is known about the Young's modulus from bending and the softening response of masonry. Moreover, to the author's knowledge, no experimental work has been performed where the bending response of masonry wallets was determined using both in-plane and out-of-plane bending tests.

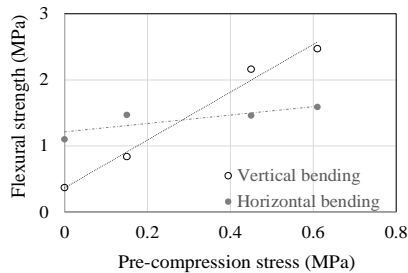


**Figure 2.19:** Variations of vertical and horizontal out-of-plane flexural strength of fly ash-lime-gypsum brick masonry under different pre-compression stress, Gourav & Reddy, 2018.

## 2.5.2 Testing procedure and data elaboration

This research studied the bending behaviour of replicated masonry wallets by performing four-point out-of-plane and in-plane bending tests on wallets, as well as bond wrench tests on stack-bond prisms. To this end, the outlines of standards EN 1052-2(CEN 2016) and EN 1052-5(CEN 2013) were followed when deciding on the size of specimens, curing, and loading rate under four-point bending and bond wrench tests, respectively. A summary of the bending properties is listed in Table 2.8–Table 2.10. To determine the flexural strength of masonry, four-point out-of-plane, and in-plane bending tests were conducted, in which masonry wallets were bent over three configurations, as follows:

- Four-point bending test with the moment vector parallel to the bed joints and in the plane of the wall, which generates a plane of failure parallel to the bed joints (denoted as *vertical out-of-plane bending test OOP1*).
- Four-point bending with the moment vector orthogonal to the bed joints and in the plane of the wall, which generates a plane of failure perpendicular to the bed joints (denoted as *horizontal out-of-plane bending test OOP2*).
- Four-point bending with the moment vector orthogonal to the plane of the wall (denoted as *in-plane bending test IP*).

To determine the flexural behaviour of masonry, two different bending set-ups were adopted, as the design of the testing set-up and measuring systems were part of the learning process. Initially, a displacement-controlled set-up was adopted for both the out-of-plane and in-plane bending tests; where the applied loads had the same direction as the self-weight of wallets, see Appendix A.4. However, controlling the progressive crack mechanism in the post-peak phase was not always possible. In addition, it was expected that the self-weight of the masonry could exacerbate the occurrence of brittle failure. Aiming to capture the post-peak response under bending loads, the testing set-up underwent extensive modifications. In the second testing phase, the crack width of the wallets under both out-of-plane and in-plane bending was used as a controlling parameter instead of the jack deformation. To this end, the crack opening was controlled using at least two LVDTs. Another improvement with respect to the previous testing set-up was the exclusion of the adverse influence of the masonry self-weight from the out-of-plane bending tests. In this regard, the general outline proposed by van der Pluijm (1999) was followed. An overview of both testing set-ups is presented in Appendix A.4. The dimensions of the wallets are listed in Table 2.2. For each loading configuration, a minimum of five wallets were tested.

The vertical flexural strength,  $f_{x1}$ , horizontal flexural strength,  $f_{x2}$ , and in-plane flexural strength of the wallets,  $f_{x3}$ , were determined as follows:

$$f_{x1} = \begin{cases} \frac{3F_{\max} d_3}{l_m t_m^2} & \text{Improved testing set-up with the exclusion of masonry self-weight} \\ \frac{3m}{l_m t_m^2} \left\{ x_i - \frac{(0.5(h_m - d_1) + x_i)^2}{h_m} \right\} & \text{Self-weight and applied load had the same direction} \end{cases} \quad (2.4)$$

$$f_{x2} = \begin{cases} \frac{3F_{\max} d_3}{h_m t_m^2} & \text{Improved testing set-up with the exclusion of masonry self-weight} \\ \frac{3m}{h_m t_m^2} \left\{ x_i - \frac{(0.5(l_m - d_1) + x_i)^2}{l_m} \right\} & \text{Self-weight and applied load had the same direction} \end{cases} \quad (2.5)$$

$$f_{x3} = \frac{3F_{\max} d_3}{t_s h_s^2} + \frac{3m}{l_s h_s^2} \left\{ x_i - \frac{(0.5(l_s - d_1) + x_i)^2}{l_s} \right\} \quad (2.6)$$

where  $F_{\max}$  is the maximum load at failure,  $d_3$  is the distance between the loading and the bearing support,  $l_m$  is the length of the masonry specimen,  $h_m$  is the height of the masonry specimen and,  $t_m$  is the thickness of the masonry specimen. In the case of the testing configuration with the applied load acting in the same direction as the self-weight of masonry (i.e. vertical bending axis), the contribution of the wallet's weight should be added to the flexural strength, where  $m$  is the weight of the wallet and  $x_i$  is the nearest distance between the crack and the outer bearings,  $d_2$ . In the case of the improved testing set-up with the horizontal bending axis, the contribution of the wallet weight was excluded. Note that all the parameters refer to as-built wallets.

Assuming a linear stress distribution over the height of the specimen's cross-section, the elastic modulus of the masonry was determined from both the force-deflection curve and the curvature-bending moment curve. The elastic modulus of masonry was calculated using the force-deflection curve in the elastic range, between 1/10 and 1/3 of the maximum force, as follows:

$$E_{3-fd(i)} = \frac{\frac{F_{el}}{2} d_3 (3d_1^2 - 4d_3^2)}{24v_{el} I_m} \quad (2.7)$$

where  $F_{el}$  and  $v_{el}$  are the load in the linear elastic stage between 10% and 30% of the maximum load and the corresponding mid-span vertical displacement, respectively,  $I_m$  is the moment of inertia of the masonry along the cross-section, and  $d_1$  and  $d_2$  are the distance between the inner and outer load bearings, respectively. Similarly, the bending stiffness was also calculated from the bending moment-curvature curve as follows:

$$E_{3-mc(i)} = \frac{M_{el}}{\kappa_{el}} \quad (2.8)$$

where  $M_{el}$  and  $K_{el}$  are the bending moment in the linear elastic stage between 10% and 30% of the maximum bending moment and the corresponding curvature,



respectively. Assuming uniform stiffness in the wallets, curvature was calculated by considering the wallet's elongation as recorded by LVDTs.

The concept of fracture energy associated with tensile cracking, as used for concrete, was applied to masonry by van der Pluijm (1999). Thanks to the use of the improved set-up, the fracture energy determined from the four-point bending tests can be calculated as the sum of the areas underneath the two point loads versus deflection curves, Figure 2.20a, taking into account the cross-sectional area of the specimen. Accordingly, the fracture energy for the specimen under vertical out-of-plane bending,  $G_{fx1}$ , horizontal out-of-plane bending,  $G_{fx2}$ , and in-plane bending,  $G_{fx3}$ , was calculated. In some instances, the post-peak softening branch reached a plateau, see Figure 2.20b. This peculiar response might be attributed to the presence of friction load between the wallets and the supporting steel plate (on the bottom), friction due to the self-weight of the wallets, and the formation of mixed cracks propagated along multiple joints. To exclude such undesirable behaviour, the fracture energy was calculated up to the point where the plateau started, see Figure 2.20b.

For both brittle and quasi-brittle materials, the stress corresponding to the onset of cracking under bending load can be considered uniaxial tensile strength. In order to be consistent, the stress at which the curve began to deviate 10% from its initial slope was used as a basis to find the tensile strength. Although this number is arbitrary, it was selected based on engineering judgment. Therefore, insight into the uniaxial tensile strength can be indirectly obtained from the bending tests. By giving the ratio between the flexural strength and the uniaxial tensile strength, this study responds to a major demand in both practice and research (e.g., see van der Pluijm, 1999; Barros & Lourenço, 2000).

The bond strength between the masonry unit and the mortar was determined using the bond wrench test, proposed by standard EN 1052-5(CEN 2013). The aim was to produce a bending moment along the brick-mortar interface of the top unit of a stack-bond prism. For each masonry type, a minimum of fifteen single joints were tested.

Assuming a linear stress distribution over the width of the top masonry unit, the bond strength,  $f_w$ , was calculated as follows:

$$f_w = \frac{F_1 e_1 + F_2 e_2 - \frac{2}{3} t_u \left( F_1 + F_2 + \frac{F_3}{4} \right)}{l_j w_j^2 / 6} \quad (2.9)$$

where  $F_i$  is the failure load, measured and applied by the jack or recorded by the analogue torque wrench,  $F_2$  is the normal force caused by the weight of the bond wrench apparatus,  $F_3$  is the weight of the masonry portion pulled off from the specimen. Furthermore,  $e_1$  is the distance from the applied load to the tension face of the specimen,  $e_2$  is the distance from the centre of gravity of the clamp to the tension face of the specimen,  $l_j$  is the mean length of the bed joint, and  $w_j$  is the mean width of the bed joint. The set-up and the definitions of the various quantities are shown in Appendix A.4.

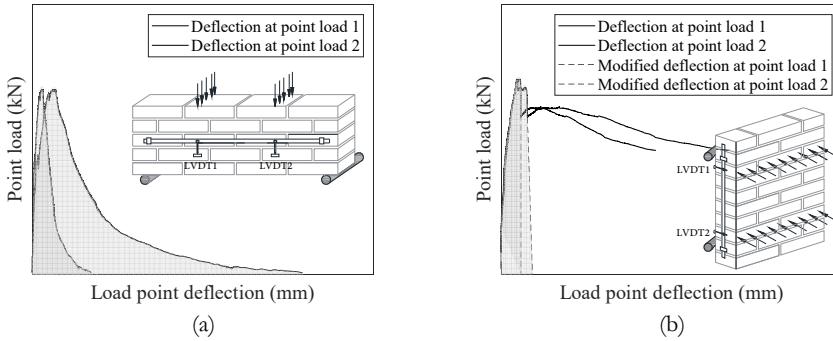


**Figure 2.20:** Point load-point deflection curve used to calculate the bending fracture energy: (a) typical curve obtained from in-plane bending test; (b) typical curve obtained from out-of-plane bending test.

**Table 2.8:**

Summary overview of the bending properties under vertical out-of-plane and bond wrench tests. Coefficient of variation in parentheses.

Masonry type	Vertical out-of-plane bending (OOP1)					Bond wrench
	$f_{x1}$ MPa	$E_{3,ft-1}$ MPa	$E_{3,mc-1}$ MPa	$f_{t1}$ MPa	$G_{fxc1}$ N/m	
MAT-1	0.26 (18%)	11356 (26%)	5435 (27%)	0.18 (33%)	-	0.27 (43%)
MAT-2	0.38 (26%)	10154 (11%)	8957 (36%)	0.28 (43%)	-	0.27 (54%)
MAT-3	0.16 (22%)	4440 (48%)	5201 (23%)	0.08 (28%)	5.25 (97%)	0.14 (46%)
MAT-4	0.14 (32%)	3958 (18%)	2189 (31%)	0.06 (40%)	14.57 (53%)	
MAT-5	0.58 (16%)	25369 (12%)	6063 (8%)	0.53 (24%)	5.89 (29%)	0.55 (17%)

**Table 2.9:**

Summary overview of the bending properties under horizontal out-of-plane bending test. Coefficient of variation in parentheses.

Masonry type	Horizontal out-of-plane bending (OOP2)				
	$f_{x2}$ MPa	$E_{3,ft-2}$ MPa	$E_{3,mc-2}$ MPa	$f_{t2}$ MPa	$G_{fxc2}$ N/m
MAT-1	0.56 (43%)	9004 (18%)	4447 (16%)	0.29 (50%)	-
MAT-2	1.14 (16%)	7796 (38%)	7965 (38%)	0.48 (21%)	-
MAT-3	0.65 (28%)	15088 (57%)	5599 (5%)	0.37 (35%)	54.21 (53%)
MAT-4	0.41 (15%)	10987 (13%)	4664 (25%)	0.22 (15%)	22.51 (38%)
MAT-5	0.73 (4%)	15206 (15%)	4178 (25%)	0.43 (17%)	11.02 (16%)

**Table 2.10:**

Summary overview of the bending properties under in-plane bending test. Coefficient of variation in parentheses.

Masonry type	In-plane bending (IP)				
	$f_{x3}$ MPa	$E_{3,ft-3}$ MPa	$E_{3,mc-3}$ MPa	$f_{t3}$ MPa	$G_{fxc3}$ N/m
MAT-1	0.39 (21%)	3160 (19%)	1601 (54%)	0.19 (34%)	-
MAT-2	0.68 (15%)	5052 (33%)	5947 (31%)	0.30 (30%)	-
MAT-3	0.48 (21%)	4239 (18%)	3779 (20%)	0.22 (17%)	109.20 (57%)
MAT-4	0.49 (22%)	4554 (11%)	4191 (9%)	0.18 (9%)	64.75 (38%)
MAT-5	0.38 (21%)	-	-	0.20 (52%)	-

### 2.5.3 Overall response

This section discusses the nonlinear bending response of masonry in terms of flexural stress-deflection, moment-curvature curves, and the final crack pattern of wallets under vertical and horizontal out-of-plane and in-plane bending loads. The response of each tested specimen (in grey) and mean curves (in black) are presented in Figure 2.21–Figure 2.25.

Disregarding the bending direction, the analysis of the flexural stress-deflection and moment-curvature curves, can be carried out over three phases: initial linear phase, pre-peak nonlinear phase, and post-peak softening phase. In the linear phase, often no cracks appeared on the wallet's surface. For the analysed masonry types, linear behaviour continued up to 35%–90% of the peak load. For each masonry type, the longest linear branch was often found for the wallets tested under vertical out-of-plane bending load. In the nonlinear pre-peak phase, the stiffness of the curves gradually decreased. As micro-cracks grew and merged into macro cracks, failure of the wallets occurred. Under vertical out-of-plane bending load, the nonlinearity began as debonding cracks appeared along bed joints. However, under horizontal out-of-plane bending and in-plane bending loads, the pre-peak nonlinearity can be ascribed to micro-crack initiation along the head joints. With continued deformation, the stiffness drastically decreased due to the complex interaction between shear and torsional effects along the bed joints (van der Pluijm, 1999, Willis, 2004). In the post-peak phase, progressive cracking of the joints/units occurred; thus, the wallets lost both strength and stiffness. Controlling the crack opening, made for the MAT-3, MAT-4, and MAT-5 wallets, instead of the jack deformation, made for MAT-1 and MAT-2 wallets, improved the insights into the softening response of masonry. Nevertheless, capturing the post-peak response of the wallets under vertical out-of-plane bending load was quite challenging, as instant and unstable cracks occurred along the bed joints. Note that a brittle failure was reported for MAT-5 CS element masonry with thin joints under both vertical and horizontal out-of-plane bending loads; thus controlling the crack opening beyond the peak load was almost impossible.

Four-point bending configurations allowed for the simultaneous testing of multiple joints, while the failure path followed the weakest link in the wallet. Under vertical out-of-plane bending load, the fracture plane was more likely to occur along the bed joint due to interface debonding rather than due to the tensile failure of brick. In this study, the failure mode was mostly characterised by the formation of one or two straight cracks along the bed joints located within the constant moment zone. Under horizontal out-of-plane bending load, the wallets failed either due to the formation of stepwise debonding cracks along multiples interfaces, or due to vertical splitting cracks. The former failure often started with debonding along a head joint followed by the formation of a stepwise crack, which underwent both shearing and twisting deformations. The vertical splitting crack running across head joints and bricks often started in a brick. The occurrence of the two different failure modes can be influenced by the brick, mortar, and interface properties. It can be assumed that stepwise debonding failure is more likely to happen in the case of masonry with a weaker bond. However, by further improvement of the bond, it is

expected that the masonry would tend to fail due to brick splitting. Note that the vertical splitting crack was noticed only in one CS brick wallet, while it was frequently observed in the case of wallets extracted from existing buildings, which will be addressed in the following chapter. The failure of the wallets in the in-plane bending test was similar to that of the horizontal out-of-plane bending test.

In this study, the flexural failure of the stack-bond prism, whereby a single joint is subjected to the bending moment, was classified as debonding along the brick-mortar interface, Figure 2.26. However, the flexural failure of the mortar as well as brick failure can be also expected, if the masonry has a rich cement mortar (Sarangapani et al., 2005).

In line with the objectives of the testing program, the following observations were made:

- The crack pattern was affected by the bending direction.
- No significant difference in the crack patterns of the single- and double-wythe wallets were noticed. Comparing the behaviour of MAT-3 single-wythe clay with that of MAT-4 double-wythe solid clay wallets, the former masonry type showed a longer linear branch than the latter. The promotion of micro-crack propagation in the double-wythe wallets could be attributed to a complex stress distribution due to the presence of the collar joint.
- The crack pattern of the MAT-5 CS element masonry with a thin mortar layer did not differ from the brick masonry with a conventional joint. In the pre-peak phase, the brick masonry types showed a linear behaviour continuing up to 70%–90% of the failure load, while a very long linear branch was found for the CS element masonry, until approximately 90% of the failure load, Figure 2.25.

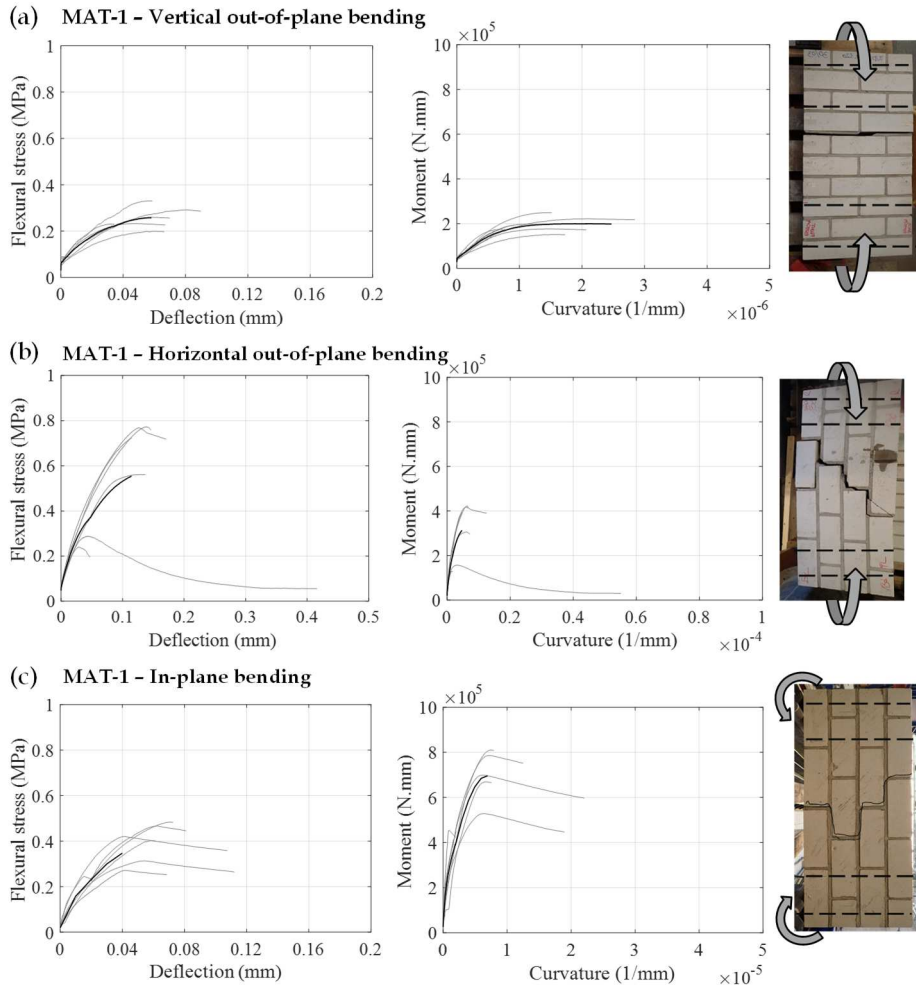


**Figure 2.21:** Flexural stress-deflection curve, moment-curvature curve, and final crack pattern of MAT-1 single-wythe CS brick masonry under: (a) vertical out-of-plane bending; (b) horizontal out-of-plane bending; (c) in-plane bending.

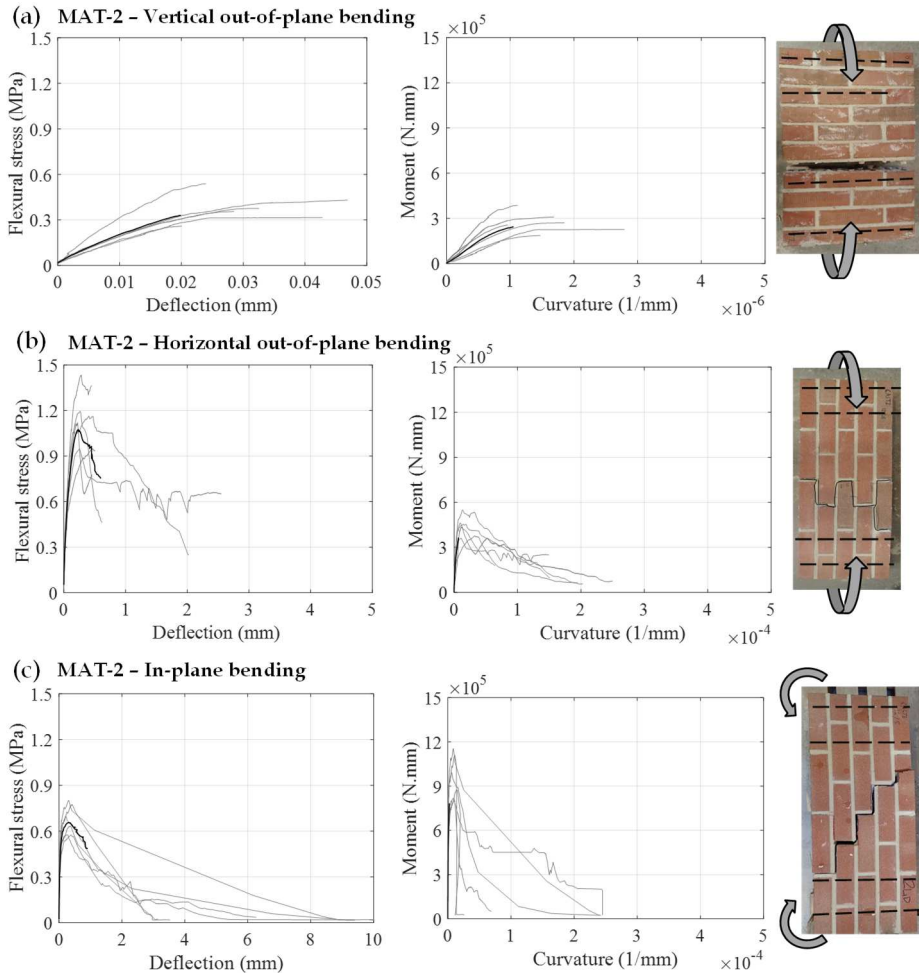


**Figure 2.22:** Flexural stress-deflection curve, moment-curvature curve, and final crack pattern of MAT-2 single-wythe perforated clay brick masonry under: (a) vertical out-of-plane bending; (b) horizontal out-of-plane bending; (c) in-plane bending.

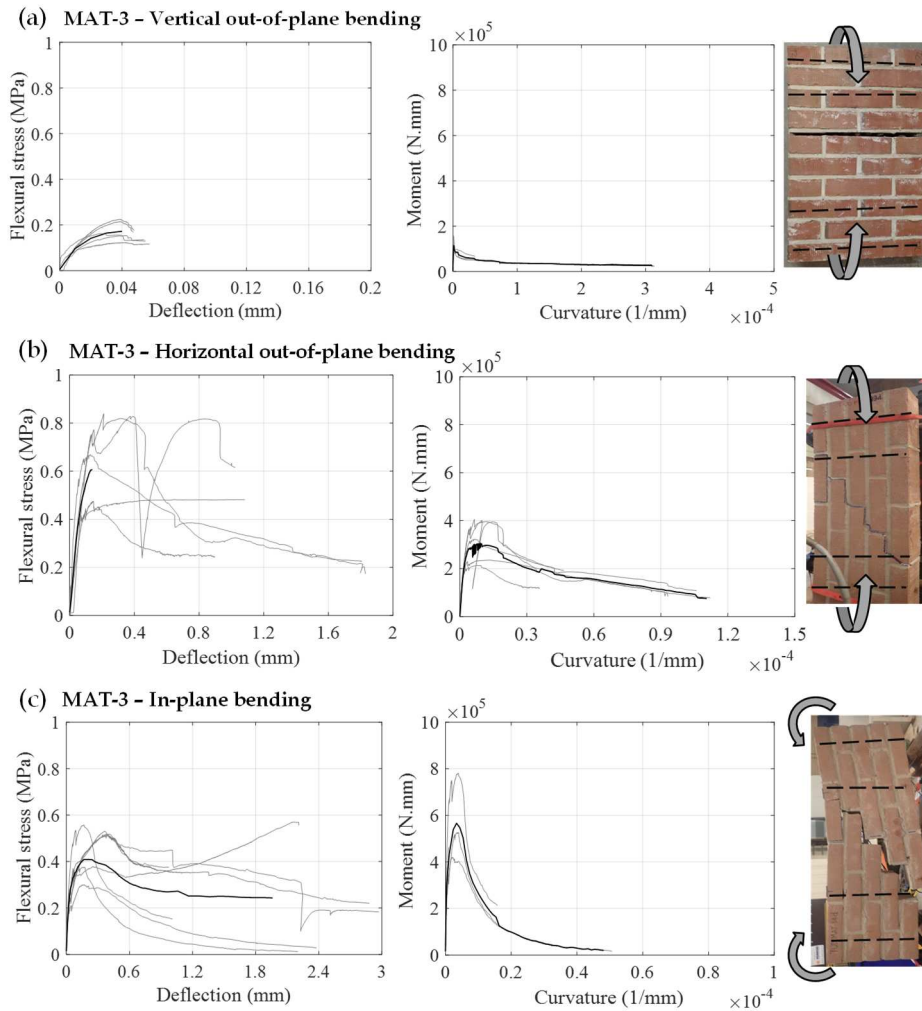


**Figure 2.23:** Flexural stress-deflection curve, moment-curvature curve, and final crack pattern of MAT-3 single-wythe slid clay brick masonry under: (a) vertical out-of-plane bending; (b) horizontal out-of-plane bending; (c) in-plane bending.

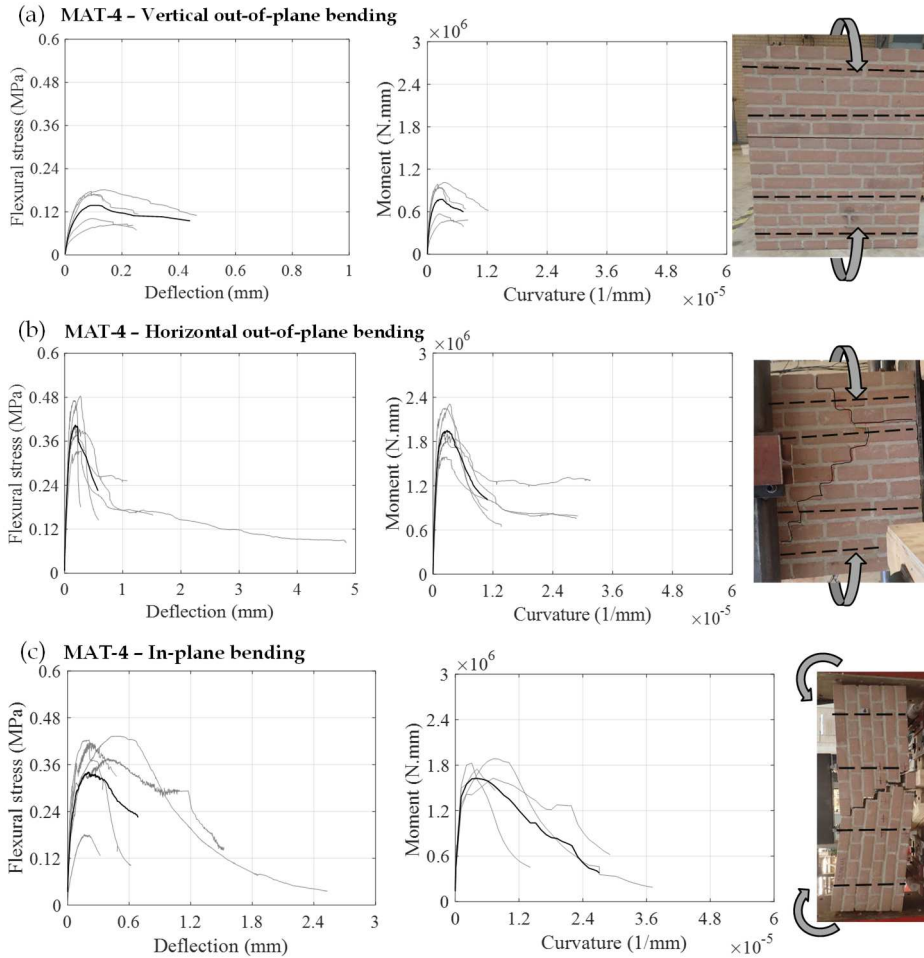


**Figure 2.24:** Flexural stress-deflection curve, moment-curvature curve, and final crack pattern of MAT-4 double-wythe solid clay brick masonry under: (a) vertical out-of-plane bending; (b) horizontal out-of-plane bending; (c) in-plane bending.



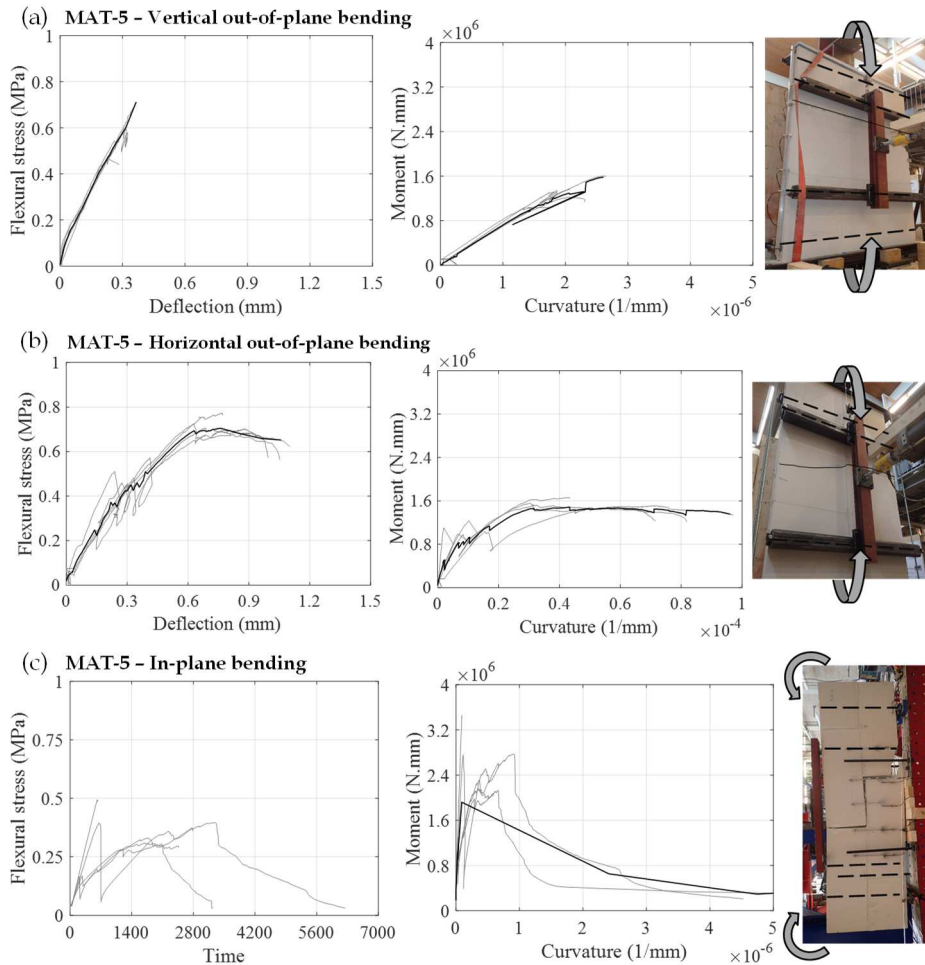


**Figure 2.25:** Flexural stress-deflection curve, moment-curvature curve, and final crack pattern of MAT-5 single-wythe CS element masonry under: (a) vertical out-of-plane bending; (b) horizontal out-of-plane bending; (c) in-plane bending. Note that in the in-plane bending test, the readings of vertical LVDTs and thus the values of deflection were not reliable.

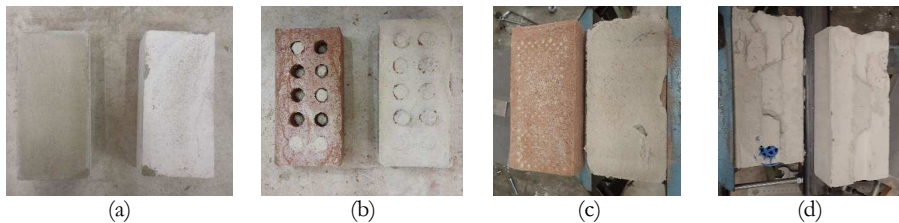


**Figure 2.26:** Typical bond failure: (a) CS brick masonry; (b) perforated clay brick masonry; (c) solid clay brick masonry; (d) CS element masonry.

### 2.5.4 Flexural strength

Under vertical out-of-plane bending tests, the flexural strength appeared to be dependent on the interface properties and the surface characteristics of the masonry unit. The highest flexural strength was obtained for the MAT-5 CS element masonry with a thin-mortar layer ( $f_{x1}=0.58$  MPa), and the lowest belonged to MAT-4 double-wythe clay brick masonry ( $f_{x1}=0.14$  MPa). Amongst the different brick masonry types, the highest flexural strength belonged to the MAT-2 perforated clay wallets ( $f_{x1}=0.18$  MPa); such high resistance can be attributed to the dowel action of the perforated bricks.

No influence of the size effect on the vertical flexural strength was found. Under vertical out-of-plane bending, both MAT-3 single-wythe and MAT-4 double-wythe clay brick masonry wallets resulted in similar strength values, Figure 2.27. As the failure of masonry under vertical out-of-plane loading is governed by the debonding of the weakest joint, disregarding masonry wythe and height, a link between the vertical flexural strength and the bond strength can be expected. In this study, a one-to-one correspondence was found between these two properties, except for MAT-2 perforated clay masonry. This masonry type showed a vertical flexural strength that was approximately 40% higher than the bond strength. Unlike the bond wrench test, by which only a single bed joint fails, multiple joints play a role in the vertical flexural testing of wallets. Accordingly, it can be assumed that the contribution of the dowel action is greater in the bending test than in the bond wrench test.

The horizontal flexural strength of masonry,  $f_{x2}$ , depends not only on the bed joint, but also on the characteristics of the head joint. Unlike the vertical bending test, the masonry with the highest bond strength did not necessarily result in the highest horizontal flexural strength. The significant importance of the dowel action is once again highlighted for MAT-2 perforated clay brick, which showed the highest horizontal flexural strength ( $f_{x2}=1.14$  MPa). Unlike vertical flexural strength, the horizontal flexural strength of double-wythe wallets was approximately 40% lower than that of the single-wythe wallets. In such a case, the contribution of the collar joint in the distribution of stress cannot be neglected. Thus, numerical and experimental studies are more broadly needed. The horizontal flexural strength of MAT-5 CS element masonry, built with the strongest mortar, did not deviate significantly from the other brick masonry types.

Similar to the horizontal flexural strength, the in-plane flexural strength of masonry,  $f_{x3}$ , was influenced by the characteristics of both the bed and head joints. The highest value of the in-plane flexural strength was found for MAT-2 perforated clay brick masonry. The in-plane flexural strength of MAT-3 single-wythe and MAT-4 double-wythe clay brick masonry wallets were similar, indicating no size effect under in-plane bending loads. The lowest value of the in-plane flexural strength belonged to MAT-5 CS element masonry wallets with thin joints that were built using the strongest mortar.

Despite the attempt to build consistent specimens, the values of the bond strength were widely dispersed, Table 2.8. The brick masonry types with conventional joints showed a larger variation in bond strength, ranging between 0.43% and 0.54%; conversely, MAT-5 CS element masonry with thin layer joints showed a low coefficient of variation equal to 17%.

Previous studies showed that the mechanism of the bond development along the interface could be regarded as a time-dependent process. Sugo et al. (2007) monitored the bond strength of one masonry type, consisting of 1:1:6 mortar and clay bricks, over a period of one year. Eventually, they came up with a hypothetical curve, whereby a marginally significant loss of bond strength was reported over two alternating ages of 18 to 90 days as well as 165 to 180 days. The reduction in strength was attributed to the development of micro-cracks caused by mortar shrinkage. Such a gain, loss, and regaining trend in bond strength was also noticed in previous studies (e.g., Baker & Franken, 1976). Using bricks and mortar from the same production batch as the current study, Gaggero (2019) investigated the possible influence of hardening time on the bond strength of CS brick masonry and clay brick masonry. Over time, she found that the bond strength of CS brick masonry did not change significantly; however, clay brick masonry gained higher resistance.

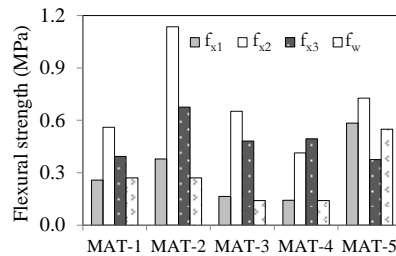


**Figure 2.27:** Overview of the vertical out-of-plane flexural strength,  $f_{x1}$ , horizontal out-of-plane flexural strength,  $f_{x2}$ , in-plane flexural strength,  $f_{x3}$ , and flexural bond strength,  $f_w$ .

## 2.5.5 Young's modulus

In this study, the analysis of the Young's modulus under bending loads rests on simple beam theory. The Young's modulus was calculated in the linear-elastic phase, assuming that the wallet deflection was much less than the wallet height. The stiffness values, reported in Table 2.8–Table 2.10, were calculated by taking into account both the flexural stress-deflection (using vertical LVDTs) and moment-curvature curves (using horizontal LVDTs). Similar values of Young's modulus can be expected using both approaches; however, higher values of Young's modulus were often found using the stress-deflection curve, using Eq. (2.7), rather than moment-curvature, i.e. using Eq. (2.8), as seen in Figure 2.28. At this moment, there is no sound explanation for such a difference between the values of the Young's modulus using the readings of different LVDTs.

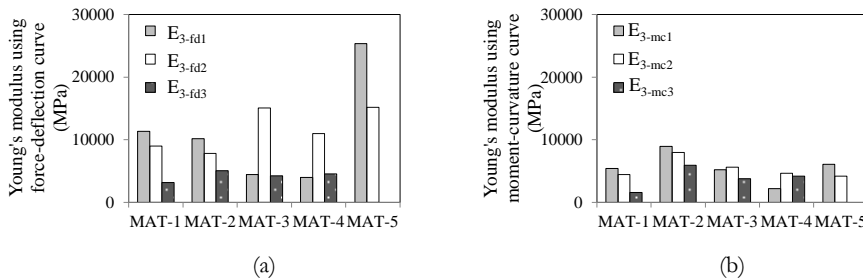


**Figure 2.28:** Overview of the Young's modulus of wallets obtained under vertical out-of-plane bending, horizontal out-of-plane bending, and in-plane bending from: (a) flexural stress-deflection (using vertical LVDTs); (b) and moment-curvature curves (using horizontal LVDTs).

## 2.5.6 Fracture energy in bending

The values of fracture energy are presented in Table 2.8–Table 2.10 and shown in Figure 2.29. Generally, wallets subjected to in-plane bending load showed the highest values of fracture energy, and the wallets under vertical out-of-plane bending had the lowest values. Note that no reliable values of fracture energy were obtained for MAT-1 CS brick masonry and MAT-2 perforated clay brick masonry tested using the displacement-controlled testing set-up.

No clear trend was observed between the fracture energy of MAT-3 single-wythe and MAT-4 double-wythe clay brick masonry. However, the outcome obtained from the in-plane bending test is contrary to that of Olivito and Stumpo (2001), who found the dependency of the ratio between the fracture energy of double-wythe wallets and single-wythe wallets to the mortar strength. For the purpose of testing, they adopted masonry samples constructed using two types of mortar: weak (compressive strength of 2.45 MPa) and strong (compressive strength of 10.10 MPa). In the case of the masonry with weak mortar, no significant difference was found between the values of fracture energy of single- and double-wythe wallets. For masonry with strong mortar, the fracture energy of double-wythe masonry was reported to be almost two times higher than that of single-wythe masonry. To derive concrete conclusions, further testing is necessary.

To date, few studies have investigated the influence of tests on the estimation of fracture energy. For instance, a close correspondence is expected between the values of fracture energy obtained under vertical out-of-plane bending and bond wrench tests, as both tests depend on the characteristics of the interface. As mentioned earlier, in a separate study, Gaggero (2019) managed to record the softening response of MAT-1 CS brick masonry and MAT-3 clay brick masonry specimens using a bond wrench test. The values of the fracture energy estimated using the bond wrench test are presented in Figure 2.29. Gaggero (2019) found the fracture energy of clay brick masonry to be dependent on the hardening time: the older the age, the higher the values of fracture energy. Figure 2.29 presents the values of fracture energy of stack bonded prisms at 56 days, which is approximately the same age at which the clay brick masonry wallets were tested. A one-to-one correspondence was found between the fracture energy of the two types of tests, though this conclusion is based on a limited number of specimens. van der Pluijm (1999) made a comparison between the fracture energy of masonry under tension loading and the fracture energy of stack-bond prisms tested under vertical out-of-plane bending loads. He reported higher values of fracture energy under the flexural tests than the tensile tests, where a ratio of three and a ratio of two were reported for clay and CS block masonry, respectively. van der Pluijm (1999) attempted to explain such differences in light of the actual bonding area, as he found a ratio of 1.7 between the bonding surface of the couplet and wallets. Nevertheless, the nature of the difference between the fracture energy in tension and in flexure remains unclear.

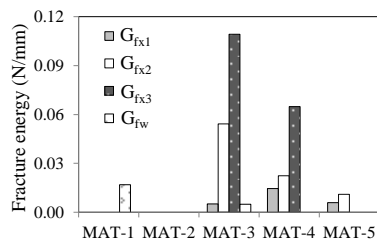


**Figure 2.29:** Overview of the fracture energy under vertical out-of-plane bending,  $G_{fx1}$ , horizontal out-of-plane bending,  $G_{fx2}$ , in-plane bending,  $G_{fx3}$ , and bond wrench test,  $G_{fw}$ , extracted from Gaggero (2019).

## 2.5.7 Uniaxial tensile strength

As mentioned earlier, the behaviour of masonry wallets under pure bending can be characterised in three regimes: elastic linear, nonlinear pre-peak, and post-peak softening. Within the elastic regime, the distribution of stress in the compression and tension zones is linear and, thus, the tensile stress is the same as the flexural stress. However, by increasing the load, micro-cracks start growing and, subsequently, the neutral axis keeps shifting toward the outermost fibres in compression. This indicates that the stress distribution is no longer linear. Therefore, tensile strength cannot be regarded as equivalent to flexural strength. As already stated, the direct tensile test has scarcely been adopted within the masonry research community, as the preparation of samples as well as the testing set-up are quite challenging (Hordijk, 1993; van der Pluijm, 1999). Nevertheless, previous studies showed that the uniaxial tensile strength of masonry can be indirectly derived from the flexural strength of masonry. To this end, van der Pluijm (1999) reported ratios of flexural strength to tensile strength between 1.1 and 1.7. Eventually, by comparing his database with data from the literature, he assumed that the uniaxial tensile strength can be determined as 0.67 times the flexural strength. In an extensive experimental campaign, Jiao et al. (2019) reported a factor of 0.5 between the horizontal flexural strength and the uniaxial tensile strength obtained in the direction perpendicular to the bed joint.

In this study, the ratio between the uniaxial tensile strength and flexural strength of the CS element masonry with a thin joint was generally higher than the one for brick masonry with a conventional joint, as seen in Figure 2.30. For different brick masonry types (MAT-1, 2, 3, 4) this ratio ranged between 0.36 and 0.73, with an average ratio of 0.51, while for CS elements (MAT-5), a ratio between 0.53 and 0.90 was found. The tensile strength was assumed to be the stress corresponding to the onset of cracking when performing bending tests; see e.g., Maalej and Li (1994).

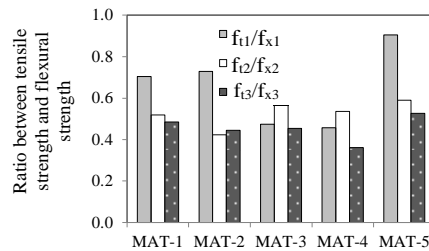


**Figure 2.30:** Ratio between the derived tensile strength and flexural strength.

## 2.6 NONLINEAR SHEAR-SLIDING BEHAVIOUR ALONG THE INTERFACE

This section first discusses the current state-of-the-art of brick-mortar shear-sliding behaviour. Second, the testing procedure and data elaboration are detailed. Third, it discusses the overall response of masonry in terms of initial shear strength (cohesion), initial and residual friction coefficient, shear modulus of the mortar joint, mode-II fracture energy, and dilatancy.

### 2.6.1 State-of-the-art: Shear response

The existing literature on the shear-sliding properties along the brick-mortar interface is extensive and focuses particularly on determination of initial shear strength (cohesion) and friction coefficient. Independent of the investigated masonry types, previous experimental studies reached a clear consensus regarding the dependency of shear strength on the applied pre-compression stress level. In other words, by increasing the pre-compression level, the shear strength increased accordingly. Nevertheless, the extent of the increase in shear strength differs based on the masonry type. In this context, the mechanical and physical characteristics of the mortar joint and the masonry unit play important roles. Rahman and Ueda (2013) found that masonry with stronger mortar showed higher values of shear strength and consequently higher values of initial shear strength; however, the friction coefficient was not reported to be dependent on the mortar strength.

Apart from the initial properties, the residual shear properties were also addressed in several studies (e.g., Lourenço & Ramos, 2004; Vasconcelos & Lourenço, 2009; Augenti & Parisi, 2011; Lizárraga & Pérez-Gavilán, 2017). As with shear strength, previous studies showed the dependency of the residual shear strength on the pre-compression level and the mortar strength (Rahman & Ueda, 2013). The residual shear strength refers to a stress in which no cohesion exists along the interface, so that the two unbonded surfaces just slide along each other. As experimental results were mapped into the framework of the Coulomb failure criterion, a zero or very small value of residual shear strength was found. Previous experimental studies showed that the residual friction coefficient could differ from the initial friction coefficient, even up to 10%. The reduction of the residual friction coefficient with respect to the initial friction coefficient can be attributed to further damage in the asperities of the plane of failure.

Several authors have investigated the influence of mortar strength, masonry unit, and the level of pre-compression on the shear modulus of the mortar. Rahman and Ueda (2013) found that the shear modulus of mortar was improved by increasing the mortar compressive strength. Abdou et al. (2006) concluded that the surface characteristics of masonry unit had a direct influence on the shear modulus, as bricks with hollows act as an abutment and consequently result in an increase in the shear modulus with respect to solid clay bricks. Regarding the dependency of the shear modulus of mortar on the level of pre-compression stress, conflicting conclusions have been presented in the literature. Augenti and Parisi (2011) found that the shear modulus of mortar was not affected by the pre-compression level. This conclusion differed from the findings of Rahman and Ueda (2013), who found

that the shear modulus of masonry with strong mortar is affected more significantly with an increase in the pre-compression level.

To date only a limited number of studies have dealt with characterising the post-peak degradation response of the brick-mortar interface under shear-sliding load, which can be quantified in terms of mode-II fracture energy. Pioneering research on clay and CS brick masonry showed that this parameter can be approximated as a linear function of the pre-compression level. Rots et al. (1997), van der Pluijm (1999), and Augenti and Parisi (2011) reported an increase between the mode-II fracture energy and pre-compression level of clay, CS brick, and tuff masonry. Nevertheless, Lizárraga and Pérez-Gavilán (2017) found an inverse trend, as the mode-II fracture energy of perforated concrete masonry with conventional mortar joints decreased with an increase in the pre-compression level.

As with mode-II fracture energy, limited attention has been paid to the characterisation of dilatancy, defined as the slope of the normal displacement to shear displacement diagram. Independent of the masonry type, previous research found that the angle of dilatancy decreased with an increase in the level of pre-compression stress (e.g., see Atkinson et al., 1989; van der Pluijm, 1993; Lizárraga & Pérez-Gavilán, 2017). In addition, it was reported by van der Pluijm (1999) that by increasing the shear sliding, the dilatancy angle gradually reduced to zero. Apart from the impact of the pre-compression level, van der Pluijm (1999) concluded that the type of failure, i.e. bond failure or mortar failure, can considerably influence the magnitude of the normal displacement and thus the angle of dilatancy.

To understand the shear response of masonry at the material level, researchers introduced different types of shear tests aiming to introduce as the best possible pure and uniform distribution of shear stress along the brick-mortar interface of specimens arranged in the shape of a couplet, triplet, or small wallet. A detailed summary of the developed testing methods in the literature can be found in Atkinson et al. (1989), Zimmermann et al. (2012), Montazerolghaem and Jaeger (2014), and Lizárraga and Pérez-Gavilán (2017).

To investigate the impact of testing method on the stress distribution along the interface, researchers performed linear or nonlinear finite element analysis. However, Zhang et al. (2018) concluded that the linear analysis did not result in a realistic estimation of the shear stress distribution, particularly when the damage was initiated. In the context of nonlinear finite element analysis, Zhang et al. (2018) and Montazerolghaem and Jaeger (2014) uncovered that almost all the available testing methods suffer from the concentration of shear stress, particularly at the extremities of the interface. Comparing different testing methods, it can be concluded that the triplet test, introduced by European standard EN 1052-3(CEN 2002), offers a reasonable compromise between simplicity of the testing set-up and accuracy of the results.

Despite the valuable contributions of the previous studies on the shear-sliding behaviour of the brick-mortar interface, not much is known about the elastic shear modulus of the mortar joint and mode-II fracture energy.



## 2.6.2 Testing procedure and data elaboration

Although various testing arrangements have been developed in the literature, this study followed the outline of the current European standard method EN 1052-3(CEN 2002). Accordingly, a progressive shear load was applied along the interface of a stack-bond specimen, which, based on the masonry unit dimensions, were either in triplet or couplet configurations, while in the direction perpendicular to the interface the specimen was subjected to a constant compressive load. To keep the pre-compression load constant, particularly when reaching the maximum shear load, a spring system was positioned between the specimen and the horizontal actuator. To capture the complete nonlinear shear-sliding behaviour along the masonry unit-mortar interface, the vertical load was applied using a displacement-controlled actuator. Both the shear-sliding deformations and the normal displacement of the joint, which is perpendicular to the bed joint, were measured using LVDTs. More information regarding the testing set-up and measuring system can be found in Appendix A.5. For each individual masonry type, the test was repeated at three different pre-compression levels. Following the outline of standard EN 1052-3(CEN 2002), for brick masonry types, triplets were adopted, consisting of one brick in length and three courses of bricks in height; however, in the case of CS element units with a height greater than 100 mm, couplets were adopted. Each couplet, with dimensions of 300×300×100 mm, was composed of two sawn-cut pieces extracted from the top and bottom of one single CS element unit. Following EN 1052-3(CEN 2002), the bonded surfaces of CS elements were the original faces and not the cut ones.

In this study, the shear-sliding behaviour along the interface was characterised in terms of cohesion (or initial shear strength), initial and residual friction coefficient, shear modulus of the mortar joint, mode-II fracture energy, and dilatancy. Assuming a uniform stress distribution along the interface, the shear strength was calculated as the ratio of maximum shear load to the shearing surface, and the normal pre-compression stress was evaluated by dividing the normal pre-compression force by the cross-sectional area of the joint. The residual shear strength was defined in the plateau phase, where no further reduction in shear stress was observed.

Under the assumption that the shear strength and residual shear strength follow the Coulomb friction relationship, the initial and residual shear properties were evaluated. The initial shear strength (or cohesion),  $f_{t0}$ , was evaluated as the shear stress corresponding to zero normal stress, and the friction coefficient,  $\mu$ , was found as the slope of the linear regression line. A similar approach was followed to evaluate the residual shear strength,  $f_{t0,res}$ , and residual friction coefficient,  $\mu_{res}$ . The residual failure criterion often passes through the origin axis, meaning that the stress is measured over two unbonded surfaces.

Due to the high stiffness of the units, it was assumed that the relative sliding and normal displacement measured across the joint could be attributed only to the deformation of the mortar. This allowed for evaluating the shear modulus of the mortar joint. The elastic shear modulus of the mortar joint was determined as the slope of the shear stress-strain curve calculated in the linear phase, between 1/10

and 1/3 of the maximum shear stress. The shear strain was calculated by dividing the shear sliding by the mortar joint thickness.

In nonlinear finite element analysis of quasi-brittle materials like masonry, not only are the stiffness and strength properties reported, but so is the toughness, i.e. the post-peak softening. The toughness for shear fracture can be expressed as the mode-II fracture energy,  $G_{f-II}$ , which is the energy required to create a one-unit area of a shear crack along the brick-mortar interface.

To determine the dilatancy from the experimental results, the following formula was adopted:

$$\tan(\psi) = -\frac{(u_p)_{n+1} - (u_p)_n}{(v_p)_{n+1} - (v_p)_n} \quad (2.10)$$

where  $v_p$  is the plastic sliding displacement,  $u_p$  is the corresponding plastic normal displacement perpendicular to the bed joint, and  $n$  is the increment of the sliding displacement. The calculation of the plastic displacements excludes the elastic deformation of the mortar. To this end, the mortar stiffness is assumed to be 200 times the compressive strength of mortar (Kaushik et al., 2007). van Zijl (2004) formulated the description of normal uplift upon shear-sliding as follows:

$$u_p = \frac{\psi_0}{\delta} \left(1 - \frac{\sigma}{\sigma_u}\right) (1 - e^{-\delta v_p}) \quad (2.11)$$

where  $\psi_0$  is dilatancy at zero normal confining stress and shear-sliding,  $\sigma_u$  is confining compressive stress at which the dilatancy becomes zero,  $\delta$  is dilatancy shear-sliding degradation coefficient,  $v_p$  and  $u_p$  are plastic shear-sliding and plastic normal displacement. In this study, these three parameters were obtained by least-squares fitting to experimental data, as suggested by van Zijl (2004). Note that in this study, the failure criterion was not modified to account for dilatancy. Note that in this study, the failure criterion was not modified to account for dilatancy.

### 2.6.3 Overall response

The characteristics of the shear stress-sliding curves of the analysed masonry types and the typical failure pattern are discussed in this section. An overview of the shear properties along the brick-mortar interface of the four masonry types is presented in Table 2.11.

As shear-sliding behaviour of the brick masonry is concerned, a nonlinear pre-peak branch was observed, followed by a post-peak softening branch that eventually reached a plateau. First, linear behaviour was found up to 10%–40% of the maximum shear load. By increasing the shear load, the curve showed signs of a decrease in stiffness that can be attributed to the initiation of debonding cracks along the interface. At the peak load, visible cracks developed simultaneously along the two interfaces. However, non-simultaneous failure of the two interfaces is often observed in the case of CS brick masonry tested at the lowest pre-compression level (0.20 MPa). In this case, two consecutive peak loads were identified in the shear-sliding curves. After reaching the peak load, cracks progressively developed throughout the interfaces until full debonding occurred, and, consequently, with a further increase in the sliding, no further reduction in the shear load was noticed.

In this phase, the resistance can be attributed only to frictional mechanisms; thus the corresponding stress was referred as ‘residual strength’ or ‘dry-friction’. Generally, by increasing the pre-compression level, the transition from the maximum shear stress to the residual strength occurred more gradually. Figure 2.31a–Figure 2.33a show that the higher the confining pressure, the higher the values of both the peak and residual shear strength. After the softening phase, no further reduction in shear stress was observed, as two unbonded surfaces were sliding along each other under constantly compression.

Regarding the CS element couplets, the shear response was not fully characterised, as the formation of the mixed failure interrupted the further propagation of shear cracks along the interface. The shear response of the CS element was characterised by two peaks, each associated with a different failure mechanism. Up to the first peak, an initial linear branch with a steep slope was observed. The first peak load corresponded to the formation of a shear crack along the interface, thus causing a sudden transition from stable to unstable crack growth. Consequently, a short softening phase was observed, followed by a hardening branch until another peak was attained. As expected, after interface debonding, the unsymmetrical configuration of the specimen influenced the flow of the load path. Accordingly, the applied load was transferred to the support, placed beneath the CS element. As a result, the second peak in the shear stress curve was associated with the formation of a diagonal splitting crack in the larger CS unit, Figure 2.34b. For testing samples in the couplet configuration, the testing set-up developed by van der Pluijm (1999) may be seen as a solution to avoid the mixed failure, and consequently to be able to capture the post-peak response.

The failure of the triplets was predominantly reported as interface debonding, while due to the configuration of the CS element masonry couplets, a mixed shear sliding-splitting failure mode was experienced, Figure 2.34b. At the lowest pre-compression level, the shear failure of the triplets was often reported along one or two interfaces without any mortar or brick failure. However, by increasing the pre-compression level, the interface debonding of triplets accompanied the mortar failure, near the extremities, Figure 2.31b–Figure 2.32b. In addition, in the case of perforated clay masonry, tiny splitting cracks also appeared in bricks, particularly corresponding to holes, Figure 2.32c.

**Table 2.11:**

Overview of shear properties of unit-mortar interface. Coefficient of variation in parentheses.

Masonry type	$f_{vo}$ MPa	$\mu$ -	$\mu_{res}$ -	$G_m$ MPa	$G_{fII}$ N/mm	$\Psi_0$ -
MAT-1	0.14	0.42	0.58	717 (65%)	$-0.09f_p+0.17$	0.26
MAT-2	0.15	0.87	0.76	1161 (%)	$-0.01f_p+0.02$	0.26
MAT-3	0.20	0.69	0.69	165 (13%)	$0.53f_p-0.04$	0.50
MAT-5	0.83	1.48	-	342 (%)	-	-

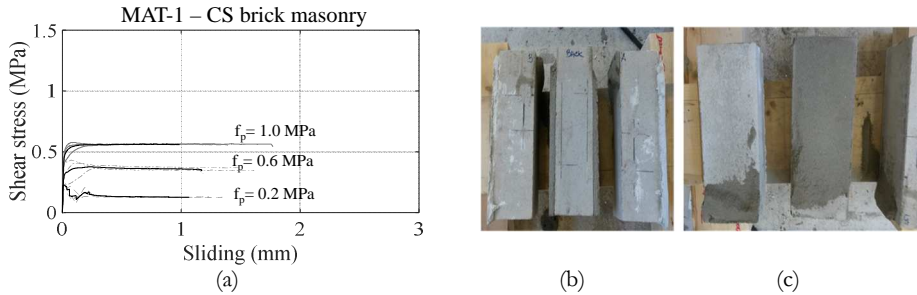


**Figure 2.31:** Shear-sliding behaviour at the brick-mortar interface of MAT-1 CS brick masonry triplet: (a) shear stress-sliding curves at three different pre-compression levels,  $f_p$ ; typical failure pattern: (b) front side; (c) lateral side.

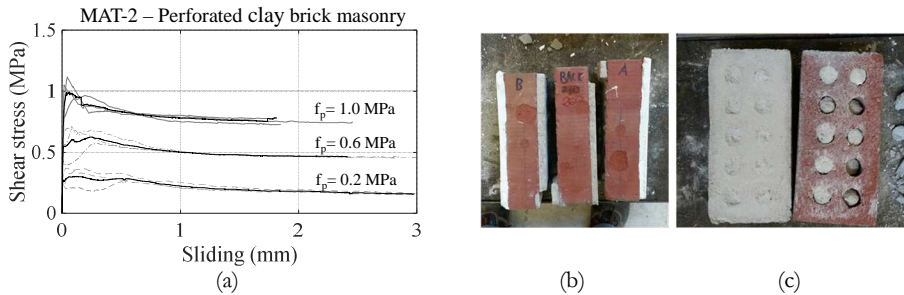


**Figure 2.32:** Shear-sliding behaviour at the brick-mortar interface of MAT-2 perforated clay brick masonry triplet: (a) shear stress-sliding curves at three different pre-compression levels,  $f_p$ ; typical failure pattern: (b) front side; (c) lateral side.

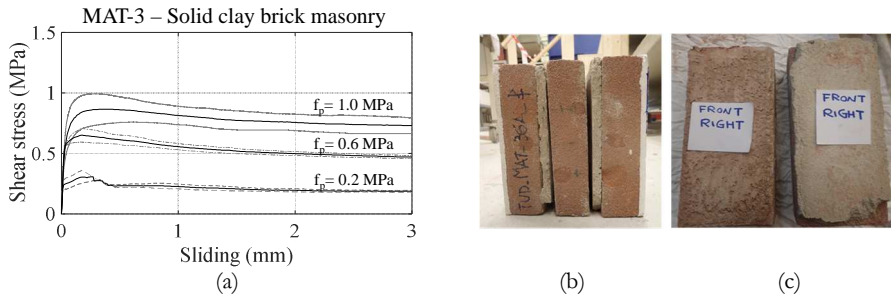


**Figure 2.33:** Shear-sliding behaviour at the brick-mortar interface of MAT-3 solid clay brick masonry triplet: (a) shear stress-sliding curves at three different pre-compression levels,  $f_p$ ; typical failure pattern: (b) front side; (c) lateral side.

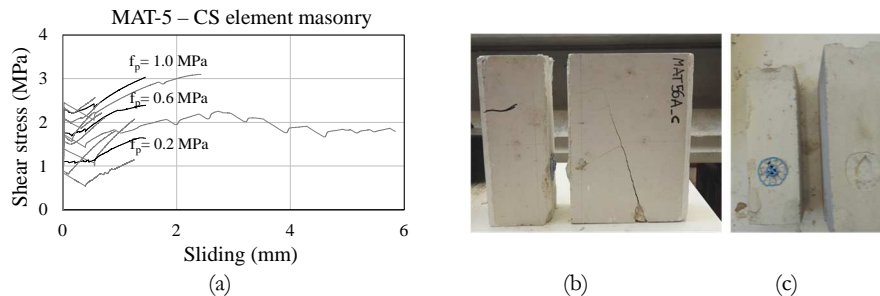


**Figure 2.34:** Shear-sliding behaviour at the brick-mortar interface of MAT-5 CS element masonry couplet: (a) shear stress-sliding curves at three different pre-compression levels,  $f_p$ ; typical failure pattern: (b) front side; (c) lateral side.

## 2.6.4 Cohesion and friction coefficient

As masonry failure was governed by the shear-sliding along the interface, the shear strength of the unit-joint interface can be represented by the Coulomb friction criterion. As reported by Atkinson et al. (1989), the linear relationship between shear strength and normal compressive stress remains valid only at moderate compressive stress levels, at which the nonlinear behaviour of mortar is trivial. Experimental investigation by Rahman and Ueda (2013) showed that at compressive stress levels higher than 1.0 MPa, the failure envelope exhibited a nonlinear trend. In this study, the pre-compressive stress was always kept lower than 1.0 MPa, thus assuming a linear failure criterion.

Previous experimental studies found that the values of cohesion could be influenced by the mortar compressive strength as well as the surface characteristics of bricks. In this study, the highest value of cohesion belonged to the CS element masonry built with a thin mortar layer, having the highest value of the mortar compressive strength,  $f_m=16.1$  MPa. However, the lowest value of cohesion was not found for the perforated clay brick masonry with the lowest values of mortar compressive strength. As concluded by Groot (1997), apart from mortar compressive strength, the mortar composition, and the physical characteristics of bricks, such as surface roughness and water retention, could largely influence the cohesion.

In this study, the initial friction coefficient of brick masonry ranged between 0.42 and 0.87, while the CS element couplets showed a much larger value,  $\mu=1.48$ . The lowest friction coefficient was found for the MAT-1 CS brick masonry triplets ( $\mu=0.42$ ), which can be explained by the very smooth surface of the CS brick. In addition, the fracture surface of the MAT-1 CS brick masonry was often described as smooth and without any mortar failure. By contrast, MAT-2 perforated clay bricks showed a rough fracture surface, thus leading to the highest value of friction coefficient for the analysed brick masonry types. Although the MAT-5 CS element masonry couplets formed a very smooth fracture surface, surprisingly a very high value for the friction coefficient ( $\mu=1.48$ ) was found. Currently there is no convincing explanation for such deviant behaviour; therefore, the author suggests performing more tests on CS element masonry to ensure the reproducibility of the test results. In conclusion, the coefficient of friction can be greatly affected by the roughness of the brick, mortar and fracture surface.

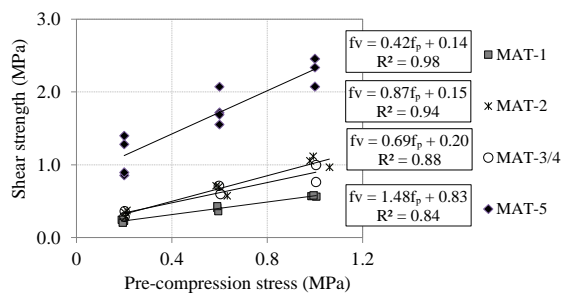


**Figure 2.35:** Evaluation of cohesion (initial shear strength) and friction coefficient in the frame of the Coulomb failure criterion.

## 2.6.5 Residual friction coefficient

In the frame of the Coulomb friction model, the residual friction coefficient was determined for brick masonry assuming a linear relationship between the residual shear strength and the pre-compression level. The residual friction coefficients of all the investigated masonry types are reported in Table 2.11. The residual friction coefficient of the MAT-5 CS element masonry was not characterised, since the testing configuration did not allow for capturing the post-peak response.

A difference was noticed between the residual and the initial friction coefficients, as the progressive debonding mechanism could alter the roughness of the fracture surface. The residual friction coefficient of the studied masonry types ranged between 0.58 and 0.76. Like the initial friction coefficient, the lowest and the highest residual friction coefficients were obtained for the MAT-1 CS brick masonry and MAT-2 perforated clay brick masonry, respectively. For the Dutch brick masonry types, van der Pluijm (1999) reported higher values of the residual friction coefficient, varying between 0.74 and 1.00. To define a single value of the residual friction coefficient independent from masonry type, van der Pluijm (1999) and Rots et al. (1997) performed a linear regression analysis considering all the results of the analysed brick masonry types. Accordingly, for the investigated brick masonry types, the mean value of the residual friction coefficient is equal to 0.68, with a high level of accuracy ( $R^2 > 0.92$ ), as seen in Figure 2.36.

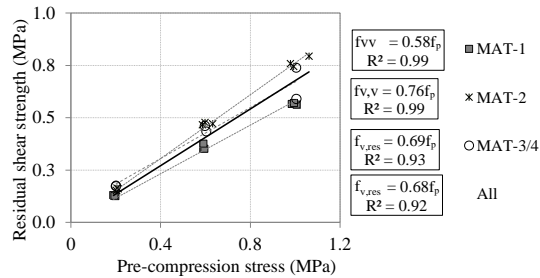


**Figure 2.36:** Evaluation of the residual friction coefficient for each masonry type as well as the mean value of residual friction coefficient by considering the results of all masonry types.

### 2.6.6 Shear modulus of the mortar joint

The variation of the shear stiffness versus the normalised shear stress is presented in Figure 2.37. For every masonry type, the curves are presented up to the peak load (i.e. a normalised stress of 1). Table 2.11 reports the mean values of the shear modulus of the mortar joint.

Generally, no considerable change in the shear modulus of the mortar joint was noticed with an increase in the pre-compression level, particularly in the case of the MAT-3 solid clay brick masonry and the MAT-5 CS element masonry. No clear dependency between the shear modulus of the mortar joint and the mortar strength was observed. The highest value of the shear modulus belonged to MAT-2 perforated clay brick masonry, while the lowest value of shear stiffness was recorded for MAT-3 solid clay brick masonry built with the weakest mortar, having a compressive strength of 3.81 MPa.

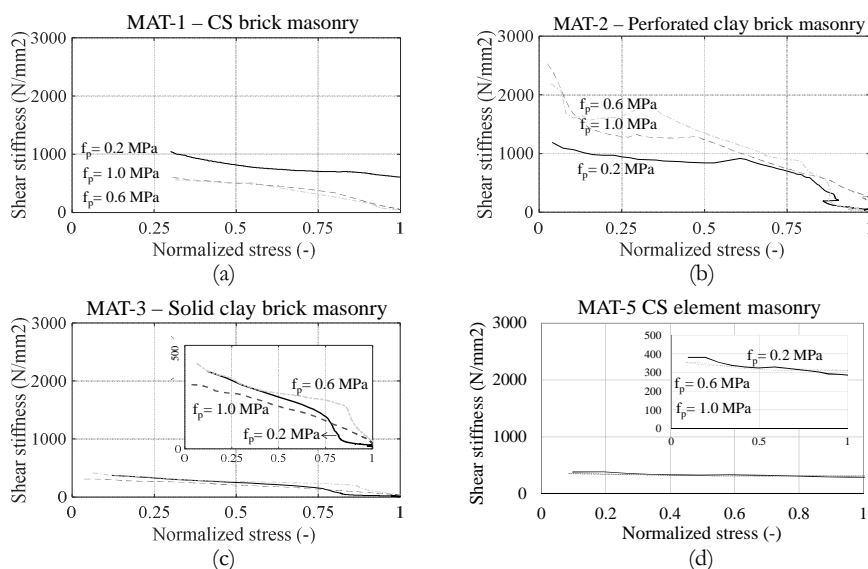


**Figure 2.37:** Variation of shear modulus of the mortar joint versus normalised shear stress: (a) MAT-1 CS brick masonry; (b) MAT-2 perforated clay brick masonry; (c) MAT-3 solid clay brick masonry; (d) MAT-5 CS element masonry.

## 2.6.7 Cohesion softening and mode-II fracture energy

The nonlinear softening attributed to the cohesion mechanism of quasi-brittle materials, like masonry, can be described by the mode-II fracture energy. The linear variation of the fracture energy,  $G_{f-II}$ , as a function of the pre-compression stress is plotted in Figure 2.38. Although these results corroborated the findings of previous researchers (e.g., van der Pluijm, 1999; Augenti & Parisi, 2011), they call into question whether mode-II fracture energy is a real material property. Nevertheless, mode-II fracture energy at zero pre-compressive stress is often used as an input for numerical analysis.

It could be expected that masonry with a rough surface corresponds to higher values of fracture energy. Using a linear regression analysis, MAT-1 CS brick masonry and MAT-3 solid clay triplets showed an increasing trend in the fracture and pre-compression stress. However, MAT-2 perforated clay brick masonry showed an inverse trend, as by increasing the pre-compression level the transition from shear strength to residual strength became very smooth. In general, clay brick masonry with a rough fracture surface corresponds to higher fracture energy than CS brick masonry with a smooth fracture surface.

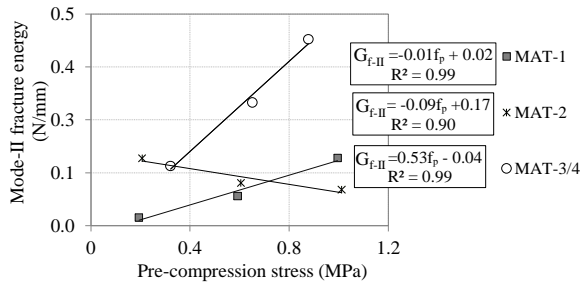


**Figure 2.38:** Variation of mode-II fracture energy as a function of the pre-compression stress for brick masonry types.

## 2.6.8 Dilatancy

As supported by experimental and numerical evidence, when a brick-mortar interface is subjected to shear loading, an uplift of the joint is expected at the onset of cracking (e.g., van der Pluijm, 1993; van Zijl, 1996). In confined masonry, this phenomenon, known as dilatancy, could lead to a local increase in normal stress and thus an increase in shear strength. Ignoring the dilatancy (i.e. assuming  $\psi=0$ ) often results in a non-conservative prediction of the masonry response (e.g., van Zijl et al., 2001; van Zijl, 2004).

The normal displacement of the joint was affected by the level of pre-compression and the surface smoothness. The variation of the normal deformation as a function of sliding is shown in Figure 2.39. The slopes of these curves reflect the dilatant behaviour of the joint. At the lowest pre-compression level, the three brick masonry types resulted in the same trend. First, a progressive uplift of the joint was observed. However, as the sliding increased further, damage to the asperities continued at a lower rate. Eventually, no further wearing of the asperities was observed, as the rate of variation of the normal deformation became almost



constant. As the pre-compression level increased, two distinct behaviours were observed for clay and CS brick masonry. Generally, by increasing the pre-compression level, both clay brick masonry types, i.e. MAT-2 perforated clay and MAT-3 solid clay brick masonry, showed a lower uplift of the joint, but the trend of the curve did not change. By contrast, the dilatant behaviour in the MAT-1 CS brick masonry disappeared with an increase in the pre-compression level. In the case of CS element masonry, no reliable measurements of uplift of the joint were obtained. In conclusion, the dilatant behaviour depends considerably on the pre-compression level and the roughness of the fracture surface. The values of dilatancy at zero normal confining stress and shear-sliding are reported in Table 2.11. The lowest value belonged to MAT-1 CS brick and the highest for MAT-3 solid clay brick masonry triplets.

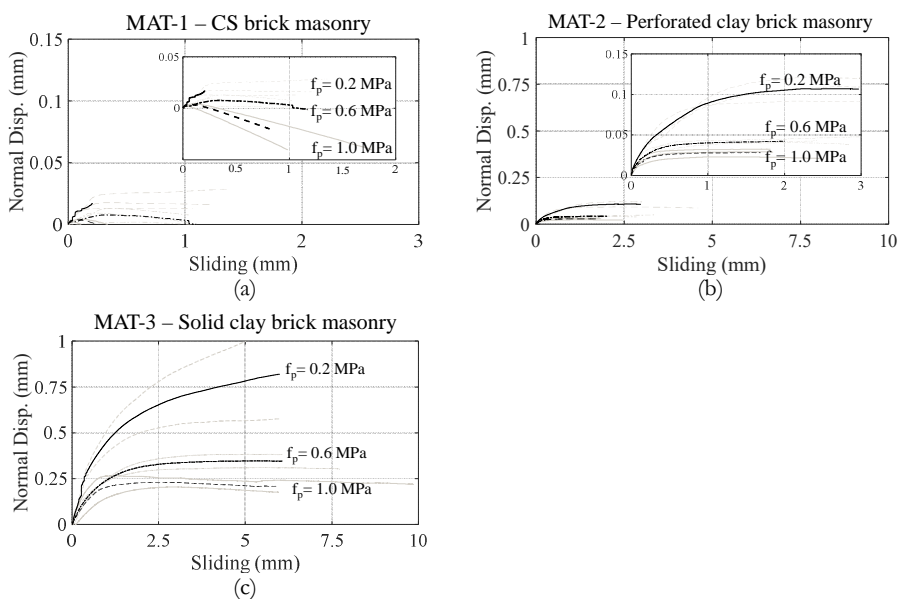


**Figure 2.39:** Variation of normal displacement versus shear-sliding of the unit-mortar interface: (a) MAT-1 CS brick masonry; (b) MAT-2 perforated clay brick masonry; (c) MAT-3 solid clay brick masonry.

## 2.7 CONCLUDING REMARKS

Through a systematic experimental approach, this chapter has presented a detailed overview of the compression, bending, and shear response of the five most common Dutch masonry types. These masonry types were reproduced in the laboratory to resemble the typical characteristics of the Dutch buildings identified in the Groningen region, as will be further discussed in Chapter 3. The adopted masonry types were as follows: MAT-1 single-wythe calcium silicate (CS) brick masonry, MAT-2 single-wythe perforated clay brick masonry, MAT-3 single-wythe solid clay brick masonry, MAT-4 double-wythe solid clay brick masonry, and MAT-5 single-wythe CS element masonry. Despite the difficulties during the construction, handling and testing of the specimens, in particular the double-wythe and CS element wallets, the specimen dimensions conformed to the outline of the European standards. The main contribution of this chapter is providing a comprehensive pool of experimental knowledge about the complete nonlinear behaviour of the five different masonry types, including the characterisation of stiffness, strength and toughness properties as well as the orthotropic response under compression and bending loads. This was achieved in light of well-designed, displacement-controlled or crack width-controlled testing set-ups. The outcomes of this chapter, together with the experimental data on field-extracted masonry presented in Chapter 3, support the definition of a constitutive law and a correlation study between different mechanical properties, which will be presented in Chapter 6.

Masonry under *compressive load* showed nonlinear behaviour caused by the complex interaction between the masonry constituents (e.g., the masonry units and mortar joints) each having different elastic properties. Upon increasing the load, diffused micro-cracks grew and coalesced into macro-cracks resulting in the localisation of deformations and thus masonry failure. The wallets showed a complex crack pattern with damage distributed across both their length and width. Generally, under vertical compression loading the nonlinearity started as splitting cracks formed in the bricks. However, under horizontal loading, the interface debonding was the prominent cause of nonlinearity. In the nonlinear pre-peak phase, the stiffness degradation under the horizontal configuration was higher than under the vertical configuration. In the post-peak phase, higher values of strain were attained under horizontal compression loading than under vertical compression loading. It was observed that unlike in brick masonry, the compressive strength of CS element masonry did not lie between the compressive strengths of its constituents; indeed it was remarkably lower than these. This observation highlights the effect of joint thickness on masonry strength. Like compressive strength, Young's modulus was significantly influenced by the wythe number and the joint thickness. Unlike the brick masonry types, the stiffness of the CS element masonry with a thin layer of joint was not affected by the loading direction and was similar to the unit stiffness. Given the compressive fracture energy of brick masonry types, similar values of fracture energy were obtained under the vertical configuration, while larger differences were observed under the horizontal configuration. The large CS element

wallets showed a local brittle failure, and thus the post-peak response was not captured.

Masonry under *bending load* showed brittle or quasi-brittle behaviour. The instant of unstable crack growth along a single or multiple bed joints often hindered the capture of the post-peak softening branch, especially in the case of CS element masonry. Generally, it was observed that the beginning of the nonlinearity in the moment-curvature diagram was earlier under horizontal out-of-plane bending than under vertical out-of-plane bending. Regarding the in-plane behaviour, a similar or a shorter linear branch was found than that under horizontal out-of-plane bending. Under vertical out-of-plane bending load, the fracture plane often occurred along the bed joint due to interface debonding rather than the tensile failure of brick. This could be interpreted as a sign of masonry with a weak bond along the interface. Under horizontal out-of-plane bending load and in-plane bending load, the masonry failed by two distinct failure modes: diagonal debonding along multiples interfaces, and vertical splitting failure. The former failure often started by debonding along a head joint and thereafter by a stepwise crack. Under out-of-plane bending loads, bed joints underwent both shearing and twisting deformations. In addition to the bending tests, bond wrench tests were performed. A one-to-one correspondence was found between the flexural strength under vertical out-of-plane bending load and the bond strength, except for MAT-2 perforated clay brick masonry which had higher values of flexural strength than bond strength. Such a difference can be explained in that the contribution of the dowel action is greater in the bending test with multiple joints than in one joint during the bond wrench test. Unlike the vertical out-of-plane bending test, the masonry with the highest value of bond strength did not show the highest value of flexural strength in the horizontal out-of-plane bending test. The highest value of flexural strength in both the horizontal out-of-plane and in-plane bending tests belonged to perforated clay brick masonry, implying the importance of the dowel action created by the portion of mortar filling the brick perforations. No size effect under vertical out-of-plane bending or in-plane bending was noticed, while under a horizontal out-of-plane bending load, a 40% reduction in the flexural strength of double-wythe masonry with respect to single-wythe masonry was observed. As expected, the values of fracture energy were higher under in-plane, horizontal out-of-plane, and vertical out-of-plane loading. Bending tests can indirectly provide insight into tensile properties, which are required for the nonlinear structural assessment. To this end, the values of uniaxial tensile strength were evaluated as the stress corresponding to the onset of cracking. For brick masonry types, the ratio between tensile strength and flexural strength ranged between 0.36 and 0.73, with an average ratio of 0.51, while for CS element masonry a higher ratio varying between 0.53 and 0.90 was found.

The behaviour of the unit-mortar interface of triplets/couplets under combined *compression-shear loading* was governed by de-cohesion and friction mechanisms. At the lowest pre-compression level, the shear failure of the triplets was often reported along one or two interfaces without any mortar or brick failure. However, by increasing the pre-compression level, interface debonding accompanied the mortar failure, near the extremities. As masonry failure was governed by the shear-sliding

along the interface, the shear strength of the unit-mortar interface can be represented by the Coulomb friction criterion. It was observed that cohesion was greatly affected by the properties of the mortar and the characteristics of the masonry unit. However, it was concluded that the coefficient of friction was influenced by the roughness of the brick, mortar and fracture surface, while it was independent from the mortar strength. Moreover, a difference was noticed between the residual and the initial friction coefficient, as a progressive debonding mechanism could alter the roughness of the fracture surface. Regarding the mortar joint shear modulus, no considerable change was noticed with an increase in the pre-compression level, particularly in the case of MAT-3 solid clay brick masonry triplets and MAT-5 CS element masonry couplets. In addition, no clear dependency of the mortar joint shear modulus on the mortar compressive strength was evident. The fracture energy was linearly affected by a change in the pre-compression level, whereas both increasing and decreasing trends were found for different masonry types. The dilatant behaviour showed considerable dependency on the pre-compression level and the smoothness of the fracture surface. Accordingly, in the case of CS brick masonry with a smooth fracture surface, the dilatant behaviour was not as dominant as in the case of solid clay brick masonry with a rough fracture surface.

# MATERIAL PROPERTIES OF DUTCH MASONRY BUILDINGS BUILT BETWEEN 1912 AND 2010: LABORATORY AND IN- SITU TESTS

---

Confidence levels in the structural analysis of existing masonry buildings can be improved by well-characterised material properties and clear insight into their statistical distributions. The negligence of uncertainties in the modelling process means that we incorporate a set of tacit assumptions. Therefore, the more rigorously the input parameters are defined, the more reliable the prediction models. The source of uncertainties regarding material properties can often be traced back to the lower accuracy of in-situ testing methods in comparison to laboratory tests, the limited possibility of performing enough tests, and a lack of insight into the statistical distribution of material properties.

The restrictions and limitations of the available testing methods add uncertainty to the material properties, and thus to the structural analysis. Many uncertainties still exist regarding the relationship between the material properties established through laboratory testing and those determined using in-situ testing methods. The invasive laboratory tests on field-extracted samples are often challenged from the viewpoint of the cutting process and transportation, threatening the integrity of the samples, and an expectation that the ‘best pieces’ of masonry have been selected for sampling. However, in-situ tests call into question the impact of unknown parameters, such as boundary conditions. Generally, the selection of the type of tests to characterise the material properties of masonry can be made based on a pragmatic compromise between the induced damage, speed, and cost.

When it is not possible to perform tests, either due to the risk of interference in the building integrity/functionality (e.g., in historical buildings) or a lack of financial resources, building codes and national regulations should give a clear indication of the material properties of the regional building stock. To this end, some countries with a long history of seismic activity, such as New Zealand, Turkey, and Italy, have broadened their knowledge on the mechanical characteristics of their most vulnerable building typologies. Often they have performed a significant number of laboratory tests on field-extracted samples as well as in-situ testing, providing insight into the compression, bending, and shear properties of existing masonry in terms of strength and stiffness, while often paying less attention to toughness (e.g., Russell, 2010; İspir, 2010; Lumantarna, 2012; Almesfer et al., 2014). Despite the valuable contributions of these studies in the realm of masonry characterisation, the mechanical properties ascertained in

one region cannot easily be extrapolated to other parts of the world, as masonry origins strongly vary from a geographical and historical perspective.

To deal with uncertainties in material properties that arise from the inter- and intra-buildings variability of material properties, knowledge about the statistical distribution of material properties is required. Traditionally, a normal distribution is typically assumed for the statistical analysis of concrete and masonry. Similarly, standard EN 1052-1 (CEN 1998) suggested finding the characteristic compressive strength of masonry, while assuming a normal probabilistic model (5% percentile). Unlike concrete, so far limited studies have delved into the statistical analysis of the material properties of existing masonry.

Considering the limitations of the Dutch as well as the international literature, the outline of this chapter is as follows: first, an overview of the testing campaign is provided, whereby 15 different buildings, representative of the Dutch unreinforced masonry (URM) building stock and built between 1912 and 2010, were selected as case studies. From each building, masonry samples were extracted and transported to the laboratories, where a complete picture of the masonry properties was investigated in terms of stiffness, strength, and toughness under compression, bending, and shear loading. Apart from the laboratory tests, in-situ semi- and non-invasive tests were performed (by a qualified engineering company). Next, a comparison is made between the material properties obtained from the tests on medium-sized specimens tested in the laboratory and from the in-situ tests. Because the tests were performed on multiple buildings, we were able to compile a dataset of material properties and analyse their statistical distributions. In addition, the material properties are further refined with respect to unit type, year of construction, and quality (when possible).

The major contributions of this chapter are to investigate the presence of any link between the material properties obtained from in-situ non- and semi-invasive testing methods and those obtained from destructive laboratory tests; to provide new insights into the nature of variation in the material properties of masonry; and to offer a regional dataset of material properties, which together with previously available literature data, is incorporated into the formulation of the Dutch standard for the assessment of existing URM buildings due to induced earthquakes.

### **3.1 OVERVIEW OF TESTING PROGRAMME ON FIELD-EXTRACTED SAMPLES**

To incorporate the uncertainty in structural analysis that arises from an insufficient number of tests, Eurocode 8 (EN 1998-3:2005) suggests reducing the mean values of material properties using a confidence factor. As stated in Eurocode 8, each type of analysis (i.e. linear elastic and nonlinear methods) requires a certain level of knowledge about material properties and geometrical and structural details. Accordingly, Eurocode 8 introduces three different knowledge levels, namely limited (KL1), normal (KL2), and full (KL3), each corresponding to a different value of confidence factor, Table 3.1. The knowledge

level depends on the extent of information gathered from the in-situ inspection and the possibility of testing on each floor. As expected, the better the knowledge level, the lower the confidence factor, which ranges from 1.35 to 1.00 from limited to full knowledge level. To move from a limited to a full knowledge level, the number of samples per test for each floor should be increased from one to three, thus avoiding a reduction in the material properties of up to 35%.

As Willis (2004) stated, a definite source of spatial variability in masonry material properties can be traced back to the intrinsic nature of masonry constituents, workmanship, weathering, and aging conditions. For instance, in the Netherlands, the masonry of Dutch URM dwellings has gradually evolved over the years, and still shows innovation in recent construction. Accordingly, it is expected that the material properties could be affected over time, either due to the improvement in the quality of masonry components or in the quality of the workmanship. At this moment, the Netherlands, with its recent experience of seismic events, suffers from the lack of a regional database containing the material properties of the most typical masonry types. Previous literature on Dutch URM mainly dealt with the laboratory testing of reproduced single-wythe clay and calcium silicate (CS) brick masonry specimens, whereas stiffness and strength were the most studied mechanical properties and emphasis was gradually also placed on the characterisation of the post-peak degradation in connection to early nonlinear FEM applications (e.g., see Rots et al., 1997; van der Pluijm, 1999; and Vermeltfoort, 2005). It could be assumed that through the replication of samples, the intrinsic variability of the material properties was to some extent overlooked.

An evaluation of the seismic assessment of URM structures in the Netherlands reveals the flaws in the Dutch standard guidelines and the international literature. The NEN 6790(2005) standard lags behind in terms of seismic provisions and suffers from the lack of a regional database of material properties. Furthermore, the international literature does not give a clear indication on the statistical distribution of material properties, and it does not thoroughly address any differences in the material properties due to the use of different testing methods.

An extensive experimental campaign was performed in the Netherlands in the context of a structural upgrading project, incorporating both laboratory tests on field-extracted samples and in-situ semi- and non-destructive tests. By means of the laboratory tests, detailed insights were gained into the comprehensive behaviour of masonry under compressive, bending, and shear loading. Through the in-situ tests, limited knowledge was gained about the masonry properties and quality.

**Table 3.1:**  
Knowledge level and corresponding confidence factors.

Knowledge level	Material test	No. tests per floor	Confidence factors
Limited knowledge (KL1)	Limited in-situ testing	1	1.35
Normal knowledge (KL2)	Extended in-situ testing	2	1.20
Full knowledge (KL3)	Comprehensive in-situ testing	3	1.00

In the first step, visual inspection along with construction drawings, if available, allowed for the collection of overall knowledge about the physical characteristics of the Dutch buildings, in terms of geometry and construction details. During the survey, information on the masonry type, floor system, and presence of connecting ties in cavity walls was gathered. Moreover, demolishing some of the damaged houses enabled the detection of hidden structural elements such as wall-to-floor connections (Figure 3.1a), connections between wall-to-timber floors (Figure 3.1b), insight into the timber joists (Figure 3.1c) as well as knowledge on the depth and types of foundation (Figure 3.1d). For more information, readers are referred to Zapico Blanco et al. (2018).

In the second step, the monitoring and instrumentation of the buildings allowed for the detection of possible sources of damage in the building. Under ambient and low excitation vibrations, the structural response was recorded for a limited number of houses. To this end, triaxial seismometers were placed in multiple locations, thus enabling the evaluation of the dynamic characteristics of the structure. For more information regarding the monitoring, readers are referred to Graziotti et al. (2014).

In the third step, laboratory destructive testing on field-extracted samples as well as in-situ tests were performed, aiming to reverse the lack of knowledge on the material properties of Dutch URM. Before any testing activity, every single building was visually surveyed. The aim was to prepare a plan of approach, whereby the potential testing activities as well as the sampling strategies, including sampling priorities, numbers and geometries of the required samples, were determined (see Zapico Blanco et al., 2018). The testing program was a collaboration between several universities, research institutions, and engineering companies, and was completed over three phases as follows:

- *Testing campaign 2014*: With technical coordination from Arup, laboratory tests on extracted samples and in-situ tests were carried out by TU Delft and EUCentre, respectively. The testing campaign was later interwoven with similar laboratory and in-situ tests conducted by B|A|S with technical coordination from Arcadis and partly Arup. After an a posteriori (re)analysis of the experimental results, only the values of compressive strength as well as bond strength provided by B|A|S were considered in this study (nonnekes, 2015a; Nonnekes, 2015b; Nonnekes, 2015c).
- *Testing campaign 2015*: Laboratory tests were carried out by TU Delft and TU/e, and in-situ tests were performed by EUCentre, with technical coordination from Arup.
- *Testing campaign 2016/2017*: Laboratory tests were performed by TU Delft, while Arup supported the extraction and transportation of samples.



The in-situ tests, performed under the supervision of EUCentre, were complementary to the laboratory tests, conducted mainly by TU Delft in collaboration with TU/e and B|A|S. The in-situ tests were planned in an aim to investigate the suitability of the semi-invasive double flat-jack and shove tests for the case of Dutch walls with low overburden and slender load-bearing walls, as well as for calibrating the non-invasive testing methods, including Schmidt hammer, penetrometer, and ultrasonic tests.

In total, 15 different buildings, deemed to be representative of the Dutch URM building stock, were selected as case studies for the inspection, monitoring and testing, comprising 12 residential buildings and three schools. During the inspection and the sampling from each building, more than one masonry type was often identified because of the extension of the building during different periods, the use of different materials, and variations in masonry quality within a wall or between different walls. Accordingly, further divisions for these buildings were made to consider such differences. As a result, we made 26 sub-divisions of masonry types, treating each as a separate object (Zapico Blanco et al., 2018). Thus, throughout this chapter ‘objects’ refer to the different masonry types. An overview of the tested buildings and their specifications, including the year of construction and their typology, are listed in Table 3.2. For the sake of simplicity, a code letter was assigned to each individual building, whereas the letter after the hyphen refers to the type of building, with ‘H’ for the houses, and ‘S’ for the schools. Despite an extensive effort, it was seldom possible to extract a full set of samples from each object to provide a complete description of its material properties. Table 3.3 presents an overview of the number of the extracted samples tested under compression, bending, and shear loading. Following the outline of ASTM C1532(2005), the extracted samples were separately packed and later delivered to the laboratories, Figure 3.2.



(a) three leaves interconnected with ties



(b) connections between planks and timber joist



(c) joist pockets



(d) footing

**Figure 3.1:** Examples of information collected during demolition of a detached house with typical architecture built in 1930. Photos taken by the author.



**Figure 3.2:** Overview of packed samples extracted from the field and delivered to Stevin II laboratory.

**Table 3.2:**

Overview of the buildings investigated within the testing campaign of 2014–2017 by TU Delft (ARUP, 2015; Jafari & Esposito, 2018), excluding the houses tested by B|A|S.

Building	Code	No. of objects	Year. const.	Description
	HOG-H	1	1912	- Detached house. - Sampling from single-wythe walls
	WIR-H	1	1920	- Detached house - Walls both in single- and double-wythe - Sampling only from single-wythe walls
	MID-H	2	1920	- Large masonry villa. - Walls both in single- and double-wythe clay brick masonry - Sampling from both single- and double-wythe walls
	ROE-S	5	1922	- School was extended in 1955 and 1985 - Cavity wall system. Inner leaf and outer leaf in clay brick masonry - Sampling from both inner and outer leaf constructed in 1922, as well as clay brick masonry built in 1955 and 1985 - Masonry with two different qualities were identified when extracting sampling from the walls built in 1985
	MOL-H	2	1932	- Detached house - Walls both in single- and double-wythe clay brick masonry - Sampling from both single- and double-wythe walls
	WIL-H	2	1952	- Terraced house - Cavity wall system. Inner leaf in CS bricks and outer leaf in clay brick masonry - Sampling from both inner and outer leaf

**Continuation of Table 3.2:**

Overview of the buildings investigated within the testing campaign of 2014–2017 by TU Delft.

Building	Code	No. of objects	Year. const.	Description
	BEA-S	2	1955	<ul style="list-style-type: none"> <li>- School was extended in 1</li> <li>- Cavity wall system. Inner leaf and outer leaf in clay brick masonry</li> <li>- Sampling only from inner leaf</li> </ul>
	BEA-H	1	1958	<ul style="list-style-type: none"> <li>- Terraced house</li> <li>- Cavity wall system. Inner leaf in CS bricks and outer leaf in clay bricks</li> <li>- Sampling only from inner leaf</li> </ul>
	ZIJL-H	1	1976	<ul style="list-style-type: none"> <li>- Corner house</li> <li>- Cavity wall system. Inner leaf in CS bricks and outer leaf in clay bricks</li> <li>- Sampling only from inner leaf</li> </ul>
	LAG-H	1	1978	<ul style="list-style-type: none"> <li>- Detached house</li> <li>- Cavity wall system. Inner leaf in CS bricks and outer leaf in clay brick masonry.</li> <li>- Sampling from both inner and outer leaf</li> </ul>
	TRIA-S	2	1984	<ul style="list-style-type: none"> <li>- School</li> <li>- Cavity wall system. Inner leaf in CS bricks and outer leaf in perforated clay brick masonry.</li> <li>- Sampling from both inner and outer leaf</li> </ul>
	SCH-H	1	1987	<ul style="list-style-type: none"> <li>- Terraced house</li> <li>- Cavity wall system. Inner leaf in CS and outer leaf in clay brick masonry</li> <li>- Sampling from both inner and outer leaf</li> </ul>

**Continuation of Table 3.2:**

Overview of the buildings investigated within the testing campaign of 2014–2017 by TU Delft.

Building	Code	No. of objects	Year. const.	Description
	TIL-H	2	1990	- Detached house - Cavity wall system. Inner leaf in CS and clay bricks and outer leaf in clay brick masonry - Sampling from both inner and outer leaf
	KWE-H	2	1995	Detached house - Cavity wall system. Inner leaf in CS and clay bricks and outer leaf in clay brick masonry - Sampling from both inner and outer leaf
	HOO-H	1	2013	- Detached house - Cavity wall system. Inner leaf in clay cellular concrete and outer leaf in clay bricks - Sampling only from outer leaf

**Table 3.3:**

Overview of tested objects and the tested number of specimens.

Type	Code	Y.o.C	Compression		Four-point bending			Bond wrench	Shear
			Vert.	Hor.	OOP1	OOP2	IP		
Clay brick masonry	Solid HOG-H1	1912	0	0	0	1	0	7	0
	Solid WIR-H1	1920	3	2	0	3	3	6	9
	Solid MID-H1.1	1920	3	0	0	0	0	0	9
	Solid MID-H1.2	1920	3	0	0	0	0	0	9
	Solid ROE-S1.1	1922	5	0	0	0	3	6	9
	Solid ROE-S1.2	1922	0	0	0	0	3	6	9
	Solid MOL-H1	1932	3	0	0	0	0	0	9
	Solid MOL-H2	1932	3	0	0	0	0	0	9
	Solid WIL-H2	1952	3	6	0	3	3	6	9
	Solid ROE-S2	1955	5	0	0	3	3	6	9
	Solid BEA-S1	1955	5	0	0	3	3	6	9
	Solid ROE-S3.1	1985	2	0	0	2	2	6	9
	Solid ROE-S3.2	1985	4	0	0	2	2	0	9
	Perforated TRIA-S2	1984	6	0	3	4	3	4	6
	Perforated TIL-H2	1990	0	0	3	3	3	13	0
Solid KWE-H2	1995	4	0	0	1	3	6	9	
perforated BEA-S2	2001	8	0	0	3	2	5	10	
Frogged HOO-H2	2013	5	0	0	0	2	3	9	
CS brick masonry	WIL-H1	1952	2	3	0	0	0	0	9
	BEA-H1	1958	2	2	0	0	0	2	9
	ZIJL-H1	1976	6	0	2	1	0	6	8
	LAG-H1	1978	3	3	0	0	2	5	9
	TRIA-S1	1984	5	0	1	0	3	8	9
	SCH-H1	1987	5	0	0	0	3	2	9
	TIL-H1	1990	3	3	0	0	0	0	6
	KWE-H1	1995	0	0	0	0	0	0	0

Tested by TUD

Tested by TU/e

Note that Y.o.C refers to the year of construction of the object. OOP1, OOP2, and IP refer to vertical out-of-plane bending, horizontal out-of-plane bending, and in-plane bending tests on wallets, respectively.

### 3.2 COMPARISON BETWEEN THE RESULTS OF LABORATORY AND IN-SITU TESTING METHODS

The in-situ tests can be classified as non-invasive tests and semi-invasive testing methods. The former are mainly adopted for the evaluation of uniformity and the diagnosis of damage and deterioration; however, due to their fast, simple, and non-intrusive nature, researchers have attempted to establish a relationship, though tenuous, between the outcomes of these tests and the material properties of masonry. Unlike non-invasive testing methods, semi-invasive test methods can provide direct information about the material properties. These tests are faster with respect to the laboratory test; nevertheless, the accuracy of the results is of concern (e.g., Binda et al., 1997; Graziotti et al., 2018a).

Non-invasive testing techniques often serve as an indication of the quality and homogeneity of brick and mortar, as well as masonry; nevertheless, attempts have been made in the literature to predict material properties. Non-invasive testing techniques do not disrupt the materials; hence, they are of particular relevance for historic preservation purposes. Brencich and Sterpi (2006) attempted to calibrate the Schmidt hammer procedure for the evaluation of the compressive strength of clay brick masonry. Unlike the standard approach that assumes a linear interpolation between the number of strokes and the compressive strength of masonry, they found that a bilinear or an exponential curve can better fit the experimental results. Nevertheless, they reported an error in the predicted compressive strength of masonry of up to 25%. They concluded that the predicted values of masonry compressive strength could be highly affected by the quality of workmanship. In addition, Benedetti and Pelà (2012) investigated the suitability of penetration equipment to predict the compressive strength of masonry constituents; however, the obtained results were considerably scattered, with a high error reaching up to 100%. In a recent study, Pelà et al. (2018) investigated the applicability of two penetrometric based techniques, namely the Helix Pull-out Test (HPT) and Pin Penetrometer Test (PPT), to evaluate the strength of historical mortar. Both testing methods, causing negligible damage to mortar, were able to capture the spatial variability of the mortar strength properties and thus allowed for discerning the different types of mortar. Although previous studies established tenuous relationships between the results of non-invasive testing methods and the mechanical properties of masonry as estimated with laboratory tests, no direct estimation of the mechanical properties can be provided using these testing methods. In addition, the accuracy of the test could be challenged with respect to the confinement of mortar exerted by the surrounding bricks (Vermeltfoort, 2005). Accordingly, it could be expected that the values of strength and stiffness are overestimated using the non-invasive tests (Benedetti & Pelà, 2012). Thus, it can be concluded that the main application of non-invasive testing techniques is narrowed down to identifying anomalies within a wall section (Schuller, 2003) as well as to providing preliminary information regarding the form and its condition (de Vekey, 1988). A review of the mainstream non-invasive testing methods can be found in a study by Schuller (2003).

The philosophy behind semi-invasive testing methods is to evaluate the mechanical properties of in-situ masonry by inducing limited and repairable damage to the structure. The double-flat jack tests and shove tests are known as the most common techniques to evaluate the deformation properties of masonry under uniaxial compressive load, and the shear properties along the brick-mortar interface, respectively. Double flat-jack tests can be performed in agreement with standard ASTM C1197-14a(2014), whereby a small portion of a masonry wall, often made of two bricks in length and five courses of brick in height, is subjected to a compressive stress-state by means of two flat-jacks placed at the extremities, Figure 3.3a. By gradually increasing the flat-jack pressure and continuously measuring the vertical deformations along the masonry portion, the elastic modulus of masonry can be evaluated. The double flat-jack test is often terminated in the linear phase, thus minimising the extent of damage to the wall, and providing the chance to perform a subsequent shove test in the same location. Accordingly, the two flat-jacks, already used during the double flat-jack test, are kept in place, and a full brick in the middle of the testing portion (both vertically and horizontally) is selected as a tested brick. In agreement with standard ASTM C1531-16(2016), the two bricks and head joints adjacent to the tested brick are removed, providing space for a horizontal jack to impose a shear load at one side of the brick and for free sliding of the brick at the other side, Figure 3.3b. Using the Coulomb strength criterion, the residual properties as well as the initial properties can be found. The difficulties in the test execution, particularly in the case of irregular stone masonry, was repeatedly reported by researchers, including Binda and Tiraboschi (1999). In addition, Simões et al. (2016) revealed that the accuracy of shove tests could be highly influenced by the wall composition (i.e. type and dimension of masonry unit and workmanship) as well as the site condition (i.e. boundary conditions and existing stress-state on the wall). Although extensive research has been carried out to determine the material properties of existing masonry using flat-jack based testing methods, there is a need for a comparative study to calibrate their results with respect to the material properties obtained from laboratory tests on extracted samples.



**Figure 3.3:** Semi-invasive in-situ tests performed by EUCentre on existing masonry: (a) double flat-jack test; (b) shove test. Photos were extracted from Graziotti et al. (2014).

As mentioned above, prior to sampling existing structures in the Groningen region, an in-situ testing campaign was conducted (Zapico Blanco et al., 2018). Within the scope of non-invasive testing methods, the rebound hammer test on brick, the penetrometric test on mortar, and the ultrasonic test on masonry walls were conducted. Besides these tests, in-situ double flat-jack tests and shove tests were conducted to evaluate the mechanical properties of the existing masonry, Figure 3.3. Due to the low overburden in the Dutch URM walls, the double flat-jack tests were conducted only in the initial linear phase (Zapico Blanco et al., 2018). Hence, no insight into the compressive strength of masonry was provided.

A correlation between the outputs of the Schmidt hammer test and the compressive strength of brick as well as the compressive strength of masonry wallets obtained from invasive laboratory tests is shown in Figure 3.4. It can be concluded that the results of the Schmidt hammer test can, in certain cases, provide an indication of the quality of brick and masonry. A similar conclusion was derived by Vasanelli et al. (2016), who found a weak correlation. Nevertheless, more tests are required to further enrich the dataset and thus allow for proper calibration of the non-invasive in-situ tests. Detailed information on the results of the non-invasive testing methods can be found in a dedicated report by EUcentre (2015).

The correlation between the mechanical properties, in terms of Young's modulus, cohesion, and friction coefficient, obtained from the laboratory tests on field-extracted samples and the in-situ semi-invasive tests is shown in Figure 3.5. A good correlation was only found for a limited number of objects, while for most of the objects a weak correlation was established. This inconsistency between the results of laboratory tests and in-situ tests may be explained by the fact that the portion of the masonry wall where the in-situ test is performed is not fully disconnected from the surrounding masonry, thus presenting different boundary conditions than in the laboratory tests. Moreover, another issue is attributed to the elaboration of the results of the shove test, as the stress distribution is altered due to the disturbance in the wall integrity. For this reason, attempts were made to re-evaluate the actual stress acting on the sliding brick due to the contribution of the flat-jacks as well as the contribution of overburden. Recent research on the effects of boundary conditions, dilatancy, and stress redistribution revealed valuable information about the shove test for single-wythe masonry walls (Graziotti et al., 2018a; Andreotti et al., 2018; Ferretti et al., 2019). However, more detailed measurements at this phase are required to further calibrate the outputs of the shove test, particularly in the case of double-wythe masonry walls.

In a complementary testing campaign, the author performed flat-jack based in-situ tests on a laboratory-made full-scale single-wythe CS brick masonry wall, aiming to minimise the influence of unknown parameters such as workmanship, quality of materials, and overburden on the testing results. Information about the testing procedure, data elaboration, testing results, and correlation with the results of laboratory tests can be found in Jafari et al. (2018a). The semi-invasive tests were performed at three different locations of the wall, while imposing different



values of overburden: 0.15, 0.25, and 0.6 MPa, Figure 3.6a. At each location, the single flat-jack, double flat-jack and shove tests were performed sequentially, Figure 3.6b. The ratio between the Young's modulus obtained from the double flat-jack tests and from the compression tests on the wallets stands for 1.1 and 2.2, as the values of the Young's modulus were evaluated, respectively, at 10% of the maximum stress and between 10% and 30% of the maximum stress. To correctly interpret the shove test results, the effective level of the normal compressive stress acting on the sliding brick was modified following the procedure suggested by Graziotti et al. (2018a). Accordingly, prior to the shove test, the double flat-jack test was performed in the shove test configuration. Assuming a linear relationship between the shear strength and the normal compressive stress acting on the sliding brick, the shear properties of the brick-mortar interface were evaluated according to the Coulomb failure criterion. Comparing the properties obtained from the shear-compression tests on triplets with the ones obtained from the shove test, it was revealed that the shove testing method overestimated the values of cohesion up to 60%. Since a limited number of shove tests was performed, more research is suggested, whereby experimental studies and numerical simulation are integrated.

In the case of the Dutch masonry with low overburden and slender load-bearing walls, no strong link between the results of laboratory tests on medium-sized specimens and flat-jack based testing methods was found, either for existing masonry or laboratory-made masonry. Moreover, the flat-jack based testing methods cannot provide information regarding the post-peak softening regime. Accordingly, there is a clear need for a testing method that can offer an acceptable compromise between the accuracy of the results and the introduced damage in the building. For this reason, Chapter 4 and Chapter 5 investigate the applicability of the core testing method, as a quick and efficient way to determine the mechanical properties of masonry.

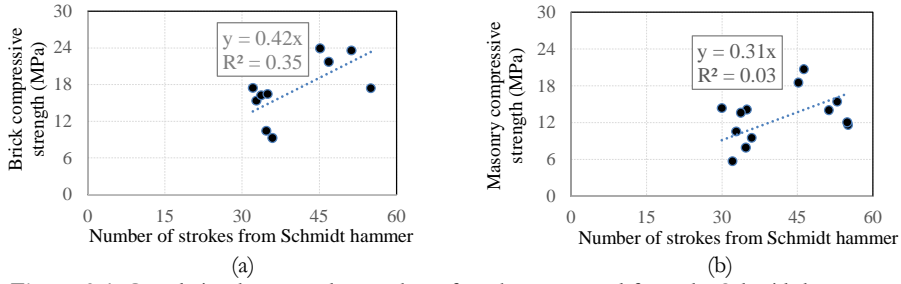


**Figure 3.4:** Correlation between the number of strokes measured from the Schmidt hammer test and (a) compressive strength of brick; (b) compressive strength of masonry wallets. Data are extracted from EUcentre (2015).

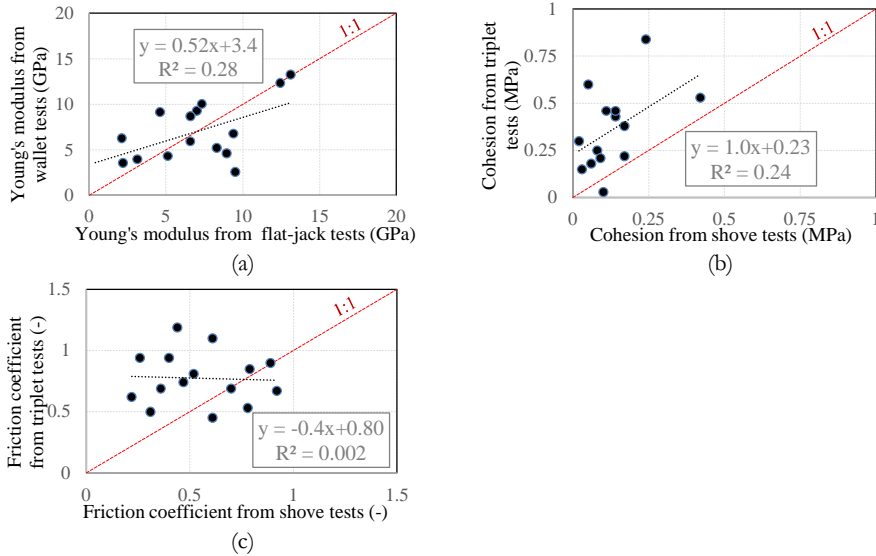


**Figure 3.5:** Correlation between the mechanical properties obtained from in-situ semi-invasive testing methods and laboratory tests on field-extracted specimens: (a) Young's modulus; (b) cohesion; (c) friction coefficient. Data are extracted from EUcentre (2015).

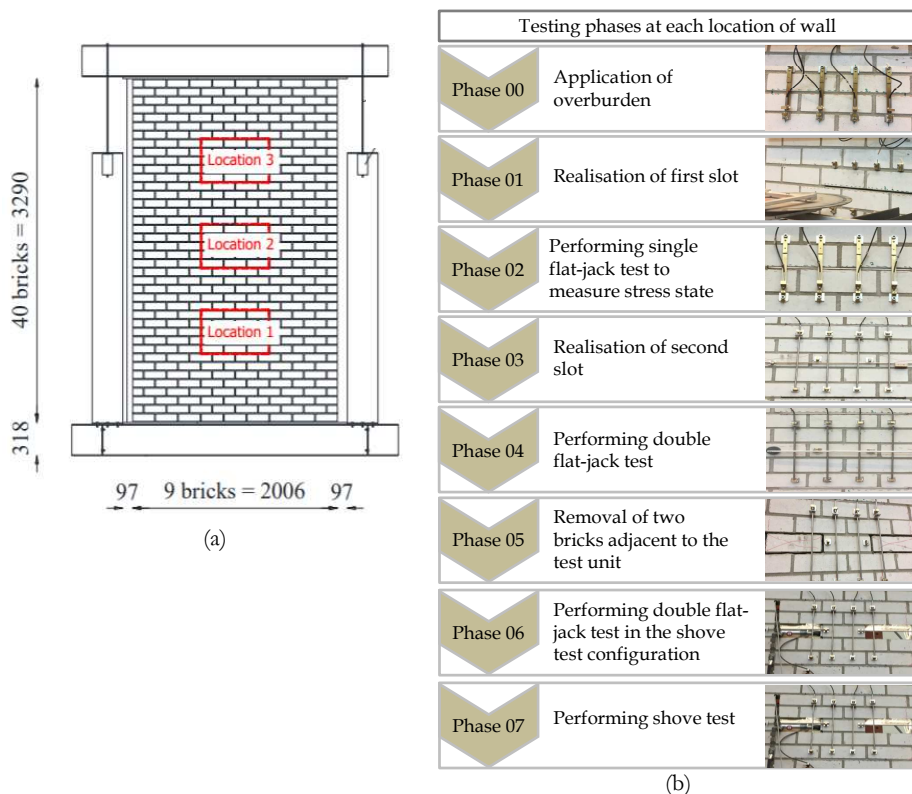


**Figure 3.6:** Replication of in-situ flat-jack based testing methods in the laboratory: (a) geometry of a built CS wall (dimensions are in mm); (b) testing sequence at each location.

### 3.3 NONLINEAR BEHAVIOUR OF FIELD-EXTRACTED MASONRY

Compression, bending, and shear properties of the field-extracted samples were evaluated following the procedures described for the laboratory-made samples in Chapter 2 and the testing methods described in Appendix A. As in the approach to laboratory-made samples, the stress-strain or stress-displacement curves as well as the final crack patterns were recorded for each individual sample. More detailed information regarding the response of each masonry object can be found in related technical reports (Jafari et al., 2015; Jafari & Esposito, 2018). To avoid repetition regarding the general response of masonry (discussed mainly in Chapter 2), the response of the field-extracted masonry is fully discussed only for one object, while the focus is on addressing any dissimilarities with respect to the response of the laboratory-made specimens.

Generally, no significant deviation was noticed in the response of the field-extracted samples with respect to the laboratory-made samples. However, higher values of the coefficient of variation were often attributed to the field-extracted samples, which are likely be related to workmanship quality as well as weathering conditions. In addition, one could argue that the variability is somehow an undesirable effect of disturbance in the sample integrity due to the cutting operation and transportation. However, high values for the coefficient of variation were also obtained when performing in-situ double flat-jack and shove tests, indicating that cutting and transportation are not the main drivers for the variability.

#### 3.3.1 Compressive response

Figure 3.7 shows a comparison between the mean stress-strain diagram of the field-extracted wallets and laboratory-made wallets under vertical as well as horizontal compression loading. From 22 objects, 87 wallets were extracted. The behaviour of six CS brick masonry wallets extracted from the inner walls of a detached house typology, namely TIL-H1, is discussed in this section. Of the tested wallets, three were compressed under a vertical configuration, and three under a horizontal configuration (indicated by grey curves in Figure 3.7); the mean curve (black line) was found following the procedure described in Chapter 2. The axial strain and the lateral strain refer to the deformations measured parallel to and perpendicular to the loading direction, respectively.

The main difference between the compression responses of the field-extracted and laboratory-made CS brick wallets lies in the post-peak response and a different orthotropic strength ratio. As for the MAT-1 CS brick masonry wallets (dashed line), the stress-strain diagrams of field-extracted wallets can be approximated by a linear branch, followed by a nonlinear response up to the peak load. However, contrary to the laboratory-made samples, the field-extracted TIL-H1 wallets showed higher values of vertical compressive strength than horizontal compressive strength. Such a difference in the orthotropic behaviour of the MAT-1 laboratory-made and TIL-H1 field-extracted samples could be ascribed to

differences between the stiffness of the masonry constituents. In the softening regime, the TIL-H1 field-extracted wallets showed a more brittle behaviour than the MAT-1 laboratory-made specimens. Generally, in most cases lower values of compressive fracture energy were found for the field-extracted brick masonry than for the laboratory-made wallets. The values of compressive strength,  $f'_m$ ,  $f'_{m,b}$ , Young's modulus,  $E_3$ ,  $E_{3,b}$ , and compressive fracture energy,  $G_{f-c}$ ,  $G_{f-c,b}$  under vertical and horizontal loading configurations are presented in Table 3.4. The intra-building variability of material properties, quantified by means of the coefficient of variation, is slightly higher for the field-extracted masonry than for the laboratory-made wallets.

Under vertical compressive loading, the cracking evolution in the two types of wallets was different, while under horizontal loading no significant difference was noticed. Under vertical compressive load, the first splitting cracks in the TIL-H1 field-extracted wallet appeared in the bricks (Figure 3.8a), while mortar cracking was often reported for the MAT-1 laboratory-made wallets (Figure 3.9a). With continued deformation, vertical splitting cracks developed through the length and thickness of the specimens, for both field-extracted and laboratory-made wallets. Under horizontal compressive load, no difference in crack evolution was noticed for TIL-H1 field-extracted and MAT-1 laboratory-made wallets. First, debonding cracks, parallel to the loading direction, appeared along the brick-mortar interface. With continued deformation, cracks mainly developed through the height of the specimen, thus creating a buckling mechanism that was eventually followed by bricks cracking (Figure 3.9c,d). Note that for the field-extracted masonry types, particularly for clay brick masonry, we often observed a wider range of failure, including splitting, crushing, spalling, debonding, friction and shear cracking. This is attributed to the complex interaction among the masonry constituents (e.g. units and mortar joints), each having different elastic properties.

**Table 3.4:**

Overview of compression properties of TIL-H1 field-extracted and MAT-1 laboratory-made wallets. Coefficient of variation in parentheses.

Masonry type	Compression properties					
	Vertical configuration			Horizontal configuration		
	$f'_m$ MPa	$E_3$ MPa	$G_{f-c}$ N/mm	$f'_{m,b}$ MPa	$E_{3,b}$ MPa	$G_{f-c,b}$ N/mm
Existing masonry (TIL-H1)	6.93 (14%)	4474 (11%)	14.52 (20%)	5.92 (10%)	3498 (42%)	26.48 (6%)
Replicated masonry (MAT-1)	5.93 (9%)	2749 (10%)	34.31 (14%)	7.56 (2%)	2079 (42%)	41.94 (12%)

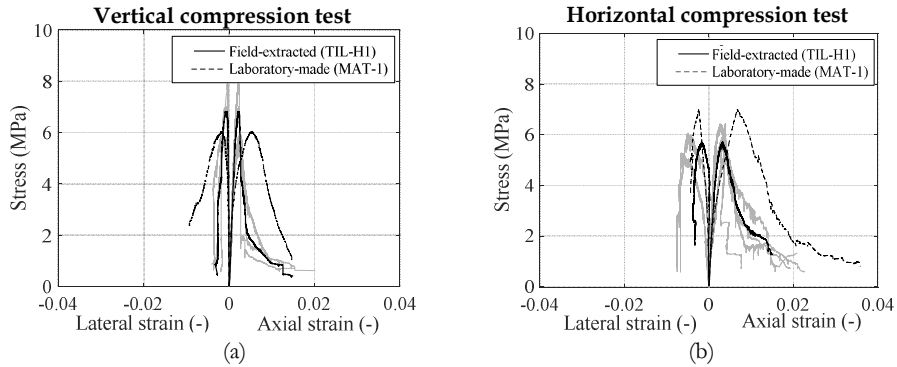


**Figure 3.7:** Stress-strain relationships of field-extracted (TIL-H1) and laboratory-made CS brick masonry (MAT-1) under: (a) vertical compressive load; (b) horizontal compressive load.

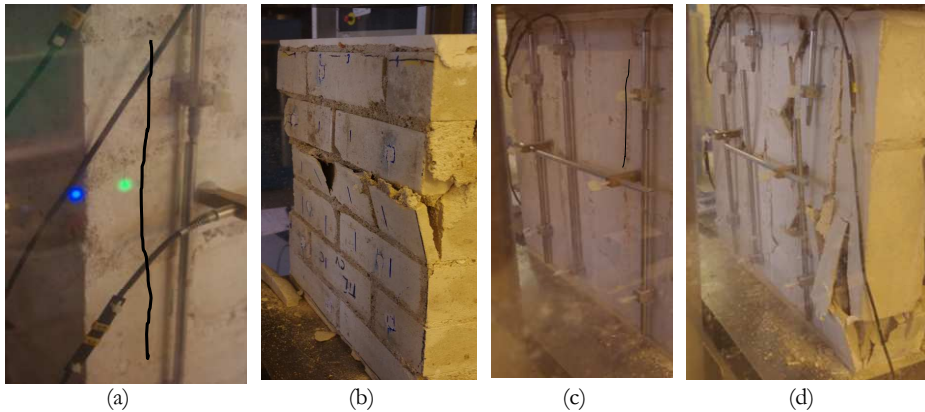


**Figure 3.8:** Crack pattern of field-extracted CS brick masonry (TIL-H1) under vertical compression loading: (a) first cracking; (b) final crack pattern; under horizontal compression loading: (c) first cracking; (d) final crack pattern.

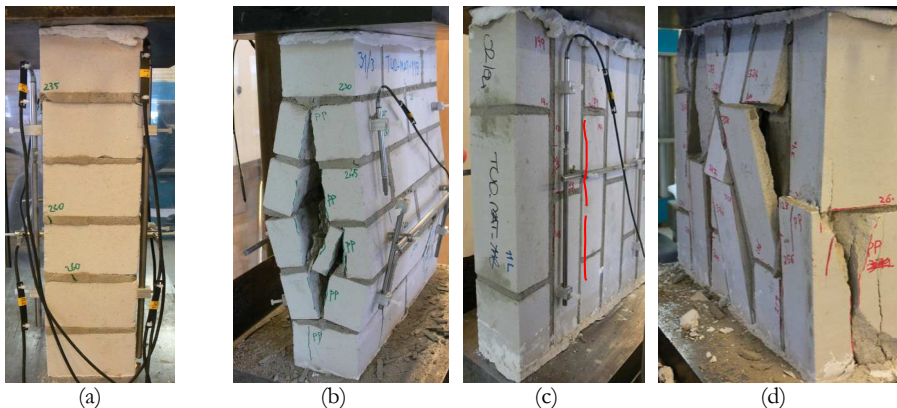


**Figure 3.9:** Crack pattern of laboratory-made CS brick masonry (MAT-1) under vertical compression loading: (a) first cracking; (b) final crack pattern; under horizontal compression loading: (c) first cracking; (d) final crack pattern.

### 3.3.2 Bending response

The extraction as well as the handling of large size wallets from existing structures often proved to be a challenging and labour-intensive task, thus it was only possible in the case of two objects to receive the three sets of wallets required for the bending tests. From 15 objects, 81 wallets were extracted, of which 9 were tested under vertical out-of-plane bending, 27 under horizontal out-of-plane bending, and 45 under in-plane bending load. Most of the field-extracted samples were tested using the displacement-controlled set-up, and the crack-width control set-up was only used for two objects, namely TIL-H2 and HOG-H1 (for more information regarding the test set-up see Appendix A.4). Accordingly, only limited insight was gained into the post-peak softening of the field-extracted wallets under bending load.

Generally, no significant deviation in the pre-peak bending response of the field-extracted samples was noticed as compared to the laboratory-made samples, while in the post-peak phase the field-extracted wallets showed a more brittle behaviour. Figure 3.10–Figure 3.12 show a comparison between the mean stress-strain diagram of the TIL-H2 field-extracted perforated clay bricks wallets and MAT-2 laboratory-made wallets under out-of-plane and in-plane bending load. Although tests on field-extracted wallets were performed by controlling the opening of cracks on the tension side of the specimen, the post-peak response of the wallets under horizontal out-of-plane bending load was not captured (Figure 3.11). Generally, higher values of strength were found for perforated clay brick masonry as compared with those for solid clay brick masonry.

The crack patterns of the wallets under vertical out-of-plane bending and in-plane bending were often similar to those of the laboratory-made samples, Figure 3.13–Figure 3.14. In the horizontal out-of-plane and in-plane bending tests, some field-extracted wallets failed due to the formation of a vertical crack through head joints and units, Figure 3.13b, rather than a stepwise debonding crack through head joints and bed joints, Figure 3.14b,c, which was always the case for the laboratory-made wallets. Thus, the variation in the post-peak response of the field-extracted specimens was often higher than that of the laboratory-made ones.

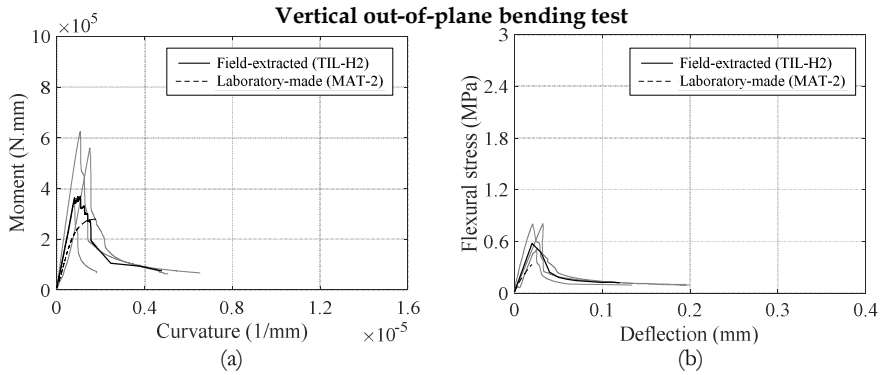


**Figure 3.10:** Behaviour of TIL-H2 field-extracted and MAT-2 laboratory-made perforated clay brick masonry under vertical out-of-plane bending: (a) moment-curvature curves; (b) flexural stress-deflection curves.

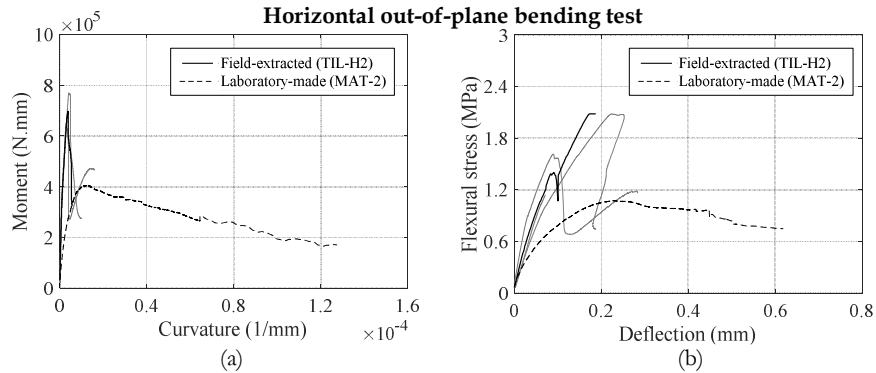


**Figure 3.11:** Typical behaviour of TIL-H2 field-extracted and MAT-2 perforated clay brick masonry under horizontal out-of-plane bending: (a) moment-curvature curves; (b) flexural stress-deflection curves.

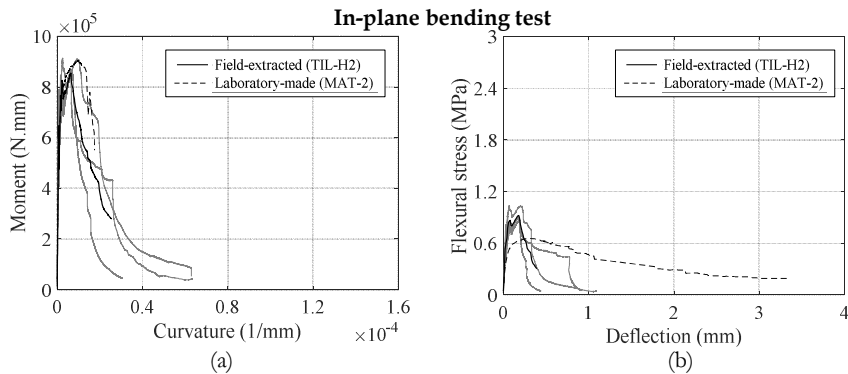


**Figure 3.12:** Typical behaviour of TIL-H2 field-extracted and MAT-2 perforated clay brick masonry under in-plane bending: (a) moment-curvature curves; (b) flexural stress-deflection curves.



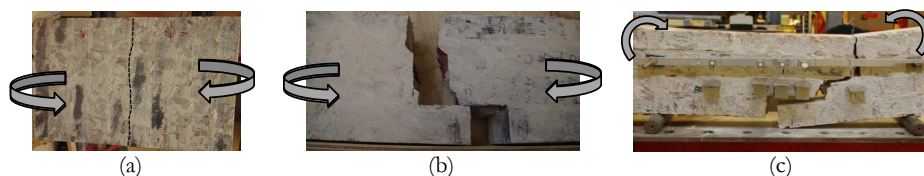


**Figure 3.13:** Crack pattern of TIL-H2 field-extracted perforated clay brick masonry under four-point bending tests: (a) vertical out-of-plane bending; (b) horizontal out-of-plane bending; (c) in-plane bending.

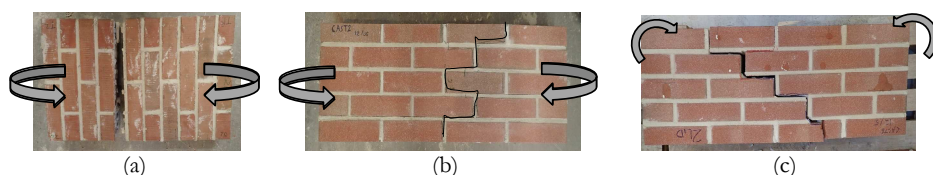


**Figure 3.14:** Crack pattern of MAT-2 laboratory-made perforated clay brick masonry under four-point bending tests: (a) vertical out-of-plane bending; (b) horizontal out-of-plane bending; (c) in-plane bending.

### 3.3.3 Shear response

Handling as well as preparing the triplets is generally a delicate task. Hence, irrespective of the construction type (i.e. laboratory-made or field-extracted) some of the triplets disintegrated during the preparation phase. Nevertheless, the debonded triplets were tested with the aim of evaluating the residual shear properties. In total, 188 triplets were extracted from 23 objects. It is worth mentioning that most of the field-extracted samples were tested in the laboratory of TU/e (Vermeltfoort, 2015).

Generally, no specific deviation in the shear stress-sliding curves of the field-extracted samples with respect to the laboratory-made samples was noticed, while differences were noted in their dilatant behaviour. Figure 3.15a shows the shear stress-sliding curves of CS brick masonry triplets extracted from the inner walls of a detached house typology, namely TIL-H1. For a given pre-compression level, there is a larger discrepancy in the shear response of the field-extracted triplets as compared to the laboratory-made triplets for which the variability in material properties was minimised, Figure 3.15a. The variations of the normal displacement (perpendicular to the joint) versus shear-sliding for both field-extracted and laboratory-made CS brick masonry are plotted in Figure 3.15b. Larger values of normal displacements were recorded for the field-extracted triplets as compared to the laboratory-made triplets.

As with the laboratory made samples, the failure mode of the field-extracted triplets was essentially characterised as shear sliding along the interface. In addition, it was noticed that the failure mode could be affected by the level of pre-compression. As shown in Figure 3.16a, the failure of triplets at the low pre-compression level of 0.2 MPa was often due to the development of a debonding crack along the interface. However, at the highest pre-compression level (1.0 MPa) mortar failure was also observed, Figure 3.16b. Similar observations were also made for the laboratory-made triplets, 3.16c,d.

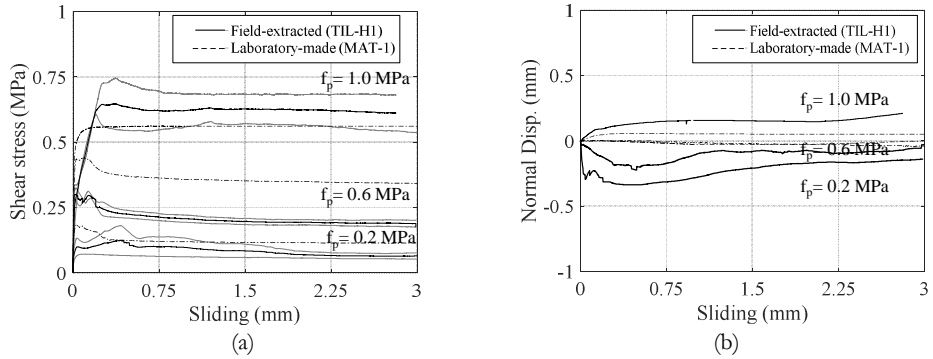


**Figure 3.15:** Shear behaviour of TIL-H1 field-extracted and MAT-1 laboratory-made CS brick masonry: (a) shear stress-sliding curves; (b) normal displacement-sliding curve.

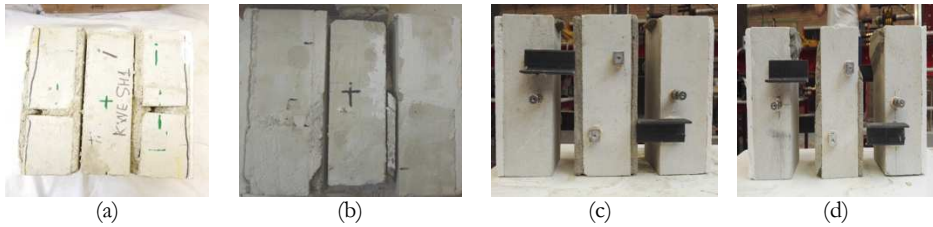


**Figure 3.16:** Crack pattern at pre-compression levels of 0.20 MPa and 0.60 MPa: (a,b) field-extracted triplets; (c,d) laboratory-made triplets.

### 3.4 INTER-BUILDING DISTRIBUTION OF MATERIAL PROPERTIES

Uncertainties in the structural assessment of unreinforced masonry (URM) structures result from decisions on the type of model, type of structure, earthquake ground motions, and the choice of material properties. As stated by Parisi and Augenti (2012), uncertainties in the response of masonry can be distinguished into two categories: aleatory and epistemic uncertainties. The former, known as statistical uncertainty, is assumed to be dependent on the randomness of the phenomenon and can be quantified using methods such as Monte Carlo. The latter, known as systematic uncertainty, could be reduced by improving the level of knowledge.

To deal with uncertainties in material properties that arise from the inter- and intra-building variability of material properties, knowledge about the statistical distribution of material properties is required. Aiming to incorporate uncertainties in the material properties, Rota et al. (2010) developed two complimentary approaches for the derivation of fragility curves based on nonlinear stochastic analysis. In the first approach, the material properties were assumed to be random variables varying within pre-defined ranges. In the second approach, not only the properties, but also the materials associated with each macro-element were random. Hacıfendioglu et al. (2017) investigated the influence of uncertainty in material properties on the stochastic response of a historic masonry bridge. To this end, they assumed that the distributions of the Young's modulus and Poisson's ratio could be fitted with normal and lognormal distributions, respectively. They concluded that the response of the URM bridge was significantly influenced by variability in the elastic modulus of masonry, while increasing the uncertainties in the values of Poisson's ratio had a negligible impact. Traditionally, a normal distribution is often assumed for the statistical analysis of concrete and masonry. In the realm of concrete, Silvestri et al. (2008) and Unanwa and Mahan (2014) showed that the distribution of the compressive strength of concrete can be captured well with the lognormal distribution rather than the normal one. However, standard EN 1052-1(CEN 1998) suggests a normal probabilistic model (5% percentile) to find the characteristic compressive strength of masonry. Unlike concrete, so far limited studies have delved into the statistical analysis of material properties of existing masonry.

### 3.4.1 Overall results of all masonry types

To understand the inter-building variability of each material property, Figure 3.17–Figure 3.19 show the histogram representations, given the complete data set of all extracted masonry types, i.e. the overall results of clay brick masonry and CS brick masonry together. In addition, using the distribution fitter functions in MATLAB software 2019b, three of the most widely used distribution types, including the normal, lognormal, and Weibull distributions, are plotted against the probability density. The aim was to determine whether they can fit desirably with the distribution of the experimental data. The following conclusions can be drawn from the statistical analysis:

- Both vertical and horizontal compressive strength better conform to the normal or Weibull distribution, although the lower tail behaviour is not always fully captured by the distribution models, while the Young's modulus and compressive fracture energy, with a skewed tail, can be better fitted with the lognormal distribution, Figure 3.17. In addition, the histogram representations reveal a larger frequency range for the vertical compression properties rather than for the horizontal compression properties.
- The distribution of the vertical flexural strength, with a skewed tail, can be better fitted with the Weibull or lognormal distribution, while the horizontal flexural strength and in-plane strength better conform to the normal or Weibull distribution, Figure 3.18a-c.
- An exponential function was used to describe the distribution of the bond strength, since zero values of the bond strength, found for three objects, restricted the application of the lognormal/Weibull distributions, Figure 3.18d. Previous studies found a link between the vertical flexural strength and the bond strength, as both properties depend on the brick-mortar interface strength (e.g., van der Pluijm, 1999). Accordingly, as expected, right-skewed histograms were found for both properties.
- The normal and lognormal distributions better postulate the variations of the cohesion and friction coefficients, respectively, Figure 3.19.

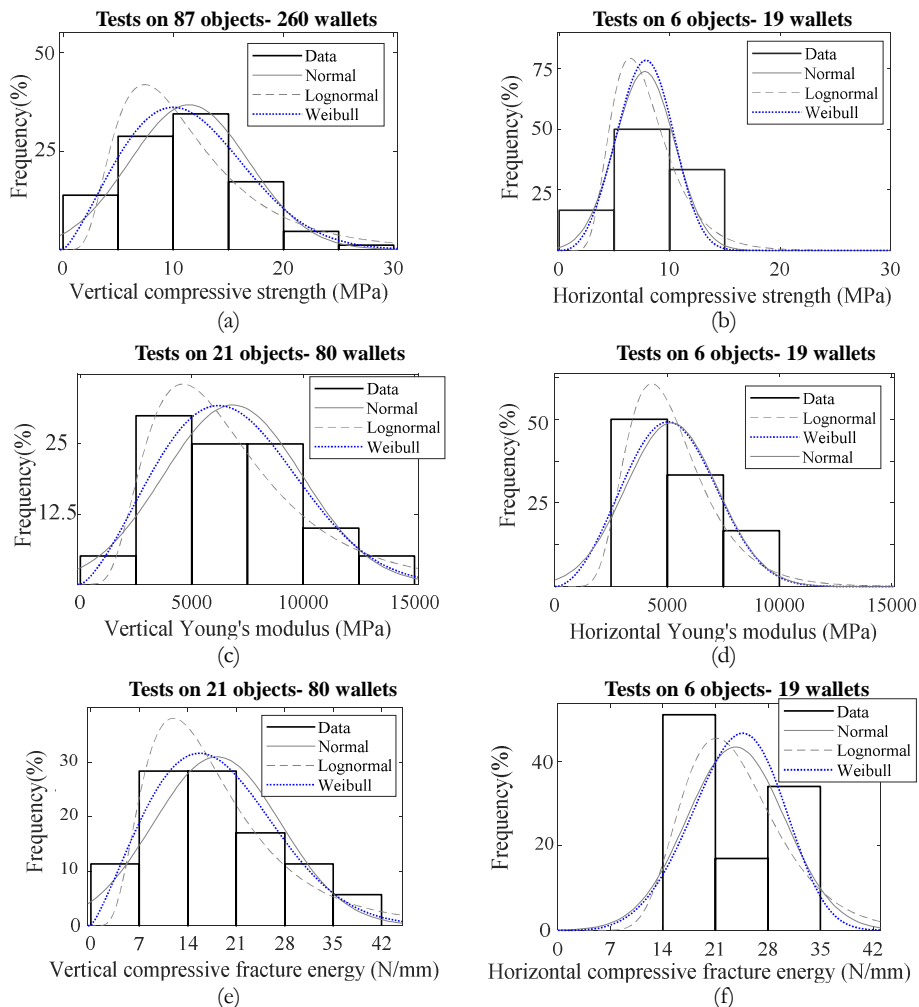


**Figure 3.17:** Distribution of compression properties of field-extracted wallets: (a,b) vertical and horizontal compressive strength; (c,d) vertical and horizontal Young's modulus; (e,f) vertical and horizontal compressive fracture energy.

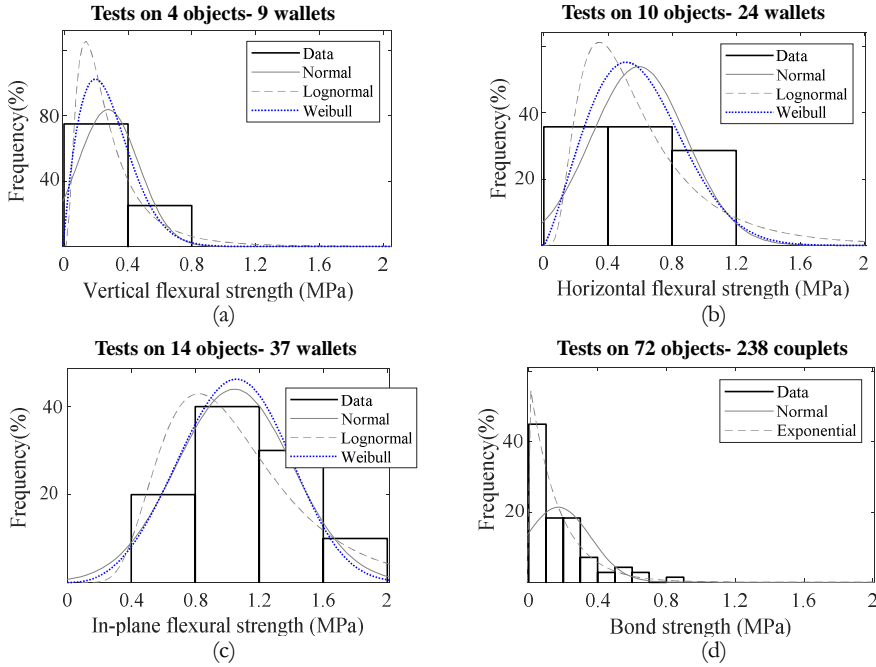


**Figure 3.18:** Distribution of bending properties of field-extracted wallets: (a) vertical flexural strength; (b) horizontal flexural strength; (c) in-plane flexural strength; (d) bond strength.

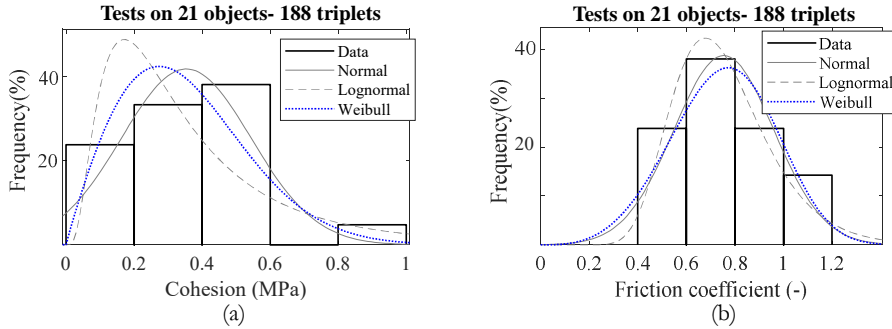


**Figure 3.19:** Distribution of shear properties of field-extracted triplets: (a) cohesion; (b) friction coefficient.

### 3.4.2 Subdivision of material properties

This study suggests subdivisions for the material properties, in an aim to eliminate the possible influence of brick type, clay brick production method, and masonry quality on the mean values of the material properties and their variations. In the construction industry in the Netherlands, a significant milestone can be recognised, coinciding with the end of the Second World War (1945). This milestone is marked by the transition from the load-bearing wall, either in double-wythe clay brick masonry or single-wythe clay brick masonry, to the cavity wall system with the inner load bearing leaf in CS brick/element masonry and the outer non-load bearing veneer leaf in clay brick masonry. With this in mind, this study first introduces a division between the properties of clay and of CS brick masonry. Note that no division was made between different types of clay bricks, as the majority of tested objects were made from solid clay bricks. It is believed that with industrialisation, the production process for bricks and thus the brick quality was improved. Hence, the second subdivision accounts for the division of the material properties of clay brick masonry constructed pre- and post-1945. Third, to incorporate the effects of poor workmanship or decay in the condition of materials due to environmental effects over time, the material properties are subdivided based on their quality.

Based on a visual inspection of the samples when they arrived in the laboratory, focusing in particular on the quality of mortar, filling of the joints, and workmanship, we determined the quality of the masonry. Generally, we noticed that poor quality masonry objects often showed bond strength values less than 0.20 MPa. Since the bond strength was not always available for every object, we attempted to define quality in a more consistent manner by correlating the values of bond strength with the corresponding values of masonry compressive strength, Figure 3.20a. Assuming a linear relationship between these two properties, a compressive strength of 14 MPa corresponds to a bond strength of 0.20 MPa. Accordingly, any masonry with values of bond strength and compressive strength lower than 0.20 MPa and 14 MPa, respectively, was ascertained to be of poor quality.

To cross-validate the reliability of the suggested approach for the definition of quality, Figure 3.20b makes a comparison with the quality of masonry defined using non-invasive testing methods. An indication of the homogeneity of materials, and thus quality, was only provided for a limited number of objects by means of non-invasive in-situ tests (EUcentre, 2015). Figure 3.20b shows that an inconsistent definition of quality was found only for two objects. Due to re-pointing on the external face of the walls of one object, the mortar joints seemed rather filled, while the joints on the inaccessible face were hardly filled at all. This could not be observed during the in-situ tests, thus making the laboratory inspection more reliable for determining the quality of the masonry.

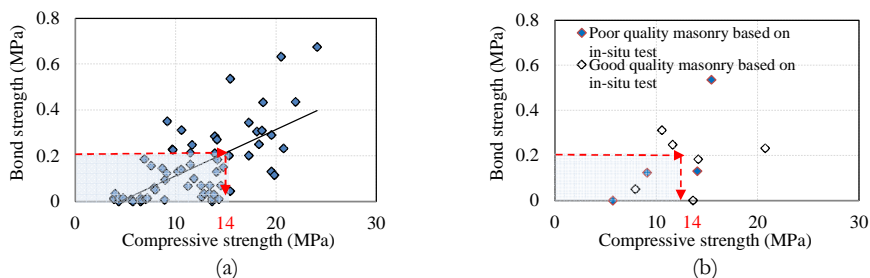


**Figure 3.20:** Definition of quality: (a) correlation between bond strength and compressive strength to define the quality threshold; (b) cross-validation of quality of masonry based on the value of the material properties and non-invasive observations.

To investigate whether there is a difference between the material properties of clay brick masonry with respect to the construction year and quality, a statistical analysis was conducted using IBM SPSS 24 statistical software. The analysis was conducted only for the compressive strength of masonry and bond strength, for which a larger database was available. Accordingly, P-values, as listed in Table 3.5, were derived from the independent sample T-test for normally distributed values of vertical compressive strength and from the Mann-Whitney U-test for exponentially distributed values of bond strength. The null-hypothesis states that there is no difference between the properties of the two sets of data. This hypothesis holds true if the P-value is higher than  $\alpha$ , which in the engineering research community is often defined as 0.05. Consequently, a subdivision is strongly needed if the P-value  $\ll 0.05$ , and no subdivision is required if the P-value  $\gg 0.05$ . The reader is referred to Field (2009) for an exhaustive discussion of the statistical analysis.

The results of the statistical analysis in Table 3.5 show that there is a statistically significant difference between the material properties of clay brick masonry constructed before and after 1945, as well as between the properties of clay brick masonry of poor and of good quality. Note that only clay brick masonry objects were categorised based on the construction year, while no division was made for CS brick masonry due to the absence of CS block or element masonry objects. Moreover, the division of CS brick masonry based on quality was not possible as a limited number of masonry objects, eight in total, were tested. As seen in Table 3.5, the total number of CS brick masonry objects is much lower than the number of clay brick masonry objects. As a result, although the higher P-value obtained for bond strength indicates that it is highly likely that the material properties do not differ by unit type, we could not rule out the size effect. Accordingly, in what follows, divisions of the material properties are discussed in further detail.



**Table 3.5:**

Statistical analysis to investigate the difference between the mean properties of two different groups.

Division of material properties based on		No. objects	P-value for compressive strength	P-value for bond strength
Unit types	Clay brick masonry	79	0.160	0.590
	CS brick masonry	8		
Year of construction of clay brick masonry	<1945	55	0.0032	0.0002
	>1945	24		
Quality of clay brick masonry	<1945	Poor quality	0.007	0.007
		Good quality		
	>1945	Poor quality	0.006	0.002
		Good quality		

### Subdivision of material properties based on unit type

An overview of the distribution of material properties obtained from tests on clay brick masonry and tests on CS brick masonry in terms of histogram representation is shown in Figure 3.21–Figure 3.23. For each masonry type, the total number of testing objects, mean values of the material property, and the coefficient of variation in percentage (in parentheses) are reported in the legend. To exclude the effect of the number of samples, the histograms' y-axes indicate the sum of weighted samples number. To this end, a weight was assigned to every sample of an object, and the total weight of each single object was assumed to be one. Note that in Figure 3.21 and Figure 3.22d there are a higher number of objects for the vertical compressive strength and bond strength, respectively, than for the other properties.

Distributions of the vertical compression properties of clay and CS brick masonry are presented in Figure 3.21. The vertical compressive strength of clay brick masonry for 218 wallets from 79 objects varies between 1.3 MPa and 28.6 MPa with an average of 12 MP, Figure 3.21a. The vertical compressive strength of CS brick masonry for 28 wallets from 8 objects varies between 5.4 MPa and 15.8 MPa with an average of 10 MP, Figure 3.21a. The mean value of the clay brick compressive strength ( $f_m=12$  MPa) is slightly higher than that of CS brick masonry ( $f_m=10$  MPa). However, a large variation in the strength of clay brick masonry objects was found. Owing to a more uniform production process of CS bricks, the compressive strength varied within a narrower range. Considering the distribution of the vertical Young's modulus and vertical compressive fracture energy, no noticeable difference between the mean values of the clay and the CS brick masonry was found; however, this could be influenced by the limited number of objects. Under horizontal compression loading, significant differences between the compression properties of clay and CS brick masonry were observed, although a limited number of objects was considered.

Figure 3.22 presents distributions of the bending properties of clay and CS brick masonry. Figure 3.22a shows a major difference between the vertical out-of-plane flexural strength of clay and that of CS brick masonry, with the results for CS brick masonry objects being located at the lower end of the histogram, and those of the clay brick masonry objects at the higher end. In addition, higher values of

horizontal flexural strength were obtained by performing tests on clay brick masonry than those found for CS brick masonry. The distribution of the in-plane flexural strength and bond strength in Figure 3.22c and Figure 3.22d, respectively, shows enormous scatter, for both masonry types. This once more highlights the decisive role of the brick-mortar bond in the bending properties of existing masonry.

Distributions of the shear properties of clay and CS brick masonry are presented in Figure 3.23. Similar to the other material properties, a higher value of cohesion was observed for clay brick masonry than for CS brick masonry (Figure 3.23a), consistent with the findings for flexural bond strength (Figure 3.22d). However, the friction coefficient was not found to be dependent on the type of masonry unit (Figure 3.23b). This indicates that the surface roughness of the mode-II shear cracks is similar for the two masonry types.

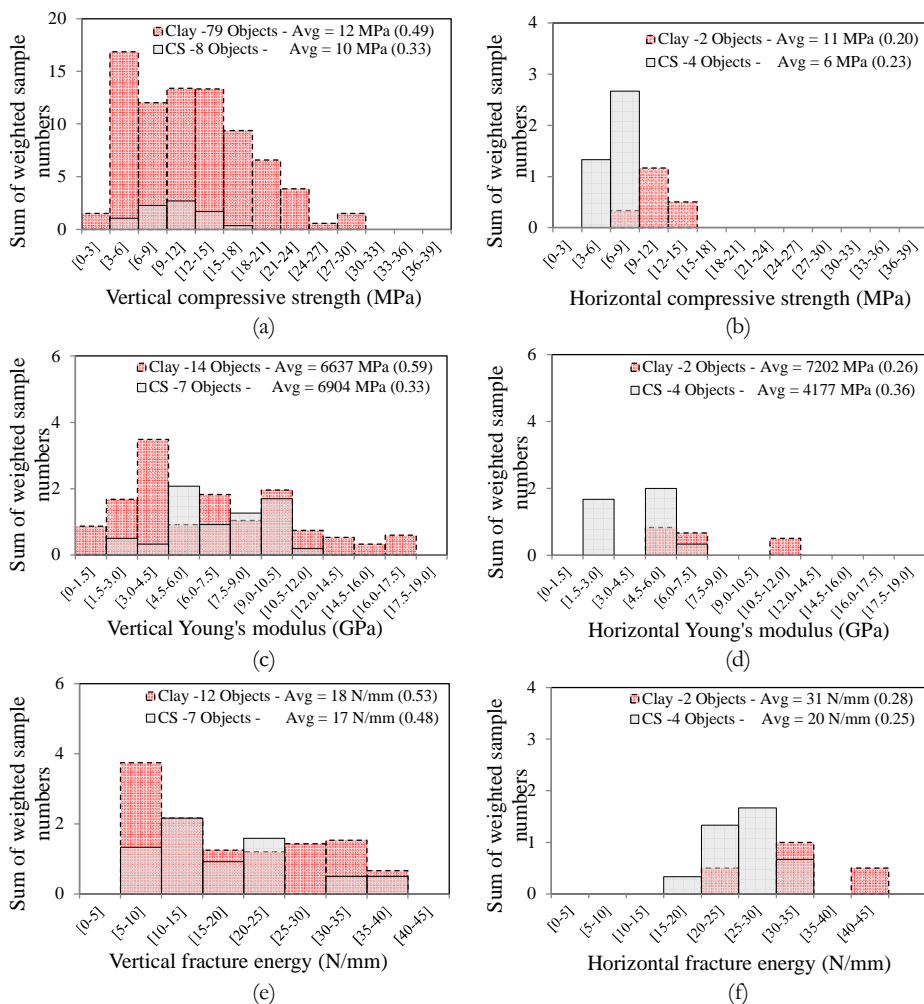


**Figure 3.21:** Distribution of experimentally determined compression properties for field-extracted existing masonry categorised according to unit type (clay brick or calcium-silicate brick): (a,b) vertical and horizontal compressive strength; (c,d) vertical and horizontal Young's modulus; (e,f) vertical and horizontal compressive fracture energy. Coefficient of variation in parentheses.

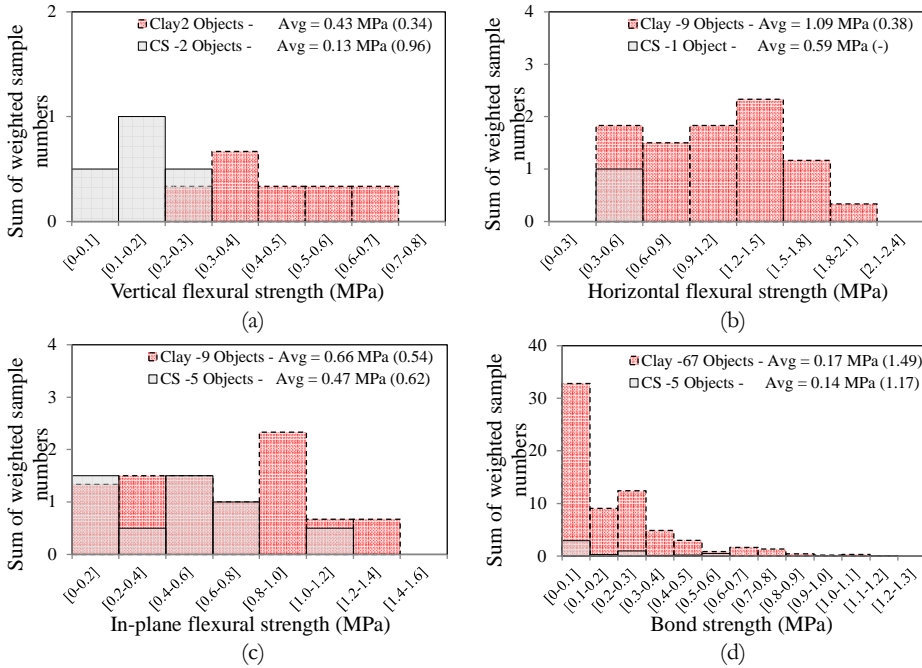


**Figure 3.22:** Distribution of experimentally determined bending properties for field-extracted existing masonry categorised according to unit type (clay brick or calcium-silicate brick): (a) vertical flexural strength; (b) horizontal flexural strength; (c) in-plane flexural strength; (d) bond strength. Coefficient of variation in parentheses.

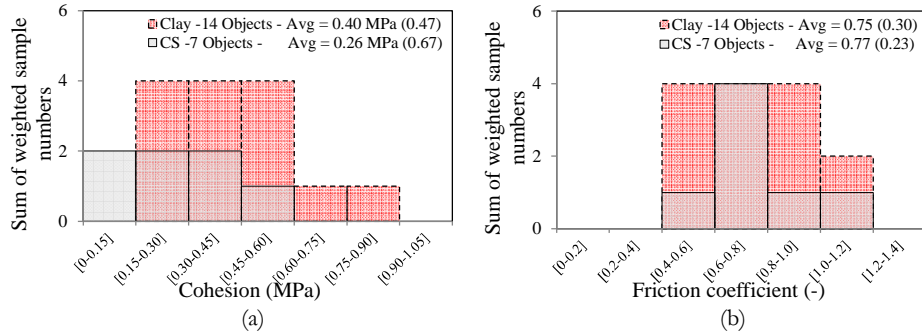


**Figure 3.23:** Distribution of experimentally determined shear properties for field-extracted existing masonry categorised according to unit type (clay brick or calcium-silicate brick): (a) cohesion; (b) friction coefficient. Coefficient of variation in parentheses.

### **Subdivision of material properties of clay brick masonry based on year of construction**

Overall, the masonry from recently built objects showed higher values for the material properties, with significant variation in both categories, but less for newly built clay brick masonry, Figure 3.24–Figure 3.26. This is mainly attributed to the fact that newer built masonry is often made of industrially produced pre-mixed mortars and bricks and thus involves more quality control. For each masonry type, the total number of testing objects, the mean values of the material property, and the coefficient of variation in percentage (in parentheses) are reported in the legend.

The vertical compressive strength of newly built clay brick masonry from 24 objects was 1.5 times higher than older masonry from 55 objects, Figure 3.24a. Moreover, a lower value of the coefficient of variation was found for newly built clay brick masonry. The vertical Young's modulus and vertical compressive fracture energy of newly built masonry objects were 1.4 and 1.8 times higher, respectively, as compared to older clay brick masonry. However, no significant reduction was observed in the values of coefficient of variation in the newly built clay brick masonry objects. Regarding the horizontal compression properties of clay brick masonry, no definite conclusion could be drawn due to the limited number of objects.

Regarding the bending properties of masonry, distinct differences between the mean values of the two groups were observed for horizontal flexural strength and bond strength, Figure 3.25. The horizontal flexural strength of newly built masonry objects was two times higher than that of older clay brick masonry, Figure 3.25b. The bond strength of newly built clay brick masonry from 21 objects was 2.6 times higher than older masonry from 46 objects, Figure 3.25d. For both properties, a lower value of the coefficient of variation was found for newly built clay brick masonry. Regarding the vertical flexural strength and in-plane flexural strength of clay brick masonry, no firm conclusions could be drawn due to the insufficient number of older masonry objects, Figure 3.25a,c.

The cohesion of newly built clay brick masonry from eight objects was 1.5 times higher than older masonry from six objects, Figure 3.26a. In agreement with the findings from the divisions of material properties based on the unit types, the mean values of the friction coefficient of the two groups were almost identical.

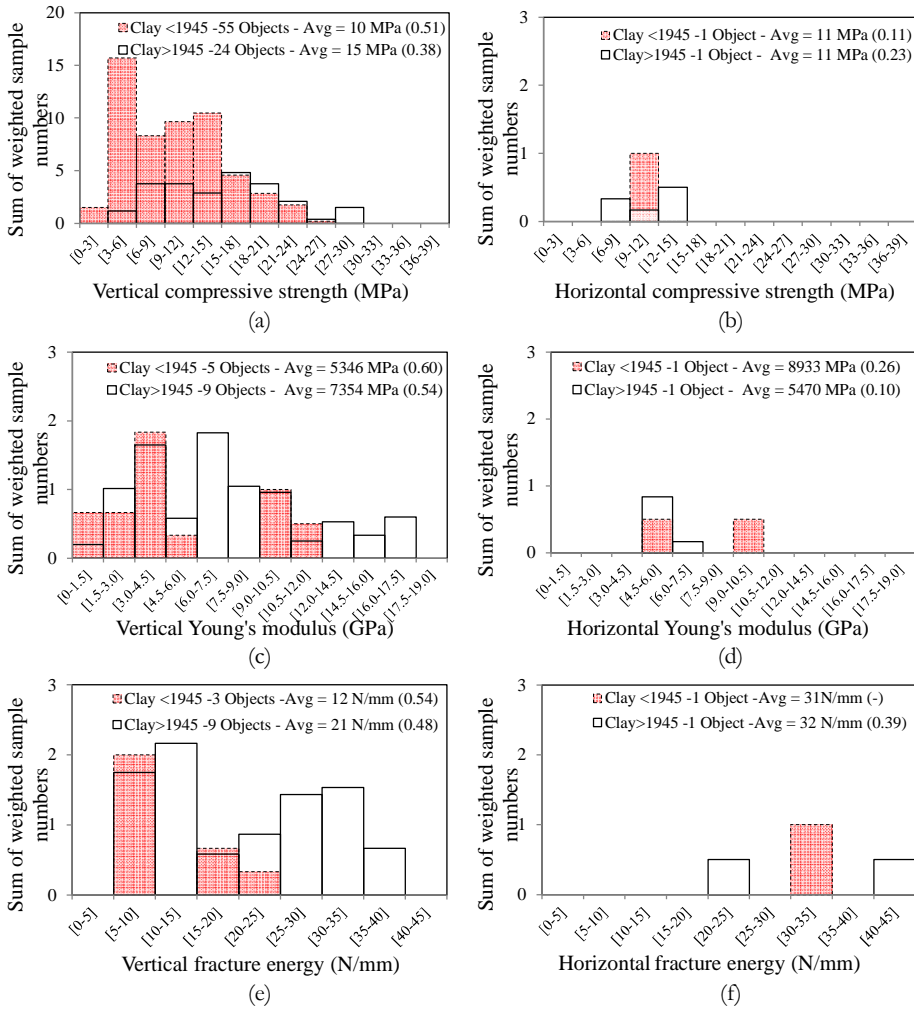


**Figure 3.24:** Distribution of experimentally determined properties of field-extracted existing clay brick masonry categorised according to year of construction (pre- and post-1945): (a,b) vertical and horizontal compressive strength; (c,d) vertical and horizontal Young's modulus; (e,f) vertical and horizontal compressive fracture energy. Coefficient of variation in parentheses.

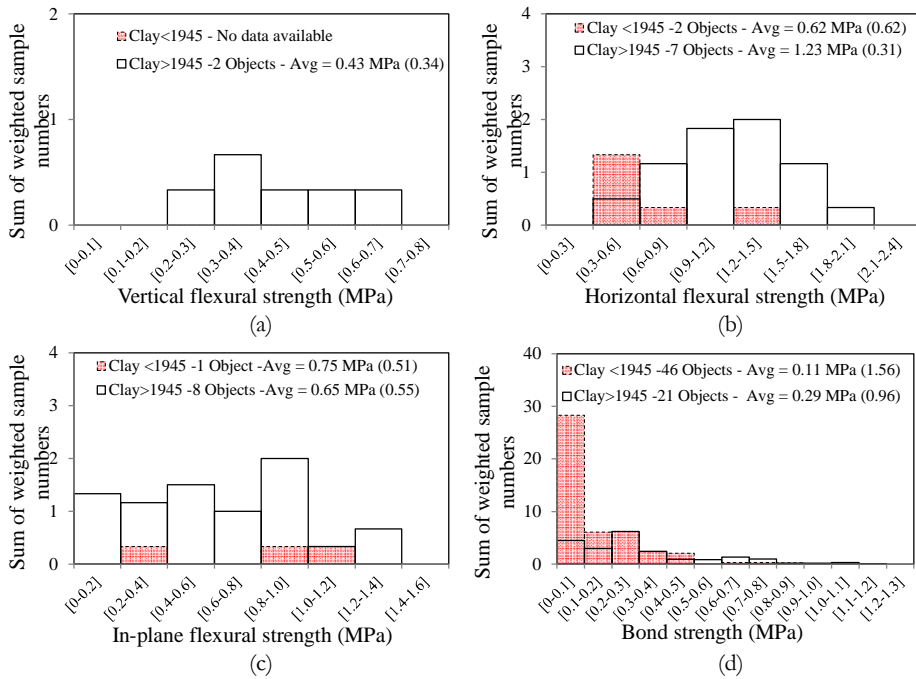


**Figure 3.25:** Distribution of experimentally determined properties of field-extracted existing clay brick masonry categorised according to the year of construction (pre- and post-1945): (a) vertical flexural strength; (b) horizontal flexural strength; (c) in-plane flexural strength; (d) bond strength. Coefficient of variation in parentheses.

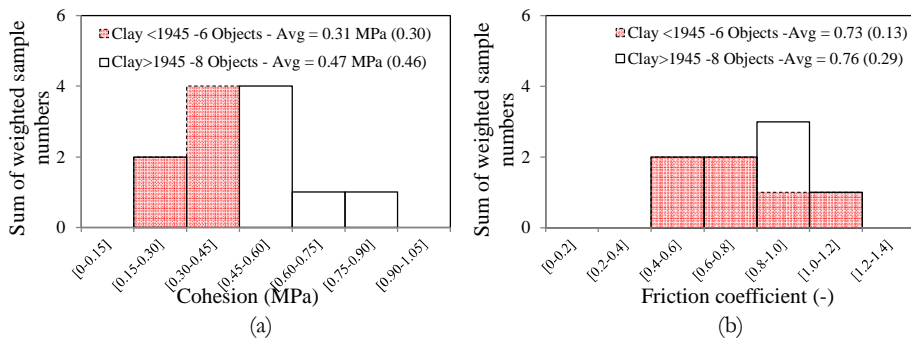


**Figure 3.26:** Distribution of experimentally determined properties of field-extracted existing clay brick masonry categorised according to the year of construction (pre- and post-1945): (a) cohesion, (b) friction coefficient. Coefficient of variation in parentheses.

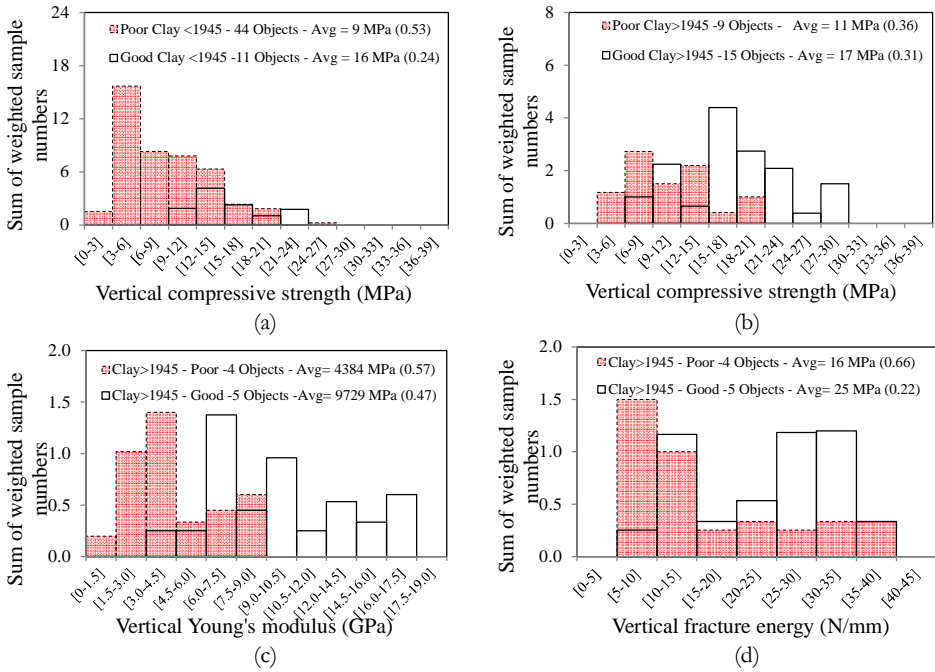
### Subdivision of material properties based on year of construction and quality

Figure 3.27–Figure 3.29 show the material properties of the clay brick masonry, for both the pre-1945 and post-1945 period, divided based on quality. As masonry objects were divided based on quality, the majority of clay brick masonry constructed before 1945 and CS brick masonry was identified as poor quality. However, having a larger database for compressive strength and bond strength of clay brick masonry, populated using the additional data of B|A|S, allowed for a division based on quality for the two construction periods. For clay brick masonry constructed after 1945, a more balanced outcome was found in terms of numbers of poor and good quality objects. Accordingly, the material properties of newly built clay brick masonry objects were categorised based on quality. However, due to the limited number of objects, such a division was not made for the compression properties of masonry under horizontal loading nor for flexural strength under out-of-plane bending load.

- As evident in Figure 3.27a,b, the values of vertical compressive strength of good quality masonry constructed pre- and post-1945 were 1.8 and 1.6 times higher, respectively, than for poor quality masonry. In addition, a lower dispersion for newly built masonry with good quality was observed. The values of the vertical Young's modulus and vertical compressive fracture energy of newly built clay brick masonry with good quality were 2.2 and 1.6 times higher, respectively, than for poor quality masonry, Figure 3.27c,d. Moreover, for masonry with good quality, a lower dispersion was found, particularly for vertical compressive fracture energy.
- For good quality masonry, higher values of bending properties were found than for poor quality masonry, Figure 3.28. The values of the horizontal flexural strength and in-plane flexural strength of newly built clay brick masonry with good quality were 1.3 and 4.6 times higher, respectively, than for poor quality masonry, Figure 3.28a,b. For both pre- and post-1945 built masonry, large differences in the mean values of bond strength as well as the coefficients of variation of poor and of good quality masonry were found, Figure 3.28c,d. The bond strength of good quality masonry constructed pre- and post-1945 was four and six times higher, respectively, than the bond strength of the poor quality masonry.
- There was not much difference between the cohesion and friction coefficients of newly built clay brick masonry with good quality and with poor quality, Figure 3.29.

In conclusion, the mean values of poor and good quality masonry showed clear and explainable differences. Such observations confirmed the necessity of the proposed subdivisions for material properties of existing masonry into year of construction combined with poor and good quality.





**Figure 3.27:** Distribution of experimentally determined properties of field-extracted existing clay brick masonry based on quality and year of construction: vertical compressive strength (a) pre-1945 and (b) post-1945; (c) vertical Young's modulus; (d) vertical compressive fracture energy.

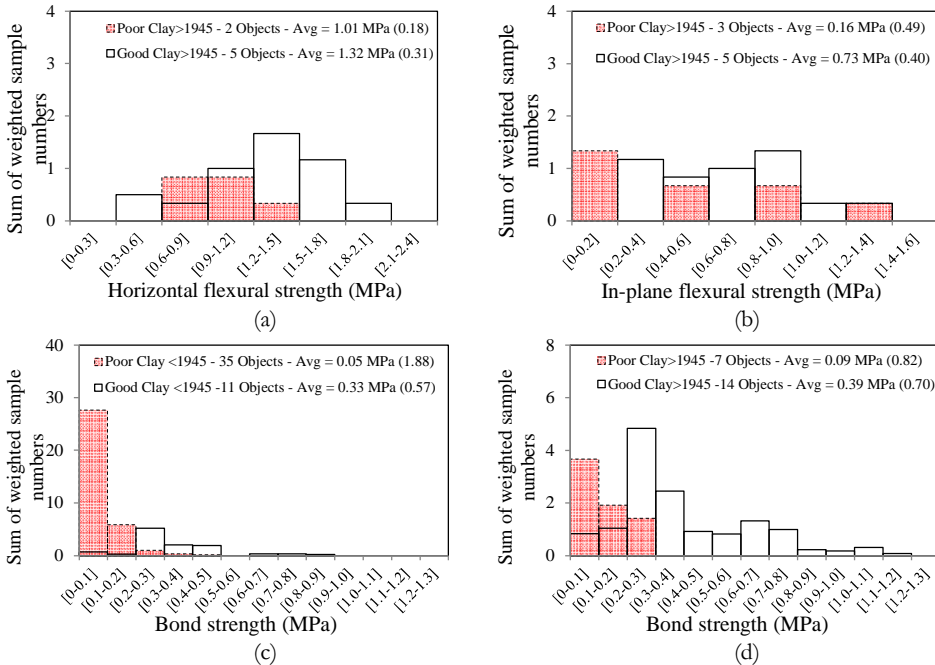


**Figure 3.28:** Distribution of experimentally determined properties of field-extracted existing clay brick masonry based on quality and year of construction: (a) horizontal flexural strength; (b) in-plane flexural strength; bond strength (c) pre-1945 and (d) post-1945.

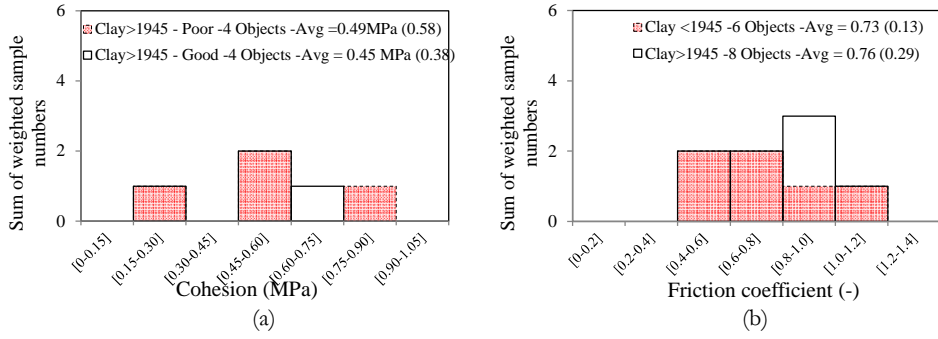


**Figure 3.29:** Distribution of experimentally determined properties of field-extracted existing clay brick masonry based on quality and year of construction: (a) cohesion; (b) coefficient of friction.

### 3.5 DATASET OF MATERIAL PROPERTIES OF DUTCH MASONRY

Table 3.6 provides an overview of the material properties obtained from tests on field-extracted masonry, which accounts for divisions based on unit type (i.e. clay brick and CS brick) and year of construction of the clay bricks (i.e. pre- and post-1945). For each property, the mean values, coefficient of variation, and number of tested specimens are identified. Note that Table 3.6 does not include any division based on quality of masonry, as most of the older clay brick masonry (pre-1945) and the CS brick masonry was of poor quality.

The dataset obtained in this study together with previously available data from the literature contributed to the formation of the material table originally presented in NEN-NPR 9998:2015 and were partially updated in the subsequent versions (the current version is NEN NPR 9998+C1:2020). As mentioned above, due to the large size of CS element masonry, no samples were extracted from the existing buildings. However, because the production process of CS element masonry has been partially standardised, the material properties obtained for the laboratory-made specimens, reported in Chapter 2, were used as a benchmark.

Table 3.7 makes a comparison between the values reported in NEN-NPR 9998+C1:2020 and the average values obtained from tests on the field-extracted clay and CS brick masonry objects and from tests on laboratory-made CS element masonry. The comparison shows that the code-based properties have been chosen with a reasonable degree of conservatism as compared to the test results. The compression properties proposed in NPR are on average 14% lower than the average test results under both vertical and horizontal configurations. The highest reduction (64%) was seen in the compressive fracture energy of older clay brick masonry, aiming to offset the large value of the horizontal compressive fracture energy found from tests on only one object. Regarding the bending properties, the highest reduction, up to 31%, was applied for the older clay brick masonry category. However, NPR suggests 15% and 37% increases in the values of vertical flexural strength of CS brick masonry and horizontal flexural strength of CS element masonry, respectively, as compared with the experimentally determined properties. Regarding the values of cohesion, NPR suggests a reduction of 3% to 15%. However, it makes 22% and 46% reductions in the friction coefficients of CS brick masonry and CS element masonry, respectively. In addition, this standard suggests a reduction of up to 40% in the material properties of clay brick masonry constructed before 1945 when the masonry is judged to be of poor quality based on a visual inspection. As mentioned in Section 3.4.2, the division of material properties of older clay brick masonry based on quality was only possible for vertical compressive strength and bond strength. Accordingly, for older clay brick masonry, the values of compressive strength of poor quality and good quality masonry were found to be 8.6 MPa and 15.6 MPa, respectively, Figure 3.27a. Thus, the suggested compressive strength of 8.5 MPa for older clay brick masonry is deemed to be relatively conservative.

**Table 3.6:**

Overview of mean values of experimentally determined material properties of field-extracted samples, including coefficient of variation, and number of tests.

Material property	Sym.	Unit	Clay brick masonry						CS brick masonry		
			Pre-1945			Post-1945			Avg.	C.o.V.	No.
			Avg.	C.o.V.	No.	Avg.	C.o.V.	No.			
Normalised compressive strength of brick	$f_b$	MPa	19.40	0.32	23	23.25	0.53	30	15.26	0.25	28
Flexural strength of brick (out-of-plane)	$f_{bb}$	MPa	6.12	0.16	42	4.38	0.38	46	4.19	0.35	59
Vertical compressive strength	$f'_m$	MPa	9.98	0.51	55	15.02	0.38	24	9.74	0.33	8
Vertical Young's modulus	$E_3$	MPa	5346	0.60	14	7354	0.54	42	6904	0.33	25
Vertical compressive fracture energy	$G_{fc}$	N/mm	11.93	0.54	14	20.58	0.48	42	17.41	0.48	25
Horizontal compressive strength	$f'_{m,b}$	MPa	10.86	0.11	2	11.00	0.23	6	6.17	0.23	11
Horizontal Young's modulus	$E_{3,b}$	MPa	8933	0.26	2	5470	0.10	6	4177	0.36	11
Horizontal compressive fracture energy	$G_{fc,b}$	N/mm	30.84	-	1	63.10	0.20	6	19.97	0.25	11
Vertical flexural strength	$f_{s1}$	MPa	-	-	-	0.43	0.34	6	0.13	0.96	3
Horizontal flexural strength	$f_{s2}$	MPa	0.62	0.62	21	1.23	0.31	19	0.59	-	1
In-plane flexural strength	$f_{s3}$	MPa	0.75	0.51	37	0.65	0.55	22	0.47	0.62	12
Bond strength	$f_b$	MPa	0.11	1.56	124	0.29	0.96	91	0.14	1.17	23
Cohesion (initial shear strength)	$f_{t0}$	MPa	0.31	0.30	72	0.47	0.46	64	0.26	0.67	56
Friction coefficient	$\mu$	-	0.73	0.13		0.76	0.29		0.77	0.23	

**Table 3.7:**

Overview of experimentally obtained properties and those presented in NEN-NPR 9998+C1:2020.

Properties	Sym.	Unit	Clay brick masonry				CS masonry			
			Pre-1945		Post-1945		Brick masonry		Element masonry	
			Tests	NPR	Tests	NPR	Tests	NPR	Tests	NPR
Vertical compressive strength of masonry	$f'_m$	MPa	9.98	8.5	15.02	10	9.53	7.0	13.93	10.0
Horizontal compressive strength of masonry	$f'_{m,b}$	MPa	10.86		11.00		6.17		9.42	
Vertical Young's modulus of masonry	$E_3$	MPa	5346	5000	7354	6000	6904	4000	8313	7500
Horizontal Young's modulus of masonry	$E_{3,b}$	MPa	8933		5470		4177		7701	
Vertical compressive fracture energy	$G_{f-c}$	N/mm	11.93	20	20.58	15	17.42	15	20.92	20
Horizontal compressive fracture energy	$G_{f-c,b}$	N/mm	30.81		63.10		20.04		12.83	
Vertical flexural strength <sup>1</sup>	$f_{s1}$	MPa	-	0.15	0.43	0.30	0.13	0.15	0.58	0.60
Horizontal flexural strength <sup>2</sup>	$f_{s2}$	MPa	0.62	0.55	1.23	0.85	0.59	0.55	0.73	1.00
Cohesion (initial bed joint shear strength)	$f_{i0}$	MPa	0.31	0.30	0.47	0.40	0.26	0.25	0.83	0.80
Friction coefficient in bed joint	$\mu$	-	0.73	0.75	0.76	0.75	0.77	0.60	1.48	0.80

<sup>1</sup>Bending strength for plane of failure parallel to the bed joints.<sup>2</sup>Bending strength for plane of failure perpendicular to the bed joints.

### 3.6 CONCLUDING REMARKS

To aid seismic assessments for induced seismicity in Groningen, an extensive experimental programme was launched, in which 15 buildings that were judged to be representative of the masonry building stock were selected as case studies. From each building, samples were extracted and delivered to the laboratories, where compression, bending, and shear tests were performed. By performing tests on different masonry types, a dataset of the material properties was established, which facilitated the selection of compatible materials. Apart from invasive laboratory tests, non- and semi-invasive in-situ tests were conducted by another party. Accordingly, direct insight into the Young's modulus of masonry, cohesion, and friction coefficient were provided using flat-jack based testing methods, i.e. double flat-jack and shove tests. However, non-invasive testing methods (i.e. penetrometer, Schmidt hammer, and ultrasonic tests) served as an indication of the quality of the masonry.

The comparison of material properties obtained from the laboratory tests and from the flat-jack based testing methods confirmed that further studies are required to validate and calibrate the outcomes of the shove tests as well as to devise a semi-invasive testing procedure specifically for Dutch masonry. By correlating the material properties obtained from the in-situ tests to those obtained from the laboratory tests on field-extracted specimens, no promising correspondence was found. Moreover, the in-situ testing campaign revealed that the flat-jack based testing methods require highly skilled technicians and equipment that is not widely available in the Netherlands.

The intra-building variability of material properties of field-extracted masonry was often slightly higher as compared to the laboratory-made masonry, which could be related to inconsistent construction quality within a wall or between walls or to material deterioration due to environmental effects. Generally, no significant deviation was noticed in terms of stress-strain relationship or the crack evolutions of the field-extracted samples with respect to the laboratory-made samples, discussed in Chapter 2. However, in some instances, the post-peak behaviour was rather brittle, which could be attributed to differences in the material properties of the masonry constituents.

The inter-building variability of material properties obtained from tests on a large variety of clay brick masonry and calcium silicate brick masonry types built in different time periods was found to be rather large. Through statistical analysis, insight into the statistical distribution of each material property was provided, which would be of prime interest when performing probabilistic analyses to derive fragility curves. As a result, vertical and horizontal compressive strength, horizontal flexural strength, in-plane flexural strength, and cohesion could be described by a normal or Weibull distribution, while the variations in vertical and horizontal Young's modulus, vertical and horizontal compressive fracture energy, vertical flexural strength, and friction coefficient were best fitted with a lognormal function. In addition, the distribution of bond strength could be approximated

with an exponential function. Moreover, it was noticed that the values of the bond strength are more spread out than those for the other properties. Accordingly, a sensitivity analysis of bond strength or any property derived from it (e.g., tensile strength) is recommended when it comes to structural assessment of existing masonry using numerical finite element models.

To improve the level of knowledge on the nature of variation in the material properties, these were subdivided according to unit type (i.e. clay brick or CS brick); additionally for clay brick masonry a subdivision based on year of construction (i.e. pre- or post-1945) was considered. Accordingly, the following conclusions were drawn:

- By subdividing the material properties based on the unit types, higher values of strength, stiffness, and toughness were found for clay brick masonry than for CS brick masonry. A ratio ranging between 0.97 and 3.3 was found between the properties of clay brick masonry and of CS brick masonry. The lowest and the highest ratios belonged to the values of friction coefficient and vertical flexural strength, respectively.
- As the material properties of clay brick masonry were further subdivided according to the year of construction, both subcategories showed significant variations in material properties, although this was less for newly built clay brick masonry. Generally, the recently built objects showed higher values for the material properties as compared to older clay brick masonry. For properties with a more balanced number of objects in each subcategory, a ratio ranging between 1.04 and 2.64 between the properties of pre- and post-1945 clay brick masonry was found. The lowest ratio was found for the values of friction coefficient and the highest for the bond strength.
- Good quality clay brick masonry showed less variation as compared to poor quality masonry. The highest difference between the material properties of poor and of good quality clay brick masonry was found for the bending properties, with a ratio of 6.6 for bond strength.

Finally, this chapter offers a regional dataset of material properties, which is of interest for practitioners when testing activities are not possible, either due to the historical relevance of the structure or to a lack of time and financial resources. The dataset obtained in this study, together with previously available literature data, contributed to the formation of the material table originally presented in NEN-NPR 9998:2015 and was partially updated in the subsequent versions (the current version, NEN-NPR 9998+C1:2020). However, the material properties suggested by NEN-NPR 9998:2020+C1 are often on the conservative side.





## CORE TESTING METHOD TO ASSESS NONLINEAR COMPRESSION BEHAVIOUR OF BRICK MASONRY\*

---

As discussed in Chapter 3, in the case of Dutch masonry with low overburden and slender load-bearing walls, no strong link was found between the results of laboratory tests on medium-sized specimens and in-situ semi-invasive testing methods. Accordingly, there is a lack of a testing method which can offer an acceptable compromise between the accuracy of the results and the introduced damage in the building. For this reason, both this chapter and the next chapter (Chapter 5) explore the suitability of the core testing method as a quick and efficient way to determine the mechanical properties of masonry under compression and shear-sliding load.

This chapter aims to evaluate the applicability of the core testing method to assess the complete nonlinear behaviour of brick masonry under compression loading in terms of Young's modulus, compressive strength and the corresponding strain, and compressive fracture energy. To this end, a comparative study was conducted in which small-diameter cores as well as companion medium-sized wallets were subjected to uniaxial compression loading. The suitability of the core testing method was investigated for two different core geometries: cores 150 mm in diameter and smaller cores 100 mm in diameter. For testing purposes, seven different masonry types were adopted, including both laboratory-made and field-extracted masonry. This chapter concludes that the core testing method can be regarded as a practical alternative to conventional semi-invasive testing techniques to evaluate both compressive strength and Young's modulus, while further studies are necessary to evaluate its potential for assessing the peak strain and the compressive fracture energy.

The outline of this chapter is as follows: A review of the current state of the art is presented in Section 4.1. A detailed account of the testing programme, including specimens' geometries and the testing procedure is provided in Section 4.2. The global response of each case study, compiled from tests on cylindrical cores and wallets, is discussed in detail in terms of crack evolution and characteristics of the stress-strain relationships in Section 4.3. The suitability of the core testing method is investigated by conducting a correlation study in Section 4.4. The chapter concludes by summarising the main findings in Section 4.5.

---

\*This chapter is based on the author's article published in the Journal of Construction and Building Materials, (Jafari et al., 2019). Minor modifications have been made to suit the thesis.

## 4.1 STATE-OF-THE-ART

Unreinforced masonry (URM) structures are primarily designed to withstand gravity loads; as a result, their compression characteristics are regarded as fundamental design parameters. As supported by experimental and numerical evidence (e.g., Haller, 1969; Lenczner, 1972; Lourenço, 1997a; Vermeltfoort, 2005; Lourenço & Pina-Henriques, 2006) URM under compressive load shows nonlinear behaviour caused by a complex interaction among the masonry constituents (e.g., masonry units and mortar joints), each having different elastic properties. This incompatibility between the properties of the masonry units and the mortar under compression leads to the formation of distributed splitting micro-cracks. Upon increasing loads, these micro-cracks grow and coalesce into macro-cracks resulting in localisation of deformations and thus masonry failure with energy release from in-plane and out-of-plane splitting, crushing, spalling, interface debonding, friction, and shear cracking (e.g., van Mier, 1984; Rots, 1991; Vonk, 1992; Bažant & Xiang, 1997).

To experimentally characterise the compression response of brick URM, conventional testing methods regulated by standards EN 1052-1 (CEN 1998) and ASTM C1197 (2014) can be employed. Following the standard procedure, compression tests can be performed on a medium-sized portion of brick masonry, made of a minimum of two bricks in length and a minimum of five brick courses in height, either extracted and tested in the laboratory or tested in-situ using flat-jacks. Despite the destructive sampling procedure, which is costly and not always practical, laboratory tests allow for capturing the full nonlinear compression behaviour of masonry, providing insights into the strength, stiffness, and the post-peak softening behaviour. The flat-jack tests are less destructive than laboratory tests, but only the elastic response of masonry can be captured, and insights into the compressive strength as well as the post-peak softening behaviour are barely provided. For a low value of overburden, due to technical challenges during test execution, uplift of the contrast portion can be expected rather than the pressurising of the masonry portion between the two flat-jacks. Thus, the range of applicability of the flat-jack test is constrained to walls with a high value of overburden. Results of the flat-jack tests can vary widely when the compressive stress field is not well-distributed due to poor quality of the masonry or to the cutting operation (e.g., Binda & Tiraboschi, 1999; Cescatti et al., 2016; Jafari 2018a). In view of the limitations of invasive laboratory tests and semi-invasive in-situ flat-jack tests, the necessity to establish an alternative testing method has been widely discussed (Noland et al., 1988; de Vekey, 1997; Brencich & Sterpi, 2006; Brencich & Sabia, 2008; Ispir et al., 2009; Sassoni & Mazzotti, 2013; Sassoni et al., 2014; Pelà et al., 2016a; Jafari et al., 2017; Segura et al., 2018).

To overcome the limitations of conventional testing methods, splitting tests on cylindrical cores have recently been studied as a promising alternative (Brencich & Sterpi, 2006; Brencich & Sabia, 2008; Ispir et al., 2009; Sassoni & Mazzotti, 2013; Sassoni et al., 2014; Pelà et al., 2016a; Jafari et al., 2017; Segura et al., 2018). Small-diameter cores cause limited invasiveness due to sampling and allow for the testing of samples in the laboratory with a standard set-up, which can make it possible to

obtain the complete nonlinear response of masonry beyond the peak strength. This information is essential for providing input parameters for nonlinear finite element analyses based on continuum models (e.g., Rots et al., 2017). According to the method first proposed by the International Union of Railways (UIC 778-3R:1995), the masonry compressive strength can be assessed using cores 150 mm in diameter made of two horizontal (bed) joints and one vertical (head) joint in the centre. To apply the compressive load on the core, UIC 778-3R(1995) recommends using steel cradles. However, Brencich and Sterpi (2006), Brencich and Sabia (2008), and Ispir et al. (2009) reported no good correlation between the properties obtained from the tests on cores and those on companion specimens. This can be caused by the stress concentration, which may arise due to the imperfect contact between the uneven core surface and the steel cradles. To minimise this effect, Sassoni and Mazzotti (2013), Sassoni et al. (2014), and Pelà et al. (2016a) used a high-strength mortar capping placed at the top and bottom of the core. Consequently, they achieved a better estimation of the compression properties. In addition, aiming to minimise the extent of damage due to drilling, Sassoni and Mazzotti (2013) and Sassoni et al. (2014) investigated the suitability of smaller diameter (100 mm) cores. In spite of valuable knowledge gained in these studies on the use of the core testing method, the case studies were always limited to clay brick masonry. In most cases, samples were extracted from walls built in a laboratory environment, disregarding the possible variability of material properties in existing buildings due to environmental conditions, long-term effects and workmanship. Moreover, these studies mainly focused on the characterisation of the pre-peak stage, in particular compressive strength and Young's modulus. Less attention was paid to the stress-strain relationship, including the post-peak softening and its relation to the damage evolution during loading.

## 4.2 MATERIAL AND METHODS

The comparative experimental study included compression tests on cylindrical cores and tests on companion wallets made of the same materials. These samples were either replicated in the laboratory, Figure 4.1a, or extracted from existing buildings, Figure 4.1b, located in the northern part of the Netherlands. Treating each masonry type replicated in the laboratory and each building as a separate object, in total, seven testing objects were investigated in this study. Of the seven tested objects, three were replicated in the laboratory using the same materials as explained in Chapter 2, and four were extracted from existing buildings. More information regarding the extraction and transportation of the samples from existing buildings can be found in Chapter 3. Table 4.1 lists an overview of the tested masonry objects, specifying unit type (solid clay or calcium silicate brick) and construction conditions (laboratory-made or field-extracted).

The flexural and compression characteristics of the mortar used in the construction of the replicated objects were determined from tests on mortar bars according to standard EN 1015-11 (CEN 1999), as discussed in Chapter 2. The flexural strength was assessed using a three-point bending test on 40×40×160 mm mortar bars, while compressive strength was determined from tests on broken specimens previously tested in the bending configuration. Table 4.1 lists the flexural strength and the compressive strength of the mortar tested at least 28 days after casting; the coefficient of variation is indicated in parentheses. The flexural strength and compressive strength of mortar for the calcium silicate brick masonry (MAT-1) were approximately two times higher than the corresponding values for the clay masonry specimens (i.e. MAT-3 and MAT-4). In the case of existing objects, the mortar properties could not be investigated due to difficulties in extracting intact mortar samples. For the laboratory-made specimens, the material properties were already discussed in Chapter 2; however, for the sake of completeness they are repeated here.

Both for replicated and existing objects, the flexural and compressive strength of bricks were evaluated according to standards NEN 6790(2005) and EN 772-1(CEN 2011), respectively. The mean value of the brick flexural strength was determined using out-of-plane three-point bending tests on six bricks; the load was applied parallel to the bed joint plane of the brick. More information regarding the testing procedure and data elaboration can be found in Appendix A. Linear behaviour was observed up to approximately 90% of the peak load; subsequently, some nonlinearity occurred just before the peak, followed by a brittle failure at maximum force. The compressive strength of brick was evaluated while load was applied perpendicular to the bed joint plane. The normalised mean value of the brick compressive strength was calculated from tests on six bricks, considering the shape factor and accounting for the height-to-thickness ratio. The brick flexural strength and normalised compressive strength are given in Table 4.1. The flexural strength of the clay bricks used to replicate samples in the laboratory (MAT-3 and MAT-4 objects) was approximately two times higher than the other brick types. A high dispersion of the flexural strength with a 76% coefficient of variation was found for the bricks extracted from the Molenweg object. The highest and lowest normalised

compressive strength belonged, respectively, to clay bricks from the Rengersweg object amounting to 41.90 MPa and to calcium silicate (CS) bricks from the MAT-1 object with the mean value of 13.26 MPa. The dispersion of the compressive strength of the existing objects was relatively low, as the coefficients of variation ranged between 12% and 17%, less than that of brick flexural strength ranging between 29% and 76%. Due to limitations of the sampling area in existing buildings, single CS bricks could not be extracted from the Tilweg object; in the case of Rengersweg object, six intact bricks were extracted and only tested in compression.

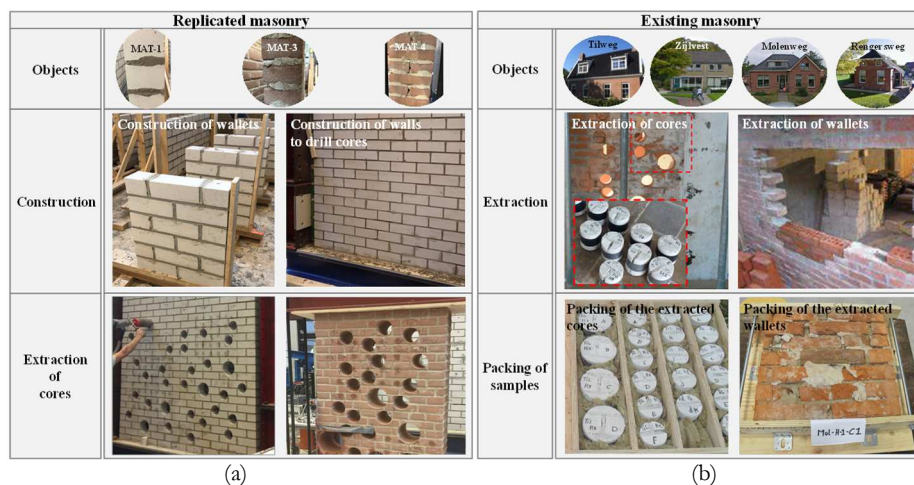


**Figure 4.1:** Overview of the masonry objects: (a) laboratory-made; (b) field-extracted.

**Table 4.1:**

Overview of the tested masonry objects including mortar and brick properties. Coefficient of variation in parentheses.

Objects	Brick types	Replicated/ Existing*	Mortar properties		Brick properties	
			Flexural strength MPa	Compressive strength MPa	Flexural strength MPa	Compressive strength MPa
MAT-1	CS	Replicated	3.21(5%)	7.57(6%)	2.79(11%)	13.26(13%)
Tilweg	CS	Existing(2000)	-	-	-	-
Zijlvest	CS	Existing(1976)	-	-	3.53(29%)	15.90(17%)
MAT-3/4	Clay	Replicated	1.40(12%)	3.81(9%)	6.31(11%)	28.31(10%)
Molenweg	Clay	Existing(1932)	-	-	2.78(76%)	21.73(13%)
Rengersweg	Clay	Existing(1920)	-	-	-	41.90(12%)

\*Year of construction of the existing building is indicated in parentheses.

**Table 4.2:**

Overview of the size of wallets and LVDTs dimension. For definition of parameters A, B, and C, see Figure 4.2c.

Objects	No. of wythe	Size of wallets mm <sup>3</sup>	A mm	B mm	C mm
MAT-1	Single	434×476×100	243	332	298
Tilweg	Single	450×490×100	250	330	290
Zijlvest	Single	460×420×100	145	210	330
MAT-3	Single	430×470×100	300	330	290
MAT-4	Double	540×650×210	360	390	290
Molenweg	Single	475×433×117	200	220	200
Rengersweg	Single	450×270×100	85	225	-

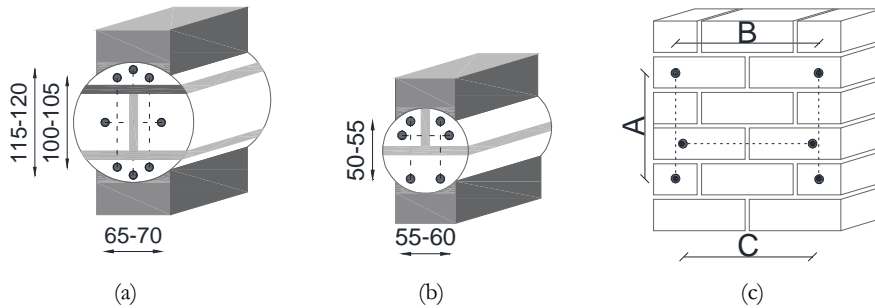


**Figure 4.2:** Overview of specimen geometry and LVDTs arrangement: (a) H-shaped core with 150 mm diameter; (b) T-shaped core with 100 mm diameter; (c) companion wallets. The length of parameters A, B, and C is given in Table 4.2.

#### 4.2.1 Testing set-ups and procedures

A displacement-controlled procedure was applied to capture the nonlinear behaviour up to and beyond the peak. The cylindrical cores and companion wallets were tested using a compression test set-up with a 3500 kN hydraulic jack (more details can be found in Appendix A.3). The peak load of the specimens was reached between 15 and 30 minutes, following the prescriptions of standard EN 1052-1(CEN 1998). The vertical and horizontal deformations, both on the front and on the backside of the specimens, were continuously measured using Linear Variable Differential Transformers (LVDTs). The LVDTs had a measuring range of 10 mm and an accuracy of  $\pm 1\mu\text{m}$ . Each face of the cylindrical cores and of the wallets was equipped with two vertical LVDTs and one horizontal LVDT, Figure 4.2. For the cores, the length of the LVDTs was kept almost unchanged, while for the companion wallets it was varied based on the wallet dimensions, Figure 4.2c and Table 4.2. In the latter case, aiming for a better estimation of the compressive fracture energy, the length of the vertical LVDTs was generally higher than the one prescribed by EN 1052-1(CEN 1998). No rotation or buckling of the vertical LVDTs in the pre-peak phase was reported. By contrast, for large out-of-plane or in-plane post-peak deformations of specimens, rotation and detachment of the LVDTs were observed; thus, the corresponding readings were not taken into account. In order to obtain the stress-strain relationship for the post-peak phase, readings of the hydraulic jack were used, Figure 2.9a.

In this study, the compressive behaviour of masonry is characterised in terms of Young's modulus, compressive strength and corresponding peak strain, and compressive fracture energy; an analyses of the stress-strain relationships for axial (i.e. vertical LVDT readings) and lateral strain (i.e. horizontal LVDT readings) are provided. The Young's modulus ( $E_3$ ) was evaluated between 1/10 and 1/3 of the maximum stress, aiming to eliminate an initial start-up of the stress-strain curve usually caused by the gradual contact between the loading plates and the specimen, which may unrealistically affect the estimation of the elastic modulus. This initial adjustment between the machine plates and the specimen was also observed by García et al. (2012) during compression tests on stone masonry. The compressive strength ( $f_m$ ) was determined as a ratio between the failure load and the loaded cross-sectional area of the individual specimen. In the case of a core, the loaded cross-sectional area can refer to the horizontal maximum cross-section (according to UIC 778-3R:1995) or to the cap cross-sectional area (as proposed by Pelà et al., 2016a); in this study the latter is considered. The peak strain was determined as the strain corresponding to the peak load. In order to describe the gradual post-peak softening, the concept of compressive fracture energy introduced by van Mier (1984) for concrete and further used by for masonry was adopted. The compressive fracture energy was calculated as the area underneath the stress-axial displacement curve over the height of the masonry specimen (thus excluding the cap's height in the case of the core). To obtain the ultimate displacement, the post-peak softening branch was approximated with a linear relation after reaching a stress level of  $0.3 f_m$ , and the slope of this line was evaluated between  $0.5 f_m$  and  $0.3 f_m$ , Figure 2.10. Considering the elastic-brittle behaviour of the capping mortar (will be explained in Section 4.3.1), it was assumed that no energy was dissipated by the capping mortar, and the energy dissipation was caused only by the fracture process in the masonry.

To compare the stress-strain relationships obtained from tests on cylindrical cores and companion wallets, the mean stress-strain curves, considering the axial and lateral strains, were derived for each object following the approach proposed by Augenti and Parisi (2010). For all individual masonry objects, the mean stress-strain curve was obtained by considering pre-defined increments of axial strain and calculating the corresponding average stress as well as the corresponding average lateral strain. In this study, an increment of the axial strain equal to  $1.5E-05 \pm 1\%$  was chosen.

#### 4.2.2 Specimen geometries

The comparative experimental study included tests on cores as well as tests on companion wallets, with a minimum of two bricks in length and a minimum of five brick courses in height. In the thickness, the specimens were either 100 mm (single-wythe with running bond) or 210 mm (double-wythe with Dutch bond).

Two core types were adopted: an H-shaped core with a diameter of 150 mm and a T-shaped core with a diameter of 100 mm. The former consisted of two bed joints and one central head joint, Figure 4.2a, while the latter was formed from one central

bed joint and one head joint, Figure 4.2b. The masonry cores were extracted perpendicular to the wall surface using a dry extraction procedure, as suggested by Pelà et al. (2016a). To preserve the integrity of the replicated walls during the sampling procedure, they were pre-compressed using pre-stressed rods. Generally, for replicated clay brick masonry (MAT-3 and MAT-4), in some cases a wet extraction procedure was adopted due to technical issues.

To evenly distribute the compressive load on the cross-sectional area of the cylindrical cores and to avoid stress concentration which may be caused due to the irregular surface of the core, cylindrical cores were capped at the top and bottom using high strength mortar, Figure 4.2a,b. This procedure, first proposed by Sassoni and Mazzotti (2013) and Sassoni et al. (2014), and subsequently applied by Pelà et al. (2016a), differs from the one proposed by the UIC 778-3R(1995), in which steel cradles are used to distribute the load. Following this procedure, a good bond between the cap and the core was reported; moreover, a confinement effect experienced in a real wall was simulated (Sassoni & Mazzotti, 2013; Sassoni et al., 2014). For capping, this study used a high strength mortar showing brittle behaviour under compressive loading. To evaluate the compression properties of the capping mortar, prisms were cast in moulds and kept in ambient laboratory conditions. Compression tests on the mortar prisms were performed 3, 7, 10, and 28 days after casting. Following standard EN 13412(CEN 2007), the compressive strength and Young's modulus of the capping mortar were evaluated as 60 MPa and 34 GPa, respectively; 95% of the cap strength was achieved after three days. Note that the capping mortar should have enough workability to create a continuous bond with the brick, as suggested by ASTM C1552(2003). After capping, cylindrical cores were kept in laboratory conditions. The caps were unmoulded after at least one day; testing took place after at least seven days.

To validate the applicability of the core testing method, companion wallets were subjected to compression loading. Following the prescriptions of standard EN 1052-1(CEN 1998), dimensions of the companion wallets depend on the size of brick and on the number of wythes (i.e. single or multiple wythe). However, due to difficulties of extracting large samples from existing buildings, only wallets from the Tilweg object had a height according to the standard prescriptions. Similar to the core samples, a dry extraction procedure was adopted to take wallets out of existing buildings. All the wallets replicated in the laboratory were constructed on a wooden frame to facilitate handling. The wallets' dimensions are specified in Table 4.2. To ensure that the loaded faces of the wallets were levelled and parallel to each other, as suggested by the standard, a 10-mm thick layer of gypsum was applied to the faces in contact with the loading plates.



## 4.3 GLOBAL BEHAVIOUR

In this section, the global response of cores, both 150 and 100 mm in diameter, and companion wallets under compression load is described in terms of crack patterns and the shape of the stress-strain relationships. First, the relation between the stress-strain relationships and the observed crack pattern is presented. Second, observations of the confinement effects due to the capping mortar on the core behaviour are presented, comparing the axial strain versus lateral strain curves. Finally, an overview of the behaviour of each object is presented separately. Note that an overview of the obtained material properties for cores and wallets is given in Section 4.4, where the correlation study is discussed.

### 4.3.1 General response

The general response of the cores and wallets is presented by correlating the stress-strain relationships with the evolution of the crack pattern, Figure 4.3. The analysis was carried out considering three phases: an initial linear-elastic phase, a pre-peak hardening phase, and a post-peak softening phase.

*Initial linear-elastic phase:* For the cores, a linear-elastic relation was observed between the stress and the axial strain up to approximately 40% of the compressive strength; no visible crack was detected on the core faces, Figure 4.3a. However, a reduction of lateral stiffness was observed, which can imply that internal micro-cracks were formed. For the wallets, no reduction of axial stiffness was observed up to approximately 50% of the compressive strength. However, the first sign of cracking was observed either along the brick-mortar interface of the head joints or as vertical splitting cracks in the bricks followed by a small reduction in lateral stiffness. In this phase, an acceptable match was found between the slopes of the stress versus axial strain curve, the so-called Young's modulus, obtained from tests on the cores and from tests on wallets. By contrast, the lateral stiffness of the cores was found to be approximately three to five times lower than that of the wallets.

*Pre-peak hardening phase:* Following the initial linear-elastic phase, both cores and wallets showed a hardening phase up to the peak strength, but a different crack pattern was observed, Figure 4.3b. In the case of cores, the first vertical splitting crack often appeared along the brick-mortar interface of the head joint. As the load was increased, more vertical splitting cracks spread in the specimen and were often localised close to the boundaries of the cap; no crushing or spalling was observed. In the case of wallets, the vertical tiny cracks, which had already appeared in the initial phase, gradually increased in length. In addition, vertical splitting cracks, uniformly spaced along the length and width of the wallets, and mortar crushing of the bed joints were also observed. For a stress level of 90% of the compressive strength, surface spalling along the length of the wallets was also detected. Generally, the values of the axial peak strain obtained for the cores, both 150 and 100 mm in diameter, were up to three times higher than the peak strain values obtained for the wallets. The CS masonry cores and wallets showed a longer

hardening regime with respect to clay masonry specimens. This can result from the gradual splitting process of the CS bricks and the stronger mortar as compared to the clay masonry.

*Post-peak softening phase.* Both cores and wallets showed a post-peak softening behaviour; a change in the slope of the curve was often observed at a residual stress of 85–90% of the compressive strength, Figure 4.3c. The tests were terminated when the specimens were fully disintegrated, and no more mechanical damage was reported due to friction. In the case of cores, the widening of the previously formed cracks was observed rather than the development of new cracks at close spacing. The localised vertical cracks aligned with the boundaries of the cap fully developed along the height and the width of the cores and thus led to the detachment of the marginal parts of the masonry that were not originally in contact with the cap. In the case of wallets, explosive splitting cracks (particularly for clay wallets) and spalling on the face of the wallets at the centre were often reported. In some cases, along the width of the wallets, in-plane branching cracks having a ‘V-shape’ or shearing cracks triggering a sliding between the front and back face of the wallets were observed.

The compression properties of the cylindrical cores can be evaluated by considering the horizontal maximum cross-sectional area either of the core or of the cap. As mentioned earlier, vertical splitting cracks in the cores generally localised at positions underneath the boundaries of the cap. This localisation often led to the detachment of the external part of the core. In agreement with the observed crack pattern, all the compression properties of the cylindrical cores were evaluated considering the cross-sectional area of the cap, although not all the cores showed localised cracks along the outer edges of the cap.

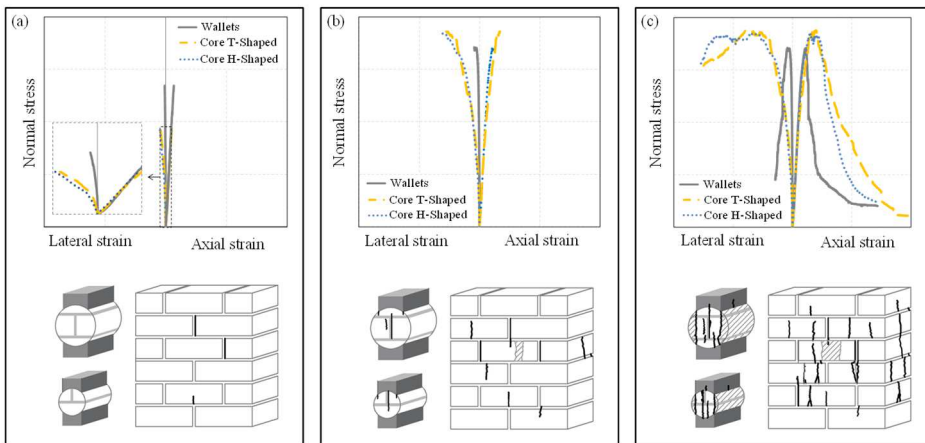


**Figure 4.3:** Typical compression response at three different phases: (a) initial linear-elastic phase; (b) pre-peak hardening phase; (c) post-peak softening phase. The shaded areas indicate detachment of material in cores and spalling in wallet.

To evaluate the effect of the difference in boundary conditions between cores and wallets, the typical stress versus axial displacement and axial strain versus lateral strain curves are analysed in Figure 4.4. The wallets showed a more ductile post-peak phase caused by fewer localised cracks with respect to the cores. Additionally, the T-shaped cores showed more brittle and more localised cracks than the H-shaped ones. Due to the frictional constraint between the masonry core and the capping mortar, it can be assumed that cores were generally more constrained than wallets. Higher peak strain was found for the cores in both axial and lateral directions with respect to the wallets. The ratio in terms of peak axial strain values between T-shaped and H-shaped cores for different objects varied between 0.6 and 1.6, while a variation between 0.31 and 1.0 was found when comparing the cores and the wallets, Figure 4.4b. Further research is ongoing to evaluate the possible influence of the cap stiffness and the cap geometry on the evaluation of the compression properties.

The evolution of cracks in the capping mortar was closely inspected to detect any undesired premature cracking of the capping mortar. Being a stiffer capping mortar bonded to a softer masonry core, cracking in the cap is expected due to the difference in stiffness of the two materials for large vertical displacements, Figure 4.5a. However, the onset of cracking is expected in the masonry core. In a few cases, a premature vertical crack, located at half the width of the cap, was observed in the capping mortar. During the curing period, an uneven top surface of the cap was often observed, which could be the cause for the premature cracking of the capping mortar during the compressive test. In the case that an uneven surface was observed, a finishing layer of gypsum was applied to restore the flat surface. This procedure was applied only in the case of cores extracted from existing structures. For the cores extracted from replicated walls, prior to the test, irregularities in the capping surface were not carefully investigated; consequently, a post evaluation was carried out based on photographic documentation. Figure 4.5b shows the influence of premature cracking in terms of stress-axial strain relations. The compressive strength was hardly affected by the premature cracking of the cap, while it often provided an underestimation of the Young's modulus and an overestimation of the peak strain as well as the compressive fracture energy. Accordingly, for specimens with the first signs of cracking in the cap, only compressive strength values were taken into account, and the other properties were excluded in the calculation of the mean values reported in Section 4.4.

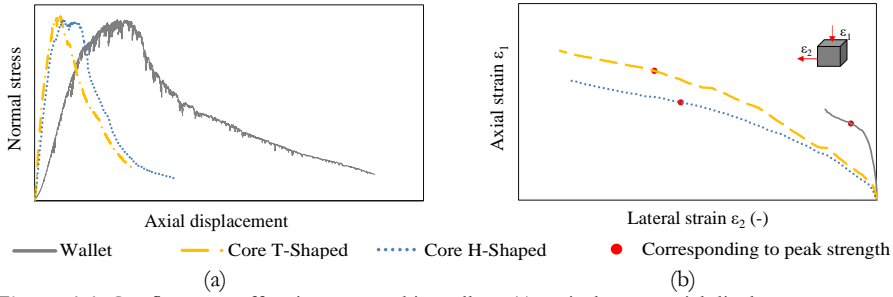


**Figure 4.4:** Confinement effect in cores and in wallets: (a) typical stress-axial displacement curves; (b) typical axial strain-lateral strain curves.

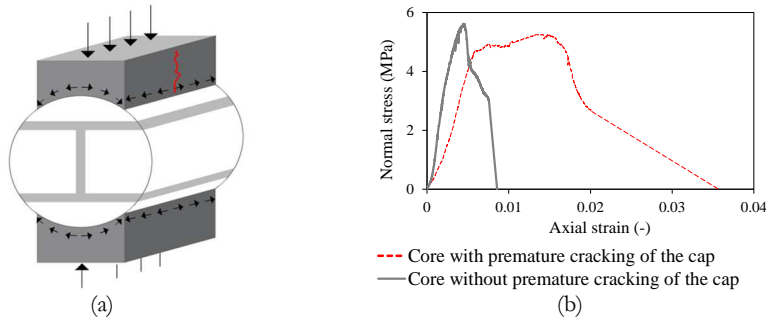


**Figure 4.5:** (a) Premature cracking of the capping mortar; (b) difference between compression response of masonry cores with and without premature cracking in the cap.

### 4.3.2 Response of each masonry object

In this section, the response of cores and companion wallets is analysed for each masonry object in Figure 4.6–Figure 4.12. Each figure comprises six parts, namely: (a) the crack pattern of the wallets; the crack pattern of the T-shaped cores (b) the front view and (c) the side view; the crack pattern of the H-shaped cores (d) the front view and (e) the side view and (f) the mean stress-strain curves for the wallets (grey line), T-shaped (yellow line) and H-shaped (blue line) cores. Due to limited data on wallets for the Rengersweg object, the mean stress-strain curve was approximated as a linear curve in the pre-peak phase, Figure 4.12f. In this section, those objects that showed a response different from the general trend (described in Section 4.3.1) are further analysed. This analysis is performed in view of the correlation study, which will be presented in Section 4.4.

For the laboratory-made CS masonry cores (MAT-1), the cracking occurred in the cap rather than in the masonry. As expected, the cores showed lower stiffness and higher peak strain with respect to the masonry wallets, Figure 4.6f. Consequently, for this object only compressive strength values can be regarded as reliable.

The compressive strength of the double-wythe clay masonry (MAT-4) was overestimated by 63% using the core method, Figure 4.10f. This difference in the compressive strength may result from the excessive confinement of the lateral expansion along the width of the core caused by the cap. The presence of a continuous cap might not allow the opening of the central joint in the width of the

core, a phenomenon that was observed for the wallets. Further studies are necessary to investigate this phenomenon and its influence on the compressive properties of masonry. Accordingly, the correlation study presented in the following section only focuses on single-wythe specimens.

The compressive strength of the existing clay masonry extracted from the Molenweg object was overestimated by 84% using the core method, Figure 4.11f. Visual inspections of the Molenweg building indicated pre-existing cracks in the bricks and only partial filling of the joints, which resulted in a very low value of the wallets' compressive strength (4.00 MPa). This non-uniform texture of the Molenweg object was probably caused by poor workmanship and aging. In the case of irregular masonry, unbiased sampling is not always achievable. In order to ensure the integrity of the core, it may be assumed that cores were extracted from 'best pieces', while for the larger wallets biased sampling was not possible. Therefore, the properties obtained from the core testing method may not be representative.

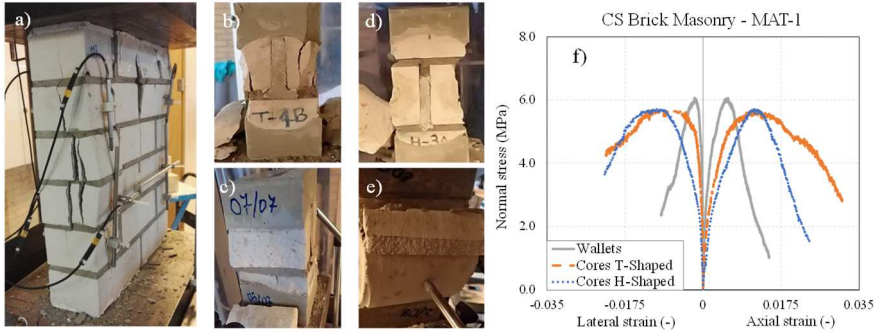


**Figure 4.6:** Laboratory-made CS brick masonry (MAT-1): (a) final crack pattern of wallets; (b,c) final crack pattern of T-shaped core; (d,e) final crack pattern of H-shaped core; (f) mean stress-strain relationships.

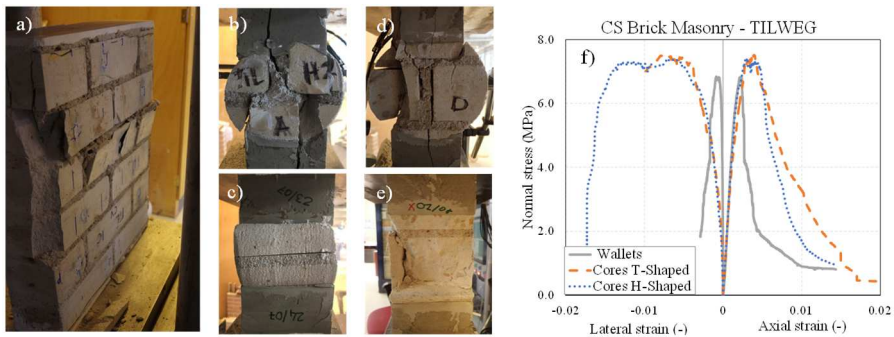


**Figure 4.7:** Field-extracted CS brick masonry (Tilweg): (a) final crack pattern of wallets; (b,c) final crack pattern of T-shaped core; (d,e) final crack pattern of H-shaped core; (f) mean stress-strain relationships.

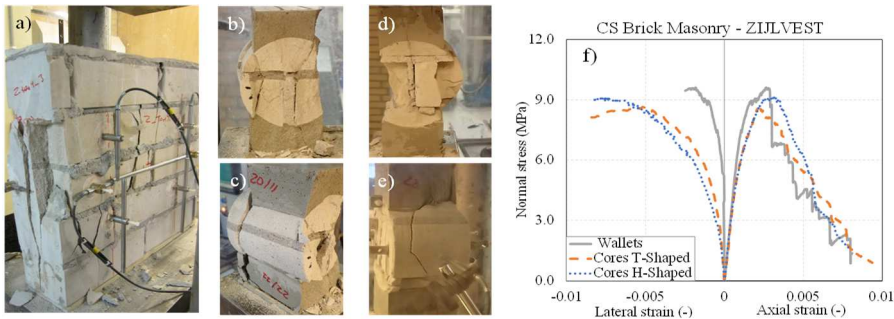


**Figure 4.8:** Field-extracted CS brick masonry (Zijlvest): (a) final crack pattern of wallets; (b,c) final crack pattern of T-shaped core; (d,e) final crack pattern of H-shaped core; (f) mean stress-strain relationships.

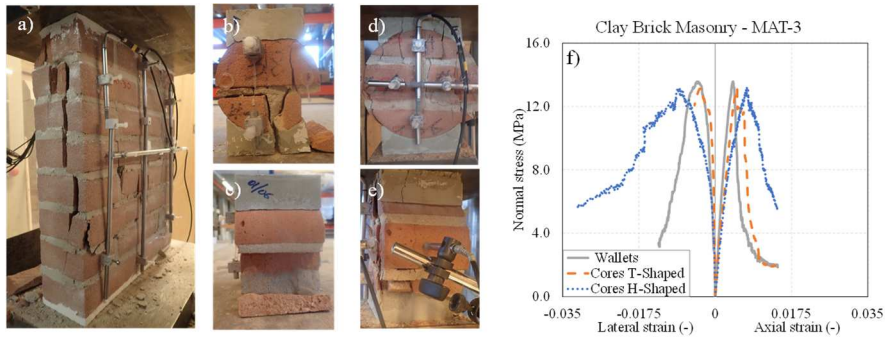


**Figure 4.9:** Laboratory-made clay brick masonry (MAT-3): (a) final crack pattern of wallets; (b,c) final crack pattern of T-shaped core; (d,e) final crack pattern of H-shaped core; (f) mean stress-strain relationships.

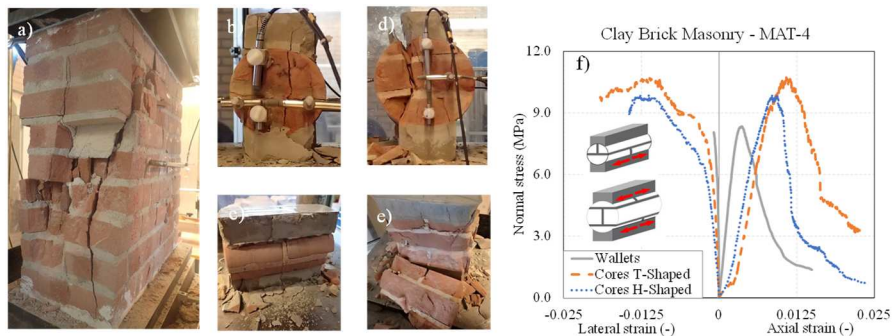


**Figure 4.10:** Laboratory-made double-wythe clay brick masonry (MAT-4): (a) final crack pattern of wallets; (b,c) final crack pattern of T-shaped core; (d,e) final crack pattern of H-shaped core; (f) mean stress-strain relationships.

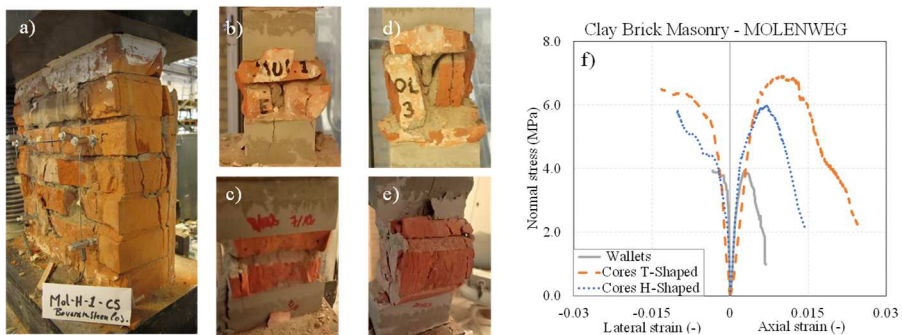


**Figure 4.11:** Field-extracted clay brick masonry (Molenweg): (a) final crack pattern of wallets; (b,c) final crack pattern of T-shaped core; (d,e) final crack pattern of H-shaped core; (f) mean stress-strain relationships (Vermeltoort, 2015).

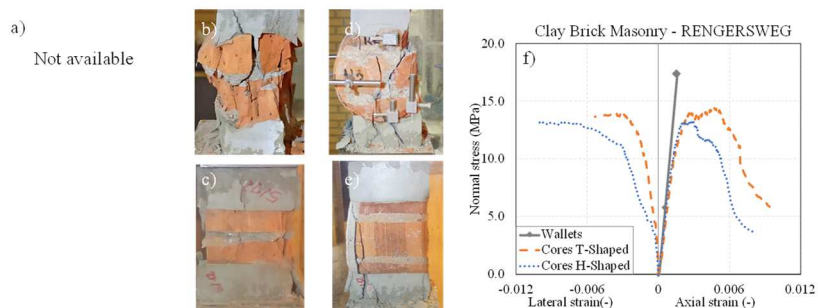


**Figure 4.12:** Field-extracted clay brick masonry (Rengersweg): (a) no information about crack pattern of wallets was available; (b,c) final crack pattern of T-shaped core; (d,e) final crack pattern of H-shaped core; (f) mean stress-strain relationships (Nonnekes, 2015a).



**Table 4.3:**

Database of compression properties from tests on cores and companion specimens.

Name / Ref	Unit <sup>1</sup>	No. Wythe <sup>2</sup>	Characteristic of cylindrical cores								Characteristic of companion specimens					
			No. Spec.	Area <sub>core</sub> / Area <sub>cap</sub>	Height of cap	$D_{core}$ mm	$f_{m,core}$ MPa	$E_{core}$ MPa	$\epsilon_{peak,core}$ ‰	$G_{fc,core}$ N/mm	No. Spec.	Size No.brick	$f'_m$ MPa	$E$ MPa	$\epsilon_{peak}$ ‰	$G_{fc}$ N/mm
MAT-1	CS/R	S	6	1.3	30	94	6.17	1674	18.73	14.92	6	2×6×1	6.35	4265	5.90	20.03
MAT-1	CS/R	S	6	1.6	29	143	6.18	1172	14.10	13.73						
Tilweg	CS/E	S	5	1.3	44	93	7.68	4515	3.85	5.46	3	2×6×1	6.93	4460	2.25	11.52
Tilweg	CS/E	S	5	1.6	45	144	8.37	4634	3.24	7.18						
Zijlvest	CS/E	S	7	1.3	43	94	9.38	9674	2.41	3.17	3	2×5×1	9.86	8639	2.44	15.95
Zijlvest	CS/E	S	7	1.6	49	144	9.52	8078	2.84	6.25						
MAT-3	C/R	S	2	1.3	24	100	13.00	3066	4.79	10.97	6	2×8×1	14.02	4590	4.26	29.34
MAT-3	C/R	S	2	1.5	20	150	14.04	2974	8.55	17.79						
MAT-4	C/R	D	6	1.4	35	100	15.08	2547	12.69	14.81	12	2×10×2	9.56	2951	4.06	33.27
MAT-4	C/R	D	5	1.7	41	150	13.76	2422	9.78	19.09						
Molenweg <sup>3</sup>	C/E	S	5	1.4	44	95	7.38	2205	5.08	10.49	3	2×7×1	4.00	3167	2.95	10.37
Molenweg	C/E	S	6	1.6	49	144	6.36	2743	5.88	9.67						
Rengersweg <sup>4</sup>	C/E	S	6	1.4	41	95	17.51	10268	3.64	6.60	3	2×5×1	17.39	11390	-	-
Rengersweg	C/E	S	6	1.6	48	144	14.70	10749	2.30	9.10						
ARCH <sup>5</sup>	C/E	S	9	1.2	40	100	15.88	-	-	-	3	2×3×1	13.20	-	-	-
MT1 <sup>6</sup>	C/R	D	9	1.3	40	100	12.69	-	-	-	3	3×12×2	8.47	-	-	-
MT2 <sup>6</sup>	C/R	D	14	1.3	40	100	17.06	-	-	-	3	3×12×2	10.23	-	-	-
3JC <sup>7</sup>	C/R	S	6	1.4	-	150	8.40	2570	-	-	6	1×5×1	5.82	2855	-	-

<sup>1</sup> Unit: CS/R = Calcium silicate masonry replicated in the laboratory  
CS/E = Calcium silicate masonry extracted from existing buildings

C/R = Solid clay masonry replicated in the laboratory  
C/E = Solid clay masonry extracted from existing buildings

<sup>2</sup> No. wythe: S = Single-wythe, D = Double-wythe.

<sup>3,4</sup> Tests on companion wallets were performed by third parties, Vermeltfoort (2015) and Nonnekes (2015a), respectively.

<sup>5,6,7</sup> Data were extracted from studies conducted by Sassoni and Mazzotti (2013), Sassoni et al. (2014), and Pelà et al. (2016a), respectively.

■ Excluded from correlation study in Section 4.4

## 4.4 CORRELATION STUDY

To evaluate the reliability of the core testing method, a correlation study was performed including the data presented in this study and those presented by Sassoni and Mazzotti (2013); Sassoni et al. (2014); and Pelà et al. (2016a). Although other references are available in the literature regarding the core testing method (e.g., Brencich & Sterpi, 2006; Brencich & Sabia, 2008; Ispir et al., 2009), in this study the attention is focused only on cores made with at least one vertical head joint and capped with high strength mortar (Table 4.3). Cores without any vertical head joint were omitted, because they could not represent the failure mode of the companion wallets, in particular when the onset of cracking is located in the head joint rather than in the brick. Sassoni and Mazzotti (2013) and Sassoni et al. (2014) studied the applicability of masonry cores 100 mm in diameter to reproduce the compressive strength of companion wallets for three masonry objects. Pelà et al. (2016a) replicated a single-wythe masonry object comparing the results of tests on cores with a diameter of 150 mm and tests on companion prisms.

Table 4.3 lists the compressive properties for every analysed object in terms of Young's modulus, compressive strength, peak strain, and compressive fracture energy of both cylindrical cores and companion wallets. The number of tested cores and tested companion wallets, the ratio between the maximum horizontal cross-sectional area of the core ( $A_{core}$ ) and of the cap ( $A_{cap}$ ), the minimum height of the cap at its centre, the core diameter ( $D$ ) and the dimension of the companion specimens are listed. As seen in Table 4.3, all the compression properties of the cylindrical cores were evaluated considering the cross-sectional area of the cap, although not for all the cores localised cracks along the outer edges of the cap were reported. In the case of literature data, this may differ from the procedure adopted in the original paper. The grey cells in Table 4.3 identify the values excluded from the correlation study in agreement with the observations made in Section 4.3.2. Consequently, the analysis is performed here considering only single-wythe specimens.

Using a linear regression analysis, the relation between compression properties of the cores and of the wallets is presented in Figure 4.13. The compressive strength ( $f_{m,core}$ ), the Young's modulus ( $E_{3,core}$ ), peak strain ( $\varepsilon_{peak,core}$ ) and the compressive fracture energy ( $G_{f-c,core}$ ) obtained by core testing are plotted against the same properties obtained by tests on companion specimens ( $f_m, E_3, \varepsilon_{peak}, G_{f-c}$ ). In each graph, the results for T-shaped cores (100 mm in diameter) are indicated with yellow markers and those for H-shaped cores with blue markers; in the case of CS masonry, partially black markers are adopted to distinguish them from clay masonry specimens. For every object, the standard deviation of the properties for the core is given with a horizontal bar, and for the wallets with a vertical bar. The red dashed line shows a one-to-one correlation curve, while the grey area gives the scatter band.

Comparing the results of the companion specimens and of the cores, a very good correlation is found in terms of compressive strength and Young's modulus. A ratio equal to 0.99 with a coefficient of determination of 0.88 is obtained for the compressive strength, Figure 4.13a. Similarly, a ratio equal to 1.05 with a coefficient

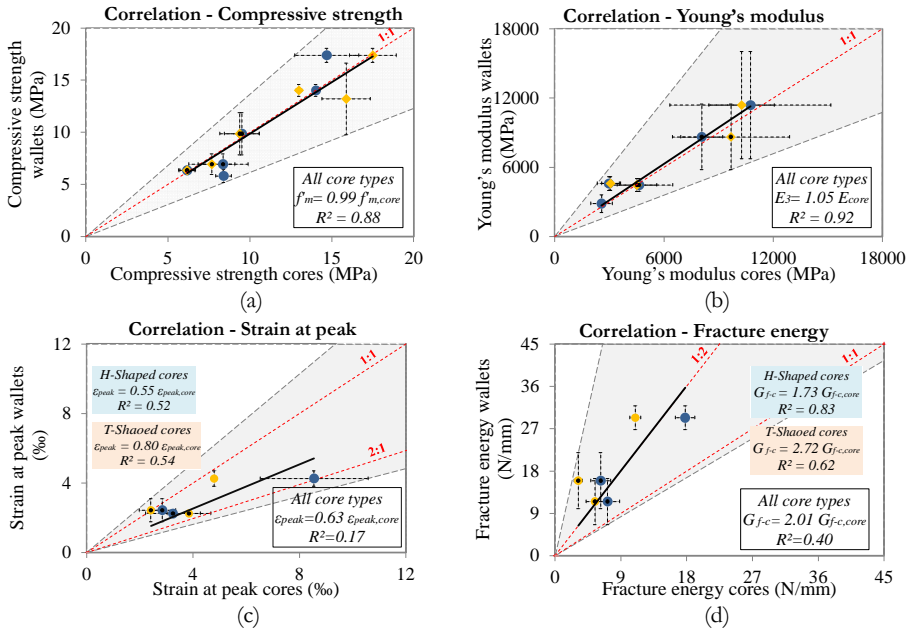
of determination of 0.92 is obtained for the Young's modulus, Figure 4.13b. For the compressive strength, the coefficient of variation was similar in the case of tests on cores and wallets, with a maximum of 21%. For the Young's modulus, wallets as well as cores from existing clay masonry objects (Rengersweg) showed the highest values of standard deviation, which may be attributed to spatial variability of masonry properties caused by workmanship and aging. The results obtained from both T-shaped cores (with 100 mm in diameter) and H-shaped ones (with 150 mm in diameter) show a good correlation with wallets. Consequently, for the analysed cases, no size effect is reported in the evaluation of compressive strength and the Young's modulus. This conclusion is in line with findings by van Mier (1984), in which the compressive strength and Young's modulus of concrete cubes having different heights were similar and independent of the specimen size.

Regarding the peak strain and the compressive fracture energy, no clear correlation is found between the results of tests on cores and tests on wallets, Figure 4.13c,d. The correlations improve if the T-shaped cores 100 mm in diameter and the H-shaped cores 150 mm in diameter are treated separately. Lower values of peak strain and higher values of fracture energy are obtained by tests on wallets with respect to the core testing method. The peak strain value obtained for the wallets is 0.80 times that for the T-shaped cores and 0.55 times the one for the H-shaped cores. The compressive fracture energy for the wallets is 2.72 times the one for the T-shaped cores and 1.73 times of the one for the H-shaped cores. Considering the energy per normalized unit of area (specific energy), it will be expected that a higher value of specific energy is needed to crack and crush small-diameter masonry cores rather than larger companion specimens.

In conclusion, despite the differences between the boundary conditions of the companion wallets and of the cores (due to the confinement effect of the capping mortar), the complete nonlinear response of existing masonry structures can be evaluated. The compressive strength and the Young's modulus obtained from the cores showed very good correlation with the properties obtained from the companion specimens. Independently of the core size (i.e. cores with a diameter of 150 or 100 mm), a correlation factor of one was found with a high correlation of determination. No clear correlation could be found for the peak strain and the compressive fracture energy obtained from tests on cores and companion specimens. A dependency on specimen size was observed in this study, which could, however, be influenced by the limited number of considered objects. Further studies are necessary for the evaluation of the post-peak softening properties.

Considering the good correlations obtained for different test methods in terms of compressive strength and Young's modulus, the database was further used to obtain correlations between these two masonry properties. Figure 4.14 gives the relation between the mean values of the Young's modulus and the characteristic compressive strength. Considering all the values obtained from both testing methods (excluding the data marked in grey in Table 4.3), a ratio between the Young's modulus and compressive strength equal to 634 with a low coefficient of determination of 0.43 was found. Approximately the same factor was found if cores and wallets were treated separately. Dutch national annex and Eurocode 6 proposed

an empirical linear formula in which the ratio between Young’s modulus and characteristic compressive strength was equal to 700 and 1000, respectively.



◆ CS Masonry Cores 100 mm ◆ Clay Masonry Cores 100 mm — Standard deviation bars — Regression line  
 ● CS Masonry Cores 150 mm ● Clay Masonry Cores 150 mm — Scatter band

**Figure 4.13:** Correlation between compression properties of the single-wythe cylindrical cores and of the companion specimens: (a) compressive strength; (b) Young’s modulus; (c) peak strain; (d) compressive fracture energy.

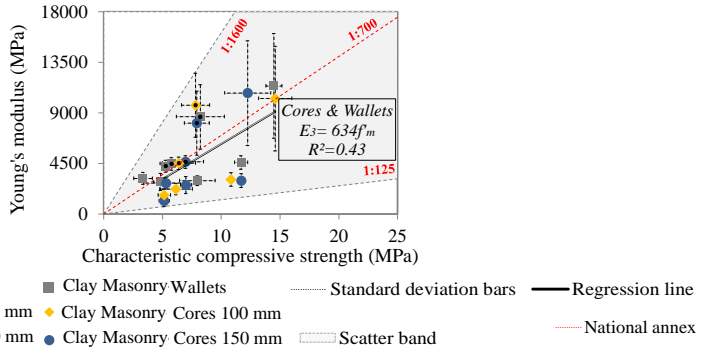


**Figure 4.14:** Correlation among the mean values of Young’s modulus and the characteristic values of compressive strength obtained from both testing methods, excluding data marked grey in Table 4.3.

## 4.5 CONCLUDING REMARKS

This chapter has illustrated and discussed the suitability of the test on small-diameter cores to evaluate the nonlinear behaviour of masonry in compression. This testing method is classified as being semi-destructive, as extraction of 150 mm (H-shaped) or 100 mm (T-shaped) diameter samples does not cause any disruption of building functionality. Seven masonry objects were selected, having either been replicated in the laboratory or extracted from existing buildings. Differently from previous studies, the present work was not limited to the evaluation of the compressive strength and the Young's modulus, but also aimed at characterizing the full nonlinear stress-strain behaviour including post-peak softening. The Young's modulus, compressive strength and corresponding strain, compressive fracture energy and the stress-strain relationship were established. To validate the accuracy of the results from the core tests, a comparative experimental approach was adopted by performing tests on companion wallets. The database established from tests on cores and tests on companion wallets was further augmented and expanded by adding literature data. The focus was on the correlation between the compression properties obtained from tests on cores and companion specimens made of single-wythe brick masonry. The following conclusions can be drawn:

- Due to the higher stiffness of the capping mortar, the lateral deformation of the masonry is restrained. Thus, tensile cracking of the capping mortar cannot be avoided due to increasing horizontal compressive stress in the masonry and the horizontal tensile stress in the capping mortar. Further experimental and numerical studies are suggested to investigate the influence of cap stiffness and cap geometry on compression properties.
- Masonry under compressive load shows nonlinear behaviour caused by a complex interaction among the masonry constituents (e.g., masonry units and mortar joints) each having different elastic properties. Upon increasing the load, diffused micro-cracks grow and coalesce into macro-cracks, resulting in the localisation of deformations and thus masonry failure. The majority of core specimens only showed the formation of out-of-plane splitting cracks and debonding cracks across the length. In addition, localised cracks formed along the end boundaries of the cap, eventually leading to the detachment of the marginal parts of the cores. The crushing and degrading of the inner part of the cores were also observed. By contrast, the wallets showed a complex crack pattern with damage distributed across both length and width. Considering the localisation of the cracks near the cap end boundaries, it is suggested to evaluate the compression properties obtained by core testing, considering stress evaluated with respect to the cap cross-sectional area.
- Despite the difference in crack pattern, the compressive stress-strain relationships obtained from cores and wallets showed remarkable similarity. They were characterised by a linear-elastic branch followed by a hardening behaviour until the peak and a post-peak softening behaviour, which can be

approximated by a linear descending branch, until reaching a residual strength of 5–10% of the compressive strength.

- By comparing the two tests' methods, a one-to-one correlation (with a coefficient of determination higher than 0.88) was obtained in terms of both compressive strength and Young's modulus. The strong correlations, which could be established only for single-wythe masonry, are independent of the masonry type (calcium silicate or clay masonry) and core size (i.e. cores 150 and 100 mm in diameter). In light of the latter finding, the use of smaller diameter cores is preferable, as the damage caused by extraction is less visible and can be easily repaired.
- The core testing method tends to overestimate the values of the peak strain, while it underestimates the evaluation of the compressive fracture energy. The differences in the post-peak response of the cores and wallets were also detected in terms of crack patterns, as cores showed no or limited in-plane splitting cracks and more widening of previously formed cracks rather than developing new cracks at close spacing. In addition, generally, higher values of the compressive fracture energy are reported from tests on H-shaped cores than on T-shaped ones. However, no specific trend is observed in terms of peak strain of both core types. As a function of the core size, the strain corresponding to the peak stress as well as the compressive fracture energy of the single-wythe cylindrical cores is only slightly correlated to the corresponding properties of the companion wallets. It should be noted that these correlations were obtained for a restricted data set that accounts separately for the core size. To clarify this size effect and the confining effect of the cap on the compression properties of the cores, more studies are suggested.
- Aiming to predict the mean values of the Young's modulus based on the characteristic values of the compressive strength of the corresponding object, a regression analysis was performed including results of both testing methods. A linear relation with a factor of 634 was found, with a low coefficient of determination of 0.43.

In conclusion, the comparative experimental study demonstrates the great suitability of the core testing method for addressing both compressive strength and Young's modulus. Moreover, the core testing method shows potential for the estimation of peak strain and compressive fracture energy. From a comparison with conventional testing methods, it can be concluded that the core testing method is less invasive than tests on wallets, but can provide comparable results; additionally, it employs conventional equipment, reducing the technical challenges of current in-situ testing methods, e.g., flat-jack tests. However, further studies, both experimentally and numerically, are suggested to investigate the effect of boundary conditions as well as the confinement effect of capping mortar on the evaluation of the compression properties.

## CORE TESTING METHOD TO ASSESS NONLINEAR SHEAR SLIDING BEHAVIOUR OF THE BRICK-MORTAR INTERFACE\*

---

Given the weak correlation found in Chapter 3 between the shear properties obtained from laboratory tests on triplets and those obtained from the in-situ shove test, this chapter investigates the suitability of the core testing method as a quick and efficient way to determine the mechanical properties of masonry under shear-sliding load. To this end, tests on 69 cores and shear-compression tests on 42 companion triplets are compared with respect to the evaluation of the nonlinear shear-sliding behaviour of masonry, including the determination of the post-peak softening response. In this context, seven brick masonry types, including clay and calcium silicate (CS) brick masonry, were selected for testing.

This chapter confirms the previous findings on the suitability of the core testing method for assessing the cohesion and friction coefficient of masonry. Additionally, the comparisons in terms of dilatancy and energy dissipation, novel aspects with respect to previous studies, provide interesting insights for further research on the cohesive and frictional mechanisms occurring at brick-mortar interfaces. Accordingly, due to its semi-invasive sampling nature and its good agreement with triplet results, the core testing method is confirmed to be a competitive technique for the in-situ assessment of the cohesion, friction coefficient, and shear modulus of mortar.

The outline of this chapter is as follows: A review of the current state-of-the-art is presented in Section 5.1. A detailed account of the experimental program, including testing procedure and elaboration of the experimental results is provided in Section 5.2. The global behaviour of the cores under shear load and of the triplets under combined shear-compression load is discussed in Section 5.3. The applicability of the core testing method to assess cohesion and friction coefficient is investigated in Section 5.4 by conducting a correlation study, including the literature data. A comparison is made between the outputs of the two testing methods in terms of elastic shear modulus of the joint in Section 5.5, dissipated energy during the formation of the shear crack linked to the cohesive mechanisms in Section 5.6, and the dilatant behaviour in Section 5.7. A summary of the findings and the lessons learned are presented in Section 5.8.

---

\* This chapter is based on the author's article published in the Journal of Construction and Building Materials, (Jafari et al., 2020). Minor modifications have been made to suit the thesis.

## 5.1 STATE-OF-THE-ART

Nonlinear numerical analyses, often used for the assessment of unreinforced masonry (URM) buildings subject to earthquake and wind loads, require a detailed description of nonlinear shear-sliding behaviour along the brick-mortar interface, including the evaluation of the post-cracking response. In fact, different modelling approaches, such as continuum approaches (e.g., Lotfi & Shing, 1991; Lourenço et al., 1998), micromechanical-based approaches (e.g., Gambarotta & Lagomarsino, 1997; Marfia & Sacco, 2012), and discrete models (e.g., Lourenço & Rots, 1997; D’Altri et al., 2019a) postulate a constitutive law to describe this behaviour. Under a combination of axial and lateral loading, the shear failure of URM walls is characterised as a stepwise diagonal shear cracking along the head joints and bed joints, and/or a shear-sliding along the bed joint. Previous experimental studies (e.g., Anthoine et al., 1995; Tomažević et al., 1996; Magenes & Calvi, 1997) indicated that the shear resistance of a URM wall was associated with the characteristics of the masonry component, such as wall geometry, overburden, and boundary conditions, as well as with the characteristics of the masonry material. Focusing on the latter, the present chapter deals with a detailed characterisation of the nonlinear shear-sliding behaviour of masonry along the brick-mortar interface in terms of cohesion, friction coefficient, shear modulus of the mortar joint, fracture energy (i.e. the energy required to create one unit area of a shear crack), and dilatancy.

In view of structural assessment, the in-situ characterisation of nonlinear shear-sliding behaviour at the brick mortar interface is of high relevance. Of the different standardised testing methods, shear-compression testing on triplets, Figure 5.1a, prescribed by standard EN 1052-3(CEN 2002), is regarded as a suitable method. By means of standard displacement-controlled equipment, both pre- and post-peak shear properties can be determined. However, the invasive extraction of multiple samples, made of three courses of bricks, is the major drawback in the practical application of this method. As an alternative, an in-situ method which involves a minimum disturbance to wall integrity was introduced by standard ASTM C1531-16(2016), known as the ‘shove test’ or ‘push test’, Figure 5.1b. Different than the laboratory triplet test, the shove test allows for determining only the cohesion and friction coefficient, and it is not likely to provide information on mode-II fracture energy. To perform a shove test, specialised technical experts should continuously monitor the deformations of the masonry wall using accurate instrumentation. This should be done to prevent the unwanted cracking of the contrast portion of the wall, which could introduce uncertainty regarding the reliability of the test (Binda & Tiraboschi, 1999; Cescatti et al., 2016). As the wall integrity is to some extent disturbed, objective interpretation of the factual normal stress acting on the tested brick due to the contribution of both flat-jacks and overburden is seldom possible. In this context, by integrating numerical and experimental approaches, Andreotti et al. (2018) and Ferretti et al. (2018a) provided better insight into the stress redistribution that occurs during the shove test. It should be pointed out that due to the differences in the boundary conditions of the triplet test and the shove test, the accuracy of



the experimental result could be argued. Nevertheless, the drawbacks and limitations of these conventional laboratory and in-situ testing methods gave rise to the development of novel methodologies, such as tube-jack testing (Manning et al., 2016) and the core testing method (Braga et al., 1992; Benedetti et al., 2008; Benedetti & Pelà, 2012; Mazzotti et al., 2014; Marastoni et al., 2016; Pelà et al., 2017).

As a minimally invasive inspection method is of paramount interest, particularly in the case of historical heritage structures, core testing was recently put forward as a novel method for characterising the shear behaviour of brick masonry along the brick-mortar interface (Braga et al., 1992; Benedetti et al., 2008; Benedetti & Pelà, 2012; Mazzotti et al., 2014; Marastoni et al., 2016; Pelà et al., 2016; Pelà et al., 2017). This method is based on the in-situ extraction of cylindrical cores having a diameter ranging from 70 to 100 mm and consisting of one central bed joint, Figure 5.1c. In the laboratory, the cores are subjected to a vertical line load along their thickness, similar to a Brazilian splitting test, ASTM C496(2017). By rotating the bed joint of the cores with respect to their original extraction position, different testing configurations can be considered by introducing various shear-compression stress states along the brick-mortar interface. As the loading condition is similar to that of the Brazilian splitting test, it is often referred to as a splitting test on the core. However, with reference to its purpose, the authors refer to this test as a shear test on the core. As stated by Pelà et al. (2017), this method was first introduced by Braga et al. (1992), who performed tests with a mortar inclination angle of  $45^\circ$ , aiming to reproduce a pure shear stress state along the brick-mortar interface that would be as comparable as possible to the diagonal-compression tests on panels standardised in ASTM E519(2015). With the aim of obtaining mortar properties, Benedetti et al. (2008) and Benedetti and Pelà (2012) performed tests on cores with mortar inclination angles of  $30^\circ$ ,  $45^\circ$ , and  $60^\circ$ . In follow-up studies (e.g., Mazzotti et al., 2014; Marastoni et al., 2016; Pelà et al., 2016; Pelà et al., 2017) extensive experimental research was performed using a mortar inclination angle between  $0^\circ$  and  $60^\circ$ . The failure mode of the cores with mortar inclination angles between  $40^\circ$  and  $55^\circ$  was predominantly described as a shear-sliding along the brick-mortar interface, enabling the calculation of the shear strength parameters in agreement with the Coulomb friction criterion (Mazzotti et al., 2014; Pelà et al., 2016; Pelà et al., 2017). In this context, to confirm the accuracy of the failure criterion established by the core testing method, Mazzotti et al. (2014) and Pelà et al. (2017) also performed shear-compression tests on companion specimens. As they reported, the shear strength of the companion specimens, characterised in terms of cohesion (initial shear strength) and friction coefficient, matched well with the results of shear tests on cores. Accordingly, the core testing method provides basic knowledge about the shear mechanical properties (i.e. cohesion and friction coefficient) for assessing the structural response. However, for accurate predictions of the failure mechanism and failure modes of masonry structures, not only the strength at peak but also a full description of the shear properties in the pre-peak and post-peak phases is often required. It should be emphasised that the reliability of the core testing method may be questioned on the grounds that it provides insight into the local behaviour

of masonry rather than the whole structure. Nevertheless, the same concern applies to all the available in-situ testing methods when a small and representative portion of masonry is tested.

In spite of the valuable contribution of previous studies on the suitability of the core testing method, the potential of this method to determine the complete nonlinear shear-sliding behaviour of masonry has not been broadly investigated (i.e. in terms of shear modulus of the mortar joint, post-peak cohesion softening behaviour, and dilatancy). In addition, previous studies focused only on clay brick masonry samples extracted from masonry that was replicated in laboratories. Thus, the possibility of offsetting the wide variation in results could be raised, as the influence of aged materials and workmanship on mechanical properties is deliberately neglected. Considering that the core testing method shows potential for in-situ characterisation of masonry due to its limited sampling invasiveness and the straightforward interpretation of the testing results, this chapter investigates the further potentialities of the method.

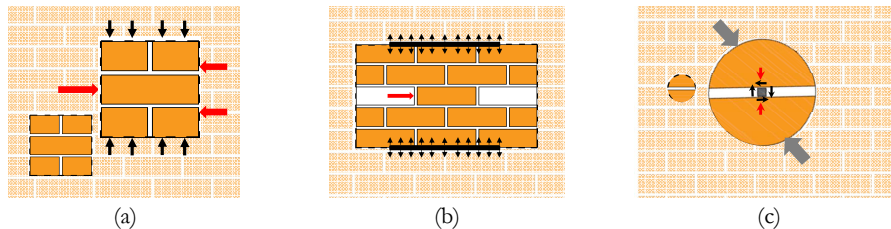


**Figure 5.1:** Characterising shear-sliding behaviour along the brick-mortar interface using: (a) laboratory shear-compression testing on triplets; (b) in-situ shove testing on a portion of masonry wall; (c) laboratory shear testing on a small-diameter core.

## 5.2 MATERIALS AND METHODS

The comparative experimental programme focused on extracted samples from existing buildings located in the northern part of the Netherlands, in the province of Groningen, and replicated samples built in the laboratory. The masonry objects adopted in this chapter are the same as discussed in Chapter 4. In total, seven different masonry objects were included in this study, as each building used for the sampling and each masonry type replicated in the laboratory were treated as separate objects, Figure 5.2. An overview of the tested masonry objects, as well as the unit type (CS brick or solid clay), construction type (built in the laboratory or extracted from existing buildings), and the measured characteristics of masonry components in terms of compressive and flexural strength can be found in Table 4.1.

Tests were conducted on small-diameter cores 92–105 mm in diameter having one central bed joint, as well as on companion triplets of one brick in length and three brick courses in height. Considering that a running bond pattern is used in existing buildings, the replicated masonry specimens were built with a running bond pattern and are here called ‘modified triplets’ (Figure B.1a, Appendix B). They differ from ‘standard triplets’ (Figure B.1b, Appendix B) composed of stack-bonded bricks, and comply with EN 1052-3(CEN 2002). To investigate the difference between the shear properties of standard triplets and modified triplets, both triplet configurations were built in the laboratory and tested under shear-compression loading. A summary of the shear strength of both modified and standard triplets is given in Appendix B. In total, 36 cores and 25 modified triplets were extracted from existing buildings, and 33 cores and 17 standards triplets were built in the laboratory.

Sampling from both existing and replicated objects was performed perpendicular to the wall surface using a dry extraction procedure, as suggested by Pelà et al. (2017). Both cores and triplets were packed and transported to the laboratory according to the recommendations of ASTM C1532(2005). Additionally, the integrity of the replicated walls during the core drilling was a cause for safety concern in the laboratory. Hence, the walls were pre-compressed using transverse beams, as suggested by Pelà et al. (2017). Note that due to the technical issues in drilling cores from the MAT-4 clay walls, in some cases, a wet extraction procedure was adopted.

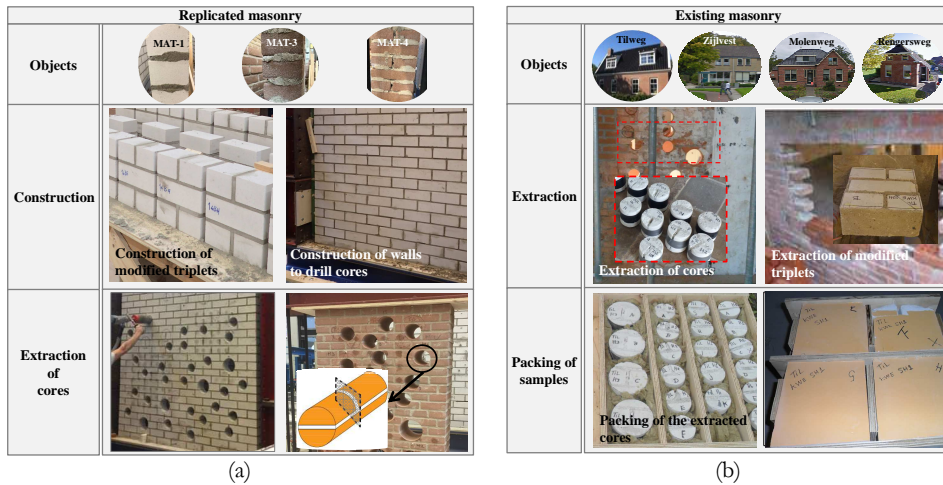


**Figure 5.2:** Overview of the masonry objects: (a) replicated in laboratory; (b) extracted from existing buildings.

### 5.2.1 Testing procedure

This section describes the testing procedure adopted for the shear tests on cores and the shear-compression tests on companion triplets. The former was performed following the provisions of the literature (Benedetti et al., 2008; Benedetti & Pelà, 2012; Mazzotti et al., 2014; Marastoni et al., 2016; Pelà et al., 2016; Pelà et al., 2017), as no standard approach currently exists, while the latter was carried out under the guidelines of standard EN 1052-3(CEN 2002).

Under a monotonic shear load, the response of masonry cores rotated with respect to their original horizontal configuration was investigated. A load was introduced along two opposite lines, where packing strips with a density of  $1099 \text{ kg/m}^3$  and dimensions of  $194 \times 15 \times 2 \text{ mm}$  were inserted between the core and the loading plates. Two different testing set-ups were used in this study, as the design of the testing procedure and measuring systems were part of the learning process. First, a displacement-controlled set-up was attempted, in which the core response was recorded by increasing the jack displacement at a rate of  $0.5 \text{ } \mu\text{m/s}$ . In addition to the jack displacement measurement, at each face of the core, the relative sliding of one brick portion over the other was measured using a linear variable differential transformer (LVDT), Figure 5.3a. However, due to brittle failure, the adopted set-up did not fully enable the measurement of the gradual post-peak degradation. Hence, as an alternative, a sliding-controlled set-up was adopted in which the relative sliding of the brick-mortar interface measured by the LVDTs was used as a control parameter. The sliding was increased at a rate of  $0.05 \mu\text{m/s}$ . Additionally, the normal deformations perpendicular to the joints were recorded at each face using one LVDT, Figure 5.3b. The LVDTs of the two testing set-ups had a measuring range of  $5 \text{ mm}$  with an accuracy of  $\pm 1 \mu\text{m}$ .

To trigger the various combinations of shear-compression stress states along the brick-mortar interface, three different inclination angles of  $45^\circ$ ,  $50^\circ$ , and  $55^\circ$  were used. For each inclination, when possible, at least three specimens were tested.

The selection of the inclination angle was made in agreement with the observations by Mazzotti et al. (2014), in which shear-sliding failure was observed for inclination angles between  $40^\circ$  and  $50^\circ$ , while unrepresentative splitting failure was observed for inclination angles less than  $40^\circ$  and greater than  $55^\circ$ . Note that for the replicated CS and clay brick masonry objects, tests on the cores with an inclination angle of  $40^\circ$  were also performed, and the failure mode was mainly reported as a shear-sliding failure along the brick-mortar interface with brick splitting failure.

The shear response of the companion triplets was investigated by subjecting a pre-compressed triplet to an increasing shear deformation along the mortar bed joints. In this study, a displacement-controlled procedure was used to apply shear load to the middle brick of a triplet at an increasing rate of  $5 \mu\text{m/s}$ , Figure 5.3c. The hydraulic jack had a 100 kN capacity. Throughout the test, a constant horizontal pre-compression force was applied to the specimen via a horizontal hydraulic jack that was operated manually. The horizontal jack had a 50 kN capacity and was kept in place by means of four steel rods positioned on opposite sides of the specimen, connecting two steel plates that acted as contrasts. To keep the transverse compressive load approximately constant (with an acceptable variation of  $\pm 2\%$ ), a spring with a stiffness of 123 N/mm or 3300 N/mm was interposed between the actuator and the specimen. The spring with lower stiffness was used for a pre-compression level lower than 0.30 MPa, while the spring with higher stiffness was used in the other cases. The shear-compression test was repeated at three different pre-compression levels: level 1 between 0.05 and 0.35 MPa, level 2 between 0.31 and 0.70 MPa, and level 3 between 1.0 and 1.2 MPa. At each level, when possible, at least two specimens were tested. During the shear-compression tests on the modified triplets, Figure 5.3c, the relative sliding of the middle brick with respect to the lateral ones was calculated as an average of the readings of all four individual vertical LVDTs. The normal displacement of the two bed joints was calculated as an average of the readings of two horizontal LVDTs: one at each side of the triplet. The LVDTs had a measuring range of 10 mm with an accuracy of  $\pm 5 \mu\text{m}$ .

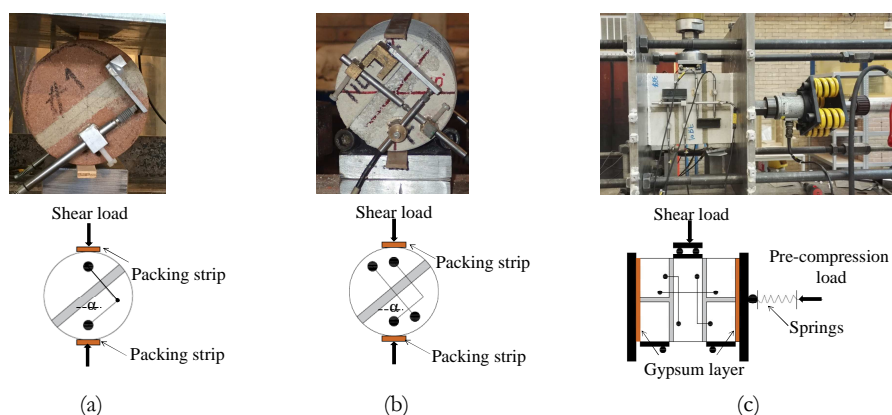


**Figure 5.3:** Experimental set-up: (a) testing cores using displacement-controlled set-up; (b) testing core using a sliding-controlled set-up; (c) shear-compression tests on modified triplets using a displacement-controlled set-up.

## 5.2.2 Elaboration of experimental results

This section builds on the elaboration of the mechanical properties characterised in terms of cohesion (or initial shear strength), friction coefficient, shear modulus of the mortar joint, energy dissipation per unit area of the shear crack, and dilatancy. In the following sections, the global behaviour of cores and triplets is first presented, and thereafter, comparisons in terms of the shear properties of the two testing methods are made.

In contrast to the literature that challenged the uniform stress distribution along the brick-mortar interface, the distribution of the tangential shear stress and the normal stress was assumed to be uniform. For cores, Benedetti et al. (2008) reported the local stress concentration beneath the applied load. For the triplets, it has been shown that the uniformity of the stress distribution deviates in the vicinity of the supporting plates (Stockl et al., 1990; van der Pluijm, 1993; Ferretti et al., 2018b). For the core, the tangential shear strength,  $f_{v,core}$ , and the corresponding normal stress,  $f_{p,core}$ , associated with the maximum vertical load,  $F_{max}$ , can be estimated as follows:

$$f_{v,core} = \frac{F_{max} \cdot \sin \alpha}{A} \quad (5.1)$$

$$f_{p,core} = \frac{F_{max} \cdot \cos \alpha}{A} \quad (5.2)$$

where  $A$  is the mortar cross-sectional area, and  $\alpha$  is the mortar inclination angle with respect to its original horizontal configuration. For the triplet test, the shear strength,  $f_v$ , and the normal pre-compression stress,  $f_p$ , were calculated as follows:

$$f_v = \frac{F_{max}}{2A} \quad (5.3)$$

$$f_p = \frac{F_h}{A} \quad (5.4)$$

where  $F_{max}$  is the maximum vertical load,  $A$  is the mortar cross-sectional area, and  $F_h$  is the (constant) horizontal pre-compression load.

The shear strength of both testing methods was assumed to follow the Coulomb friction criterion, as the failure mode of the cores and the triplets was characterised as a shear-sliding crack along the brick-mortar interface. Assuming a linear relation between the shear strength and the corresponding normal stress, the cohesion,  $f_{i0,core}$ ,  $f_{i0}$ , and the friction coefficient,  $\mu_{core}$ ,  $\mu$ , were evaluated, respectively, as the shear stress corresponding to the zero normal stress and the slope of the linear regression line, Figure 5.4. For a given inclination angle, the core testing results appear along a line passing through the origin and having a slope similar to the mortar inclination, Figure 5.4a. Accordingly, to exclude the effect of the number of data points, linear regression analysis was performed by considering the mean values of each inclination angle, as suggested by Mazzotti et al. (2014). For each tested object, Table 5.1 summarises the cohesion and the friction coefficient obtained using the two testing methods, together with the mean values of the maximum shear stress and the corresponding normal stress.

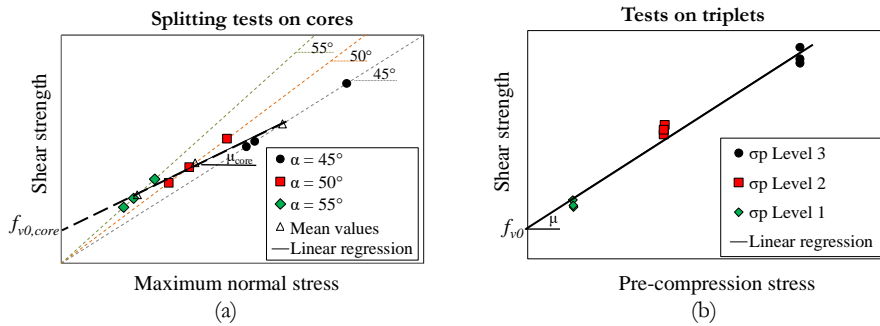


**Figure 5.4:** Establishing failure criterion: (a) shear tests on cores; (b) shear-compression tests on triplets.

Recording the relative sliding of the bricks allowed for the evaluation of the shear modulus of the mortar joint during the shear tests on cores and the shear-compression tests on triplets. The shear modulus of the mortar joint was determined to be the secant stiffness of the shear stress-strain curve, considering that the shear stress was calculated based on the same principal as in Eq. (5.1) and Eq. (5.3), and the strain was obtained by dividing the relative sliding by the joint thickness. Table 5.1 presents the values of the shear modulus evaluated in the linear-elastic phase at a stress level corresponding to 1/3 of the maximum shear stress,  $G_{m,core}$ ,  $G_m$ . It should be noted that the sliding deformations include both the sliding of the joint as well as brick deformation. However, the brick deformation was disregarded, as the brick is much stiffer than the mortar.

In nonlinear finite element analysis of quasi-brittle materials like masonry, not only are the stiffness and strength properties reported, but so is the toughness, i.e. the post-peak softening. The toughness for shear fracture can be expressed by the mode-II fracture energy,  $G_{fII}$ , which is the energy required to create a one-unit area of a shear crack along the brick-mortar interface. Nevertheless,  $G_{fII}$  cannot be simply calculated as the area underneath the shear stress-sliding curve, as the shear stress incorporates the contribution of both cohesive and frictional stress. In other words, the notion behind the fracture energy in shear is to distinguish the cohesion mechanism from the contribution of friction. The latter, arising from the surface roughness along the brick-mortar interface, is calculated by multiplying the friction coefficient for normal stress.

No direct comparison can be made between the shear fracture energy in the cores and in the triplets, due to the differences between them in the state of normal stress. Throughout the shear test on triplets, the pre-compression stress was kept constant, meaning that the frictional stress did not change, Figure 5.5a. Accordingly, the mode-II fracture energy in the triplets was approximated as the area underneath the shear stress-sliding curve over which the cohesion decreases to zero, Figure 5.5b. The stress corresponding to the zero cohesion is known as residual shear strength,  $f_{v,res}$ . Unlike in the triplet test, the friction contribution was not constant throughout the shear tests on cores, as the applied load and thus the normal stress component were continuously changing. For the cores, the frictional contribution was also estimated by multiplying the friction coefficient ( $\mu_{core}$ ) for the

normal stress component. Accordingly, the cohesive contribution was found by subtracting the frictional stress from the shear stress, Figure 5.5c. The friction coefficient was evaluated by treating the results of all the core samples together, as shown in Figure 5.5a. The area underneath the cohesive stress-sliding curve could somehow reflect the dissipated energy during the shear cracking in the cores, Figure 5.5d. The dissipated energy,  $G_{f-core}$ , was calculated only for the cores in which the pre-peak and the entire post-peak curve were successfully captured by means of the sliding-controlled set-up. As no direct comparison can be made in terms of the fracture energy of the two testing methods, Section 5.6 deals with predicting the post-peak response of the triplets using the results of the cores.

As supported by experimental and numerical evidence (e.g., Rots et al., 1997; van Zijl et al., 2001; van Zijl, 2004; Ferretti et al., 2018b), when a brick-mortar interface is subjected to shear loading, upon the onset of cracking, an uplift of the joint is expected. This expansion of the joint often diminishes with larger sliding, as no further damage or degradation of asperities occurs. In confined masonry, this phenomenon, known as dilatancy, could lead to a local increase in the normal stress and thus an increase in the shear strength. Ignoring the dilatancy (i.e. assuming  $\psi=0$ ) often results in a non-conservative prediction of masonry response. To determine the dilatancy from the experimental results, the following formula is adopted (e.g., van Zijl et al., 2001; van Zijl, 2004):

$$\tan(\psi) = -\frac{(u_p)_{n+1} - (u_p)_n}{(v_p)_{n+1} - (v_p)_n} \quad (5.5)$$

where  $v_{pl}$  is the plastic sliding displacement,  $u_{pl}$  is the corresponding plastic normal displacement perpendicular to the bed joint, and  $n$  is the increment of the sliding displacement. The calculation of the plastic displacements excludes the elastic deformation of the mortar. To this end, the mortar stiffness is assumed to be 200 times the compressive strength of mortar (Kaushik et al., 2007).



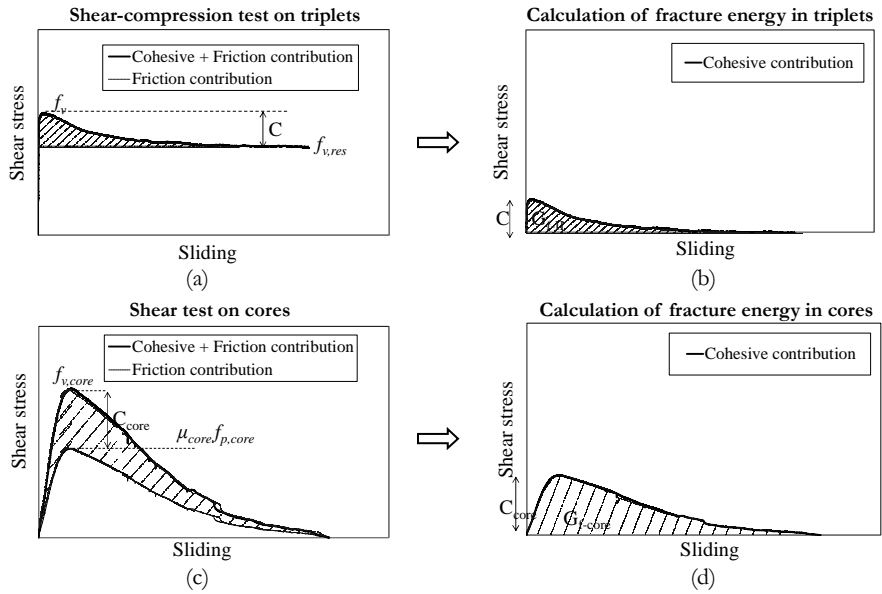


**Figure 5.5:** Calculation of fracture energy from shear stress-sliding curves and excluding the friction contribution from the shear stress: (a,b) triplets; (c,d) cores.

**Table 5.1:**

Database of shear properties obtained from tests on cores and on companion specimens.

Objects	Shear tests on cores							Shear-compression tests on companion triplets/panels					
	$\alpha$	<sup>1</sup> Failure(No.)	<sup>2</sup> $f_{r,core}$	<sup>2</sup> $f_{p,core}$	$f_{t0,core}$	$\mu_{core}$	<sup>2</sup> $G_{m,core}$	$f_p$	<sup>1</sup> Failure(No.)	<sup>2</sup> $f_r$	$f_{t0}$	$\mu$	<sup>2</sup> $G_m$
	(No.)		MPa	MPa	MPa	-	MPa	MPa		(No.)	MPa	MPa	-
MAT-1	40 (4)	S (1), ST (3)	0.36 (38)	0.43 (38)	0.13	0.58	-	0.20 (3)	S (3)	0.23 (24)	0.15	0.48	290 (67)
Replicated CS masonry	45 (6)	S (3), ST (3)	0.37 (25)	0.37 (25)	-	-	-	0.60 (4)	S (4)	0.46 (5)	-	-	462 (9)
	50 (5)	S (5)	0.25 (51)	0.21 (51)	-	-	-	1.20 (3)	S (3)	0.71 (3)	-	-	402 (23)
	55 (5)	S (5)	0.22 (67)	0.22 (67)	-	-	-	-	-	-	-	-	-
	-	-	-	-	-	-	-	-	-	-	-	-	-
Zijlvest	45 (3)	S (1), T (2)	1.49 (-)	1.49 (-)	0.42	0.76	856 (-)	0.05 (1)	S (1)	0.32 (-)	0.29	0.79	-
Existing CS masonry	50 (3)	S (2), T (1)	0.83 (19)	0.70 (19)	-	-	281 (62)	0.35 (2)	S (1), T (1)	0.63 (-)	-	-	-
	55 (3)	S (2), ST (1)	1.10 (15)	0.77 (15)	-	-	660 (23)	0.70 (2)	S (2)	0.75 (17)	-	-	-
	-	-	-	-	-	-	-	1.00 (3)	S (3)	1.13 (27)	-	-	-
Tilweg	45 (2)	S (2)	0.42 (3)	0.42 (3)	0.13	0.71	199 (8)	0.10 (1)	S (1)	0.18 (-)	0.12	0.62	202 (-)
Existing CS masonry	50 (3)	S (2), ST (1)	0.35 (22)	0.30 (22)	-	-	226 (41)	0.31 (2)	S (2)	0.32 (3)	-	-	404 (40)
	55 (3)	S (2), ST (1)	0.24 (21)	0.17 (21)	-	-	199 (35)	1.00 (1)	S (1)	0.74 (-)	-	-	179 (-)
MAT-3	40 (3)	ST (3)	1.33 (7)	1.58 (7)	0.22	0.80	-	0.20 (3)	S (3)	0.30 (23)	0.15	0.79	296 (27)
Replicated clay masonry	45 (3)	ST (2), T (1)	0.60 (25)	0.60 (25)	-	-	-	0.60 (2)	S (2)	0.61 (11)	-	-	297 (12)
	50 (3)	ST (2), T (1)	1.43 (16)	1.20 (16)	-	-	-	1.00 (3)	S (3)	0.91 (11)	-	-	248 (9)
MAT-4	45 (5)	ST (4), T (1)	1.07 (32)	1.07 (32)	0.22	0.80	284 (56)	The same as MAT-3					
Replicated clay masonry	50 (6)	S (6)	0.50 (37)	0.42 (37)	-	-	169 (32)						
	55 (6)	S (6)	0.62 (45)	0.44 (45)	-	-	162 (53)						
Molenweg <sup>3</sup>	45 (2)	S (1), ST (1)	1.00 (40)	1.00 (40)	0.35	0.67	1252 (44)	0.20 (3)	-	0.36 (14)	0.34	0.48	-
Existing clay masonry	50 (2)	S (2)	0.90 (27)	0.76 (27)	-	-	326 (42)	0.60 (3)	-	0.79 (1)	-	-	-
	55 (2)	S (2)	0.63 (48)	0.44 (48)	-	-	241 (-)	1.00 (3)	-	0.73 (15)	-	-	-
Rengersweg <sup>3</sup>	45 (3)	ST (1), T (2)	2.47 (-)	2.47 (-)	0.49	0.85	2532 (-)	0.20 (2)	-	0.74 (12)	0.54	1.00	-
Existing clay masonry	50 (3)	S (1), T (2)	0.97 (-)	0.82 (-)	-	-	496 (52)	0.40 (2)	-	0.94 (5)	-	-	-
	55 (3)	S (1), ST (1), T (1)	2.03 (8)	1.42 (8)	-	-	1238 (43)	-	-	-	-	-	-
Mazzotti et al., 2014	40 (2)	S (1), ST (1)	1.38 (3)	1.64 (3)	0.18	0.75	-	0.23 (3)	-	0.34 (16)	0.20	0.72	-
Replicated clay masonry	45 (5)	S (4), ST (1)	0.91 (15)	0.91 (15)	-	-	-	0.64 (3)	-	0.69 (4)	-	-	-
	50 (2)	S (2)	0.40 (7)	0.34 (7)	-	-	-	1.03 (3)	-	0.92 (8)	-	-	-
Pelà et al., 2017	40 (5)	S (2), ST (3)	0.39 (34)	0.46 (34)	0.14	0.59	-	0.30 (3)	S (3)	0.26 (17)	0.08	0.60	-
Replicated clay masonry	45 (5)	S (4), ST (1)	0.41 (11)	0.41 (11)	-	-	-	0.60 (3)	S (3)	0.45 (2)	-	-	-
	50 (5)	S (2), ST (3)	0.26 (20)	0.22 (20)	-	-	-	1.00 (3)	S (3)	0.68 (5)	-	-	-

<sup>1</sup>Letter refers to the observed failure mode, (i.e. ‘S’ shear-sliding failure, ‘ST’ mixed sliding along joint and tensile failure of the brick, ‘T’ tensile failure), and the digit indicates the number of specimens having the observed failure mode.

<sup>2</sup>Coefficient of variation in percentage is indicated in parentheses.

<sup>3</sup>Tests on companion triplets were performed by third parties (Vermeltoort, 2015; Nonnekes, 2015b); no information was available regarding the failure mode.

Note: Calculation of mean values excluded the results of specimens with tensile failure (‘T’ failure mode in Figure 5.6d–Figure 5.7c).

### 5.3 GLOBAL BEHAVIOUR

In this section, the global behaviour of the cores under shear load and of the triplets under combined shear-compression load is discussed and analysed. The typical final crack pattern of the cores and of the companion triplets is presented in Figure 5.6 and Figure 5.7, respectively. An overview of the number of cores and triplets with each specific crack pattern and typical mean shear stress-sliding curves are presented in Figure 5.8. The mean shear stress-sliding curves were obtained by considering pre-defined increments of sliding and, thus, calculating the corresponding average shear stress from individual test results. In this study, an increment of the sliding equal to  $1.5E-05 \pm 1\%$  was chosen. This approach was proposed by Augenti and Parisi (2011) and has already been adopted in Chapter 2 and Chapter 4.

Cores generally failed along the brick-mortar interface, but a mixed failure mode that involved the cracking of the brick was also observed in some cases, Figure 5.8. In 60% of the cases, the failure mode of the cores was characterised as a shear-sliding along one interface, Figure 5.6a, or along two interfaces, including mortar cracking, Figure 5.6b. Throughout the chapter, this failure mode is labelled as ‘S’. However, 25% of the total number of cores showed a combination of pure shear-sliding failure along the interface with a tensile failure of the brick(s), which appeared as a wedge-shaped splitting crack, Figure 5.6c. This mode of failure was labelled as ‘ST’. Apart from the mentioned failure modes, 15% of the total number of cores showed a predominant tensile splitting failure with a vertical tensile crack along the loading axis, rather than only shear-sliding failure along the joint, Figure 5.6d. This mode of failure is introduced as ‘T’.

Almost all triplets failed with pure shear-sliding failure either along one interface, Figure 5.7a, or two interfaces, Figure 5.7b, the ‘S’ failure mode. In addition, only one triplet showed a combination of pure shear-sliding with tensile failure of the middle brick, Figure 5.7c, the ‘T’ failure mode. Neither cores nor triplets with the ‘T’ failure mode could be regarded as representative of the shear-sliding failure along the brick-mortar interface; hence, all the mean shear properties were evaluated by excluding the outputs of these specimens. For the sake of completeness, the failure modes of all the individual specimens in terms of ‘S’, ‘ST’, and ‘T’ are presented in Table 5.1.

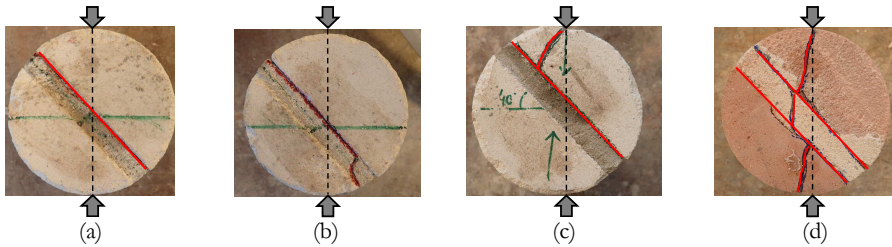


**Figure 5.6:** Typical failure mode of cores under shear load: (a) shear-sliding failure along one interface (‘S’); (b) shear-sliding failure along two interfaces including mortar failure (‘S’); (c) mixed sliding-tensile failure (‘ST’); (d) tensile failure (‘T’).

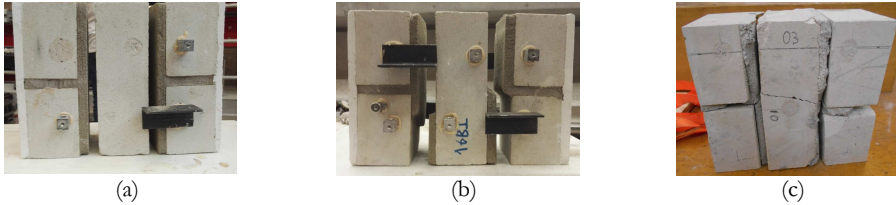


**Figure 5.7:** Typical failure of triplets under shear-compression loading: (a) shear-sliding failure along one interface (‘S’); (b) shear-sliding failure along two interfaces (‘S’); (c) tensile failure of the middle brick (‘T’).

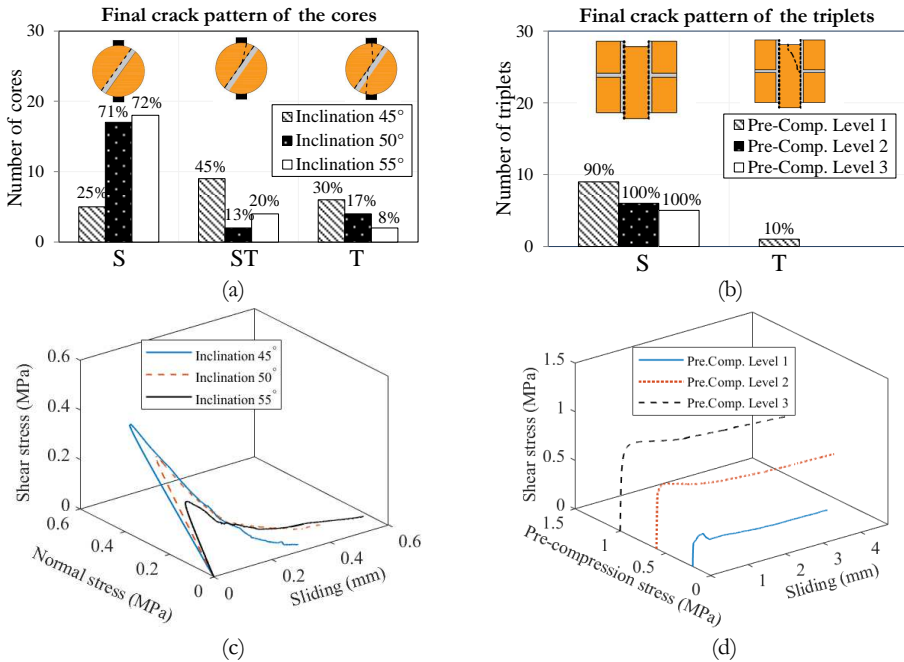


**Figure 5.8:** Overview of different failure modes with respect to the number of cores (a) and number of triplets (b); typical mean stress-sliding relationship observed during shear tests on the cores (c); and shear-compression tests on triplets (d). The number of cores and triplets were counted independently of the objects.

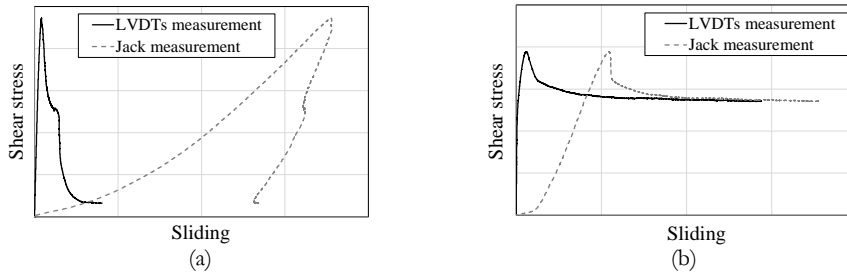


**Figure 5.9:** Typical shear stress-sliding curve obtained from the jack and LVDT measurements: (a) shear test on core with sliding-controlled set-up; (b) shear-compression test on triplet with displacement-controlled set-up.

Apart from the testing configuration itself, which could cause non-uniform stress distribution along the interface, the difference between the properties of the mortar relative to the brick and the quality of the bond between them could have a great influence on the stress distribution. It can be assumed that the stronger the mortar and interface, the higher the homogeneity of the material. In the case of a homogeneous material, the core is more likely to fail due to vertical splitting (such as a concrete core) than due to shear-sliding along the interface. In this study, such behaviour was more pronounced for the cores extracted from the clay masonry building of Rengersweg, where five out of nine cores clearly showed the ‘T’ failure mode rather than the other acceptable failure modes (i.e. ‘S’ or ‘ST’). Despite the replicated objects, no information was available regarding the mortar properties and the bond strength of the Rengersweg building. However, the shear properties of the triplets shown in Table 5.1 reveal a very high cohesion of the Rengersweg object compared with the others. This confirms the assumption of a strong bond leading to the tensile failure mode (‘T’) of the core. This may result in limiting the applicability of the core testing method. Accordingly, further experimental and numerical investigations are suggested to clarify the possible influence of mortar properties on the applicability of the core testing method.

The final crack pattern of the cores and of the triplets may be influenced by the imposed inclination angles and the pre-compression levels, respectively (Figure 5.8a,b). The occurrence of shear-sliding failure (‘S’) was more pronounced when cores were tested at the highest inclination angle ( $55^\circ$ ). However, testing the cores at the lowest inclination angle ( $45^\circ$ ) increased the probability of the mixed failure mode (‘ST’ and ‘T’). With regard to the triplets, when the pre-compression level was increased, the failure mode was mostly governed by failure along two interfaces rather than the failure along one interface that prevailed for the lowest pre-compression level.

Because dissimilar boundary and loading conditions were imposed, the shear stress-sliding curves obtained from the two testing methods showed similarities as well as differences. In the pre-peak phase, the mean shear stress-sliding curves obtained from the two testing methods is characterised by linear behaviour up to a

stress of approximately 35–60% of the peak stress, followed by a nonlinear branch until the peak load was reached, Figure 5.8c,d. The maximum values of the shear and normal stress for the cores could be considered a function of the inclination angle (Table 5.1). At the inclination angle of  $45^\circ$ , the normal component had the same magnitude as the shear one; however, when the inclination angle was increased, the normal stress had a lower magnitude than the shear stress. As is frequently observed, the higher the value of the mortar joint inclination angle, the lower the values of the shear and the normal strength. In the post-peak phase, both testing methods showed softening behaviour caused by damage and wear of the asperities along the brick-mortar interface. In this phase, the mean shear stress-sliding curves obtained from both methods could be approximated with an exponential curve. With an increase in the plastic shear-sliding deformation of the cores, both the shear and normal stress progressively decreased to a zero value. Note that when using the sliding-controlled set-up, full gradual post-peak softening behaviour was obtained only for the cores with pure shear-sliding failure (i.e. ‘S’). However, the post-peak phase of the cores with the mixed sliding-tensile failure (i.e. ‘ST’) was not or only partially recorded. Unlike the cores with variable normal stress, the pre-compression stress on the triplets was kept constant during the entire test. Accordingly, after the occurrence of decohesion in the triplets (representing mode-II cohesion softening), no further reduction in the shear stress was found due to the presence of friction. Generally, with the increase in pre-compression stresses in the triplets, the transition of the shear stress from peak strength to zero cohesion became smoother.

To capture the gradual post-peak softening of the cores, and thus to avoid sudden instability, control of the shear-sliding deformations along the interface of the core is required rather than control of the displacement of the jack. Due to the stable propagation of the shear crack, the internal measuring system of the jack showed snap-back behaviour, Figure 5.9a, meaning that the masonry relaxes along the load lines while the shear crack propagates in a stable manner. Contrary to this, the LVDTs on the cores always showed a progressive sliding deformation. Although the snap-back behaviour occurred during the shear-sliding failure along the brick-mortar interface, it was not as pronounced as was reported by van der Pluijm (1993) and Rots et al. (1997) for other cases with tension or shear cracking. In the case of triplets, both the LVDTs and jack measuring system showed an increase in sliding deformation, because the applied pre-compression load prevented any lateral instability, Figure 5.9b. Due to the inherent stiffness of the testing set-up, the deformations measured by the jack differed from the measurement by the LVDTs; however, only the LVDT recording was considered.

## 5.4 COHESION AND FRICTION COEFFICIENT

The Coulomb failure criterion was used to estimate the shear strength properties, as both cores and triplets showed shear-sliding failure along the brick-mortar interface. Accordingly, the cohesion (initial shear strength) and the friction coefficient obtained from both testing methods provided a basis for comparison. To this end, a database was created, Table 5.1, that included the results of the seven objects investigated in this study along with data from the literature on two replicated clay masonry objects (Mazzotti et al., 2014; Pelà et al., 2017). As mentioned in Section 5.3, all the specimens that showed the tensile failure mode ‘T’ were excluded from the analysis.

To directly correlate the shear properties of the two testing methods, a linear regression analysis was performed on the nine masonry objects. For this reason, the values for cohesion and the initial friction coefficient obtained from the shear test on the cores were plotted against the values obtained from the triplet tests, Figure 5.10. The regression line, forced to pass through the origin, is shown as a black solid line. A one-to-one correlation line (the red dashed line) is also added to Figure 5.10, while the grey area indicates the scatter band. The errors, calculated as the deviations with respect to the regression lines, are also presented.

The regression analysis indicates that there is an acceptable statistical relationship both in terms of cohesion and friction coefficient regardless of masonry types, where the shear property values of the triplets were found to be approximately 0.90 times lower than the ones obtained from the core tests. In addition, low dispersion of the shear properties can be observed, as all the experimental results fall within a narrow scatter band (grey area). In conclusion, a minimally invasive core testing method can be regarded as a reliable alternative to the conventional triplet and shove test method for evaluating the shear strength properties of existing structures.

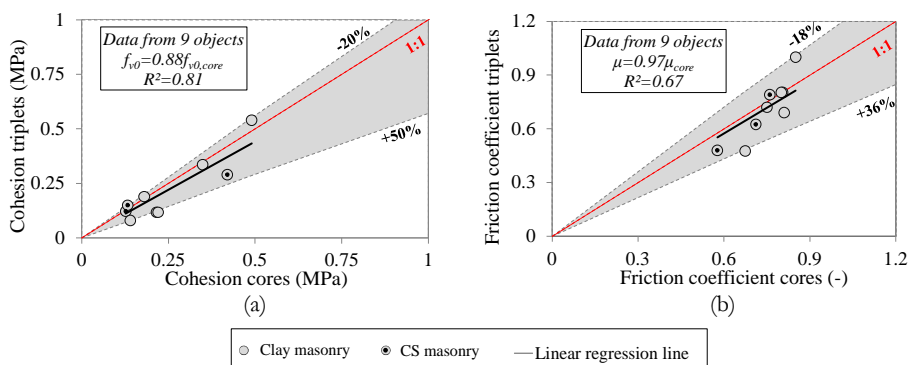


**Figure 5.10:** Correlation between shear properties of cores and of companion specimens: (a) cohesion; (b) friction coefficient. The shaded grey area identifies the scatter band. The errors, which are the deviations with respect to the regression line, are reported.

## 5.5 PLASTIC SHEAR MODULUS OF THE MORTAR JOINT

Large scatter was found in the mortar shear modulus by performing tests on the cores, Table 5.1. This was attributed to the heterogenous nature of masonry, which may cause complex distribution of stress along the joint even in the elastic phase. Due to the lack of data for the triplet tests, a direct comparison of the results with those from the core tests could be made for only two objects, namely Tilweg field-extracted CS brick masonry and MAT-4 laboratory-made clay masonry. For these two objects, the variation in mean shear modulus in the pre-peak phase as a function of normalised shear stress is shown in Figure 5.11. For each testing method, the mean shear modulus curve was found by evaluating the average results of every single specimen with the shear-sliding ('S') and mixed sliding-splitting failure mode ('ST'), regardless of the imposed inclination angle or the pre-compression level. The shear stress was normalised with respect to the shear strength. At the very beginning of the tests, the resolution of the measuring system could have influenced the accuracy of the measured sliding; accordingly, the shear modulus was reported only for normalised shear stresses higher than 0.2. The mean shear modulus curves of the cores and of the triplets are presented with a solid line and a dashed line, respectively. The corresponding 95% confidence intervals based on a Gaussian distribution are also presented (Marastoni et al., 2016).

An acceptable correspondence between the elastic shear stiffness of the two methods was found, although due to an increase in the shear stress, the shear modulus of the cores decreased at a higher rate than that of the triplets, Figure 5.11. Such a difference in the response of the two testing methods can be attributed to the different boundary conditions imposed, as shear cracks developed at a lower rate in the pre-compressed triplets than in the cores with the constant change in the normal stress. The ratio of the shear modulus of the triplets to the cores at a stress level corresponding to 1/3 of the maximum shear stress ranges from 1.1 to 1.3 (Figure 5.11), although this comparison was made for only two masonry objects. This finding brings to light the potential of shear tests on cores to address the elastic shear modulus of the mortar joint; however, further research is required to draw concrete conclusions.



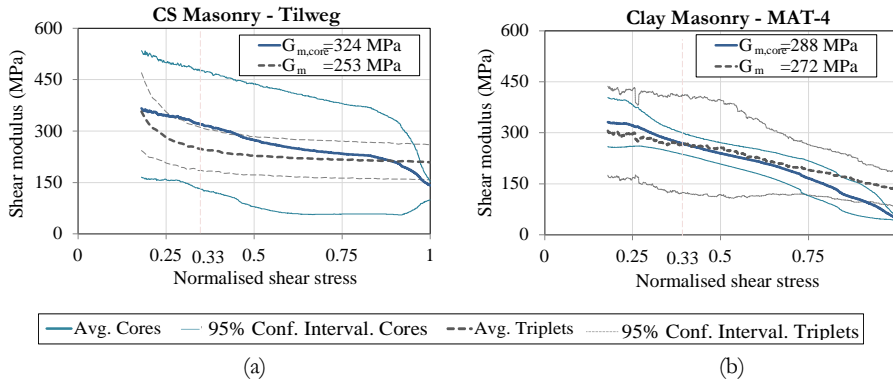


**Figure 5.11:** Variation in the shear modulus of the mortar joint as a function of normalised shear stress: (a) Tilweg field-extracted CS brick masonry; (b) MAT-4 laboratory-made clay brick masonry.

## 5.6 FRACTURE ENERGY FOR SHEAR-SLIDING CRACKING

To evaluate the dissipated energy during the formation of the shear crack linked to the cohesive mechanisms, the frictional contribution arising from the surface roughness along the brick-mortar interface is excluded. In other words, the notion behind the fracture energy in shear is to distinguish the cohesion mechanism from the contribution of friction, see Figure 5.5. For both cores and triplets, the variations in the fracture energy of cores as a function of maximum normal stress,  $f_{p,cores}$ , and of triplets as a function of pre-compression stress,  $f_p$ , are plotted in Figure 5.12. To illustrate this trend, the linear regression line for each given masonry type is also added.

With an increase in the maximum normal stress, the fracture energy in the cores consistently followed a downward trend, while no clear trend was observed from the results of the triplet tests, Figure 5.12. Regarding the trends of fracture energy, a comparison between the two testing methods can be made for only two objects, namely the CS brick masonry from the Tilweg and Zijlvest buildings. The cores and triplets taken from the Tilweg object showed a similar trend in which an increase in normal stress was accompanied by a decrease in fracture energy. However, for the Zijlvest object, an inconsistency between the trends of the fracture energy in the cores and triplets was obvious. At this time, no potential explanation for such a discrepancy can be offered; thus further research is suggested.

The clay masonry clearly showed higher values of energy dissipation than the CS brick masonry. This observation is in line with the findings of van der Pluijm (1993), where at a constant pre-compression level of 1.0 MPa, the fracture energy of clay brick specimens (0.19 N/mm) was almost four times higher than that for CS brick masonry (0.05 N/mm). For shear-sliding failure along the interface, the CS specimens, both cores and triplets, often showed a smoother crack surface than did the clay specimens, Figure 5.13. This may explain why less energy was

required to create a shear crack at the brick-mortar interface of the CS masonry than was required by the clay masonry specimen.

Although fracture energy is commonly acknowledged as a size-independent property, in this study, as in previous studies (e.g., van der Pluijm, 1993; Augenti & Parisi, 2011), a clear dependency of the mode-II fracture energy on pre-compression levels was observed. The triplets showed variation in the mode-II fracture energy up to 85% (with respect to an average value of fracture energy). On the contrary, for the cores, a nearly constant trend in fracture energy with respect to the maximum normal stress was obtained, with a maximum variation of approximately 38%. These conflicting observations pose a challenging question: Is the mode-II fracture energy in masonry an independent property or not? It should be pointed out that the definition of mode-II fracture energy remains a debatable issue for quasi-brittle material, as shown by several discussions in the field of concrete material. Bažant and Pfeiffer (1986) explained that breaking the interlocking of concrete aggregate due to shear resistance requires an energy that is almost 25 times larger than the tensile (mode-I) fracture energy. On the contrary, Carpinteri et al. (1993) stated that for mixed mode crack propagation, mode-I fracture energy can be obtained by excluding the energy dissipation due to the friction and interlocking of concrete aggregate. In addition, they observed that the energy dissipation due to the interlocking of aggregate and asperities disappeared with an increase in specimen size as well as a decrease in aggregate size. Furthermore, Carpinteri et al. (1993) reported on the dependency of mode-II fracture energy to specimen geometry (i.e. size and shape) and loading and testing conditions, and thus concluded that mode-II fracture energy in concrete is not a real material property. To produce an answer, extensive research in this realm is suggested.

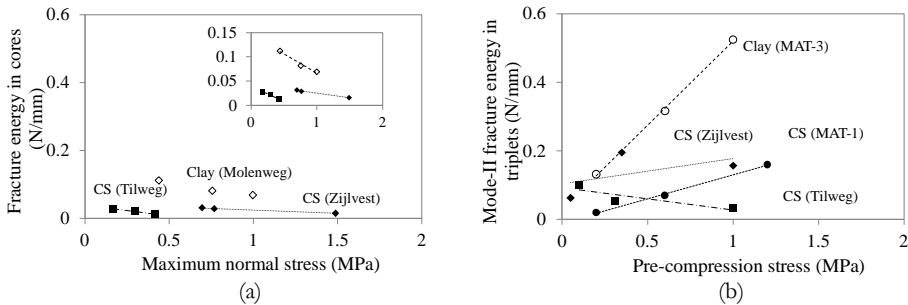


**Figure 5.12:** Variation in the values of fracture energy as a function of: (a) maximum normal stress in cores; (b) pre-compression stress in triplets.

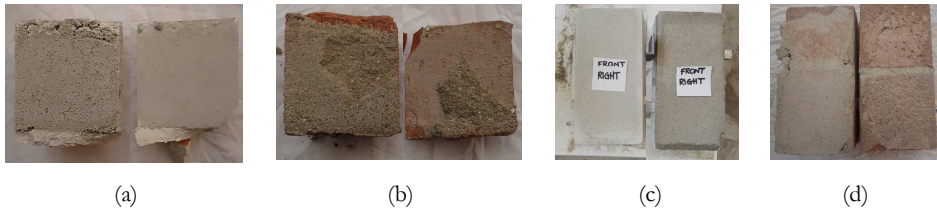


**Figure 5.13:** Top view from the debonded surface of CS and clay masonry specimens: (a-b) cores; (c-d) triplets.

Although the dissipated energy during the formation of shear cracks in both cores and triplets can be considered fracture energy, due to the influence of the lateral boundary conditions, there is a substantial difference between them. Throughout the shear-compression tests on triplets, the confinement level was kept constant, while during the core tests, the level of confinement decreased in the post-peak phase due to the reduction in the stress state along the joint. Considering such differences in the boundary conditions of the two testing methods, no direct comparison can be made in terms of energy dissipation. As found in Section 5.4, an acceptable correspondence was found between the failure criteria of the two testing methods. For this reason, an attempt was made to extrapolate the post-peak softening behaviour of the triplets using the data gathered from the core tests. For the triplets, the descending cohesive branch beyond the peak shear stress can be approximated by an exponential curve. As introduced by van der Pluijm (1993), the post-peak response can be predicted as:

$$c_p = c_{core} \cdot e^{\frac{-c_{core} \cdot \delta_p}{G_{f,avg(core)}}} \quad (5.6)$$

where  $c_p$  is the post-peak cohesive stress,  $c_{core}$  is the maximum cohesive stress (Figure 5.5),  $G_{f,avg(core)}$  is the average value of the fracture energy in the cores at different inclination angles, and  $\delta_p$  is the predicted shear-sliding deformation in the post-peak phase. The steps taken to find the analytical post-peak softening of the triplets based on the data obtained from core tests are as follows:

- 1 The shear strength was retrieved at three given pre-compression levels using the Coulomb failure criterion established from the core tests;
- 2 The residual friction strength was calculated by multiplying the given pre-compression stress by the friction coefficient obtained from the core tests;
- 3 The maximum cohesive stress,  $c_{core}$ , was found by subtracting the residual shear strength from the peak shear stress (please note that  $c_{core}$  as defined here will be the same as that in Figure 5.5c if  $f_{p,core} = f_p$ );
- 4 The post-peak cohesive stress,  $c_p$ , was defined by dividing the maximum cohesive stress over 100 equal steps in descending order;
- 5 The corresponding predicted sliding,  $\delta_p$ , was found from Eq. (5.6), considering  $c_{core}$ ,  $c_p$ , and  $G_{f,avg(core)}$  as inputs. The fracture energy in the cores did not vary significantly when the inclination angle was changed.

Accordingly, for the sake of simplicity, the fracture energy was assumed to be constant and was calculated as an average value of the fracture energy at different inclination angles;

- 6 The post-peak shear stress corresponding to the sliding was found as the sum of the post-peak cohesive stress and the residual shear strength.

In Figure 5.14, a comparison is made between the experimental and analytical results in terms of the post-peak behaviour of the triplets. Note that the comparison could be made for only two objects, namely the CS masonry from the Tilweg and Zijlvest buildings; however, the data from the latter object were excluded due to insufficient testing and the wide spread of the testing results. At pre-compression levels of 0.10 MPa and 0.30 MPa, there is an acceptable correspondence between the post-peak softening from the experiment and the analytical calculation. However, at the highest pre-compression level, the shear stress decreases at a lower rate than the analytical calculation. This difference can be traced back to the disagreement between the failure criteria of the two testing methods. In conclusion, the core testing shows some potential for evaluating the post-peak softening, though this conclusion is derived based on the results for only one object.

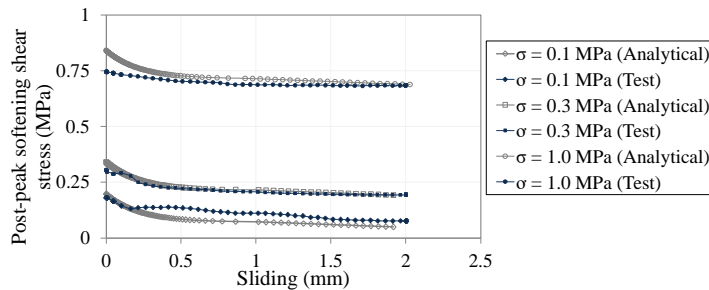


**Figure 5.14:** Comparison between the experimental post-peak softening during the shear-compression tests on triplets and the analytical model extrapolated from the core tests on the CS Tilweg object.

## 5.7 DILATANT BEHAVIOUR

The volumetric normal expansion of the masonry bed joint during the shear-sliding deformations was measured for both cores and triplets. For a given inclination angle or pre-compression level, the mean values of dilatancy as a function of normalised sliding are presented in Figure 5.15. The sliding was normalised with respect to the sliding that corresponded to the maximum shear stress. To compare the results of the two testing methods, only half of the normal displacement measured across the two bed joints was considered for the triplet tests. As mentioned in Section 5.2.2, the dilatancy was evaluated over the constant sliding increment, and the corresponding normal deformations were subsequently found. Herein, for the sake of consistency, the increment was defined as 0.25 times the sliding corresponding to the peak shear stress; this increment was regarded as sufficiently small to qualitatively capture the trend. Note that the normal expansion of the joint was recorded only for the cores extracted from the four existing buildings (i.e. Tilweg, Zijlvest, Molenweg, and Rengersweg) and for the triplets replicated in the laboratory (i.e. MAT-1, MAT-3), and was extracted only from the Tilweg building. As a result, a comparison between the dilatant response of the cores and the triplets can be made for only one object, namely the CS brick masonry from the Tilweg building, Figure 5.15a. For all the investigated masonry types, a similar trend of variations in dilatancy over the normalised sliding was found as presented in Figure 5.15a,b.

No specific trend was detected between the progressive normal expansion of the cores and the imposed inclination angles, while the lateral expansion of the triplets depended on the pre-compression levels. As mentioned earlier, the confinement condition of the two testing methods in the direction perpendicular to the bed joint differed. Accordingly, in the post-peak phase, with the decrease in the stress state in the cores, the lateral confinement constantly decreased, and the joint expanded more easily. The three sets of mean dilatancy curves obtained from the tests on the cores at different inclination angles clearly followed the same trend, Figure 5.15a. First, a contraction of the mortar joint was observed. With the increase in sliding deformation, the joint tended to expand progressively. A turning point was found at a normalised sliding of approximately 0.25. Eventually, at larger values of sliding, due to wear and damage to the asperities along the brick-mortar interface of the unconfined cores, the dilatancy became stable at a non-zero value. The dependence of dilatancy on the pre-compression level was observed in tests on the triplets; the lower the pre-compression level, the higher the dilatancy. At the highest pre-compression level, the dilatant behaviour in the triplets was either not observed or vanished at a higher rate as the damage to the fracture surface accelerated. In addition, the roughness of the brick surface played an important role in the dilatancy effect (van Zijl, 2004). All the triplets showed dilatant behaviour, with the exception of the replicated CS triplets tested at a pre-compression level of 1.2 MPa, Figure 5.15b. In conclusion, the lateral expansion of the cores, with constant change in the normal stress, was greater than that of

the triplets with constant pre-compression. Accordingly, by further increasing the shear-sliding deformation along the brick-mortar interface, the dilatant behaviour of the cores remained stable, while the dilatant behaviour of the triplets progressively vanished.

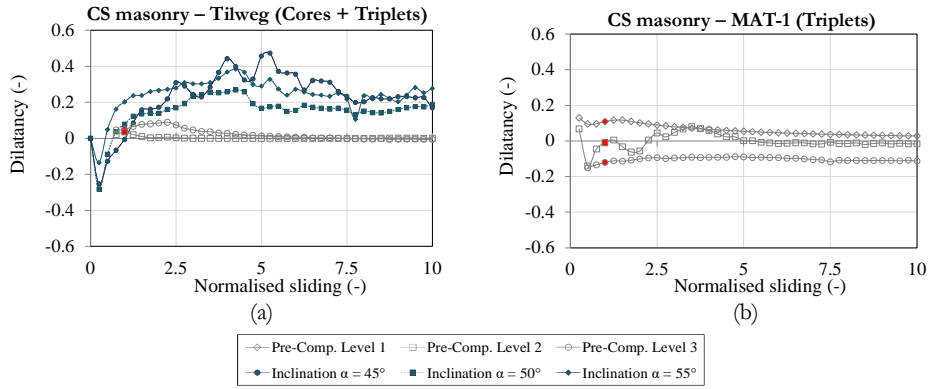


**Figure 5.15:** Dilatancy versus normalised sliding: (a) Tilweg field-extracted CS brick masonry; (b) MAT-1 laboratory-made CS brick masonry. The sliding was normalised with respect to the sliding that occurred at maximum shear stress, as indicated with a red marker.

## 5.8 CONCLUDING REMARKS

Through a comparative experimental approach, this chapter examined the suitability of shear tests on small-diameter cores to assess nonlinear shear-sliding behaviour along a brick-mortar interface. For this purpose, an experimental programme was set-up to compare the results obtained from shear tests on cores and from triplet tests on seven masonry objects. The masonry objects were either replicated in the laboratory or extracted from residential buildings located in the northern part of the Netherlands (Groningen area). The boundary condition imposed in the direction perpendicular to the bed joint of the core was different from that of the triplets, as the level of confinement in the core was not constant throughout the test, while during the triplet test the confinement level was kept constant. Cores with a diameter of about 100 mm and composed of a single bed joint were rotated with respect to their original horizontal position and subsequently subjected to vertical line load along their thickness, similar to a Brazilian splitting test. The test was carried out at different inclination angles of 45°, 50°, and 55°, thus inducing various combinations of shear-compression stress states along the brick-mortar interface. Unlike previous research, in this study a sliding-controlled set-up was also used to characterise the post-peak softening behaviour. Consequently, a more complete description of the nonlinear shear-sliding behaviour along the brick-mortar interface was provided in terms of cohesion, friction coefficient, shear modulus of the mortar joint, as well as some insight into shear softening, energy dissipation, and dilatancy.

The failure of the cores under shear load can be influenced by the imposed inclination angle and can also be affected by the mortar strength and bond strength of the interface, which introduces limitations in the application of the core testing method to determine the shear-sliding behaviour at a brick-mortar interface. At the highest inclination angle (55°), 83% of the cores failed along the brick-mortar interface, while at the lowest inclination angle (45°), the number of cores that showed pure shear-sliding failure dropped to 25%. For this inclination angle, 45% of the cores failed with mixed shear-sliding and brick splitting failure, and the remaining 30% showed tensile failure, characterised by an evident vertical crack aligned with the loading axis and a shear-sliding crack along the interface. The results of tensile failure could not be regarded as representative of shear-sliding behaviour, and thus were excluded from the evaluation of the shear properties. The presence of the tensile-splitting failure mode was attributed to the homogeneous performance of the masonry, which was due to the good quality mortar or/and good bond at the brick-mortar interface. Accordingly, the accuracy of the obtained results from the core testing method can be questioned with respect to the observed failure mode and masonry characteristics. Therefore, further research is suggested to investigate the range of applicability of the core testing method for masonry with a strong bond as well as for masonry with different ratios of stiffness of the mortar to the brick.

This study confirms the suitability of the core testing method in assessing the cohesion and friction coefficient of brick masonry. To predict a relationship between the cohesion obtained from the two testing methods as well as the friction coefficient, a regression analysis was performed on nine masonry objects, including data from the literature. As derived from this analysis, the cohesion of the triplets was found to be 0.88 times lower than that of the cores with a strong correlation ( $R^2=0.81$ ). The friction coefficient of the triplets was found to be 0.96 times lower than the friction coefficient of the cores with a moderate correlation ( $R^2=0.62$ ).

In the elastic phase, the core testing method shows the potential for evaluating the shear modulus of the mortar joint, although the comparison between the outputs of the two testing methods applies to only two masonry objects. Accordingly, with the aim of augmenting the established dataset, further studies are suggested. In general, tests on the cores resulted in a large scattering of the shear modulus that could be attributed to the heterogeneous nature of the masonry.

Unlike previous studies, this chapter provides a comparison of core and triplet tests in terms of mode-II fracture energy. In both tests, the energy dissipation is governed by fracture and friction mechanisms. To consider only the cohesive contribution associated with fracture, the cohesive stress was calculated by excluding the stress associated with friction, determined as the product of the normal stress and the friction coefficient. The fracture energy was then calculated as the area under the cohesive shear stress-sliding curve. Unlike the triplets, the cores showed a nearly constant trend between the mode-II fracture energy and the maximum normal stress. For one masonry type, an acceptable agreement was found between the post-peak softening of the triplets predicted using the core testing results and the experiments. The difference between the cores and the triplets in terms of mode-II fracture energy and the dependency of the mode-II fracture energy of the triplets on the pre-compression stress raises some doubt about this parameter as an independent material property. Nevertheless, the comparison between the two testing methods points to a new research direction.

Due to the difference in the lateral confinement of the bed joint during the shear sliding, the cores showed larger dilatancy than the triplets did. In the post-peak phase, with the decrease in the stress state in the cores, the lateral confinement constantly decreased, and the joint expanded more easily, while in the triplets the lateral confinement was kept constant throughout the test. By increasing the shear-sliding, the dilatancy of the cores gradually decreased and eventually reached a steady non-zero value. The same trend was observed for the cores tested under different inclination angles. With the increase in the pre-compression level and the sliding, the dilatancy behaviour of the confined triplets slowly vanished and almost reached zero. However, understanding the influence of boundary conditions on shear properties involves an extensive debate (e.g.,



Rots et al., 1997; van Zijl et al., 2001; van Zijl, 2004; Ferretti et al., 2018a; Ferretti et al., 2018b; Andreotti et al., 2019).

This study confirms that the applicability of the core testing method can be extrapolated to both clay and CS brick masonry types extracted from existing URM buildings. It was observed that the reliability and the variability of the experimental results were not influenced by the brick types, i.e. clay or CS brick masonry, or construction types, i.e. laboratory-made or field-extracted. However, the results were influenced by the mortar properties. From the perspective of in-situ application, the core testing method can be regarded as a reliable alternative to conventional standardized methods, such as triplet and shove tests, as far as evaluations of shear strength and shear stiffness are concerned, while evaluations of the softening parameters and dilatancy require further study.



# STRATEGY FOR THE MATERIAL CHARACTERISATION OF EXISTING STRUCTURES: CORRELATION AND CONSTITUTIVE LAWS\*

---

The reliability of the structural assessment can be improved by well-defined input parameters, in terms of material properties, as listed in Table 1.1, as well as stress-strain constitutive functions describing the nonlinear response of materials for cracking, crushing, and shearing. Obtaining such information mainly relies on conducting extensive experimental investigations, which are often restricted by a lack of financial resources or the need to limit intervention in, and damage to the building. Accordingly, practitioners aim to reach a compromise between the damage to the structure caused by extraction and intervention and the extent of knowledge on the material properties. Therefore, a need exists for developing a framework, though ambitious, which could offer a direct/indirect evaluation of material properties for existing masonry structures. Finding relationships and correlations between different material properties and formulating constitutive equations can be seen as a gateway to a coherent strategy for material characterisation in support of the assessment of existing structures.

Exploring the possible correlations between different material properties can reduce the burden associated with extraction, transportation, and testing of medium-sized samples, and thus could save time and costs. A survey of the literature revealed that some researchers have investigated the possible relationships between a few material properties (e.g., Rots et al., 1997; van der Pluijm, 1999; Kaushik et al., 2007; Lumantarna et al., 2014a; Lumantarna et al., 2014b). Apart from the literature, Eurocode 6 provides brief insights into the relationship between the compressive strength and the Young's modulus of masonry, and implicitly gives the ratio between the vertical and horizontal out-of-plane bending strength of masonry. However, investigating the correlations between the key input parameters, such as fracture energy in compression, bending, and shear, has received little attention in the literature and international/national standards.

Stress-strain constitutive functions are required as essential inputs to the continuum damage model, describing the nonlinear response of masonry to exter-

---

\* This chapter is based on the author's article submitted to *Building Engineering*.

nal compression, bending, and shear forces. To date, several models have been introduced in the literature to define the pre- and post-peak response of masonry. However, a consistent effort has not yet been devoted to investigating the accuracy of the proposed constitutive formulations for a large dataset of different masonry types as well as their capability to accurately predict the softening response.

Aiming to formulate a strategy by filling the gaps in the literature, this chapter first conducts a correlation study to predict the input material properties as a function of strength, in particular the easy-to-obtain properties. The main contribution of this research lies in addressing the relationships between properties that quantify the post-peak response of masonry, i.e. fracture energy. This is achieved through the comprehensive database obtained from tests on medium-sized specimens, i.e. the outcomes of Chapter 2 and Chapter 3.

Second, this chapter proposes stress-strain laws for compression, bending, and shear loading. To this end, first a summary of the available models in the literature is provided and a comparison is made between the predicted response and the experimental results. This comparison demonstrates the necessity of further improvement in the available constitutive laws. Next, this study develops promising constitutive functions, in which the reliability of the proposed models is investigated for the five laboratory-made masonry specimens, including brick and element masonry.

Finally, this chapter formulates a strategy, which is currently missing in the literature/design codes, for material characterisation in support of the structural assessment of existing structures. Following this strategy, an acceptable level of knowledge on material properties can be achieved, while intrusiveness and damage due to sampling remains limited.

## 6.1 PREDICTION OF MATERIAL PROPERTIES

This section investigates the presence of a link between different material properties found from the invasive tests on the laboratory-made and field-extracted specimens reported in Chapter 2 and Chapter 3, respectively. To this end, one material property is first plotted against a predictor variable. To predict the relationship between the two variables, linear regression analysis, often forced to pass the origin, is conducted. To quantify the accuracy of the relationships, values of the correlation of determination ( $R^2$ ) are also presented.

To estimate the minimum number of masonry types required for an 80% chance of finding a statistically significant correlation, an a priori power analysis using G\*Power 3.1 software (Faul et al., 2007) was conducted. Considering the desired level of significance ( $\alpha=0.05$ ) and a medium effect size (Cohen, 2013), 67 data points would be required. However, at best, 27 objects were treated in this study, including both the laboratory-made and field-extracted objects. Through a post hoc power analysis, it was determined that by using 27 data points the chance of finding a statistically significant correlation would be 46%. This means that there is a medium chance that the relationship found between two variables exists

and that it is not due to chance. This highlights the need for further studies to obtain more observations. For this reason, the data in this thesis are available in an open-access database<sup>1</sup> for future research.

Although comparisons with other correlation rules from the literature and codes are included in this section, these were not incorporated into the correlation study, as the specimens' dimensions and testing conditions, i.e. their boundary conditions and loading rates, could differ. The literature data were presented when the material properties of at least three different masonry types were reported, thus allowing us to conduct a regression analysis. The literature review, used to examine the applicability of the established relationships, is mainly built on the following references:

- Rots et al. (1997), who reported the findings of an extensive joint research and development project in the Netherlands (based on CUR Report 171, 1994). This section benefits from the results of an experimental campaign on laboratory-made masonry at material-scale, which are mainly written by van der Pluijm and A.Th. Vermeltoort.
- Outlines of the New Zealand Society for Earthquake Engineering (NZSEE), as well as experimental studies in their support by Lumantarna et al. (2014a), Lumantarna et al. (2014b), and Almesfer et al. (2014). These researchers investigated the relationships between flexural bond strength, shear strength, and compressive strength of masonry and mortar for historical clay brick masonry structures. The experimental data were obtained from in-situ tests as well as laboratory tests.
- A study by Ghiassi et al. (2019), who reviewed expressions in the literature for deriving material properties. However, some of the suggested expressions were borrowed from the literature on concrete and they were not experimentally verified for masonry.
- Findings from De Villiers (2019), who exhaustively discussed the relationship between different material properties of typical masonry in South Africa, namely conventional concrete (CON), geopolymer (GEO), compressed stabilised earth (CSER), and adobe (ADB). De Villiers (2019) seemed not to pay much attention to the statistics underlying the relationships between the properties.

---

<sup>1</sup> The experimental results of the presented tests are available via the 4TU.ResearchData repository at <https://doi.org/10.4121/15131979>. The data are distributed under the license type CC BY.

### 6.1.1 Mortar properties

Characterising the material properties of mortar in existing structures is often acknowledged as a challenging task. Up to now, researchers have deployed a number of techniques to estimate the compressive strength of mortar, either using laboratory tests on extracted mortar, such as the double punch test, or using semi- or non-invasive in-situ testing methods, e.g., the penetrometer test and Helix pull-out test. In this framework, the double punch test can be regarded as the most common testing method, and it is proposed by the German standard (DIN 1999). Following this method, intact pieces of mortar – when it is technically feasible to extract them – are subjected to compression loading. However, it turns out that the testing results should be interpreted with caution, as they depend on the thickness of the mortar (e.g., Sassoni et al., 2015; Łątka & Matysek, 2020). The calibration of the testing results on mortar strength became more challenging, as the results of the double punch tests on mortar extracted from joints and those obtained from the standard tests on cubic mortar casted in mould did not show satisfactory agreement (Sassoni et al., 2013). Such a difference could be expected, as the curing conditions for the two types of mortar samples are different. Considering the limitations of the available testing methods, as expected, the pool of experimental data on the properties of existing mortar is limited in the literature; in this research, we only characterised the properties of mortar used for the replication of samples in the laboratory with the standard mortar bar tests. To evaluate the Young's modulus of mortar, researchers have either performed compression tests on casted mortar prisms/cubes, or indirectly found it from tests on masonry wallets. Insight into the tensile behaviour of mortar can be gained by performing a direct tensile test. However, due to the difficulties encountered during the application of direct tensile tests, three-point bending tests are more popular and widely accepted among the masonry research community.

Table 6.1 lists the ratio between the elastic modulus,  $E_{3m}$ , and the compressive strength of mortar,  $f_m$ , as well as the ratio between flexural strength,  $f_{bm}$ , and the compressive strength of mortar,  $f_m$ , found from linear regression analysis. A wide ratio, ranging between 57 and 869, was found between the Young's modulus and mortar compressive strength. In this study, we found a ratio of 239 for one mortar type, in agreement with the findings of Kaushik et al. (2007), De Villiers (2019), and Barattucci et al. (2020). A ratio lower than 100 was found by Vermeltfoort (2005) and Raj et al. (2020), while Sarangapani et al. (2005) suggested a much higher ratio, 869. Among the aforementioned studies, only Rots et al. (1997) and Barattucci et al. (2020) reported the values of mortar flexural strength. In this study, we found a ratio of 0.32 between the flexural strength and compressive strength of mortar, which is higher than the findings in the literature. Concerning tensile properties of mortar, Ugama and Ejuh (2014) performed both three-point bending and uniaxial tests on iron ore tailing mortar. Though the mortar type is different than the one adopted in this study, the ratio between the flexural strength and compressive of mortar ranged from 0.14 to 0.23, similar to the literature data. However, a lower ratio of tensile strength to compressive strength of mortar was found, ranging from 0.03 to 0.05.

**Table 6.1:**

Ratio between properties of mortar (Young's modulus,  $E_{m3}$ , compressive strength,  $f_m$ , flexural strength,  $f_{bm}$ , and tensile strength,  $f_{tm}$ ). Correlation of determination in parentheses.

Reference	$E_{m3}/f_m$	$f_{bm}/f_m$	$f_{tm}/f_m$
Rots et al. (1997)	155 (0.02)	0.15 (0.85)	-
Vermeltoort (2005)	97 (0.58)	-	-
Sarangapani et al. (2005)	869 (0.68)	-	-
Kaushik et al. (2007)	200 (0.90)	-	-
Ugama and Ejeh (2014)	-	0.14–0.23	0.03–0.05
De Villiers (2019)	319 (0.90)	-	-
Raj et al. (2020)	57 (0.97)	-	-
Barattucci et al. (2020)	157 (0.55)	0.19 (0.81)	-
This work	239 (-)*	0.32 (0.83)	-

\*Only from tests on one type of mortar used for replication of samples.

### 6.1.2 Unit properties

Few studies have investigated the relationship between the material properties of units in a systematic way. A compression test on a unit is easy to perform; however, in most cases the compressive strength is the only property that has been quantified. To assess the brick elastic modulus, Vermeltoort (2005) proposed performing a compression test on a pile of bricks bonded together with a very thin layer of stiff material. This study applied the same method for the new production of units. The limited number of units extracted from existing buildings did not allow us to build stack-bond prisms and thus measure the elastic modulus. Apart from this testing method, some researchers (e.g., Binda et al., 1997; De Villiers, 2019) have adopted the procedure recommended by standard EN 12390-13 (CEN 2019) to assess the Young's modulus of concrete, in which the compressive load is applied parallel to the stretcher face of the brick. However, as reported by Pelà et al. (2016a), due to the heterogeneous nature of brick, the stiffness differed along the two principal directions. To evaluate the tensile response of a unit, direct tensile tests can be performed that require more effort in terms of preparation and testing set-up (Lourenço et al., 2005; Ghiassi et al., 2019). Thus, researchers have adopted the wedge splitting test or three-point out-of-plane bending tests to evaluate unit tensile properties.

The values of the elastic modulus of units versus the compressive strength of units found in this study are plotted in Figure 6.1a, showing a decreasing trend in the Young's modulus with an increase in compressive strength. This relationship, based on limited data, contrasts with previous studies, in which an upward trend was found, see Table 6.2 Table 6.2. Generally, previous studies found an average ratio of 266–450, with the exception of De Villiers (2019), who found a higher ratio for typical units in South Africa; however, these differ substantially in terms of material composition and dimension from the typical Dutch units used in this study. Note that the values of the Young's modulus listed in Table 6.2 were evaluated in the stretcher direction, meaning that compression load was applied perpendicular to the bed face.

The values of unit flexural strength obtained from bending tests,  $f_{bb}$ , versus the compressive strength of units,  $f_b$ , found in this study are plotted in Figure 6.1b. No specific relationship is found, as the results are widely scattered, and the ratio between unit flexural strength and compressive strength varies between 0.11 and 0.45 (dashed lines in Figure 6.1b). For the typical South African unit, De Villiers (2019) found a ratio of 0.02, see Table 6.2. A difference can be expected between the direct tensile strength of a unit,  $f_{tb}$ , and the flexural strength obtained from the bending tests,  $f_{bb}$ . Hence, in Table 6.2, a division is made between these two properties. The ratio between the tensile strength,  $f_{tb}$ , and the unit compressive strength is reported in Table 6.2. A lower ratio was reported in the literature when considering the tensile strength rather than the flexural strength of a unit. In the literature, the ratio between the tensile strength and compressive strength of units ranged from 0.03 to 0.14.

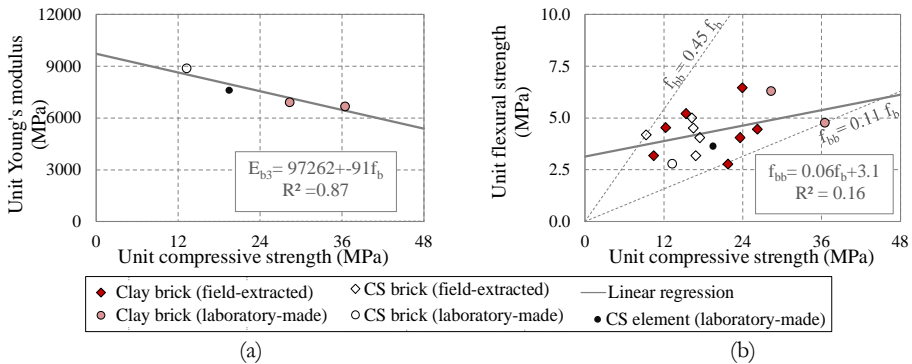


**Figure 6.1:** Correlation between unit compressive strength and: (a) unit Young’s modulus; (b) unit flexural strength.

**Table 6.2:**

Ratio between properties of units (Young’s modulus,  $E_{3b}$ , compressive strength,  $f_b$ , flexural strength,  $f_{bb}$ , and tensile strength,  $f_{tb}$ ). Correlation of determination in parentheses.

Reference	Unit type	$E_{3b}/f_b$	$f_{bb}/f_b$	$f_{tb}/f_b$
Schubert (1994)	Clay, CS brick	-	-	0.03–0.05 (0.70)
Rots et al. (1997)	Clay, CS brick	266 (0.58)	-	0.04–0.07
Lourenço et al. (2005)	Clay	-	-	0.05
Vermeltfoort (2005)	Clay brick	430 (0.81)	-	-
Kaushik et al. (2007)	Clay brick	300 (0.39)	-	-
Ghiassi et al. (2019)	Historical	350	-	0.12–0.14
De Villiers (2019)	Typical African	911 (0.36)	0.02 (0.65)	-
NZSEE	Clay bricks	-	-	0.12 (1.0)
This work	Clay, CSB, CSE	-	0.11-0.45	-



### 6.1.3 Masonry compressive strength

The compressive strength of masonry is regarded as the most central mechanical property for the design and safety assessment of existing structures. However, in practice, only minimal intrusion into the building functionality is allowed, if any, and the possibility of extracting large masonry samples is highly limited. As a result, attempts have been made in the literature to associate the compressive strength of masonry with the mechanical properties of masonry constituents, as the extraction of individual masonry units and mortar is not as invasive as the extraction of a large sample.

Postulating a series of assumptions, researchers introduced a large variety of predictive models, from simple linear models with one variable up to complex nonlinear models incorporating the effects of multiple variables. Bennett et al. (1997) and Garzón-Roca et al. (2013) proposed linear models, while nonlinear expressions were introduced by, for example, Eurocode 6(CEN 2005), Kumavat (2016), and Kaushik et al. (2007), correlating the compressive strength of masonry with the compressive strength of the masonry units as well as the compressive strength of the mortar. In most instances, the proposed expressions in the literature did not account for any divisions based on the masonry types (e.g., Hendry, 1998; and Kaushik et al., 2007). However, some researchers, including Hendry and Malek (1986), proposed two empirical formulas, depending on the bonding pattern of the masonry and thus the thickness. Apart from the compressive strength of masonry constituents, researchers such as Thaickavil and Thomas (2018) proposed a mathematical model to account for the slenderness ratio (height to thickness ratio) as well as the volume fraction of a unit,  $V_{F_b}$ , and the volume ratio of bed joint to mortar,  $V_{R_{mb}}$ . Table 6.3 lists a summary of the proposed equations in the literature, where  $f_b$  and  $f_m$  are the normalised compressive strength of units and the compressive strength of mortar, respectively. It should be emphasised that unlike the literature, Eurocode 6 refers to the characteristic compressive strength of the masonry rather than the mean value. However, as suggested by standard EN 1052-1(CEN 1998), the ratio between the mean value and the characteristic value of masonry compressive strength can be assumed to be 1.2, if fewer than five specimens were tested. It should be noted that mean properties are often used for the assessment of existing structures, while design values are adopted when dealing with new structures.

Figure 6.2 shows the error between the predicted compressive strength and the experimental values. The analysis was made only for the laboratory-made masonry types with known properties of mortar. In general, the analytical expressions tend to underestimate the values of masonry compressive strength. In order to define the best model proposed in literature, the error was calculated for each expression. The lowest and the highest errors are associated with the models proposed by Eurocode 6 and Hendry and Malek (1986), respectively. Accordingly, although a variety of models were introduced in the literature, the model introduced in Eurocode 6 still can be considered the most reliable one for the analysed cases.

**Table 6.3:**

Overview of a selection of expressions in the literature to calculate the mean value of masonry compressive strength,  $f'_m$ , and characteristic compressive strength,  $f'_k$ , using compressive strength of mortar,  $f_m$ , and compressive strength of unit,  $f_b$ .

Reference	Model	Valid for/Calibrated
Eurocode 6 (CEN 2005)*	$f'_k = 0.55 f_b^{0.70} f_m^{0.30}$ $f'_k = 0.80 f_b^{0.85}$	Clay and CS brick masonry CS element masonry
Hendry and Malek (1986)	$f'_m = 0.317 f_b^{0.531} f_m^{0.208}$	Clay brick masonry
Kaushik et al. (2007)	$f'_m = 0.63 f_b^{0.49} f_m^{0.32}$	Stack-bond clay brick masonry
Gumaste et al. (2007)	$f'_m = 1.242 f_b^{0.531} f_m^{0.208}$ $f'_m = 0.334 f_b^{0.778} f_m^{0.234}$	Single-wythe masonry wallet Double wythe masonry wallet
Thaickavil and Thomas (2018)	$f'_m = \frac{0.54 f_b^{1.06} f_m^{0.004} V F_b^{3.3} V R_{mH}^{0.6}}{H / t^{0.28}}$	Single-wythe clay brick masonry prism
Ferretti (2020)	$f'_m = 0.91 f_b^{0.33} f_m^{0.67}$	Single-wythe clay brick masonry wallets

\*Valid for Group 1 with general purpose mortar.

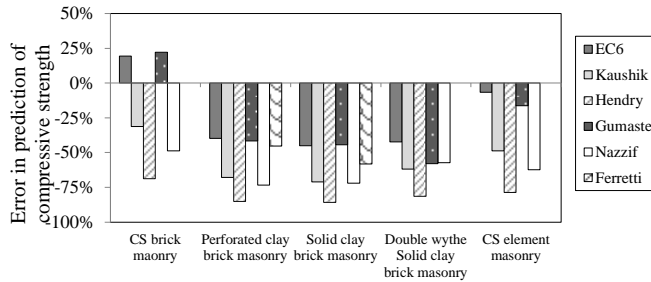


**Figure 6.2:** Error between the predicted values obtained from literature equations and the experimental results for laboratory-made masonry types.

### 6.1.4 Young’s modulus of masonry

Establishing a correlation between the Young’s modulus and compressive strength of masonry is of great interest, as it could reduce the amount of effort required to accurately measure longitudinal deformations. National standards often introduce a linear expression between the Young’s modulus and the mean values of masonry compressive strength or characteristic compressive strength. Eurocode 6 recommended a linear relationship, with the elastic modulus of masonry to be evaluated as 1000 times higher than the characteristic compressive strength of masonry, i.e.  $k_k=1000$ . However, supplementary information is often available in national annexes for each country; a value equal to 700 was suggested for Dutch masonry in NEN 6790 (NEN 2005). Unlike Eurocode 6, NZSEE and the majority of studies in the literature investigated the ratio between the Young’s modulus and the mean values of compressive strength,  $k_m$ , rather than the characteristic value,  $k_k$ .

Variations in the Young’s modulus with respect to the mean values of compressive strength obtained under a vertical configuration are plotted in Figure 6.3a. Through the regression analysis of 26 different Dutch masonry types, a ratio of 521 was obtained, though the correlation of determination was relatively low ( $R^2=0.36$ ). However, a breakdown of the data based on the masonry types, as listed in Table 6.3, revealed a higher ratio for the CS brick masonry wallets, 702, than for clay brick masonry, which had an average ratio of 477. Moreover, the results of the literature studies are set out in Table 6.3, which lists the ratio between the Young’s modulus and the mean values of compressive strength,  $k_m$ . In the literature, values of  $k_m$  ranged from 300 to 526. The upper limit is in line with the ratio of 521 that we found by considering all masonry types. Table 6.3 also lists the ratio between the Young’s modulus and characteristic compressive strength,  $k_k$ , found in this study and reported in the literature. Considering all masonry types studied in this research, a ratio of 624 was found. It can be seen that NEN 6790 (NEN 2005) provides an acceptable estimate of the Young’s modulus, although it slightly overestimates the value of the Young’s modulus for clay brick masonry.

Variations in the Young’s modulus with respect to the mean values of compressive strength obtained under horizontal configuration are plotted in Figure 6.3b. It can be seen that the data are quite scattered and the ratio of the horizontal Young’s modulus to horizontal compressive strength ranged from 243 to 1268. The simple linear regression analysis indicated that no clear relationship exists between these two properties ( $R^2=0.05$ ). However, this could be influenced by the limited amount of data.

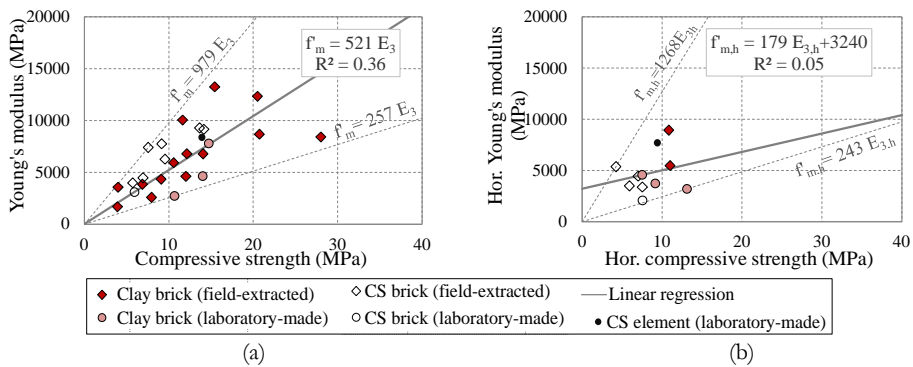


**Figure 6.3:** Relationship between Young’s modulus and mean values of compressive strength under: (a) vertical compressive load; (b) horizontal compressive load.

**Table 6.3:**

Ratio between the Young's modulus,  $E_3$ , and mean value of compressive strength,  $f_m$ , as well as characteristic compressive strength of masonry,  $f_k$ , under a vertical loading configuration. Correlation of determination in parentheses.

Reference	Masonry type	$k_m = E_3/f_m$	$k_k = E_3/f_k$
Rots et al. (1997)	Clay and CSB masonry	526 (0.80)	-
Vermeltoort (2005)	Clay brick masonry	304 (0.88)	-
Gumaste et al. (2007)	Clay brick masonry	425 (0.91)	-
Kaushik et al. (2007)	Clay brick masonry	550 (0.63)	-
Lumantarna et al. (2014b)	Clay brick masonry	290 (0.76)	-
Costigan et al. (2015)	Clay brick masonry	-	85-230 (0.46)
De Villiers (2019)	Typical South African	-	1951 (0.88)
Eurocode 6	No division	-	1000
NEN 6790	Dutch masonry	-	700
NZSEE	Clay brick masonry	300	-
This work	Clay brick masonry	477 (0.42)	575 (0.28)
	CS brick masonry	702 (0.79)	833 (0.19)
	CS element masonry	602 (-)	686 (-)
	All masonry types	521 (0.36)	624 (0.16)

Insight into the Young's modulus of masonry can be obtained not only from compression tests, but also by performing bending tests. Assuming a linear stress distribution over the height of the specimen's cross-section under bending load, the Young's modulus of masonry can either be evaluated as the initial slope of the moment-curvature curve divided by the moment of inertia or by using the stress-deflection curve. Figure 6.4 shows the ratio between the Young's modulus of masonry obtained from vertical compression tests,  $E_3$ , and from bending tests using both force-deflection curves, Figure 6.4a, and moment-curvature curves, Figure 6.4b. As mentioned in Chapter 2, we generally did not find an acceptable agreement between these two values of the Young's modulus; often higher values of the Young's modulus were found using moment-curvature rather than stress-deflection curves. Thus, further research is needed to explain such a difference.

A ratio of around one between the Young's modulus under compressive load and under bending load was only observed for MAT-2 perforated clay brick masonry and MAT-3 solid clay brick masonry wallets. A better agreement between the compressive and the bending Young's moduli was found using the moment-curvature rather than the stress-deflection curves. Using the former curve, this ratio for the five laboratory-made masonry types ranged from 0.51 to 2.00, while using the latter curve it varied from 0.24 to 1.64. Nevertheless, van der Pluijm (1993) reported higher values of the elastic modulus under bending load than under compressive load. He explained this difference in terms of the difference in the loading rates of these two types of tests. However, in this study the Young's modulus of MAT-2 perforated clay brick masonry and MAT-3 solid clay brick masonry under compressive load corresponded well with the ones obtained under bending load, using the moment-curvature curves, though the loading rate differed.

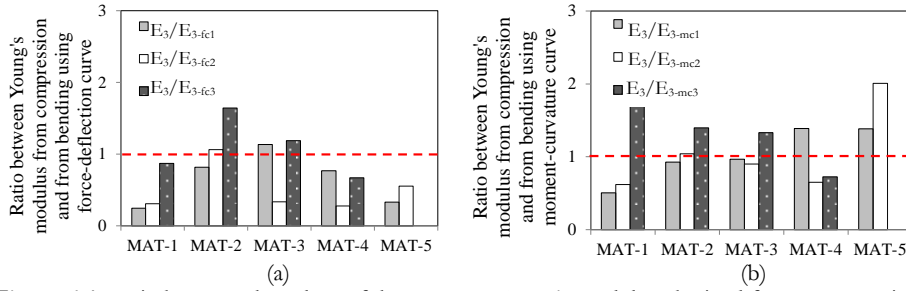


**Figure 6.4:** Ratio between the values of the masonry Young’s modulus obtained from compression tests,  $E_3$ , and from bending tests: the Young’s modulus under bending load was evaluated using: (a) moment-curvature; (b) flexural stress-deflection curves.

### 6.1.5 Strain corresponding to masonry compressive strength

So far, there has been limited discussion about the indirect estimation of the strain corresponding to masonry compressive strength, referred to as peak strain. In this context, Kaushik et al. (2007) introduced an expression in which the predicted peak strain,  $\epsilon_{pp}$ , of a stack-bond prism is a function of the mortar compressive strength,  $f_m$ , the masonry compressive strength,  $f'_m$ , and the elastic modulus of masonry,  $E_3$ , as follows:

$$\epsilon_{pp} = \frac{0.27 f'_m}{E_3^{0.7} f_m^{0.25}} \tag{6.1}$$

The proposed model by Kaushik et al. (2007) leads to an overestimation of the values of peak strain for the wallets studied in this research; as shown in Figure 6.5a, a ratio of 2.01 was found between the peak strain and the predicted values of the peak strain. In this figure, the experimental data obtained for the laboratory-made wallets are supplemented with calculated data for the field-extracted masonry by calculating the compressive strength of mortar as 1/0.036 of the flexural bond strength. This expression was proposed by Lumantarna et al. (2014a), and its validity for the studied data set is presented in Section 6.1.7.

To improve the accuracy of the predicted values of peak strain, an attempt was made to calibrate the coefficients of Eq. (6.1) using the data obtained in this study from tests on wallets. An acceptable agreement between the predicted values and the experimental data was found in Figure 6.5b, using the following revised equation:

$$\epsilon_{pp} = \frac{0.18 f'_m}{E_3^{0.73} f_m^{0.20}} \tag{6.2}$$

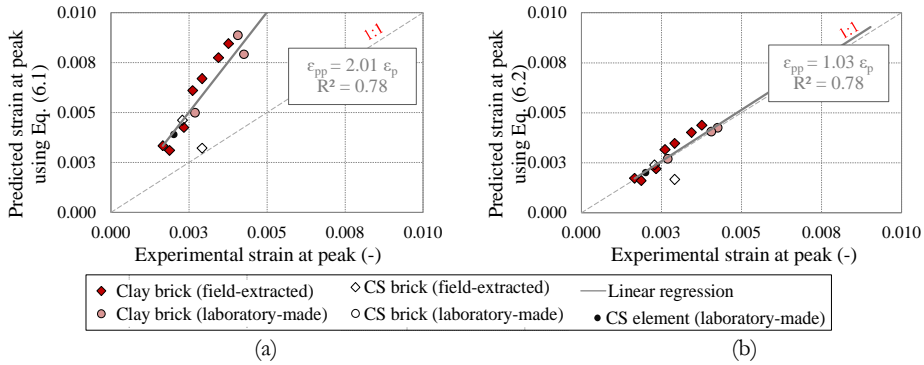


**Figure 6.5:** Relationship between the experimental values of peak strain,  $\epsilon_p$ , and the predicted value,  $\epsilon_{pp}$ , using: (a) the equation introduced by Kaushik et al. (2007) for stack-bond specimens; (b) the equation calibrated in this study for wallets.

### 6.1.6 Compressive fracture energy of masonry

Several researchers, e.g., Ghiassi et al. (2019), have argued that the compressive fracture energy of masonry should be treated as a structural property rather than a true material property, as it is measured upon the formation of multiple cracks and not a single crack. Nevertheless, in finite element softening macro-models, the compressive fracture energy along with some crush band width parameters is required to achieve mesh-objective results. Also, the original experimental work by van Mier (1984) on concrete clearly showed that compressive stress-displacement curves were objective for different specimen lengths, while stress-strain curves were non-objective.

A systematic understanding of the gradual decrease of masonry compressive resistance in the softening phase is still lacking. In the absence of data on the post-peak behaviour of masonry, scholars such as Lourenço (1996) recommended the use of the parabolic curve proposed by Model Code 90 (CEB-FIP 1990) for concrete to model the nonlinear behaviour in compression, as in Eq. (6.3). The proposed model to predict the compressive fracture energy of masonry,  $G_{f-cp}$ , reads only the compressive strength of masonry,  $f'_m$ , and is applicable only for masonry with a compressive strength between 12 MPa and 80 MPa.

$$G_{f-cp} = 0.15 + 0.43 f'_m - 0.0036 (f'_m)^2 \quad (6.3)$$

In this framework, Lourenço (1996) introduced the concept of the ductility index, which is defined as the ratio of compressive fracture energy,  $G_{f-c}$ , to the value of masonry compressive strength,  $f'_m$ . Lourenço (1996) recommended the values of average ductility index as 1.6 mm and 0.68 mm, respectively, for masonry with a mortar compressive strength lower than 12 MPa and between 12 and 80 MPa. In the present study, the average value of the ductility index for masonry with a mortar strength lower than 12 MPa was found to be 1.9 mm, which is comparable with the value of 1.6 mm suggested by Lourenço (1996). However, for masonry with a mortar strength higher than 12 MPa, the average value of the ductility index was found to be 1.5 mm, almost two times higher than the one recommended by Lourenço (1996).

For the masonry types analysed in this research, neither the parabolic equation of Model Code 90 (CEB-FIP 1990) nor the linear function could accurately show the relationship between the compressive fracture energy and the compressive strength of masonry along the two loading directions, as shown in Figure 6.6a for vertical compression and Figure 6.6b for horizontal compression. A wide ratio, ranging from 0.88 to 5.8, was found between the compressive fracture energy and the compressive strength of masonry wallets under vertical compressive load, Figure 6.6a. The regression analysis indicated no linear relationship between these two properties. Unlike vertically compressed wallets, the values for horizontal compressive fracture energy are more concentrated along the linear regression line, and thus are less scattered than the values for vertical compressive fracture energy, Figure 6.6b. Such differences could be explained by the different failure modes. The failure of the vertically compressed wallets showed various forms of brick tensile failure or shear failure, while failure in the horizontally compressed wallets consistently occurred in only one form, namely interface debonding, see Figure 2.11–Figure 2.14.

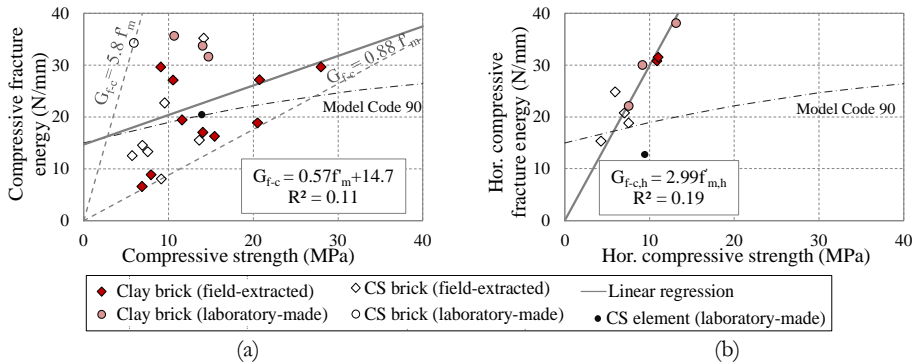


**Figure 6.6:** Relationship between compressive fracture energy and compressive strength of masonry under: (a) vertical configuration; (b) horizontal configuration.

### 6.1.7 Bond strength

Since the bond wrench test has the advantage of simplicity and repeatability with minimum intervention in building functionality (Nichols & Holland, 2011), finding relationships between the values of bond strength, measured using the bond wrench test, and the compression properties of mortar/masonry is of particular interest. To this end, Figure 6.7 shows the relationships between the bond strength and the compressive strength of masonry as well as the compressive strength of mortar obtained in this research from tests on laboratory-made and field-extracted masonry types.

The very low correlation of determination value obtained from the regression analysis ( $R^2=0.09$ ) proves the absence of a relationship between the bond strength and masonry compressive strength, Figure 6.7a. The dashed lines show a wide ratio between the bond strength and compressive strength of masonry, varying from 0.01 to 0.07. Apart from the masonry types studied in this research, Table 6.4 lists the ratio between the bond strength and masonry compressive strength

reported by several researchers; the values in parentheses are the correlation of determination. Generally, researchers found very low values for the correlation of determination over a broad range, varying from 0.005 to 0.065, thus confirming the conclusion of the current research. However, Lumantarna et al. (2014a) reported a strong relationship, with a ratio of 0.012 obtained from tests on historical clay brick masonry types in New Zealand.

Unlike the compressive strength of masonry, an acceptable correlation with a strong relationship ( $R^2=0.96$ ) was found between the bond strength and the compressive strength of mortar for laboratory-made specimens, Figure 6.7b. Although this correlation was found based on the analysis of a limited number of objects, the obtained ratio of 0.036 is comparable to those reported by Reddy and Vyas (2008) and Lumantarna et al. (2014a), as shown in Table 6.4. However, it should be noted that Sarangapani et al. (2005) and Dehghan et al. (2018) reported very low values for the correlation of determination, indicating the absence of a linear relationship between the mortar compressive strength and bond strength.

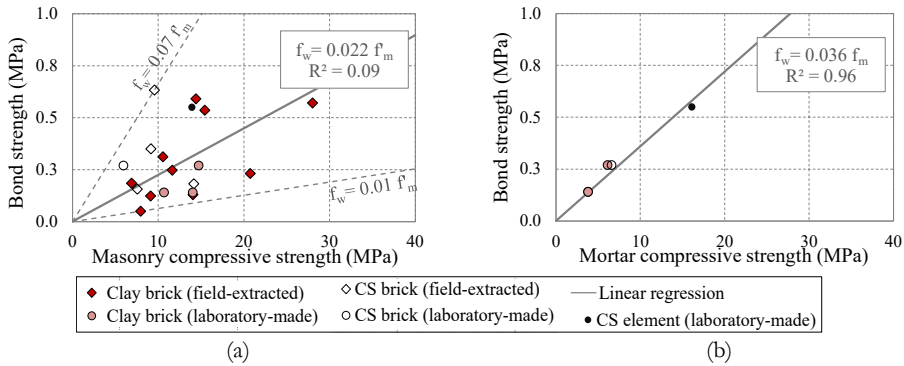


**Figure 6.7:** Correlation between bond strength and: (a) masonry compressive strength; (b) mortar compressive strength.

**Table 6.4:**

Ratio between the bond strength,  $f_w$ , and compressive strength of masonry,  $f_m$ , and of mortar,  $f_m$ . Correlation of determination in parentheses.

Reference	Masonry type	$f_w/f_m$	$f_w/f_m$
Sarangapani et al. (2005)	Clay masonry	0.065 (0.31)	0.012-0.077
Reddy and Vyas (2008)	Soil-cement masonry	0.033 (0.10)	0.035 (0.35)
Lumantarna et al. (2014a)*	Clay brick masonry	0.012 (0.89)	0.031 (0.82)
Dehghan et al. (2018)	Clay masonry	0.130 (0.11)	0.05-0.14
This work	All masonry types	0.022 (0.09)	0.036 (0.96)**

\*Values reported by Lumantarna et al. (2014a) are re-calculated excluding the outliers.

\*\*The ratio is obtained by considering only the laboratory-made masonry types.



From a physical point of view, a link could be expected between the flexural bond strength obtained from the bond wrench test and the flexural strength of the wallets determined by the vertical bending test. In both tests, the failure often occurred along the brick-mortar interface in the bed joint plane, and thus these strength parameters depend on the strength of the brick-mortar interface. Figure 6.8 shows a moderate correlation ( $R^2=0.55$ ) between these two properties, for which a ratio of 0.99 was found. As seen in the graph, the widely dispersed values belonged to the field-extracted masonry types, while a better correlation was observed for the laboratory-made masonry than for the field-extracted masonry. Several researchers also reported a one-to-one correspondence between the vertical flexural strength and the bond strength of masonry, e.g., Zhou et al. (2008).

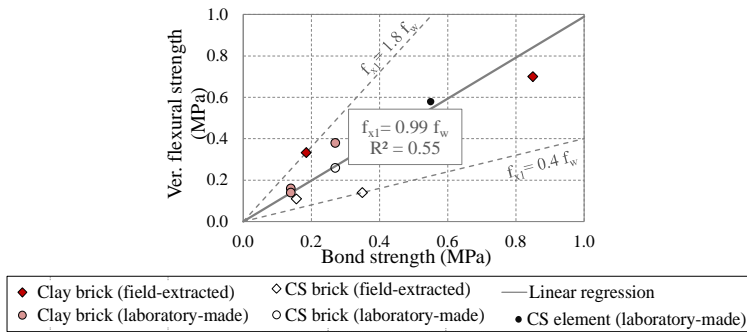


**Figure 6.8:** Correlation between flexural strength of masonry obtained from vertical out-of-plane bending tests and bond strength obtained from bond wrench tests.

### 6.1.8 Cohesion

No clear link between the compressive strength of masonry and cohesion was found in this study, which accords with the findings of previous studies, Table 6.5. Figure 6.9a plots the values of cohesion versus the masonry compressive strength obtained in this research from tests on laboratory-made and field-extracted masonry types. The very low correlation of determination ( $R^2=0.02$ ), obtained from the regression analysis of all masonry types, indicates the absence of a linear relationship between these two properties, Figure 6.9a. As seen in the graph, the data are very scattered, and the ratio between the cohesion and masonry compressive strength ranged from 0.002 to 0.07 (dashed lines in Figure 6.9a). In addition, Table 6.5 lists the breakdown of these ratios for different masonry types, though this division does not lead to an improvement in the correlation of determination (presented in parentheses).

As shown in Figure 6.9b, the very low correlation of determination value ( $R^2=0.03$ ) indicates that there was no clear relationship between the mortar strength and cohesion. A wide ratio was found between these two properties, ranging from 0.01 to 0.13 (dashed lines in Figure 6.9b). Note that the database was augmented to include the data from existing masonry, for which the mortar compressive strength was calculated from the bond strength (Section 6.1.7). The significant influence of mortar compressive strength on cohesion was previously

investigated by several researchers. However, it can be concluded that apart from the mortar strength, the brick and mortar composition, the physical characteristics of bricks, such as surface roughness, and the water retention of bricks and mortar can largely influence the quality of the bond along the brick-mortar interface (Groot, 1997). This conclusion is in line with the recommendations of Eurocode 6 (CEN 2005), which gives an indication of cohesion based on unit type, the compressive strength of the mortar, and joint thickness. Among the researchers, only Lumantarna et al. (2014b) found a strong relationship, in which the cohesion of clay brick masonry was found to be approximately 0.0471 times the mortar compressive strength, see Table 6.5. Using the extensive experimental results from laboratory-made clay brick masonry, CS brick and block masonry reported by van der Pluijm (1999), a similar relationship was also found.

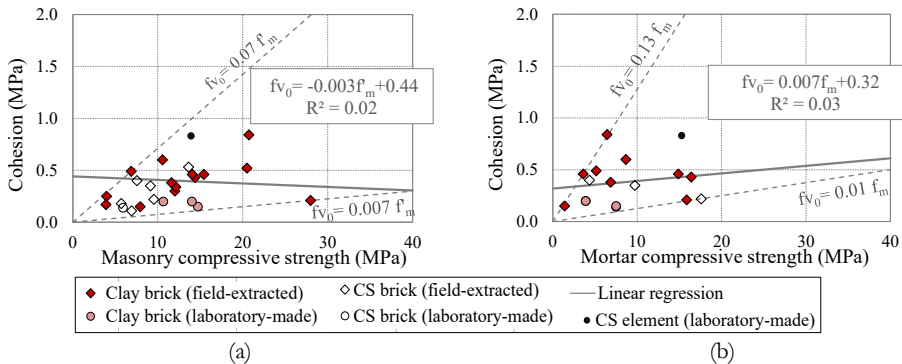


**Figure 6.9:** Correlation between cohesion and: (a) masonry compressive strength; (b) mortar compressive strength.

**Table 6.5:**

Ratio between cohesion,  $f_{v_0}$ , and compressive strength of masonry,  $f_m$ , and compressive strength of mortar,  $f_m$ . Correlation of determination in parentheses.

Reference	Masonry type	$f_{v_0}/f_m$	$f_{v_0}/f_m$
Rots et al. (1997)	Clay and CSB	0.008-0.096	0.023-0.135
van der Pluijm (1999)	Clay and CSB	-	0.043 (0.34)
Lumantarna et al. (2014b)	Clay masonry	0.032 (-0.15)	0.047 (0.83)
De Villiers (2019)	Typical South African	-	0.350 (0.30)
Barattucci et al. (2020)	Clay brick masonry	-	0.071 (-0.15)
This work	Clay brick masonry	0.007-0.071(0.09)	0.013-0.131(0.02)
	CS brick masonry	0.034 (0.60)	0.013-0.092 (0.16)
	CS element masonry	0.060 (-)	0.054 (-)
	All masonry types	0.002-0.071 (0.02)	0.013-0.131 (0.03)

A correlation between the values of cohesion and uniaxial tensile strength might be expected, as both parameters depend on brick-mortar interface properties. Although this research did not include a direct tensile test, uniaxial tensile strength was indirectly evaluated from the bending tests. As explained in Chapter 2, the stress corresponding to the onset of cracking can be considered uniaxial tensile strength. Figure 6.10a shows the relationship between the derived tensile strength and the flexural strength of laboratory-made wallets tested under vertical out-of-plane bending (OOP1), horizontal out-of-plane bending (OOP2), and in-plane bending (IP) loads. The ratios found were not similar, as the wallets were bent over three configurations. The highest ratio was found under vertical bending, 0.78, and the lowest ratio was obtained under in-plane bending, 0.44. The obtained ratio of 0.78, found between indirect uniaxial tensile strength and vertical flexural strength, is in agreement with the ratio of 0.80 found by van der Pluijm (1999), as direct tensile tests and vertical out-of-plane bending tests were performed. Nevertheless, researchers such as Lourenço (1997a) and Milani et al. (2006) indicated a lower ratio of 0.33, meaning that there is a factor of three between tensile and flexural strength.

Figure 6.10b shows the ratio between cohesion and tensile strength derived using the values of bond strength. To augment the database, the values of tensile strength were indirectly evaluated using the relationships established earlier: 1) a one-to-one correspondence exists between the bond strength and vertical out-of-plane strength of wallets; 2) there is a factor of 0.78 between the tensile strength and vertical out-of-plane strength. As evident in Figure 6.10b, no clear relationship was found between cohesion and uniaxial tensile strength. A wide range of ratios was obtained, varying between 0.43 and 3.84. These results seem to be consistent with those of van der Pluijm (1999), who found a wide range varying between 1.3 and 7.5. Nevertheless, instead of a regression analysis, he reported an average ratio of 2.0, with a coefficient of variation of 0.55. Taking a similar approach, an average ratio of 2.18 was found with a coefficient of variation of 0.66.

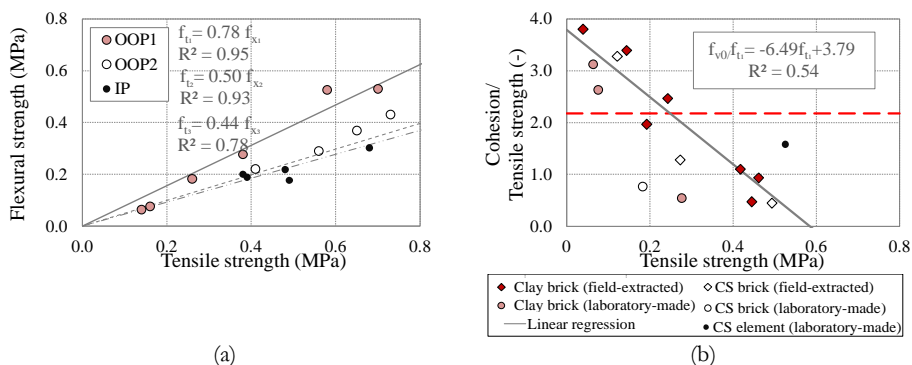


**Figure 6.10:** (a) Correlation between flexural strength and derived uniaxial tensile strength under vertical out-of-plane bending load (OOP1), horizontal out-of-plane bending (OOP2), and in-plane bending (IP); (b) correlation between cohesion and derived tensile strength.

### 6.1.9 Tensile fracture energy of mortar, units, and mode-I fracture energy

As mentioned earlier, the brittle nature of masonry and its constituents often hinders a full appreciation of the post-peak response, and thus the ability to quantify the fracture energy. Accordingly, to date, only a few studies have experimentally characterised the fracture energy of mortar, unit, and masonry under tensile loading. A summary of the available literature data is presented in Table 6.6.

So far there has been little discussion on the fracture energy of mortar under tensile load. In a recent study, Moreno Regan et al. (2018) established a relationship between mortar tensile strength,  $f_{tm}$ , and the fracture energy of mortar,  $G_{f-tm}$ , as follows:

$$G_{f-tm} = 100(f_{tm})^{0.8} \quad (6.4)$$

Moreover, in the absence of experimental results, several researchers, such as Angelillo et al. (2014) and Drougkas et al. (2016), have relied on the recommendation of Model Code 90 for concrete, whereby the tensile fracture energy of mortar,  $G_{f-tm}$ , can be found as a function of mortar compressive strength,  $f_m$ , as follows:

$$G_{f-tm} = 0.025\left(\frac{f_m}{10}\right)^{0.7} \quad (6.5)$$

From the linear regression analysis of the experimental results presented by van der Pluijm (1999), the tensile fracture energy of the clay and CS bricks can be approximated as 0.038 times the unit tensile strength. For one unit type, namely multi-perforated clay brick, Sandoval and Arnau (2017) found a ratio in line with the findings of van der Pluijm (1999). However, this ratio is almost two times higher than that of Lourenço et al. (2005), which was found from tests on three types of clay bricks. For the typical South African units, De Villiers (2019) found a ratio ranging widely from 0.013 to 0.071. As with mortar, in the absence of experimental results, the tensile fracture energy of brick is estimated in the literature using the expression from Model Code 90, Eq. (6.5).

Using the data reported by van der Pluijm (1999) obtained from uniaxial tests on 17 different masonry types, a ratio of 0.016 between the mode-I fracture energy and the tensile strength of masonry was found, though the correlation of determination was not strong ( $R^2=0.35$ ). In this research, uniaxial tensile tests were not performed; however, the bending properties obtained from the vertical out-of-plane bending tests can give an indication of the tensile properties of masonry. To this end, Table 6.6 lists the ratio between the fracture energy and flexural strength of wallets under vertical out-of-plane bending tests. Though based on a limited amount of data, an average ratio of 0.032 was found, which accords with the findings of van der Pluijm (1999). As mentioned in Chapter 2, in a separate study, Gaggero (2019) managed to record the softening response of MAT-1 CS brick masonry and MAT-3 clay brick masonry specimens using a bond wrench test. Table 6.6 reports the ratio for MAT-1 CS brick masonry and MAT-3 clay brick masonry tested at 28 days. As seen in the table, the ratio of 0.029 found

for clay brick masonry matched our findings from the vertical out-of-plane bending test, 0.032. However, the ratio found for CS brick masonry is much higher as compared to clay brick masonry.

**Table 6.6:**

Ratio between unit tensile fracture energy,  $G_{f_{tb}}$ , and tensile strength of unit,  $f_{tb}$ , and Mode-I fracture energy,  $G_{f_{I}}$ , and tensile strength,  $f_t$ . Correlation of determination in parentheses.

Reference	Masonry type	$G_{f_{tb}}/f_{tb}$	$G_{f_{I}}/f_t$
van der Pluijm (1999)	Clay and CS brick	0.038 (0.51)	0.016 (0.35)
Lourenço et al. (2005)	Clay brick	0.018 (-)	-
Sandoval and Arnau (2017)	perforated clay brick	0.038	-
De Villiers (2019)	Typical South African	0.013–0.071	-
Gaggero (2019)*	Clay brick	-	0.029
	CS brick	-	0.052–0.064
This work**	Clay brick	-	0.032

\* Values are obtained from bond wrench tests.

\*\*Values are obtained from vertical out-of-plane bending tests.

### 6.1.10 Shear fracture energy

Although fracture energy is commonly acknowledged as a size-independent property, in this study, as in previous studies (e.g., van der Pluijm, 1999; Augenti & Parisi, 2011), a clear dependency of the mode-II fracture energy on pre-compression levels was observed. As discussed in Chapter 2, a linear relationship was established between mode-II fracture energy and pre-compressive stress. As depicted in Figure 2.38, MAT-1 CS brick masonry and MAT-3 solid clay brick masonry showed an increasing trend between mode-II fracture energy and pre-compressive load, while mode-II fracture energy in MAT-2 perforated clay brick masonry decreased with an increase in the pre-compressive stress. This can be explained by a sudden reduction in the shear stress upon reaching the peak load. Accordingly, it can be concluded that mode-II fracture energy is affected not only by the pre-compressive stress, but also by the unit type.

Although a large body of literature exists regarding the shear properties of masonry, the current state of knowledge on mode-II fracture energy mainly relies on the experimental studies conducted by van der Pluijm (1999). Table 6.7 lists the expressions established in this study and found by van der Pluijm (1999) for CS brick masonry and clay brick masonry. Generally, in this study higher values of mode-II fracture energy were found than did van der Pluijm (1999). Such a difference can be attributed to the use of different testing methods and specimen geometry, as discussed in Chapter 5. In this study, we adopted triplet specimens tested under shear-compression loading accordingly to EN 1052-3(CEN 2002), while van der Pluijm (1999) used couplet specimens and an ad-hoc set up, aiming for a homogeneous shear distribution. As a coarse estimate, the mode-II fracture energy is often estimated to be ten times that of the mode-I fracture energy (Nazief, 2014; De Villiers, 2019). However, Drougkas et al. (2016) assumed that the mode-II fracture energy can be estimated as 1/10 of cohesion. Assuming that mode-II fracture is evaluated at zero pre-compressive stress, neither approach suggested in the literature was able to provide an acceptable estimation of mode-II fracture energy for the analysed masonry types. To draw more precise conclusions

regarding mode-II fracture energy and its influencing parameters, additional experimental studies are suggested.

**Table 6.7:**

Mode-II fracture energy as a function of pre-compressive stress.

Reference	Masonry type	Expression
van der Pluijm (1999)	Lab-made CS brick masonry (lower limit)	$G_{f-II} = 0.02f_p + 0.005$
	Lab-made CS brick masonry (upper limit)	$G_{f-II} = 0.04f_p + 0.01$
	Lab-made clay brick masonry (lower limit)	$G_{f-II} = 0.02f_p + 0.005$
	Lab-made clay brick masonry (upper limit)	$G_{f-II} = 0.13f_p + 0.06$
This research	Lab-made CS brick masonry	$G_{f-II} = -0.01f_p + 0.02$
	Lab-made perforated clay brick masonry	$G_{f-II} = -0.09f_p + 0.17$
	Lab-made solid clay brick masonry	$G_{f-II} = 0.53f_p - 0.04$

### 6.1.11 Orthotropic behaviour of masonry under compression and bending loads

Masonry is treated as an orthotropic material, meaning that it exhibits distinct directional properties due to the bond stacking pattern and different arrangements of head joints and bed joints (Page, 1981). Accordingly, the influence of the bed joint orientation with respect to the principal stress needs to be considered. Under compression loading, the stiffness, strength and softening response of masonry could change depending on the loading direction. The same holds for in-plane tensile loading and in-plane bending, where either a line crack in bed joints, a stepped crack through bed joints and head joints, or a line crack through head joints and bricks may emerge. Finally, for out-of-plane bending load, the orthotropic behaviour of masonry is also essential, as bed joints act as a plane of weakness, and stepped cracks or line cracks may again emerge as distinct failure modes. Experimental and numerical attempts have been made in the literature to address the orthotropic behaviour of masonry by introducing a failure surface. Lourenço et al., (1997) proposed a composite yield criterion, in which the strength and the hardening/softening behaviour differed along each material axis. It is worth mentioning that the bending properties are not always directly implemented in assessment methods; however, they are often used indirectly to provide insights into the uniaxial tensile strength along with the softening parameters.

The orthotropic behaviour of masonry under compression loading is certainly not limited to strength but can be extended to other properties, such as stiffness, strain corresponding to the peak stress, and fracture energy. The ratios between the compression properties of wallets under vertical and horizontal loading for the clay and CS masonry are shown in Figure 6.11a and Figure 6.11b, respectively. Lower strength and stiffness can be expected under horizontal compression loading, since failure generally occurred by debonding of the bed joint interfaces rather than splitting of the bricks. In addition, under horizontal loading, the head joints are compressed, and these are often not adequately filled with mortar and considered to be of a poorer quality. As a result, under horizontal action, the Young's modulus is expected to be lower and the peak strain higher. In addition,

more energy is expected to be consumed under horizontal loading, as bricks form a series of columns that can sustain further load (Dhanasekar et al., 1985). However, the findings from tests on different masonry types showed that the orthotropic behaviour of masonry is not as straightforward as assumed, and the differences between the elastic properties of masonry constituents and unit types can lead to completely different behaviour. The average values of the orthotropic ratio under compression loading are listed in Table 6.8. Irrespective of the masonry type, the horizontal compressive strength and Young’s modulus can be approximated to be 30% lower than the corresponding properties in the vertical direction. In line with the reduction of Young’s modulus, the peak strain of the clay wallets can be estimated to be 30% higher than the peak strain in the vertical direction. However, the peak strain of the CS brick as well as the CS element masonry in the horizontal direction is found to be 20% lower than the corresponding values obtained in the vertical direction. Regarding the compressive fracture energy, no significant difference between horizontal and vertical direction was noticed; thus the orthotropic ratio was 1.

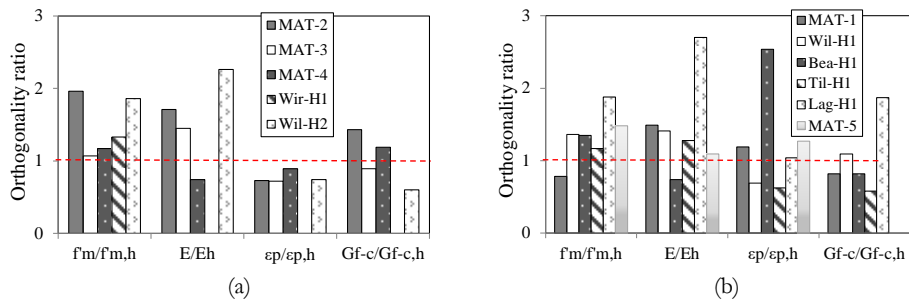


**Figure 6.11:** Orthotropic behaviour under compression loading: (a) clay brick masonry types; (b) CS brick and MAT-5 CS element masonry.

**Table 6.8:**

Mean values of orthotropic ratio under compressive loads. Number of masonry objects are in parentheses.

Masonry type	$f_{m,h}/f_m$	$E_{3h}/E_3$	$\epsilon_{p,h}/\epsilon_p$	$G_{f-c,h}/G_{f-c}$
Clay brick masonry	0.68 (5)	0.65 (4)	1.30 (4)	0.97 (4)
CS brick masonry	0.76 (5)	0.66 (5)	0.82 (5)	0.97 (4)
CS element masonry	0.69 (1)	0.69 (1)	0.81 (1)	-

It is worth mentioning that Eurocode 6(CEN 2005) also provided insight into the characteristic flexural strength of different masonry types. Accordingly, it implicitly indicates a ratio of 4 between the horizontal and vertical flexural strength of brick masonry for both clay and CS brick wallets, while a ratio of 2 is suggested for CS element masonry with thin layer joints. The ratio between the horizontal and vertical flexural strength of masonry with general-purpose mortar, i.e. both clay and CS brick masonry, and CS element masonry with thin layer joints was found to be approximately 3.0 and 1.3, respectively. These ratios are slightly lower than the ones recommended by Eurocode 6(CEN 2005). Regarding the Young's modulus, clay brick masonry showed a higher stiffness under horizontal bending than under vertical bending, while for CS brick and CS element masonry an inverse trend was found. Regarding the fracture energy, orthotropic ratios of 6 and 2 were found, respectively, for clay brick masonry and the element masonry. Note that the post-peak softening branch was captured only for a limited number of specimens. Accordingly, further tests are suggested to ensure the repeatability of the obtained ratios.

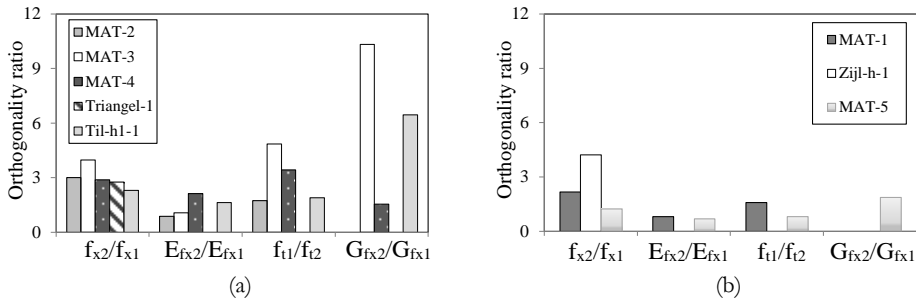


**Figure 6.12:** Orthotropic behaviour under out-of-plane bending loading: (a) clay brick masonry types; (b) CS brick and MAT-5 CS element masonry.

**Table 6.9:**

Orthotropic ratio under out-of-plane bending loads. Values in parentheses are number of masonry objects.

Masonry type	$f_{x2}/f_{x1}$	$E_{fx2}/E_{fx1}$	$f_{t2}/f_{t1}$	$G_{fx2}/G_{fx1}$
Clay brick masonry	2.99 (5)	1.43 (4)	2.99 (4)	6.11 (3)
CS brick masonry	3.19 (2)	0.82 (1)	1.59 (1)	-
CS element masonry	1.24 (1)	0.69 (1)	0.82 (1)	1.87 (1)



## 6.2 PREDICTION OF STRESS-STRAIN RELATIONSHIP

Accurate structural analysis relies on well-defined constitutive laws, describing the nonlinear response of materials for cracking, crushing, and shearing. These constitutive laws, either in an analytical setting or in a computational finite element setting, require precise descriptions of the stress-strain functions for compression, shear, and tension/bending. To date, several stress-strain functions have been introduced in the literature to define the pre- and post-peak uniaxial compressive response of masonry, such as Hendry (1981) and Sawko and Rouf (1984), as well as to define behaviour under shearing load and tension load, such as van der Pluijm (1999). The majority of the constitutive models for masonry were mainly built on the relationships proposed for concrete by researchers including Hordijk (1993), Feenstra (1993), Hoshikuma et al. (1997), and Lourenço (1997b). Despite the importance of developing analytical stress-strain laws, a consistent effort has not yet been devoted to investigating the accuracy of the proposed analytical forms for different masonry types.

This section proposes analytical models to represent the compression, bending, and shear response of masonry. The proposed models are examined for their ability to predict by comparing them with experimentally characterised mean curves obtained in the current study from tests on the five different laboratory-made masonry types.

### 6.2.1 Compression

Thus far, several constitutive laws have been introduced in the literature to define the uniaxial nonlinear compressive response of masonry. As will be further discussed, however, these models could not accurately represent the nonlinearities in the pre-peak branch as well as the post-peak softening branch of the typical Dutch masonry types tested under vertical and horizontal compression loading. Accordingly, this research proposes a compressive constitutive law, which was calibrated based on the experimental results for the five different laboratory-made masonry specimens, as discussed in Chapter 2.

The previous constitutive laws for the compression response of masonry often made a distinction between the ascending pre-peak branch, and the post-peak softening behaviour, Figure 6.13. Researchers such as Hendry (1981), Sawko and Rouf (1984), and Kaushik et al. (2007) approximated the pre-peak response of clay brick masonry tested under vertical compression loading with a second-order parabola. For Dutch masonry, Vermeltfoort (2005) found that the pre-peak response of wallets matched the second-order parabola introduced by Hendry (1981). However, Augenti and Parisi (2010) showed that nonlinearity in the pre-peak branch of tuff masonry tested under both vertical and horizontal compression loading was best captured by means of a cubic curve. To predict the pre-peak response of clay brick masonry, Facconi et al. (2017) adopted a model, previously proposed for concrete by Hoshikuma et al. (1997), which requires several input parameters, in terms of compressive strength and corresponding strain, and the Young's modulus. The post-peak degradation response of clay

brick masonry was often approximated either by a combination of a parabola followed by a linear curve (Kaushik et al., 2007), or by a simple parabola (e.g., Hendry, 1981; Sawko & Rouf, 1984; and Facconi et al., 2017). However, Augenti and Parisi (2010) suggested third-order and fifth-order curves for the post-peak response of tuff masonry tested under vertical and horizontal compression loading, respectively. Note that among these studies, only Augenti and Parisi (2010) proposed two different models for the uniaxial compression response of wallets tested under vertical and horizontal configurations.

Figure 6.14–Figure 6.18 show a comparison between the experimental stress-strain curves and the constitutive models proposed by Kaushik et al. (2007), Augenti and Parisi (2010), and Facconi et al. (2017). For the experiment, the mean stress-strain curve, obtained using the results of six tested wallets, is indicated by a black solid line, as also presented in Chapter 2. It was calculated following the approach proposed by Augenti and Parisi (2010) and adopts an increment of the axial strain equal to  $1.5\text{E-}05 \pm 1\%$ . To appreciate the variability of the experimental results, the area between the lower and the upper bounds is shaded in grey. Generally, a narrower band is noticed in the pre-peak phase, implying that the experimental data is less scattered than in the post-peak phase. Furthermore, the compression response of masonry under horizontal compression loading results in higher variability than masonry under a vertical loading configuration. It can be seen that the parabolic pre-peak curve proposed by Kaushik et al. (2007) deviated significantly from the mean experimental curves in the majority of cases. However, the accuracy increased significantly when a cubic curve or polynomial curve was adopted, as suggested by Augenti and Parisi (2010) and Facconi et al. (2017), respectively. However, for the MAT-1 CS brick masonry, these two models still do not capture the pre-peak response well, Figure 6.14a. In the post-peak phase, neither the linear nor the parabolic function, as suggested by Facconi et al. (2017) and Kaushik et al. (2007), respectively, could adequately represent the masonry response. To overcome the limitations of the current models, an effort was made to develop an analytical model that conforms better to the experimental mean stress-strain curves obtained in this study for typical Dutch masonry.

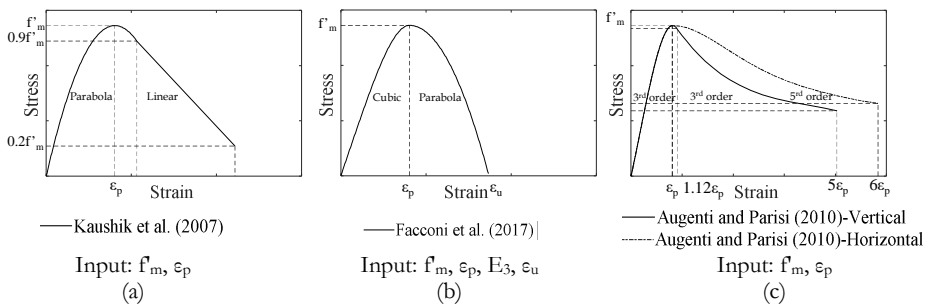


**Figure 6.13:** Overview of proposed constitutive laws in the literature.

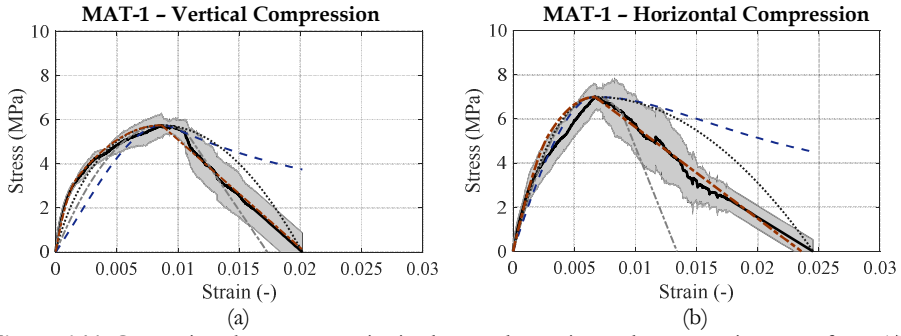


**Figure 6.14:** Comparison between constitutive laws and experimental stress-strain curves for MAT-1 CS brick masonry: (a) under vertical compression loading; (b) under horizontal compression loading.

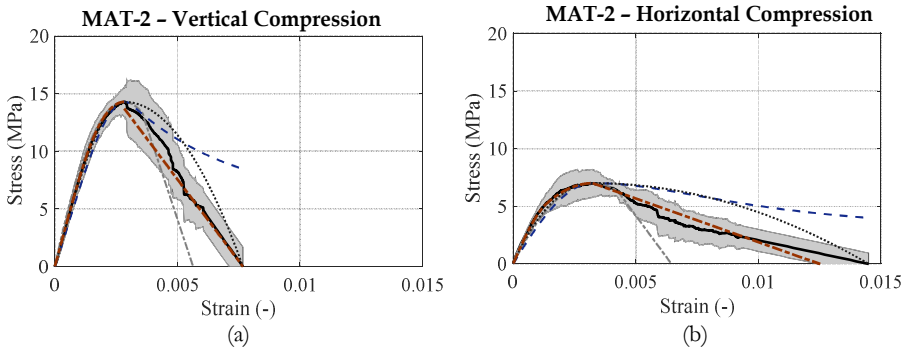


**Figure 6.15:** Comparison between constitutive laws and experimental stress-strain curves for MAT-2 perforated clay brick masonry: (a) under vertical compression loading; (b) under horizontal compression loading.

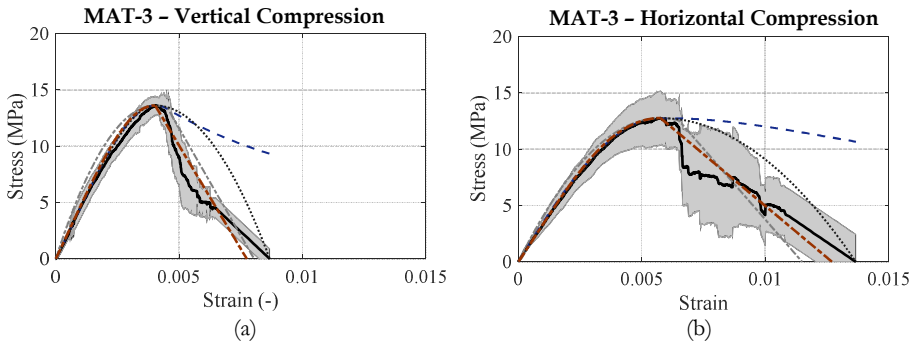


**Figure 6.16:** Comparison between constitutive laws and experimental stress-strain curves for MAT-3 solid clay brick masonry: (a) under vertical compression loading; (b) under horizontal compression loading.

**Legend for Figure 6.14-Figure 6.16**



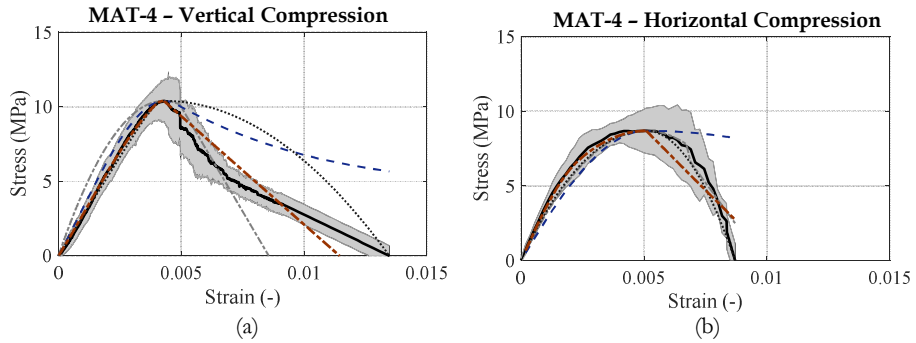


**Figure 6.17:** Comparison between constitutive laws and experimental stress-strain curves for MAT-4 double-wythe solid clay brick masonry: (a) under vertical compression loading; (b) under horizontal compression loading.

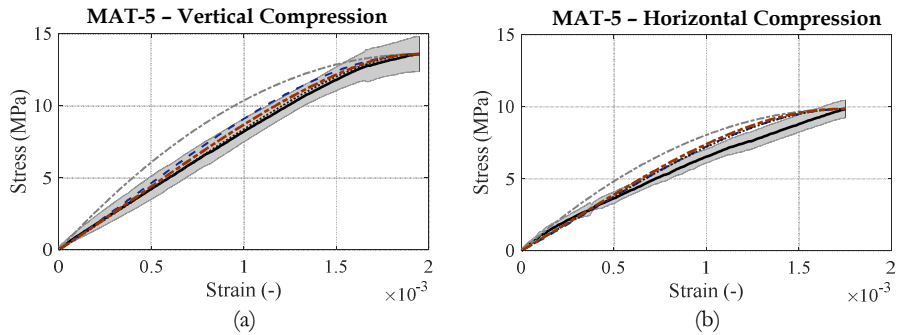


**Figure 6.18:** Comparison between constitutive laws and experimental stress-strain curves for MAT-5 CS element masonry: (a) under vertical compression loading; (b) under horizontal compression loading.

**Legend for Figure 6.17 and Figure 6.18.**

Lower and Upper bound	Kaushik	Facconi
Mean Curve	Augenti	Proposed model

To formulate the stress-strain relationship under vertical and horizontal compression loading, this study proposes a three-stage envelope curve consisting of two nonlinear pre-peak branches, and one post-peak softening branch. The pre-peak part is defined by a third-order curve followed by a second-order curve until the peak stress attained. The post-peak part is idealised by a linear curve. The proposed constitutive law can be described as:

$$\sigma = \begin{cases} A \left( \frac{E_3 \varepsilon}{f'_m} \right)^3 + B \left( \frac{E_3 \varepsilon}{f'_m} \right)^2 + E_3 \varepsilon & \varepsilon < \frac{f'_m}{E_3} \\ f'_m \left( \frac{1-\alpha}{\alpha} \left( \frac{E_3(\varepsilon - \varepsilon_p)}{f'_m - E_3 \varepsilon_p} \right)^2 + 1 \right) & \frac{f'_m}{E_3} < \varepsilon < \varepsilon_p \\ f'_m \left( \frac{\varepsilon - \varepsilon_u^*}{\varepsilon_p - \varepsilon_u^*} \right) & \varepsilon > \varepsilon_p \end{cases} \quad (6.6)$$

where  $f'_m$  is the compressive strength of masonry,  $\varepsilon_p$  is the corresponding strain,  $E_3$  is the chord modulus, and  $G_{f-c}$  is the compressive fracture energy. Parameters  $A$ ,  $B$ , and  $\alpha$  are calculated in Eq. (6.7) to Eq. (6.9). The ultimate strain,  $\varepsilon_u^*$ , can be traced back using Eq. (6.10). In this equation,  $H$  is the height of the wallet, over which the longitudinal deformations were measured.

$$\text{with } A = f'_m \left( \frac{\alpha - 2}{\alpha} + 2 \frac{1 - \alpha}{\alpha} \frac{f'_m}{f'_m - E_3 \varepsilon_p} \right) \quad (6.7)$$

$$B = f'_m \left( \frac{3 - 2\alpha}{\alpha} - 2 \frac{1 - \alpha}{\alpha} \frac{f'_m}{f'_m - E_3 \varepsilon_p} \right) \quad (6.8)$$

$$\alpha = \left( \frac{\varepsilon_p E_3}{f'_m} \right)^{1/3} \quad (6.9)$$

$$\varepsilon_u^* = 2 \frac{H(G_{f-c} - \int_0^{\varepsilon_p} \sigma_\varepsilon)}{f'_m} + \varepsilon_p \quad (6.10)$$

From Figure 6.14–Figure 6.18 it can be seen that the proposed equation captures well the typical behaviour of masonry in the pre-peak phase, while the post-peak is adequately predicted. To allow for a rigorous comparison between the experimental results and the proposed constitutive models, the mean squared error (MSE) is listed in Table 6.10, which is the average squared difference between the predicted stress and the mean stress-strain curve at each increment of strain. Accordingly, the lower the values of MSE, the better the agreement among the experiments and the predicted stress. To allow for a firm conclusion, Table 6.10 makes a division between the values of MSE calculated in the pre- and post-peak phases. In the pre-peak phase, the comparison of MSE is made only between the model by Facconi et al. (2017) and the proposed model, as the analogies between them are obvious, see Figure 6.14–Figure 6.18. The proposed model often results in lower values of MSE than does the model by Facconi et al. (2017), thus implying better agreement with the experimental results. The responses of

the different masonry types in the post-peak phase did not follow a predictable pattern. As a result, apart from the linear and parabolic curves adopted in the literature, the values of MSE are listed using an exponential equation. In some instances, the exponential equation is better fitted with the mean stress-strain curve than the linear equation, though the difference in the values of MSE are not significant. Accordingly, it is concluded that the strength degradation in the post-peak phase of the typical Dutch brick masonry types can be adequately represented by the simpler linear curve. In conclusion, the validity of the proposed formulation for predicting the uniaxial compressive response of masonry is justified, by comparing the MSE values with those obtained using the literature formulations.

Taking into account all the laboratory-made and field-extracted wallets, Figure 6.19 offers a glance at the possible variation in the value of parameter  $\alpha^3$ , defined as a function of the Young's modulus, compressive strength, and the corresponding peak strain, as calculated in Eq. (6.9). Excluding the outlier (MAT-1 CS brick masonry), the mean value remains fairly constant at 1.6. Thanks to the other experimental campaigns that were performed at Delft University of Technology (Korswagen et al., 2019; Drougkas et al., 2020), an opportunity was provided to rebuild MAT-1 CS brick masonry and MAT-3 solid clay brick masonry using the same materials, as explained in Chapter 2. For each construction phase, the mean curve was obtained by averaging the response of a minimum of five or six wallets, as shown in Figure 6.20. Moreover, a mean curve was obtained from the average of all the mean curves, as shown by the black line. In the linear range, no clear difference is noticed in the response of the CS brick masonry wallets constructed in different phases. However, a deviation in the nonlinear pre-peak response of MAT-1 CS brick wallets constructed in the first phase (presented in Chapter 2) is obvious in comparison to the other construction phases. Nevertheless, the values of compressive strength were not much affected. Accordingly, the value of  $\alpha^3$  for the first construction phase was higher than for the other phases. The workmanship quality and/or the temperature and humidity conditions are a possible explanation for the distinct response of MAT-1 CS brick masonry constructed in the first phase, as all the materials used for the construction of the wallets came from the same batch, and no variation in testing set-up or procedure occurred over time.

**Table 6.10:**

Values of mean squared error (MSE) calculated from the deviation of the analytical curve from experimental results. Minimum values of MSE are in grey.

	Masonry	Pre-peak			Post-peak			Full-curve		
		Facconi	Linear	Linear	Parabola	Expo.	Kauschik	Augenti	Facconi	Proposed
Vertical comp.	MAT-1	0.14	0.04	0.05	1.23	0.59	0.72	3.37	1.37	0.09
	MAT-2	0.04	0.02	0.43	6.37	4.18	12.38	11.02	6.30	0.45
	MAT-3	0.14	0.29	1.78	14.50	0.92	9.00	32.68	21.02	2.07
	MAT-4	0.07	0.02	0.87	12.58	0.24	4.95	9.89	12.62	0.89
	MAT-5	0.02	0.10	-	-	-	2.34	0.33	0.02	0.10
Horizontal comp.	MAT-1	0.25	0.42	0.05	2.71	0.62	6.19	4.64	2.95	0.47
	MAT-2	0.09	0.01	0.26	4.88	0.22	5.09	5.55	4.96	0.27
	MAT-3	0.01	0.04	1.51	10.08	1.61	4.48	30.09	13.43	1.55
	MAT-4	0.18	0.03	2.62	8.60	3.49	3.05	33.06	0.42	2.65
	MAT-5	0.29	0.42	-	-	-	1.25	0.30	0.29	0.42

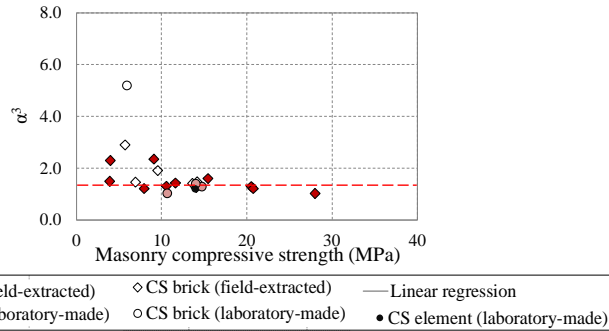


**Figure 6.19:** Variation of  $\alpha^3$  parameter with respect to the masonry compressive strength. The definition of  $\alpha$  can be found in Eq. (6.9).

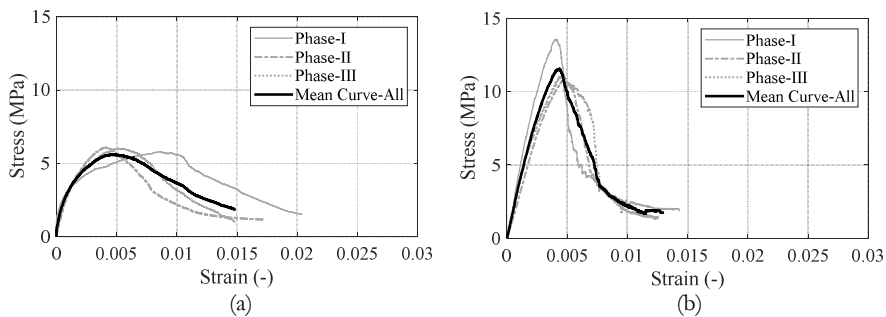


**Figure 6.20:** Mean curves of the stress-strain relationships constructed at three different phases: (a) MAT-1 CS brick masonry constructed in three different phases; (b) MAT-3 solid clay brick masonry.

## 6.2.2 Bending

Constitutive relationships under bending load are of importance to the development of analytical models for the design and analysis of URM walls subjected to out-of-plane bending loads. Such relationships are of interest, as they can be used to indirectly understand the tension response of masonry. The experimental characterisation of the post-peak softening response of masonry under bending load is a challenging task; hence, very little is known about it in the literature. In this study, efforts were made to capture the softening response of a limited number of laboratory-made wallets under bending load.

Figure 6.21–Figure 6.25 present the mean curves of the bending moment divided by the cross-sectional moment of inertia versus curvature obtained from tests on a minimum of five wallets tested under both vertical and horizontal out-of-plane bending load. The grey area indicates the lower and upper bounds. In the initial elastic phase, the slope of the mean curve reflects the Young's modulus of masonry. A comparison between the Young's modulus of masonry obtained from compression tests and bending tests on wallets is made in Figure 6.4. Beyond the elastic stage, nonlinear behaviour was observed in the further cracking of the bed joints and/or head joints. In the case of horizontal bending tests, the flexural response is governed more by the torsional behaviour of the bed joints (Willis, 2004). In the post-peak phase, any increase in the curvature can be associated with the progressive damage to the bed joints. The vertical bending can be interpreted as indirect tension, while the horizontal bending can be interpreted as indirect (torsional) shear combined with indirect tension. The (indirect) properties for bending can thus be interpreted as stemming from the underlying, more fundamental micro-properties for direct uniaxial tension and direct shear at interfaces.

In most cases, the pre-peak response of the wallets, shown in Figure 6.21–Figure 6.25, can be better fitted by a parabolic curve, rather than a linear/bilinear curve as suggested by van der Pluijm (1999). Table 6.11 lists the values of mean squared error (MSE) obtained from a comparison between the pre-peak response of the mean curve and the linear as well as the parabolic equations. In this study, the pre-peak response of MAT-5 CS element masonry with a thin joint under vertical out-of-plane bending load showed a better agreement with a linear fit than with the parabolic equation, Figure 6.25b.

The post-peak branch, though it was captured only for limited masonry types, can be approximated by an exponential curve rather than a linear equation. This conclusion was drawn by comparing the values of MSE listed in Table 6.11. The MSE values are derived by calculating the mean squared error between the experimentally characterised post-peak response of wallets and the predicted values using linear as well as exponential equations. The suitability of an exponential softening curve corresponds with the notion that bending is an indirect combination of direct tension and shear, for which an exponential curve has been observed in the literature. The proposed equation is as follows:



$$M / I = \begin{cases} \left( \frac{-E_3}{2\chi_p} \right) \chi^2 + E_3\chi & 0 < \chi < \chi_p \\ \alpha e^{-\beta\chi} & \chi_p < \chi < \chi_u \end{cases} \quad (6.11)$$

$$\text{with } \beta = \frac{\ln(M_p / M_u)}{(\chi_p - \chi_u)} \quad (6.12)$$

$$\alpha = \frac{M_p / I}{e^{-\beta\chi_p}}$$

where  $M_p$  is the bending moment at peak load,  $I$  is the moment of inertia,  $E_3$  is the Young's modulus,  $\chi_p$  is the curvature corresponding with the peak moment,  $M_u$  is the ultimate moment, and  $\chi_u$  is the curvature corresponding with the ultimate moment.

**Table 6.11:**

Values of mean squared error (MSE) calculated from the deviation of the analytical curve from the experimental results. Values are in percentage. Minimum values of MSE are in grey.

Masonry		Pre-peak		Post-peak	
		Linear	Parabola	Linear	Expo.
Vertical Bending	MAT-1	0.3	0.04	-	-
	MAT-2	0.06	0.005	-	-
	MAT-3	0.25	0.002	-	-
	MAT-4	400	192	-	-
	MAT-5	0.01	0.3	-	-
Horizontal bending	MAT-1	1.3	0.02	-	-
	MAT-2	220.8	0.63	1.22	0.08
	MAT-3	1.83	0.06	0.09	0.01
	MAT-4	5.92	0.11	0.11	0.11
	MAT-5	200	10	-	-

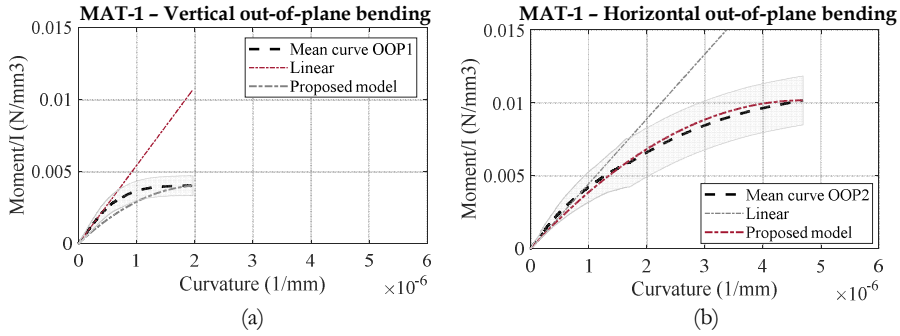


**Figure 6.21:** Comparison between constitutive laws and experimental stress-strain curves for MAT-1 CS brick masonry under: (a) vertical out-of-plane bending (OOP1); (b) and horizontal out-of-plane bending (OOP2).  $I$  is the moment of inertia.

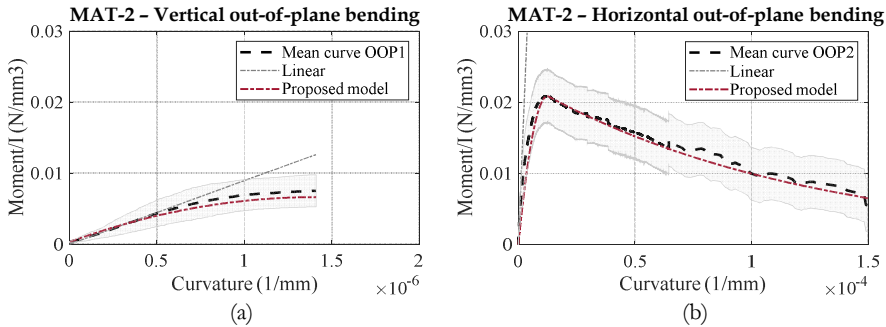


**Figure 6.22:** Comparison between constitutive laws and experimental stress-strain curves for MAT-2 perforated clay brick masonry under: (a) vertical out-of-plane bending (OOP1); (b) and horizontal out-of-plane bending (OOP2).  $I$  is the moment of inertia.

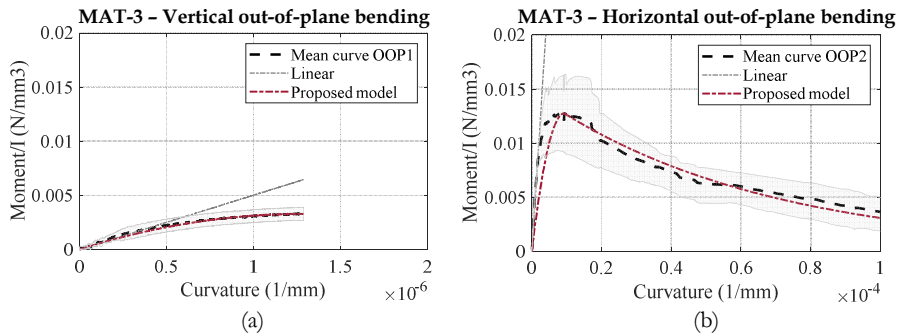


**Figure 6.23:** Comparison between constitutive laws and experimental stress-strain curves for MAT-3 solid clay brick masonry under: (a) vertical out-of-plane bending (OOP1); (b) and horizontal out-of-plane bending (OOP2).  $I$  is the moment of inertia.

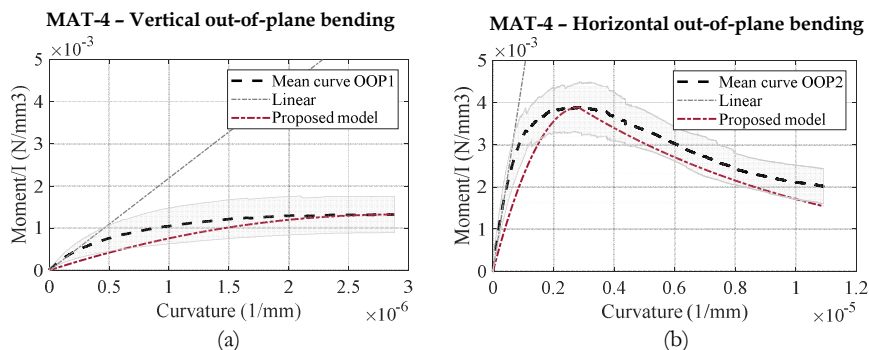


**Figure 6.24:** Comparison between constitutive laws and experimental stress-strain curves for MAT-4 double-wythe solid clay brick masonry under: (a) vertical out-of-plane bending (OOP1); (b) and horizontal out-of-plane bending (OOP2).  $I$  is the moment of inertia.

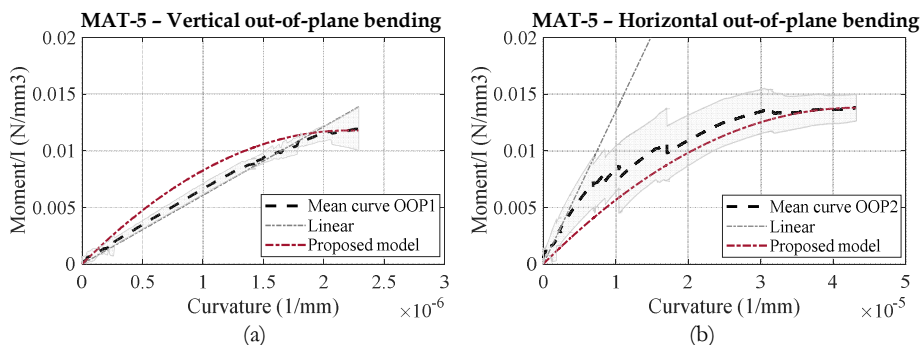


**Figure 6.25:** Comparison between constitutive laws and experimental stress-strain curves for MAT-5 CS element masonry under: (a) vertical out-of-plane bending (OOP1); (b) and horizontal out-of-plane bending (OOP2).  $I$  is the moment of inertia.

### 6.2.3 Shear

To describe the shear cracking along the masonry unit-mortar interface, the cohesion softening equation and its shape are required for numerical models. To this end, researchers such as Lourenço (1997b), van der Pluijm (1999), Augenti and Parisi (2011), and Rahman and Ueda (2013) proposed constitutive models. These models are often used by both continuum damage and brick-to-brick models. The pre-peak shear response of masonry was often approximated with a simple linear curve. However, Rahman and Ueda (2013) proposed an exponential equation, which incorporates the elastic modulus of unit and mortar, joint thickness, pre-compression stress, and the compressive strength of mortar. To describe the post-peak shear response along the brick-mortar interface, the nonlinear softening model of Hordijk (1993), widely used for concrete, was investigated by researchers such as van Zijl (1996). Moreover, Lourenço (1997b) and van der Pluijm (1999) suggested an exponential equation, and Augenti and Parisi (2011) proposed a fourth-order polynomial curve to model the shear stress-strain relationships of tuff masonry.

The applicability of the models proposed in the literature was investigated for the laboratory-made triplets by calculating the values of MSE as listed in Table 6.12. It can be concluded that neither the linear equation nor the proposed model by Rahman and Ueda (2013) can precisely describe the pre-peak shear response. However, the softening response was better captured by the exponential function suggested by Lourenço (1997b) and van der Pluijm (1999), than by the proposed model by Rahman and Ueda (2013). Accordingly, this study focuses only on developing an analytical model for the pre-peak shearing response of masonry, while the post-peak response of Dutch masonry can be defined using the exponential function proposed in literature that reads:

$$f_v = f_{v_p} \left( \frac{-f_{v_p}}{G_{f-II}} \delta \right) \quad \delta > \delta_{peak} \quad (6.13)$$

where  $f_{v_p}$  is shear strength,  $G_{f-II}$  is mode-II fracture energy, and  $\delta$  is sliding. Detailed information regarding the definition of the shear properties can be found in Chapter 2.

To capture the nonlinearity in the pre-peak shearing response of masonry, this study suggests a mixed model defined over two ranges. First, a linear branch is fitted to the experimental data which continues up to 65% of the shear strength. Second, the nonlinearity in the ascending branch is then described with a natural logarithmic function. The proposed equation is as follows:

$$f_v = \begin{cases} \frac{G_3}{t} \delta & 0 < \delta < 0.65 \frac{f_{vp} t}{G_3} \\ \alpha \ln(\delta) + \beta_v & 0.65 \frac{f_{vp} t}{G_3} < \delta < \delta_{peak} \end{cases} \quad (6.14)$$

$$\begin{aligned} \text{with } \gamma &= \frac{\ln(0.65 \frac{f_{vp} t}{G_3})}{\ln(\delta_{peak})} \\ \beta_v &= \frac{f_{vp} (0.65 - \gamma)}{(1 - \gamma)} \\ \alpha &= \frac{(f_{vp} - \beta_v)}{\ln(\delta_{peak})} \end{aligned} \quad (6.15)$$

where  $\delta_{peak}$  is the shear sliding corresponding with the shear strength,  $G_3$  is the mortar shear modulus, and  $t$  is the joint thickness.

An acceptable agreement between the proposed model and the pre- and post-peak shearing response of triplets is observed, see Figure 6.26–Figure 6.28. Moreover, the MSE values reported in Table 6.12 confirmed the suitability of the proposed model. As mentioned earlier, the proposed model incorporates the mortar shear modulus,  $G_3$ , shear strength,  $f_{vp}$ , and the corresponding value of sliding,  $\delta_{peak}$ . An attempt was made to minimise the number of input parameters by establishing a correlation between shear strength and the values of sliding at peak stress. However, due to the limited number of samples and a wide scattering of the experimental results, no clear trend was evident.

**Table 6.12:**

Values of mean squared error (MSE) calculated from the deviation of the analytical curve from the experimental results. The values are in percentage. Minimum values are in grey.

Masonry	Pre-Comp.	Pre-peak			Post-peak		Full-curve	
		MPa	Rahman	Linear	Log.	Rahman	Expo.	Rahman
MAT-1	0.20	0.63	4.45	0.02	0.92	0.02	1.54	0.04
	0.60	0.66	6952	0.01	5.98	0.001	6.64	0.01
	1.00	1.92	43444	0.13	9.18	0.01	11.10	0.13
MAT-2	0.20	0.63	4124	0.01	3.53	0.15	4.17	0.17
	0.60	2.78	38798	0.03	11.09	0.04	13.87	0.07
	1.00	8.58	506	0.11	6.25	0.03	14.83	0.14
MAT-3	0.20	0.34	1658	0.04	2.83	0.01	3.17	0.05
	0.60	2.33	542	0.02	8.29	0.09	10.62	0.11
	1.00	2.37	2012	0.31	3.75	0.21	3.75	0.52

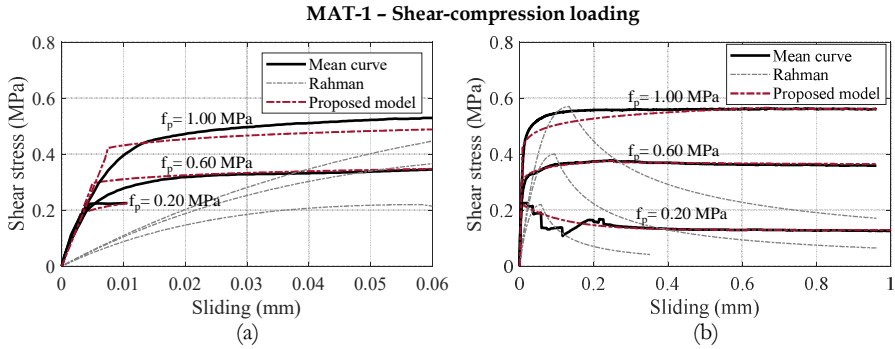


**Figure 6.26:** Comparison between analytical models and the shear stress-sliding relationships from tests on MAT-1 CS brick masonry: (a) pre-peak branch, (b) full response.

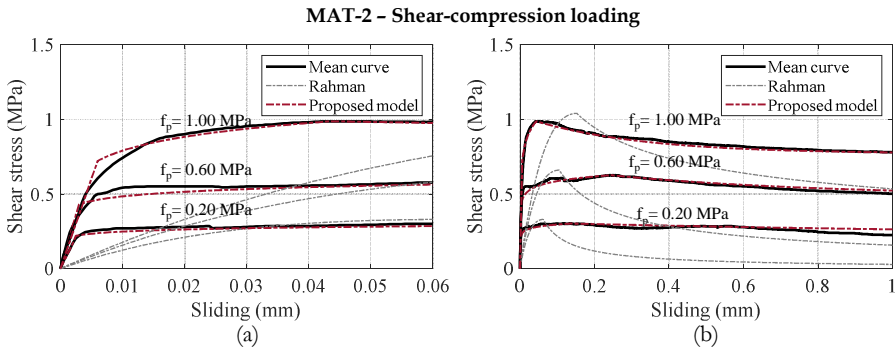


**Figure 6.27:** Comparison between analytical models and the shear stress-sliding relationships from tests on MAT-2 perforated clay brick masonry: (a) pre-peak branch, (b) full response.

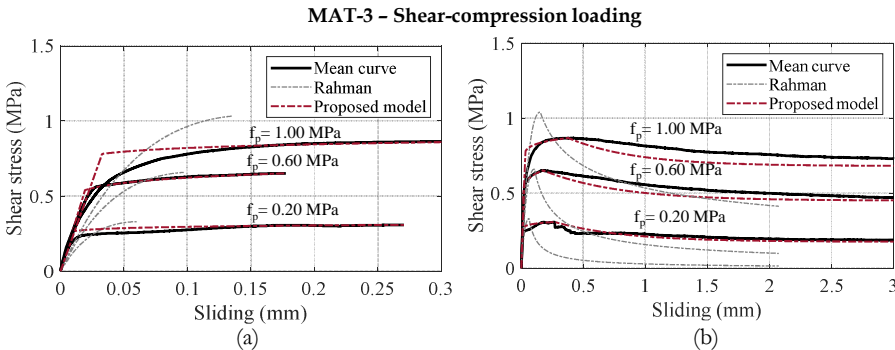


**Figure 6.28:** Comparison between analytical models and the shear stress-sliding relationships from tests on MAT-3 solid clay brick masonry: (a) pre-peak branch, (b) full response.

### 6.3 CONCLUDING REMARKS

Based on the correlations between material parameters from Sections 6.1 and on the stress-strain functions from Section 6.2, this section formulates a strategy for material characterisation of existing masonry, integrating the material properties obtained in Chapter 2 and Chapter 3 from laboratory tests on medium-sized specimens, representing typical Dutch masonry.

As mentioned in previous chapters, the direct evaluation of the material properties of existing brick masonry structures can be achieved either by means of invasive or semi-invasive testing methods. Such a division in the testing methods is made based on the extent of damage caused to the wall integrity. As a result, laboratory testing methods which require the extraction of medium-sized samples as well as invasive in-situ tests, such as the in-place diagonal compression test, belong to the category of invasive testing methods. By contrast, the extraction of small-diameter cores or performing double flat-jack and shove tests, which induce minor and easy-to-repair damage to the walls, are considered semi-invasive testing methods. In the interest of minimising the extent of damage to existing masonry structures, semi-invasive testing methods are gaining more ground. In this context, the direct evaluation of compression properties of masonry in terms of Young's modulus and compressive strength is possible by performing in-situ double flat-jack tests as well as by compressing small-diameter cores in the laboratories. Moreover, the direct estimation of shear properties along the brick-mortar interface in terms of cohesion and friction coefficient is feasible by conducting laboratory shear-sliding tests on small-diameter cores as well as in-situ shove tests. However, insights into toughness, bending and tensile properties can be gained only by performing laboratory tests on extracted samples.

To support indirect evaluations of material properties of existing brick masonry, and thus minimise the burden associated with performing complex and invasive experimental studies, this chapter has explored the statistical relationships between different material properties. This is mainly achieved in light of the rich database established from tests on field-extracted and laboratory-made masonry specimens. To predict the relationship between the two variables, a linear regression analysis, often forced to pass through the origin, was conducted. To quantify the accuracy of the relationships, values of the correlation of determination ( $R^2$ ) were also presented.

Table 6.13 offers recommendations for directly/indirectly deriving the material properties of existing masonry. To this end, first, direct insight into the material properties can be obtained by performing a limited number of tests as follows: (i) direct evaluation of the compression and shear properties of masonry in terms of strength and stiffness either using conventional semi-invasive testing methods or tests on small-diameter cores; (ii) bond wrench tests to find the bond strength; (iii) laboratory compression tests on intact bricks that remain from bond wrench tests. Second, other properties can be indirectly evaluated using expressions found in Section 6.1 or established in the literature. Note that the recommendations on the tensile properties of masonry

are mainly extracted from the literature data, given that tensile tests were not performed in this study. Accordingly, an acceptable level of knowledge on material properties can be obtained by performing a limited number of tests, thus minimising the number and the extent of invasiveness.



**Table 6.13:**

Recommendations to define input parameters for structural analysis based on correlation studies found from laboratory tests on limited number of specimens. These recommendations have been validated mainly for typical single-wythe Dutch masonry.

Properties	Sym.	Unit	Recommendation
<b>Masonry properties</b>			
Vertical compressive strength	$f_m$	MPa	Direct tests or indirectly derived as recommended in Eurocode 6 using compressive strength of brick and mortar.
Vertical Young's modulus	$E_3$	MPa	$E_3 = (500 - 700) f_m'$
Horizontal compressive strength	$f_{m,h}$	MPa	$f_{m,h}' = (0.70 - 0.80) f_m'$
Horizontal Young's modulus	$E_{3,h}$	MPa	$E_{3,h} = 0.70 E_3$
Vertical flexural strength	$f_{x1}$	MPa	$f_{x1} = f_w$
Horizontal flexural strength	$f_{x2}$	MPa	$f_{x2} = 3 f_w$ $f_{x2} = 1.3 f_w$
Tensile strength	$f_{t1}$	MPa	$f_{t1} = 0.8 f_w$
Fracture energy in vertical compression	$G_{f-c}$	N/mm	$G_{f-c} = (0.88 - 5.3) f_m'$
Fracture energy in horizontal compression	$G_{f-c,h}$	N/mm	$G_{f-c,h} = G_{f-c}$
<b>Mortar and brick properties</b>			
Mortar compressive strength	$f_m$	MPa	$f_m = f_w / 0.036$
Mortar Young's modulus <sup>1</sup>	$E_{3m}$	MPa	$E_{3m} = (200 - 240) f_m$
Mortar tensile strength <sup>2</sup>	$f_{tm}$	MPa	$f_{tm} = (0.15 - 0.32) f_m$
Mortar fracture energy in tension <sup>3</sup>	$G_{f-tm}$	N/mm	$G_{f-tm} = 0.025 (f_m / 10)^{0.7}$
Brick compressive strength	$f_b$	MPa	Direct test
Brick Young's modulus <sup>4</sup>	$E_{3b}$	MPa	$E_{3b} = (300 - 430) f_b$
Brick tensile strength <sup>5</sup>	$f_{tb}$	MPa	$f_{tb} = (0.04 - 0.07) f_b$
Brick fracture energy in tension <sup>6</sup>	$G_{f-tb}$	N/mm	$G_{f-tb} = 0.038 f_{tb}$
<b>Interface properties</b>			
Bond strength	$f_w$	MPa	Direct test
Initial shear strength/cohesion	$f_{t0}$	MPa	Direct test
Initial friction coefficient	$\mu$	-	Direct test
Fracture energy in tension <sup>7</sup>	$G_{f-I}$	N/mm	$G_{f-I} = 0.16 f_{t1}$
Fracture energy in shear <sup>8</sup>	$G_{f-II}$	N/mm	$G_{f-II} = 10 G_{f-I}$

<sup>1</sup> Based on studies from Vermeltoort (2005) and Kaushik et al. (2007).

<sup>2</sup> Based on studies from Rots, van der Pluijm, Vermeltoort et al. (1997) and Barattucci et al. (2020). Note that in the lack of experimental results the tensile strength of mortar assumed to be the same as its flexural strength.

<sup>3</sup> Expression is extracted from Model Code 90 for concrete.

<sup>4</sup> Based on studies from Rots, van der Pluijm, Vermeltoort et al. (1997), Vermeltoort (2005), and Kaushik et al. (2007).

<sup>5</sup> Based on studies from Rots, van der Pluijm, Vermeltoort et al. (1997).

<sup>6,7</sup> Based on study from van der Pluijm (1999).

<sup>8</sup> Based on studies from Nazief (2014) and De Villiers (2019).

Apart from the material parameters, this study has also provided stress-strain functions for compression, bending, and shear loading, for the five different masonry types.

For *compression loading*, a multi-polynomial model was introduced which could accurately capture both the pre- and post-peak response of masonry under two different loading directions, perpendicular and parallel to the bed joints. The pre-peak compressive branch was approximated with a cubic curve followed by a parabolic curve, while the softening branch was fitted with a linear curve.

Concerning the *bending response* of masonry, the pre-peak branch of the wallets tested under out-of-plane bending loads can be fitted by a parabolic curve. The post-peak branch for bending, though it was captured for a limited number of samples, can be approximated by an exponential curve.

As for the *shear response* of masonry, the pre-peak response was defined over two shear-sliding ranges, aiming to better capture the nonlinearity caused by cracking along the interface. First, a linear branch was fitted to the experimental data, which continued up to 65% of the shear strength. Second, the nonlinearity in the ascending branch was described with a natural logarithmic function. The shearing post-peak response was well represented by an exponential equation.

## CONCLUSIONS

---

Understanding the response of unreinforced masonry (URM) structures functioning as a holistic system requires in-depth insight into the mechanical characteristics of the masonry, its constituents, and their interaction under compression, tension, and shear loading. Such characterisation of masonry is a challenging task because of the inherent diversity of masonry types, the variability due to workmanship, the often limited possibility of disturbing the integrity of the structure through testing activities, and the dependency of strength, stiffness and toughness on the loading direction due to the orthotropic nature of masonry. This thesis presented an integrative approach to help practitioners navigate the decision-making process by prioritising the type of tests and optimising the identification of input parameters for structural assessment.

The main objective of this study was to provide input parameters with a distinct level of refinement for use in the numerical and analytical assessment methods of existing URM structures. To this end, an experimental approach was followed, using both field-extracted and laboratory-made masonry samples. The focus was on Dutch unreinforced masonry dwellings with a view to induced seismicity in the Groningen area, but also to other actions like climate induced settlements. As a result, for the five most typical Dutch masonry types, the entire set of specimens required to characterise compression, bending and shear behaviour of masonry was replicated in the laboratory. Moreover, samples were extracted from fifteen different unreinforced masonry dwellings and schools in the Groningen region, built between 1910 and 2010, and then packed and transported to the laboratories. The studied masonry types in this research included both brick masonries with conventional joints (such as single-wythe solid clay brick masonry, double-wythe solid clay brick masonry, single-wythe perforated clay brick masonry, and single-wythe calcium silicate brick masonry), and large element masonry with thin-layer joints (such as single-wythe calcium-silicate element masonry).

In this chapter, the findings of this study are reflected. The conclusions are articulated in Section 7.1, while Section 7.2 suggests avenues for further research.

## 7.1 SUMMARY OF MAIN RESEARCH FINDINGS

Although the aim of this research stems from a need to expand the knowledge on the material properties of masonry in the Netherlands, a series of how-to questions, presented in Chapter 1, signified at least one main quest at the international masonry research community level: to provide input parameters for the analysis methods for the structural assessment of existing URM structures. To this end, the study included two different testing programmes, whereby medium-sized samples in both wallet and triplet configurations (Chapter 2 and Chapter 3) as well as small-diameter cores (Chapter 4 and Chapter 5) were used. Both testing programmes were conducted on field-extracted as well as laboratory-made specimens. The construction of samples in the laboratory allowed for the replication of the entire set of samples to provide comprehensive insight into the behaviour of masonry for a statistically sufficient number of samples.

Chapter 2 and Chapter 3 improved the understanding of the behaviour of different masonry types pertaining to strength, stiffness, and toughness under different stress-states. This was achieved by: 1) compressing wallets in two directions<sup>1</sup>, 2) bending wallets over three configurations<sup>2</sup>, and 3) subjecting the brick-mortar interface of triplets to shear-compression loading. Chapter 2 exhaustively discussed the complete nonlinear response of the five different laboratory-made masonry types, while Chapter 3 focused on the statistical analysis and inter-building variability of material properties compiled from tests on a wide range of field-extracted masonry types. The systematic testing campaign on medium-sized laboratory-made (Chapter 2) and field-extracted (Chapter 3) masonry specimens were complimentary and supported the broader conclusions as follows:

- i. *Characterising the complete nonlinear response and the crack evolutions of five different masonry types under compressive, bending, and shear loading, thus providing a groundwork for development and validation of models for structural analyses.* The compression and bending properties of masonry, provided in terms of stiffness, strength, and toughness, as well as the crack evolutions, turned out to be affected not only by the mechanical properties of units and mortar, but also by the loading direction, surface characteristics of units, joint thickness, and number of wythes. In a similar way, the shear properties of masonry in terms of strength and stiffness were affected by the mortar compressive strength and the surface characteristics

---

<sup>1</sup> Uniaxial compressive tests were performed along two directions: perpendicular and parallel to the bed joints, denoted as vertical and horizontal configurations, respectively.

<sup>2</sup> Four-point bending tests were performed along three directions: four-point bending with the moment vector parallel to the bed joints and in the plane of the wall, which generated a plane of failure parallel to the bed joints and was denoted as vertical out-of-plane bending; four-point bending with the moment vector orthogonal to the bed joints and in the plane of the wall, which generated a plane of failure perpendicular to the bed joints and was denoted as horizontal out-of-plane bending; and four-point bending with the moment vector orthogonal to the plane of the wall, denoted as in-plane bending.

of the units. However, the toughness, expressed in terms of mode-II fracture energy, proved to also be dependent on the pre-compression stress applied at the interface.

- The orthotropic behaviour of masonry under compression and bending is certainly not limited to strength but can be extended to other properties, such as stiffness and toughness. Table 7.1 lists the mean values of the orthotropic ratio in terms of strength, stiffness, and toughness under compression and four-point out-of-plane bending. Moreover, as expected, the loading direction affected the formation of cracks and their subsequent propagation, which was discussed in Chapter 2.

**Table 7.1:**

Overview of the average orthotropic ratio for compression and bending properties of masonry wallets. Values in parentheses are the number of investigated masonry types.

Orthotropic ratio (horizontal to vertical properties)	Clay brick masonry	CS brick masonry	CS element masonry
Compressive strength	0.68 (5)	0.76 (5)	0.69 (1)
Young's modulus	0.65 (4)	0.66 (5)	0.69 (1)
Strain at peak	1.30 (4)	0.82 (5)	0.81 (1)
Compressive fracture energy	0.97 (4)	0.97 (4)	-
Flexural strength	3.14 (5)	3.19 (2)	1.26 (1)
Tensile strength (derived)	3.35 (4)	1.57 (3)	0.82 (1)
Fracture energy in bending	6.11 (3)	-	1.87 (1)

- The effect of surface characteristics of the units can be demonstrated by analysing the response of perforated clay brick masonry. It was found that the presence of holes in perforated clay brick masonry reduced the strength and toughness under horizontal compression loading, since it triggered vertical cracks parallel to the loading direction, localised in the vicinity of the holes. By contrast, the presence of holes under bending load accounted for the dowel action effect from bed joint mortar that had partially flowed into the holes; thus the highest values of flexural strength for brick masonry belonged to the wallets made out of perforated clay bricks. However, no significant difference in the values of cohesion and bond strength of perforated clay brick masonry with respect to solid clay brick masonry was found.
- To investigate the effect of number of wythes on compression and bending properties, both laboratory-made single- and double-wythe solid clay brick masonry wallets were tested. Generally, the compression properties of double-wythe wallets were lower as compared to those for single-wythe masonry; however, the influence of the size effect in terms of the height to thickness ratio should not be ruled out. Regarding the bending properties, both single and double wythe masonry were found to have similar values of vertical flexural strength and in-plane flexural strength, thus indicating no influence of the wythe number or size effect, while the horizontal flexural strength of the single-wythe wallets was 1.6 times higher than that of the double-wythe wallets.

- Regarding the influence of thin joint glued mortar, it was found that CS element masonry with thin-layer joints behaved more as a homogeneous continuum rather than an ordered discontinuum. Thus, the compression and bending properties of CS element masonry with thin-layer joints were often less affected as the loading direction was changed. As an example, for CS element masonry wallets the orthotropic ratio for bending strength (determined as a ratio between the horizontal flexural strength and the vertical flexural strength) stands at 1.2, while for brick masonry a higher orthotropic ratio was found, ranging from 2.2 to 4.0, with an average ratio of 3.
- ii. *Providing a comprehensive database of material properties, which can be applied not only towards the assessment of URM buildings in the Netherlands but also for like masonry in other countries with similar construction methods (e.g., in Belgium).* The work herein has contributed to filling and underpinning a database that accounts for divisions based on the unit types, clay and calcium silicate units, and the year of construction of clay bricks, pre- and post-Second World War periods. The database, reported in Table 7.2. supported the formulation of the table of material properties originally presented in NEN NPR 9998:2015 and partially updated in the subsequent versions (the current version being NEN NPR 9998+C1:2020). The code-based properties have been chosen with a reasonable degree of conservatism as compared to the test results.

**Table 7.2:**

Overview of mean values of experimentally determined material properties of field-extracted samples, including coefficient of variation, and number of tests.

Material property	Sym.	Unit	Clay brick masonry						CS brick masonry		
			Pre-1945			Post-1945			Avg.	C.o.V.	No.
			Avg.	C.o.V.	No.	Avg.	C.o.V.	No.			
Normalised compressive strength of brick	$f_b$	MPa	19.40	0.32	23	23.25	0.53	30	15.26	0.25	28
Flexural strength of brick	$f_{bb}$	MPa	6.12	0.16	42	4.38	0.38	46	4.19	0.35	59
Vertical compressive strength	$f'_m$	MPa	9.98	0.51	55	15.02	0.38	24	9.74	0.33	8
Vertical Young's modulus	$E_3$	MPa	5346	0.60	14	7354	0.54	42	6904	0.33	25
Vertical compressive fracture energy	$G_{fc}$	N/mm	11.93	0.54	14	20.58	0.48	42	17.41	0.48	25
Horizontal compressive strength	$f'_{m,b}$	MPa	10.86	0.11	2	11.00	0.23	6	6.17	0.23	11
Horizontal Young's modulus	$E_{3,b}$	MPa	8933	0.26	2	5470	0.10	6	4177	0.36	11
Horizontal compressive fracture energy	$G_{fc,b}$	N/mm	30.84	-	1	63.10	0.20	6	19.97	0.25	11
Vertical flexural strength	$f_{s1}$	MPa	-	-	-	0.43	0.34	6	0.13	0.96	3
Horizontal flexural strength	$f_{s2}$	MPa	0.62	0.62	21	1.23	0.31	19	0.59	-	1
In-plane flexural strength	$f_{s3}$	MPa	0.75	0.51	37	0.65	0.55	22	0.47	0.62	12
Bond strength	$f_w$	MPa	0.11	1.56	124	0.29	0.96	91	0.14	1.17	23
Cohesion (initial shear strength)	$f_{i0}$	MPa	0.31	0.30	72	0.47	0.46	64	0.26	0.67	56
Friction coefficient	$\mu$	-	0.73	0.13		0.76	0.29		0.77	0.23	

iii. *Providing knowledge on the variability of material properties of field-extracted masonry, thus offering a further step towards the probabilistic analysis of existing masonry structures.*

- The inter-building (between-building) variability of different material properties was described using normal, Weibull, lognormal and exponential distribution functions, as listed in Table 7.3. It was concluded that normal and Weibull functions better represent the distributions of vertical and horizontal compressive strength, horizontal and in-plane flexural strength, and values of cohesion, while the log-normal distribution is more suitable in the case of vertical and horizontal Young's modulus, vertical and horizontal compressive fracture energy, vertical flexural strength, and friction coefficient. For the values of bond strength, an exponential function gave a better fit.
- The intra-building (within-building) variability of material properties, represented by the coefficient of variation, was lower for compression properties than for bending properties. For compression properties, the intra-building coefficient of variation ranged from 3% to 54%, while for the bending properties, particularly for bond strength, the upper range was much higher, even reaching 92%. Accordingly, the sensitivity analysis of bond strength is recommended when it comes to the structural assessment of existing URM structures.

**Table 7.3:**

Statistical distribution function to capture the inter-building variability of material properties in existing structures.

Properties	No. masonry types	Distribution function			
		Normal	Weibull	Log-normal	Expo.
Vertical compressive strength	87	•	•		
Horizontal compressive strength	9	•	•		
Vertical Young's modulus	21			•	
Horizontal Young's modulus	6			•	
Vertical comp. fracture energy	21			•	
Horizontal comp. fracture energy	6			•	
Vertical flexural strength	4			•	
Horizontal flexural strength	10	•	•		
In-plane flexural strength	14	•	•		
Bond strength	72				•
Cohesion	21	•			
Friction coefficient	21			•	



Chapter 4 and Chapter 5 investigated the suitability of tests on small-diameter cores as a quick and efficient alternative to laboratory testing methods that demand the extraction of wallets/triplets, and to semi-invasive in-situ flat-jack based testing methods that aim to understand the pre-peak stage but show restrictions when it comes to the peak and post-peak characterisation of the masonry response. To this end, a comparative experimental study was conducted, including tests on small-diameter cores as well as conventional laboratory tests on companion specimens. Chapter 4 discussed the compression properties of masonry obtained from compressing two different core geometries: cores 150 mm in diameter and smaller cores 100 mm in diameter. Prior to compressing the cores, they were capped on the top and bottom faces using high strength mortar. Chapter 5 dealt with the characterisation of shear properties along the brick-mortar interface using small-diameter cores. To this end, cores with a diameter of 100 mm and composed of a single bed joint were rotated with respect to their original horizontal position and subsequently subjected to vertical line load along their thickness, similar to a Brazilian splitting test. The tests were carried out at different inclination angles of 45°, 50°, and 55°, thus inducing various combinations of shear-compression stress states along the brick-mortar interface. The following conclusions were drawn from performing compression as well as shear-sliding tests on cores extracted from seven different masonry types, both laboratory-made and field-extracted:

- i. Introducing compression tests on small-diameter cores as a favourable method for in-situ characterisation of single-wythe masonry with statistically accurate estimations of compressive strength and Young's modulus.* Owing to the displacement-controlled testing set-up, the full response of the masonry cores was captured. This study showed no influence due to the core size; thus the use of 100 mm rather than 150 mm diameter cores was preferable, as the damage caused by extraction is lower and can be easily repaired. Considering a relatively large dataset of laboratory-made and field-extracted specimens, a 1:1 correlation with standard tests on medium-sized specimens (i.e. wallets) was established in terms of compressive strength and Young's modulus. At this juncture, the values of peak strain and compressive fracture energy determined from tests on cores should be treated carefully. An underestimation of the compressive fracture energy and overestimation of peak strain was observed with respect to wallet tests, which can be attributed to the different boundary conditions.
- ii. Introducing shear tests on small-diameter cores as a reliable and comprehensive alternative to conventional in-situ shear tests with statistically accurate estimations of cohesion, friction coefficient, and shear modulus of mortar joint.* Unlike previous research, this study also used a sliding-controlled set-up to characterise the post-peak softening behaviour, a novel aspect compared to previous studies. Consequently, a more complete description of the nonlinear shear-sliding behaviour along the brick-mortar interface was provided in terms of cohesion, friction coefficient, and shear modulus of the mortar joint, as well as some insight into shear softening and thus energy dissipation. As derived from a correlation study on nine different masonry objects, including data from the literature, the cohesion of the triplets was found to be 0.88 times lower than that of the cores, with a strong

correlation ( $R^2=0.81$ ). The friction coefficient of the triplets was found to be 0.96 times lower than that of the cores, with a moderate correlation ( $R^2=0.62$ ). The ratio between the shear modulus of the triplets and that of the cores, evaluated at a stress level corresponding to 1/3 of the maximum shear stress, ranged from 1.1 to 1.3, although this comparison was only possible for two masonry objects. This study also provided a comparison of core and triplet tests in terms of mode-II fracture energy. In both tests, the energy dissipation is governed by fracture and friction mechanisms. To consider only the cohesive contribution associated with fracture, the cohesive stress was calculated by excluding the stress associated with friction, determined as the product of the normal stress and the friction coefficient. The fracture energy was then calculated as the area under the cohesive shear stress-sliding curve. Unlike the triplets, the cores did not show much variation in the values of fracture energy with normal stress. The difference between the cores and the triplets in terms of mode-II fracture energy and the dependency of the mode-II fracture energy of the triplets on the pre-compression stress raises some doubt about this parameter as an independent material property.

*iii. Extrapolating the applicability of the core testing method to both clay and calcium silicate brick masonry types extracted from existing URM buildings.* It was observed that the reliability and the variability of the experimental results were not influenced by the brick types (i.e. clay or CS brick masonry) or construction types (i.e. laboratory-made or field-extracted).

Considering the pool of experimental data obtained from tests on wallets and triplets using laboratory-made (Chapter 2) and field-extracted (Chapter 3) masonry types, Chapter 6 conducted a correlation study to investigate the presence of statistical associations between different material properties. The aim was to minimise the burden associated with performing complex and invasive experimental studies. Although Chapter 6 included comparisons with other correlation rules from the literature, these were not incorporated into the correlation study, as specimens' dimensions and testing conditions, i.e. boundary conditions and loading rate, could differ. In addition, this chapter supported the definition of constitutive laws under compression, bending, and shear loading. The main conclusions of Chapter 6 were as follows:

*i. Developing a coherent strategy for material characterisation in support of assessment of existing structures.* From the correlation study, intriguing trends were observed between different material properties. Table 7.4 summarises the recommendations to indirectly derive elastic and toughness properties as a function of strength properties; in the absence or lack of data, expressions were borrowed from the literature. Note that these recommendations have been validated mainly for typical single-wythe Dutch masonry.

*ii. Formulating constitutive stress-strain curves under compression, bending, and shear loading, which can be adopted to formulate or validate models for structural analyses.* The constitutive laws were calibrated for five different masonry types under vertical and horizontal compression, vertical and horizontal out-of-plane bending, and shear loading. The proposed compressive stress-strain model was a three-staged envelope curve consisting of two nonlinear pre-peak branches, and one post-peak softening branch. The pre-peak part was defined by a third-order curve followed by a second order curve until the peak stress was attained. The post-peak part was idealised by a linear curve. With respect to the literature, the proposed model can better represent the pre-peak nonlinearities under both vertical and horizontal compressive loading. The stress-strain relationship established under compression loading was already incorporated into the formulation of the Engineering Masonry Model, which is a continuum-based model, available in the software package DIANA FEA BV since 2016. The proposed bending stress-strain model was defined as a parabolic curve in the pre-peak phase, rather than a linear/bilinear curve as in the literature, and an exponential curve in the post-peak phase. The proposed shear stress-sliding curve in the pre-peak phase was a mixed model defined over two ranges to better capture the nonlinearities. First, a linear branch was fitted to the experimental data, which continued up to 65% of the shear strength. Second, the nonlinearity in the ascending branch was described with a natural logarithmic function. The softening response was well captured by an exponential function, as already suggested in the literature.

**Table 7.4:**

Recommendations to define input parameters for structural analysis based on correlation studies found from laboratory tests on limited number of specimens. These recommendations have been validated mainly for typical single-wythe Dutch masonry.

Properties	Sym.	Unit	Recommendation	
<b>Masonry properties</b>				
Vertical compressive strength	$f_m$	MPa	Direct tests or indirectly derived as recommended in Eurocode 6 using compressive strength of brick and mortar.	
Vertical Young's modulus	$E_3$	MPa	$E_3 = (500 - 700) f_m'$	Masonry with conventional joint & Masonry with thin joint
Horizontal compressive strength	$f_{m,h}$	MPa	$f_{m,h}' = (0.70 - 0.80) f_m'$	Masonry with conventional joint & Masonry with thin joint
Horizontal Young's modulus	$E_{3,b}$	MPa	$E_{3,b} = 0.70 E_3$	Masonry with conventional joint & Masonry with thin joint
Vertical flexural strength	$f_{x1}$	MPa	$f_{x1} = f_w$	Masonry with conventional joint & Masonry with thin joint
Horizontal flexural strength	$f_{x2}$	MPa	$f_{x2} = 3 f_w$	Masonry with conventional joint
			$f_{x2} = 1.3 f_w$	Masonry with thin joint
Tensile strength	$f_{t1}$	MPa	$f_{t1} = 0.8 f_w$	Masonry with conventional joint & Masonry with thin joint
Fracture energy in vertical compression	$G_{f-c}$	N/mm	$G_{f-c} = (0.88 - 5.3) f_m'$	Masonry with conventional joint
Fracture energy in horizontal compression	$G_{f-c,h}$	N/mm	$G_{f-c,h} = G_{f-c}$	Masonry with conventional joint
<b>Mortar and brick properties</b>				
Mortar compressive strength	$f_m$	MPa	$f_m = f_w / 0.036$	
Mortar Young's modulus <sup>1</sup>	$E_{3m}$	MPa	$E_{3m} = (200 - 240) f_m$	
Mortar tensile strength <sup>2</sup>	$f_{tm}$	MPa	$f_{tm} = (0.15 - 0.32) f_m$	
Mortar fracture energy in tension <sup>3</sup>	$G_{f-tm}$	N/mm	$G_{f-tm} = 0.025 (f_m / 10)^{0.7}$	
Brick compressive strength	$f_b$	MPa	Direct test	
Brick Young's modulus <sup>4</sup>	$E_{3b}$	MPa	$E_{3b} = (300 - 430) f_b$	
Brick tensile strength <sup>5</sup>	$f_{tb}$	MPa	$f_{tb} = (0.04 - 0.07) f_b$	
Brick fracture energy in tension <sup>6</sup>	$G_{f-tb}$	N/mm	$G_{f-tb} = 0.038 f_{tb}$	
<b>Interface properties</b>				
Bond strength	$f_w$	MPa	Direct test	
Initial shear strength/cohesion	$f_{f0}$	MPa	Direct test	
Initial friction coefficient	$\mu$	-	Direct test	
Fracture energy in tension <sup>7</sup>	$G_{f-I}$	N/mm	$G_{f-I} = 0.16 f_{t1}$	
Fracture energy in shear <sup>8</sup>	$G_{f-II}$	N/mm	$G_{f-II} = 10 G_{f-I}$	

<sup>1</sup> Based on studies from Vermeltoort (2005) and Kaushik et al. (2007).

<sup>2</sup> Based on studies from Rots, van der Pluijm, Vermeltoort et al. (1997) and Barattucci et al. (2020). Note that in the lack of experimental results the tensile strength of mortar assumed to be the same as its flexural strength.

<sup>3</sup> Expression is extracted from Model Code 90 for concrete.

<sup>4</sup> Based on studies from Rots, van der Pluijm, Vermeltoort et al. (1997), Vermeltoort (2005), and Kaushik et al. (2007).

<sup>5</sup> Based on studies from Rots, van der Pluijm, Vermeltoort et al. (1997).

<sup>6,7</sup> Based on study from van der Pluijm (1999).

<sup>8</sup> Based on studies from Nazief (2014) and De Villiers (2019).

## 7.2 RECOMMENDATIONS FOR FUTURE RESEARCH

The following topics require further research attention:

- *Experimental characterisation of masonry under cyclic loading, both in the pre- and post-peak phases under compression, bending, and shear loading.* Even though no significant difference in the stiffness and strength of masonry under monotonic and cyclic compressive load was noticed in Chapter 2, further research could enhance the pool of experimental data on the cyclic behaviour of masonry. This would support the characterisation of the unloading/reloading hysteresis loops in constitutive models, in addition to the characterisation of pre- and post-peak loading stages as focused upon in this thesis.
- *Experimental and numerical investigations to evaluate the potential of different shear testing set-ups for capturing the toughness of large element masonry with thin-layer joints.* Chapter 2 revealed that the unsymmetrical configuration of the calcium silicate element masonry couplet, suggested in EN 1052-3(CEN 2005), negatively influenced the flow of the load path and thus hindered recording the post-peak response of couplets under shear-compression loading.
- *Systematic laboratory testing to incorporate intra-wall spatial variability of material properties in existing masonry structures.* This research investigated the intra- and inter-building variability of material properties. However, a lack of information regarding the sampling locations hindered further analysis of the variability in material properties.
- *Systematic laboratory and numerical investigations focussing on the influence of boundary conditions and size effect on the strength, stiffness, and toughness under compressive, bending, and shear loading.* Although comparing the strength and stiffness of the small-diameter cores with those of the wallets/triplets revealed no evidence of the influence of the boundary conditions and size effect, further studies, both experimentally and numerically, are suggested with particular attention paid to addressing their effects on the toughness.
- *Expanding the pool of experimental data to gain insights into the softening response of masonry under bending load.* To capture the post-peak softening response of masonry under bending load, a crack-controlled set-up was found to be a better alternative to a displacement-controlled set-up. Nevertheless, further experimental studies are suggested, which could allow for formulating the post-peak phase of the constitutive functions as well as enriching the database, and thus the correlation study.
- *Experimental and numerical investigation of the influence of cap stiffness and cap geometry on the compression properties and failure mode of small-diameter cores.* In this study, the stiffness of the capping mortar was much higher than the one for masonry, thus restraining the lateral deformation of the masonry and potentially being responsible for an underestimation of the compressive fracture energy. Consequently, exploring the influence of other capping materials on the estimation of compression properties of masonry, particularly

toughness, is of interest.

- *Extension of experimental studies to investigate the influence of wythe number on the compression properties of small-diameter cores.* The current research proved the suitability of the core testing method for single-wythe masonry; however, further research is required to characterise the compression properties of multi-wythe masonry.
- *Further experimental investigations on the post-peak response of small-diameter cores under shear-sliding load.* In this study, the potential of the core testing method for evaluating the post-peak softening was exploited for only one masonry type. Thus, further research could allow the drawing of further conclusions for other masonry types.
- *Additional research to dissolve the doubt over mode-II fracture as an independent material property.* The comparison between the toughness measured from shear-sliding tests on small-diameter cores and from triplet tests, quantified in terms of mode-II fracture energy, as well as the dependency of mode-II fracture on the pre-compression stress, points to a new research direction.
- *Further experimental investigations to clarify the difference between the values of Young's modulus of masonry obtained under compressive load and the values found under bending load.* As discussed in Chapter 2, a difference was noticed between the elastic moduli of wallets tested under compressive loads and those obtained from wallets under out-of-plane bending load. This difference should be better understood, as parameters and models should be valid for masonry under in-plane as well as out-of-plane conditions and combinations thereof.

## MATERIAL TESTING

---

This appendix provides short descriptions of material tests, including the preparation of specimens, testing set-up, measuring systems, and loading protocols, performed as part of the experimental studies in Chapter 2 and Chapter 3. The main experimental outputs were:

- Bending and compression properties of hardened mortar (Section A.1).
- Bending and compression properties of units (Section A.2).
- Compression properties of masonry wallets (Section A.3).
- Bending properties of masonry wallets (Section A.4).
- Shear properties along the brick-mortar interface (Section A.5).

## A.1 Bending and Compression Properties of Hardened Mortar

### Flexural and compression tests on mortar bars (EN 1015-11:1999)

**Preparation** During each day of construction, at least three mortar bars were collected and cast in moulds. The moulds had a length of  $l_m = 160$  mm, a height of  $h_m = 40$  mm and a thickness of  $t_m = 40$  mm. The samples were stored in controlled conditions. The first two days they were placed in a fog room ( $T = 20 \pm 2^\circ\text{C}$ ,  $\text{RH} = 95 \pm 5\%$ ) with the moulds. After two days, they were un moulded and kept for another five days in the fog room. Eventually, they were placed in a conditioning room with a temperature of  $20 \pm 2^\circ\text{C}$  and a relative humidity of  $50 \pm 5\%$  until testing. After at least 28 days from construction, the flexural and compression tests were performed.

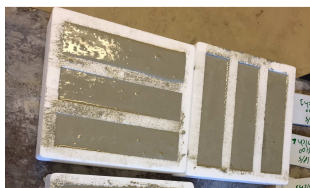


Figure A.1: Mortar bars after casting.

**Test set-up** A force-controlled Instron Universal Testing Machine was used for both flexural and compression tests. The testing machine allowed for registering only the maximum load.

The flexural strength of mortar was determined by a three-point bending test. The test set-up comprised two steel bearing rollers having a diameter of  $10 \pm 0.5$  mm and spaced  $100 \pm 0.5$  mm. A third roller was centrally placed on top of the sample to apply the load.

The compression test was performed on the broken pieces obtained from the flexural test, which had at least a length of 40 mm. The specimen was placed between two steel plates with a length of 40 mm.

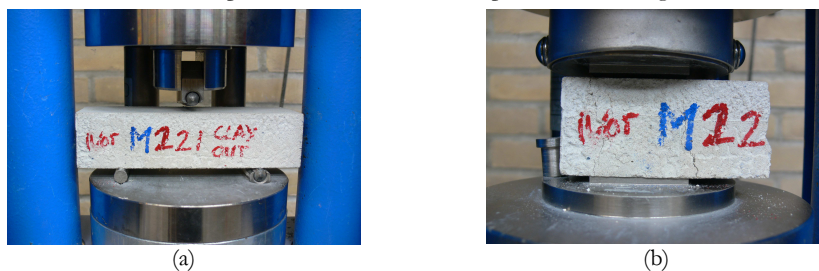


Figure A.2: Test on mortar bars: (a) three-point bending test; (b) compression test.

**Loading protocol** In both tests, a monotonic load was applied. The testing rate was selected to obtain a failure within 30 to 90s. The loading rate under bending and compression test was, respectively, 0.03 kN/s and 0.1-0.2 kN/s.



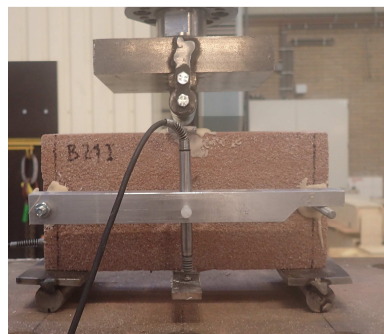
## A. 2 Bending and Compression Properties of Units

### Flexural tests on masonry unit (NEN 6790:2005)

**Test set-up** A three-point bending test was performed using a displacement-controlled apparatus including a hydraulic jack with a 50 kN capacity. The specimen was supported by two roller bearings, which were placed 10 mm far from the end of the masonry unit. A third roller was used to apply the load at mid-span. The masonry unit was positioned such that the bed face was parallel to the applied load (out-of-plane bending).



(a)



(b)

**Figure A.3:** Three-point bending test on brick: (a) measuring elongation; (b) measuring deflection at mid-span.

**Measuring system** To measure elongation between the two supports and vertical deflection at mid-span, each unit was equipped with a horizontal and a vertical LVDT, respectively. The LVDTs had a measuring range of 10 mm with an accuracy of  $\pm 1 \mu\text{m}$ .

**Loading protocol** A monotonic load was applied. The testing rate was selected to obtain a failure within 30 to 90s. The loading rate was 0.2 mm/s.

### Compression tests on single brick (EN 772-1:2011)

**Test set-up** A displacement-controlled apparatus, including a hydraulic jack with 3500 kN hydraulic capacity was used. The load was applied perpendicular to the bed face.



**Figure A.4:** Compression test on a single brick.

**Loading protocol** The masonry unit was subjected to monotonic loading. The testing rate was selected to obtain a failure within 30 to 90s. The loading rate was 0.02 mm/s.

### Compression tests on stack-bond samples (Vermeltoort, 2005)

**Preparation** A stack-bond prism, with a height-to-thickness ratio between 4 and 5, was built.

**Test set-up** A displacement-controlled apparatus, including a hydraulic jack with 3500 kN hydraulic capacity was used. The load was applied perpendicular to the bed face.



**Figure A.5:** Compression test on stack-bond prism.

**Measuring system** To record brick deformations throughout the test, four vertical LVDTs with variable lengths were placed along the stretcher face. The LVDTs had a measuring range of 10 mm with an accuracy of  $\pm 1 \mu\text{m}$ .

**Loading protocol** The loading rate was 0.002 mm/s for every brick types.

### A. 3 Compression Properties of Masonry Wallets

#### Compression tests on wallets (EN 1052-1:1998)

**Sample preparation** To ensure an even distribution of the compressive load, a thin layer of gypsum was applied to the faces in contact with the loading plates.

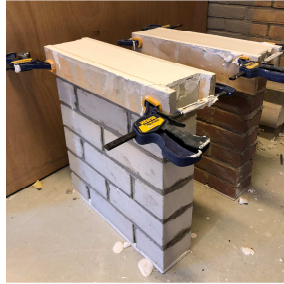


Figure A.6: Applying gypsum.

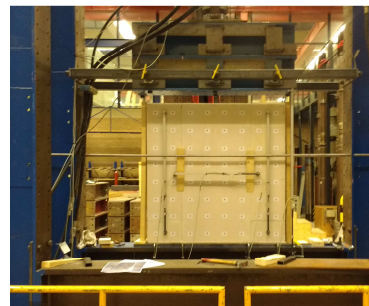
**Test set-up** Two different displacement-controlled testing set-ups were adopted based on the wallet's height. In both testing set-ups, the jack displacement was constantly increased, and the load required to crush the wallets was measured.

wallets with height lower than 550 mm The testing apparatus was provided with a 3500 kN hydraulic jack, positioned at the bottom, Figure A.7a. The hydraulic jack lifted a steel plate, the active side, and there was a passive load plate at the top. A hinge between the load cell and the top steel plate reduced possible eccentricities during loading. A load cell that measures the applied force is attached to the top steel plate.

wallets with height higher than 550 mm The designed set-up was composed of two identical steel frames positioned parallel to each other, connected on top and bottom, Figure A.7b. Each of the contrast frames was composed of two HEB300 columns and two HEB1000 beams. The bottom steel beam acted as a support for the tested specimen, while the top one held the load cell. The load was applied through two spreading beams, which were connected to the load cell by a hinge to reduce possible eccentricities during loading. A load cell that measured the applied force was attached to the top steel plate.



(a)



(b)

Figure A.7: Compression testing set-up for wallets with height: (a) lower than 550 mm; (b) higher than 550 mm.

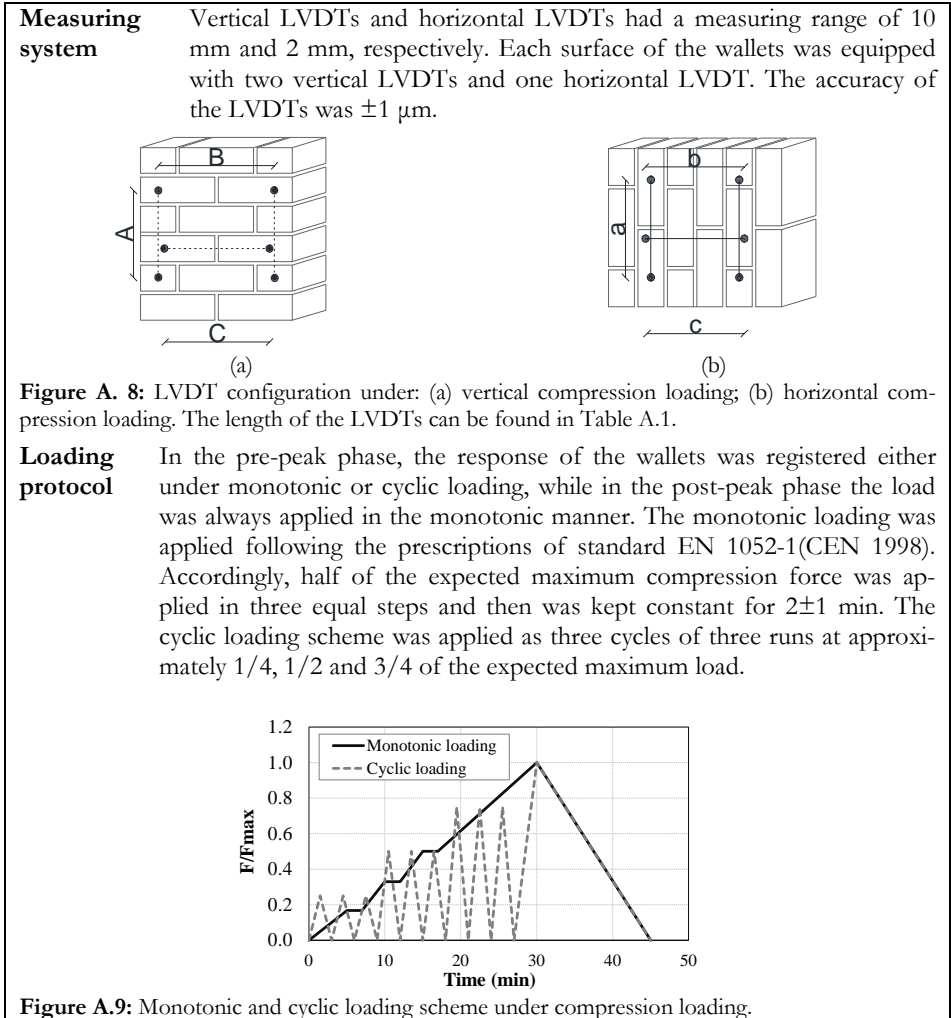


**Table A. 1:**

Overview of wallet size, LVDT dimensions, and loading rate under compression loading.

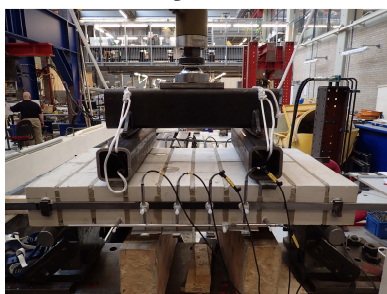
Masonry	Wallet size $l_m \times h_m \times t_m$ $\text{mm}^3$	Vertical compression			Horizontal compression			Loading rate	
		A mm	B mm	C mm	a mm	b mm	c mm	cyclic mm/s	monotonic mm/s
MAT-1	434×476×100	243	332	298	265	300	280	0.006	0.002
MAT-2	430×470×100	300	332	290	265	300	280	0.006	0.002
MAT-3	430×470×100	300	330	290	265	300	280	0.006	0.002
MAT-4	540×650×210	360	390	290	363	360	250	0.040	0.007
MAT-5	1283×1290×100	969	697	883	1093	968	775	0.050	0.010

## A. 4 Bending Properties of Masonry Wallets

### Four-point out-of-plane and in-plane bending tests on wallets (EN 1052-2:2016)

**Test set-up** Two different testing set-ups were used: initially a displacement-controlled set-up was adopted which was later replaced by a crack-controlled set-up. In both set-ups, the bending load was applied using a hydraulic jack with 100 kN capacity. The distances between the loading,  $d_2$ , and bearing rollers,  $d_1$ , were reported in Table A.2.

**Displacement-controlled set-up** The applied load was distributed along two lines via steel profiles, Figure A. 10. To assure a uniform distribution of the load, rubber strips were placed between the wallet and the steel profiles. Using the displacement-controlled set-up, the post-peak branch of the wallets under out-of-plane bending load was hardly captured, as controlling the progressive crack mechanism was not possible, which could be exacerbated due to the self-weight of masonry. To overcome such limitations, the testing set-up was re-designed in the second testing phase.



(a)



(b)

**Figure A. 10:** Four-point bending set-up: (a) vertical out-of-plane bending; (b) in-plane bending.

**Crack-controlled set-up** To exclude the effect of the self-weight of the wallet, the configuration of the out-of-plane bending set-up was modified Figure A.11. The bending load was transferred to an I-shaped, steel column connected to two steel profiles. To distribute the load along the two lines, roller bearings were mounted to the steel profiles via springs. This loading system was suspended from the top beam of the test rig using a counterweight. In fact, this system could help to minimise the friction forces between the specimen and the loading supports. In the back face of the wallets, two hollow steel profiles, mounted to the column of the test rig, where bearing rollers through a spring connection were placed. At the base, the specimen was supported by a steel plate positioned on top of flat ball bearings. Note that under in-plane bending load the orientation of the testing set-up was not changed with respect to the displacement-controlled set-up.

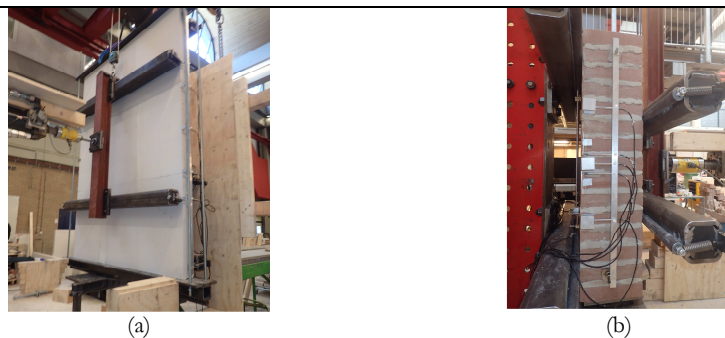


**Figure A.11:** Four-point out-of-plane bending: (a) CS element masonry wallet; (b) double-wythe clay brick masonry wallet.

**Measuring system** Within the constant moment zone, vertical and horizontal LVDTs were placed at both sides of the wallet. The LVDTs had a measuring range of 10 mm with an accuracy of 0.1%.

In the case of *displacement-controlled set-up*:

Under both out-of-plane and in-plane bending load, the deflection of wallets was measured using vertical LVDTs and elongation using horizontal LVDTs.

In the case of *cracked-controlled set-up*:

Under out-of-plane bending load the deflection of wallets was measured using horizontal LVDTs and the elongation using vertical LVDTs. The measurements of vertical LVDTs at the back face were used to control the jack's deformation.

Under in-plane bending load the deflection of wallets was measured using vertical LVDTs and the elongation using horizontal LVDTs. The latter measurements were used to control the jack's deformation.

**Loading protocol** The bending load was monotonically applied, and the loading rate is given in Table A.2.

**Table A. 2:**

Overview of the dimensions of specimens adopted for the bending tests;  $d_1$  and  $d_2$  are the distances between the loading and bearing rollers, respectively.

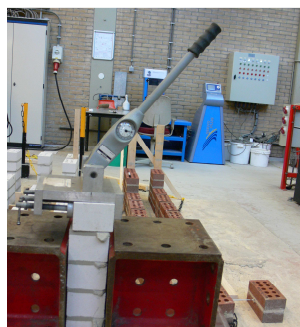
Type of test	Masonry	$t_s$ mm	$l_s$ mm	$h_s$ mm	$d_1$ mm	$d_2$ mm	Rate mm/sec	Test Set-up
Moment vector parallel to the bed joints and in the plane of the wall	MAT-1	100	430	800	360	720	0.002	Disp.Cont.
	MAT-2	100	430	600	360	720	0.002	Disp.Cont.
	MAT-3	100	430	590	220	420	0.001	Crack.Cont.
	MAT-4	210	760	890	360	720	0.001	Crack.Cont.
	MAT-5	100	1350	1930	1750	950	0.004	Crack.Cont.
Moment vector orthogonal to the bed joints and in the plane of the wall	MAT-1	100	880	315	360	720	0.002	Disp.Cont.
	MAT-2	100	880	230	220	440	0.002	Disp.Cont.
	MAT-3	100	870	290	360	660	0.001	Crack.Cont.
	MAT-4	210	1200	650	600	1100	0.001	Crack.Cont.
	MAT-5	100	2250	1290	1750	950	0.004	Crack.Cont.
Moment vector orthogonal to the bed joints and in the plane of the wall	MAT-1	100	880	315	360	720	0.002	Disp.Cont.
	MAT-2	100	880	230	360	720	0.002	Disp.Cont.
	MAT-3	100	870	290	360	660	0.001	Crack.Cont.
	MAT-4	210	1420	350	410	990	0.001	Crack.Cont.
	MAT-5	100	2247	645	1750	950	0.004	Crack.Cont.

**Bond wrench tests on couplets or stack-bond prism (EN 1052-5:2013)**

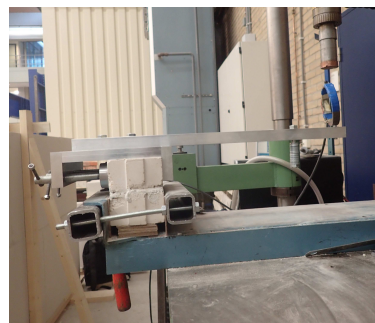
**Test set-up** Two different testing set-ups were used; the difference lied in the loading application, Figure A.12. Initially, load was applied manually; later, the testing set-up was modified, and the load was applied using a manually operated jack. In both set-ups, the specimen was rigidly held at the bottom using a support frame; however, the support system of the second testing set-up was modified. The weight of clamp,  $F_2$ , the distance from the applied load to the tension face of the specimen,  $e_1$ , the distance from the centre of gravity of the clamp to the tension face of the specimen,  $e_2$ , the mean length of the bed joint,  $l_j$ , and the mean width of the bed joint,  $w_j$ , are given in Table A.3.

With manual application of load A lever attached to the clamp is used to create a bending moment in the mortar joint. The moment applied is registered on an analogue scale. The apparatus is officially calibrated in the range of 20–215 Nm. The tolerance is 4%. Readings are accurate to 10 Nm.

With application of load using a manually operated jack The load was applied using a 100 kN hydraulic jack. A load cell attached to the jack, with an accuracy of  $\pm 1$  N, made the continuous recording of the applied force possible.



(a)



(b)

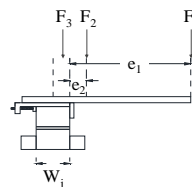
**Figure A.12:** Bond wrench testing set-up: (a) manual application of load; (b) application of load using a manually operated jack.

**Loading protocol** The load was applied smoothly so the failure occurred in 1 to 5 min. However, it was hardly possible to meet such criteria using the first testing set-up.

**Table A. 3:**

Overview of dimensions of specimens and bond wrench testing set-up specifications.

Masonry	$W_j$ mm	$l_j$ mm	$e_1$ mm	$e_2$ mm	$F_2$ N	Test Set-up
MAT-1	100	212	320	25	72.3	a
MAT-2	100	210	320	25	72.3	a
MAT-3/4	110	210	500	51	50.9	b
MAT-5	100	200	500	51	50.9	b

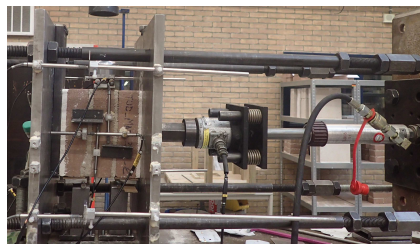


## A.5 Shear Properties along Brick-Mortar Interface

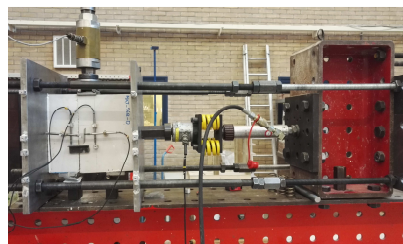
### Shear-compression tests on triplets (EN 1052-3:2002)

**Specimen preparation** To achieve a uniform distribution of the compression load along the interface, a thin layer of gypsum, 10 mm thick, was applied to the faces in contact with the loading plates. Following the outlines of the standard EN1052-3(CEN 2002), for brick masonry and CS element masonry, triplet and couplet configurations were adopted, Figure A.13.

**Test set-up** Two independently operated jacks were adopted to apply shear and pre-compressive load along the masonry unit-joint interface. The shear load was applied using a displacement-controlled hydraulic jack with 100 kN capacity. The pre-compressive load was applied perpendicular to the bed joint plane using a manually controlled horizontal jack. To this end, the specimen was enclosed between two lateral steel plates acting as contrasts. The horizontal jack was kept in place by means of four steel rods positioned on opposite sides of the steel plates. In order to keep the transverse compressive load constant ( $\pm 2\%$ ), a spring system was interposed between the hydraulic jack and the load cell. Two different springs with stiffness of 123 and 3300 N/mm were used, respectively, at the pre-compression levels lower and higher than 0.30 MPa.



(a)



(b)

**Figure A.13:** Shear-compression set-up: (a) test on brick masonry triplets; (b) test on CS element masonry couplet.

### LVDTs range

At each surface of the specimen, two vertical LVDTs and one horizontal LVDT measured the relative sliding of the central brick with respect to two lateral ones and the normal deformations of the joint, respectively. Vertical LVDTs and horizontal LVDTs had a measuring range of 10 mm and 2 mm, respectively. The accuracy of the LVDTs was  $\pm 1 \mu\text{m}$ .

### Loading protocol

The displacement of the vertical jack, introducing a shearing-sliding deformation on the joint, was increased at a rate of 0.005 mm/s.

The shear-compression test was repeated at three different pre-compression levels, namely 0.20, 0.60 and 1.0 MPa. These levels were chosen because the compressive strength of unit was higher than 10 MPa, EN 1052-3(CEN 2002).



## INFLUENCE OF TRIPLETS' GEOMETRY ON SHEAR PROPERTIES

---

This appendix contains additional detail related to Chapter 5.

To study the influence of triplet geometry on shear properties, both standard triplets (stack-bond triplets) and modified triplets (half-bonded triplets) were constructed in the laboratory, Figure B.1. Shear-compression tests on triplets were generally performed on standard triplets following EN 1052-3(CEN 2002). In the case of existing buildings with a running bond, half-bonded specimens, including two head joints, were extracted for testing purposes.

For the two masonry objects replicated in the laboratory, the difference between the Coulomb failure criterion of the standard triplets and of the modified triplets is shown in Figure B.2 and Table B.1. Considering all the results obtained by the standard and modified triplets, no significant statistical difference was found for CS masonry at any imposed pre-compression level, as the coefficient of variation ranged from 3% to 13%. On the contrary, the shear strength of the clay modified triplets differed slightly from that of the standard triplets; the coefficient of variation was between 11% and 23%. Because these results were found from tests on a limited amount of data, further experimental and numerical study is suggested to fully comprehend the impact of the head joint on the shear-sliding behaviour.

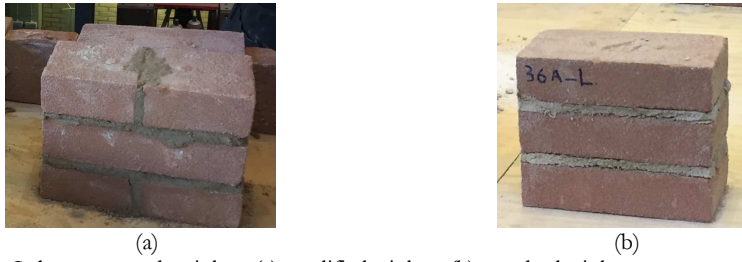


**Figure B.1:** Laboratory made triplets: (a) modified triplets; (b) standard triplets.

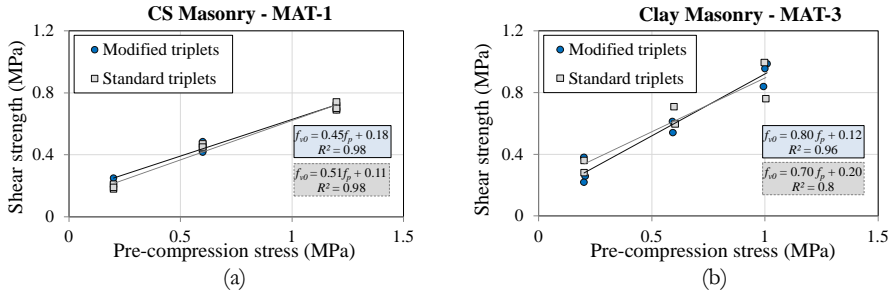


**Figure B.2:** Comparison between shear properties of the standard and modified triplets: (a) MAT-1 laboratory-made CS brick masonry; (b) MAT-3 laboratory-made clay brick masonry.

**Table B.1:**

Summary of the shear properties of standard triplets and modified triplets for two replicated objects. Coefficient of variation in percentage in parentheses.

	CS masonry MAT-1			Clay masonry MAT-3		
Pre-compression level (MPa)	0.20	0.60	1.20	0.20	0.60	1.00
<i>Standard triplets</i>						
Number of specimens	2	2	2	3	3	3
Shear strength (MPa)	0.19(8)	0.45(3)	0.71(4)	0.32(17)	0.65(12)	0.88(19)
<i>Modified triplets</i>						
Number of specimens	3	2	3	3	3	3
Shear strength (MPa)	0.27(22)	0.46(8)	0.71(3)	0.29(29)	0.58(9)	0.93(8)
<i>Standard triplets + Modified triplets</i>						
Shear strength (MPa)	0.21(13)	0.46(5)	0.71(3)	0.30(23)	0.61(11)	0.91(15)

## BIBLIOGRAPHY

- Abdou, L., Saada, R. A., Meftah, F., & Mebarki, A. (2006). Experimental investigations of the joint-mortar behaviour. *Mechanics research communications*, 33(3), 370-384.
- Almesfer, N., Dizhur, D. Y., Lumantarna, R., & Ingham, J. M. (2014). Material properties of existing unreinforced clay brick masonry buildings in New Zealand. *Bulletin of the New Zealand Society for Earthquake Engineering*, 47(2), 75-96.
- Andreotti, G., Graziotti, F., & Magenes, G. (2019). Expansion of mortar joints in direct shear tests of masonry samples: implications on shear strength and experimental characterization of dilatancy. *Materials and Structures*, 52(4), 64.
- Angelillo, M., Lourenço, P. B., & Milani, G. (2014). Masonry behaviour and modelling. In *Mechanics of masonry structures* (pp. 1-26). Vienna: Springer.
- Anthoine, A., Magonette, G., & Magenes, G. (1995). *Shear-compression testing and analysis of brick masonry walls*. Paper presented at the 10<sup>th</sup> European conference on earthquake engineering.
- Arup. (2013). *Structural Upgrading Study* (REP/229746/SU003). Amsterdam, The Netherlands: Nederlandse Aardolie Maatschappij.
- Arup. (2015). *Testing objects passport (dataset)*. Amsterdam, The Netherlands: Nederlandse Aardolie Maatschappij.
- ASTM International (2003), *ASTM C1552-3: Practice for capping concrete masonry units, related units and masonry prisms for compression testing*, West Conshohocken, PA: American Society for Testing and Materials.
- ASTM International (2005), *ASTM C1532: Standard practice for selection, removal, and shipment of manufactured masonry units placed in usage (withdrawn 2006)*, West Conshohocken, PA: American Society for Testing and Materials.
- ASTM International (2014), *ASTM C1197-14a: Standard test method for in situ measurement of masonry deformability properties using the flatjack method*, West Conshohocken, PA: American Society for Testing and Materials.
- ASTM International (2015), *ASTM E519/519M - 15: Standard test method for diagonal tension (shear) in masonry assemblages*, West Conshohocken, PA: American Society for Testing and Materials.
- ASTM International (2016), *ASTM C1531: Standard test methods for in situ measurement of masonry mortar joint shear strength index*, West Conshohocken, PA: American Society for Testing and Materials.
- ASTM International (2017), *ASTM E111 (2017): Standard test method for Young's modulus, tangent modulus, and chord modulus*, West Conshohocken, PA: American Society for Testing and Materials.

ASTM International (2017), *ASTM C496/ C496M-17, Standard test method for splitting tensile strength of cylindrical concrete specimens*, West Conshohocken, PA: American Society for Testing and Materials.

ASTM International (2018), *ASTM C1314-18 (2018): Standard test method for compressive strength of masonry prisms*, West Conshohocken, PA: American Society for Testing and Materials.

Atkinson, R., Amadei, B., Saeb, S., & Sture, S. (1989). Response of masonry bed joints in direct shear. *Journal of Structural Engineering*, 115(9), 2276-2296.

Augenti, N., & Parisi, F. (2010). Constitutive models for tuff masonry under uniaxial compression. *Journal of Materials in Civil Engineering*, 22(11), 1102-1111.

Augenti, N., & Parisi, F. (2011). Constitutive modelling of tuff masonry in direct shear. *Construction and Building Materials*, 25(4), 1612-1620.

Backes, H. (1985). *Tensile strength of masonry*. Paper presented at the 7<sup>th</sup> International Brick Masonry Conference.

Baker, L., & Franken, G. (1976). *Variability aspects of the flexural strength of brickwork*. Paper presented at the 4<sup>th</sup> International Brick and Block Masonry Conference, Brussels, Belgium.

Barattucci, S., Sarhosis, V., Bruno, A. W., D'Altri, A. M., de Miranda, S., & Castellazzi, G. (2020). An experimental and numerical study on masonry triplets subjected to monotonic and cyclic shear loadings. *Construction and Building Materials*, 254, 119313.

Barros, J. A., & Lourenço, P. B. (2000). *Size effect on masonry subjected to out-of-plane loading*. Paper presented at the 12<sup>th</sup> International Brick and Block Masonry Conference.

Bažant, Z., & Pfeiffer, P. (1986). Shear fracture tests of concrete. *Materials and Structures*, 19(2), 111.

Bažant, Z. P., & Xiang, Y. (1997). Size effect in compression fracture: splitting crack band propagation. *Journal of engineering mechanics*, 123(2), 162-172.

Benedetti, A., Pelà, L., & Aprile, A. (2008). *Masonry properties determination via splitting tests on cores with a rotated mortar layer*. Paper presented at the Proceedings of 8<sup>th</sup> International Seminar on Structural Masonry, Istanbul, Turkey.

Benedetti, A., & Pelà, L. (2012). *Experimental characterization of mortar by testing on small specimens*. Paper presented at the 15<sup>th</sup> International Brick & Block Masonry Conference, Florianopolis, Brazil.

Bennett, R. M., Boyd, K. A., & Flanagan, R. D. (1997). Compressive properties of structural clay tile prisms. *Journal of Structural Engineering*, 123(7), 920-926.

Binda, L., Baronio, G., & Ferrieri, E. (1997). *Durability of brick masonry surface treatments to salt crystallization*. Paper presented at the 11<sup>th</sup> International Brick & Block Masonry Conference, Tongji University, Shanghai.

- Binda, L., & Tiraboschi, C. (1999). Flat-jack test: A slightly destructive technique for the diagnosis of brick and stone masonry structures. *Restoration of Buildings and Monuments*, 5(5), 449-472.
- Braga, F., Dolce, M., Filardi, B., Masi, A., & Nigro, D. (1992). *A test method to assess the shear strength of existing masonry structures-theoretical basis and first experimental results*. Paper presented at the Int. Work. CNR-GNDT. Effectiveness of injection techniques for retrofitting of stone and brick walls in seismic areas, Milan, Italy.
- Brencich, A., & Sterpi, E. (2006, 06-08 November). *Compressive strength of solid clay brick masonry: Calibration of experimental tests and theoretical issues*. Paper presented at the 5<sup>th</sup> Structural Analysis of Historical Constructions, New Delhi, India.
- Brencich, A., & Sabia, D. (2008). Experimental identification of a multi-span masonry bridge: The Tanaro Bridge. *Construction and Building Materials*, 22(10), 2087-2099.
- Burd, H., Houlsby, G., Augarde, C., & Liu, G. (2000). Modelling tunneling-induced settlement of masonry buildings. *Proceedings of the institution of civil engineers-geotechnical engineering*, 143(1), 17-29.
- Bureau of Indian Standards (IS: 1905-1987), *Code of practice for structural use of unreinforced masonry*.
- Burton, C., Visintin, P., Griffith, M., & Vaculik, J. (2020). *Field testing of vintage masonry: Mechanical properties and anchorage strengths*. Paper presented at the Structures.
- Can, E., Kuşcu, Ş., & Kartal, M. E. (2012). Effects of mining subsidence on masonry buildings in Zonguldak hard coal region in Turkey. *Environmental Earth Sciences*, 66(8), 2503-2518.
- Carpinteri, A., Valente, S., Ferrara, G., & Melchiorri, G. (1993). Is mode II fracture energy a real material property? *Computers & structures*, 48(3), 397-413.
- Cescatti, E., Dalla Benetta, M., Modena, C., & Casarin, F. (2016, 26-30 June). *Analysis and evaluations of flat jack test on a wide existing masonry buildings sample*. Paper presented at the 16<sup>th</sup> Brick & Block Masonry Conference, Padova, Italy.
- Chaimoon, K., & Attard, M. M. (2009). Experimental and numerical investigation of masonry under three-point bending (in-plane). *Engineering Structures*, 31(1), 103-112.
- Cohen, J. (2013). *Statistical Power Analysis for the Behavioral Sciences*: Academic press.
- Comité Euro-International du Béton (1993), *Model Code 90,CEB Bulletin No. 213/214,ISBN 978-0-7277-1696-5, 460, CEB-FIP (1993)*.
- Costigan, A., Pavía, S., & Kinnane, O. (2015). An experimental evaluation of prediction models for the mechanical behavior of unreinforced, lime-mortar masonry under compression. *Journal of Building Engineering*, 4, 283-294.
- Crowley, H., Uilenreef, J., & Scheefhals, R. (2020). *Data Documentation, technical report & post-processing to produce the v7, Exposure Mode*. The Netherlands: ARUP.

- D'Altri, A. M., Messali, F., Rots, J., Castellazzi, G., & de Miranda, S. (2019a). A damaging block-based model for the analysis of the cyclic behaviour of full-scale masonry structures. *Engineering Fracture Mechanics*, 209, 423-448.
- D'Altri, A. M., Sarhosis, V., Milani, G., Rots, J., Cattari, S., Lagomarsino, S., Sacco, E., Tralli, A., Castellazzi, G., & de Miranda, S. (2019b). Modeling strategies for the computational analysis of unreinforced Masonry structures: Review and classification. *Archives of Computational Methods in Engineering*, 1-33.
- D'Ayala, D., & Speranza, E. (2003). Definition of collapse mechanisms and seismic vulnerability of historic masonry buildings. *Earthquake Spectra*, 19(3), 479-509.
- Damiola, M., Esposito, R., Messali, F., & Rots, J. G. (2018, 9-11 July). *Quasi-static cyclic two-way out-of-plane bending tests and analytical models comparison for URM walls*. Paper presented at the 10<sup>th</sup> international masonry conference (IMC), Milan, Italy.
- de Felice, G. (2011). Out-of-plane seismic capacity of masonry depending on wall section morphology. *International Journal of Architectural Heritage*, 5(4-5), 466-482.
- de Vekey, R. (1988, 19-21 September 1988). *Non-destructive test methods for masonry structures*. Paper presented at the Proceedings of the 8<sup>th</sup> International Brick & Block Masonry Conference, Dublin, Ireland.
- de Vekey, R. (1997). A review of the work of the RILEM committee 127-MS: testing masonry materials and structures. *Materials and Structures*, 30(1), 12-16.
- De Villiers, W. I. (2019). *Computational and Experimental Modelling of Masonry Walling towards Performance-Based Standardisation of Alternative Masonry Units for Low-Income Housing*. (Doctoral dissertation), Stellenbosch University, Stellenbosch.
- Dehghan, S., Najafgholipour, M., Baneshi, V., & Rowshanzamir, M. (2018). Mechanical and bond properties of solid clay brick masonry with different sand grading. *Construction and Building Materials*, 174, 1-10.
- Dhanasekar, M., Page, A., & Kleeman, P. (1985, June). *The failure of brick masonry under biaxial stresses*. Paper presented at the Proceeding of the Institution of Civil Engineers.
- DIN (1999), *Prüfung von Mörteln mit mineralischen Bindemitteln - Teil 9:Festmörtel; Bestimmung der Fugendruckfestigkeit.*, DIN 18555-9 (1999).
- Drougkas, A., Roca, P., & Molins, C. (2016). Material characterisation and micro-modeling of a historic brick masonry pillar. *International Journal of Architectural Heritage*, 10(7), 887-902.
- Drougkas, A., Roca, P., & Molins, C. (2016). Material characterization and micro-modeling of a historic brick masonry pillar. *International Journal of Architectural Heritage*, 10(7), 887-902.
- Esposito, R., Messali, F., & Rots, G. J. (2016). *Tests for the Characterisation of Replicated Masonry and Wall Ties* (C31B60-4). The Netherlands: Delft University of Technology.

- Esposito, R., Messali, F., Ravenshorst, G. J., Schipper, H. R., & Rots, J. G. (2019). Seismic assessment of a lab-tested two-storey unreinforced masonry Dutch terraced house. *Bulletin of Earthquake Engineering*, 17(8), 4601-4623.
- EUcentre. (2015). *Material characterisation*. Pavia, Italy: Nederlandse Aardolie Maatschappij.
- Facconi, L. (2012). *Fiber Reinforced Concrete and Mortar for Enhanced Structural Elements and Repair of Masonry Walls*. (Doctoral dissertation), University of Brescia, Brescia, Italy.
- Facconi, L., Minelli, F., & Vecchio, F. J. (2017). Predicting uniaxial cyclic compressive behavior of brick masonry: New analytical model. *Journal of Structural Engineering*, 144(2), 04017213.
- Faul, F., Erdfelder, E., Lang, A., & Buchner, A. (2007). A flexible statistical power analysis program for the social, behavioral and biomedical sciences. *Behavior Research Methods*.
- Feenstra, P. H. (1993). *Computational Aspects of Biaxial Stress in Plain and Reinforced Concrete*. (PhD thesis), Delft University of Technology, The Netherlands.
- Ferretti, D. (2020). Dimensional analysis and calibration of a power model for compressive strength of solid-clay-brick masonry. *Engineering Structures*, 205, 110064.
- Ferretti, F., Jafari, S., Esposito, R., Rots, J. G., & Mazzotti, C. (2018a). *Investigation of the shear-sliding behavior of masonry through shove test: experimental and numerical studies*. Paper presented at the 11<sup>th</sup> International Conference on Structural Analysis of Historical Constructions, Cusco, Perú.
- Ferretti, F., Mazzotti, C., Esposito, R., & Rots, J. (2018b). Shear-sliding behavior of masonry: numerical micro-modeling of triplet tests. In *Computational Modelling of Concrete Structures* (pp. 941-951): CRC Press.
- Field, A. (2013). *Discovering statistics using IBM SPSS statistics*: Sage.
- Gaggero, M. B. (2019). *Comparison of Test Methods to Determine Masonry Bond Flexural Strength*. (Master thesis), Politecnico Di Torino, Italy.
- Gambarotta, L., & Lagomarsino, S. (1997). Damage models for the seismic response of brick masonry shear walls. Part I: the mortar joint model and its applications. *Earthquake Engineering and Structural Dynamics*, 26(4), 423-439.
- García, D., San-José, J. T., Garmendia, L., & Larrinaga, P. (2012). Comparison between experimental values and standards on natural stone masonry mechanical properties. *Construction and Building Materials*, 28(1), 444-449.
- Garzón-Roca, J., Marco, C. O., & Adam, J. M. (2013). Compressive strength of masonry made of clay bricks and cement mortar: Estimation based on Neural Networks and Fuzzy Logic. *Engineering Structures*, 48, 21-27.
- Gentile, R., del Vecchio, C., Pampanin, S., Raffaele, D., & Uva, G. (2019).

- Refinement and validation of the Simple Lateral Mechanism Analysis (SLaMA) procedure for RC frames. *Journal of Earthquake Engineering*, 1-29.
- Ghiassi, B., Vermelfoort, A., & Lourenço, P. (2019). Masonry mechanical properties. In *Numerical Modeling of Masonry and Historical Structures: From Theory to Application*. (pp. 239-261): Woodhead Publishing.
- Giardina, G., Hendriks, M. A., & Rots, J. G. (2015). Damage functions for the vulnerability assessment of masonry buildings subjected to tunneling. *Journal of Structural Engineering*, 141(9), 0401421-0401413.
- Gourav, K., & Reddy, B. V. (2018). Out-of-plane flexure behaviour of fly ash-lime-gypsum brick masonry walls. *Engineering Structures*, 173, 241-250.
- Graziotti, F., Senaldi, I., Peloso, S., & Rossi, A. (2014). *Results of in-situ tests Building unit: Loppersum, Zijlvest 25*. Pavia, Italy: Nederlandse Aardolie Maatschappij.
- Graziotti, F., Guerrini, G., Rossi, A., Andreotti, G., & Magenes, G. (2018a). Proposal for an improved procedure and interpretation of ASTM C1531 for the in situ determination of brick-masonry shear strength. In *Masonry 2018: ASTM International*.
- Graziotti, F., Penna, A., & Magenes, G. (2018b). A comprehensive in situ and laboratory testing programme supporting seismic risk analysis of URM buildings subjected to induced earthquakes. *Bulletin of Earthquake Engineering*, 1-25.
- Groot, C. (1997, 16 October 1997). *The characterisation of brick and mortar considering mortar/brick bond*. Paper presented at the 11<sup>th</sup> International Brick/Block Masonry Conference, Shanghai, China.
- Guinea, G., Hussein, G., Elices, M., & Planas, J. (2000). Micromechanical modeling of brick-masonry fracture. *Cement and Concrete Research*, 30(5), 731-737.
- Gumaste, K., Rao, K. N., Reddy, B. V., & Jagadish, K. (2007). Strength and elasticity of brick masonry prisms and wallettes under compression. *Materials and Structures*, 40(2), 241-253.
- Hacıfendioğlu, K., Başağa, H. B., & Banerjee, S. (2017). Probabilistic analysis of historic masonry bridges to random ground motion by Monte Carlo Simulation using Response Surface Method. *Construction and Building Materials*, 134, 199-209.
- Haller, P. (1969). Load capacity of brick masonry. *Designing, engineering and constructing with masonry products*, 129-149.
- Hendry, A., & Malek, M. (1986). Characteristic compressive strength of brickwork walls from collected test results. *Mason. Int*(7), 15-24.
- Hendry, A. W. (1998). *Structural brickwork*. London: Macmillan.
- Hordijk, D. A. (1993). *Local Approach to Fatigue of Concrete*. (Doctoral dissertation), Delft University of Technology, Delft, The Netherlands.
- Hoshikuma, J., Kawashima, K., Nagaya, K., & Taylor, A. (1997). Stress-strain model for confined reinforced concrete in bridge piers. *Journal of Structural*



*Engineering*, 123(5), 624-633.

IBM SPSS Statistics for Windows. (2020). from IBM Corporation, Armonk, NY

International Union of Railways (1995), *Recommendations for the assessment of the load carrying capacity of the existing masonry and mass-concrete arch bridges*, UIC 778-3R (1995).

Ispir, M., Demir, C., Ilki, A., & Kumbasar, N. (2009). Material characterization of the historical unreinforced masonry Akaretler row houses in Istanbul. *Materials in Civil Engineering*, 22(7), 702-713.

Ispir, M., & Ilki, A. (2013). Behavior of historical unreinforced brick masonry walls under monotonic and cyclic compression. *Arabian Journal for Science and Engineering*, 38(8), 1993-2007.

İspir, M. (2010). *A Comprehensive Experimental Research on the Behavior of Historical Brick Masonry Walls of 19<sup>th</sup> Century Buildings*. (Doctoral dissertation), Istanbul Technical University, Turkey.

Jafari, S., Rots, G. J., & Panoutsopoulou, L. (2015). *Tests for the characterisation of original Groningen masonry* (C31B60-3). The Netherlands: Delft University of Technology.

Jafari, S., & Esposito, R. (2017a). *Material tests for the characterisation of replicated solid clay brick masonry* (C31B67WP1-12). The Netherlands: Delft University of Technology.

Jafari, S., & Esposito, R. (2017b). *Material characterisation of replicated calcium silicate element masonry* (C31B67WP1-11). The Netherlands: Delft University of Technology.

Jafari, S., Esposito, R., & Rots, J. (2017). *Literature review on the assessment of masonry properties by tests on core samples*. Paper presented at the 4<sup>th</sup> WTA International PhD Symposium, Delft, Netherlands.

Jafari, S., & Esposito, R. (2018). *Material characterisation of existing masonry for URM abacus*. The Netherlands: Delft University of Technology.

Jafari, S., Esposito, R., & Rots, J. (2018a, 9-11 July). *A Comparative study on the evaluation of different testing techniques: Evaluating the mechanical properties of masonry*. Paper presented at the 10th International Masonry Conference, Milan, Italy.

Jafari, S., Ferretti, F., & Esposito, R. (2018b). *Flat-jack and shove tests: Method validation and correlation*. The Netherlands: Delft University of Technology.

Jafari, S., Rots, J. G., & Esposito, R. (2019). Core testing method to assess nonlinear behavior of brick masonry under compression: A comparative experimental study. *Construction and Building Materials*, 218, 193-205.

Jafari, S., Rots, J. G., & Esposito, R. (2020). Core testing method to assess nonlinear shear-sliding behaviour of brick-mortar interfaces: A comparative experimental study. *Construction and Building Materials*, 244, 118236.

Jiao, Z., Wang, Y., Zheng, W., Huang, W., & Zhao, Y. (2019). Bond properties of

alkali-activated slag concrete hollow block masonry with different mortar strength grades. *Construction and Building Materials*, 216, 149-165.

Kaushik, H. B., Rai, D. C., & Jain, S. K. (2007). Stress-strain characteristics of clay brick masonry under uniaxial compression. *Journal of Materials in Civil Engineering*, 19(9), 728-739.

Khalaf, F. M. (2005). New test for determination of masonry tensile bond strength. *Journal of Materials in Civil Engineering*, 17(6), 725-732.

Korff, M., Hemel, M. j., & Esposito, R. (2021). *Bezwijken Grimburgwal: Leerpunten voor het Amsterdamse areaal*. The Netherlands: Delft University of Technology.

Korswagen, P. A., Longo, M., Meulman, E., & Rots, J. G. (2019). Crack initiation and propagation in unreinforced masonry specimens subjected to repeated in-plane loading during light damage. *Bulletin of Earthquake Engineering*, 17(8), 4651-4687.

Kumavat, H. R. (2016). An experimental investigation of mechanical properties in clay brick masonry by partial replacement of fine aggregate with clay brick waste. *Journal of the Institution of Engineers*, 97(3), 199-204.

Lagomarsino, S., Penna, A., Galasco, A., & Cattari, S. (2013). TREMURI program: an equivalent frame model for the nonlinear seismic analysis of masonry buildings. *Engineering Structures*, 56, 1787-1799.

Łątka, D., & Matysek, P. (2020). Determination of Mortar Strength in Historical Brick Masonry Using the Penetrometer Test and Double Punch Test. *Materials*, 13(12), 2873.

Lawrence, S., & Page, A. (1994, 5-7 July). *Bond studies in masonry*. Paper presented at the 10<sup>th</sup> International Brick and Block Masonry Conference, Calgary, Canada.

Lenczner, D. (1972). *Elements of load bearing brickwork* (Vol. Vol. 5): Pergamon Press, New York.

Lizárraga, J. F., & Pérez-Gavilán, J. (2017). Parameter estimation for nonlinear analysis of multi-perforated concrete masonry walls. *Construction and Building Materials*, 141, 353-365.

Lotfi, H., & Shing, P. (1991). An appraisal of smeared crack models for masonry shear wall analysis. *Computers and Structures*, 41(3), 413-425.

Lourenço, P. B. (1996). *A user/programmer guide for the micro-modeling of masonry structures* (03.21.1.31.35).

Lourenço, P. B. (1997a). *Computational Strategies for Masonry Structures*. (Doctoral dissertation), Delft University of Technology, The Netherlands.

Lourenço, P. B. (1997b). *An anisotropic macro-model for masonry plates and shells: Implementation and validation* (03.21.1.31.07). The Netherlands: Delft University of Technology.

Lourenço, P. B., De Borst, R., & Rots, J. G. (1997). A plane stress softening

plasticity model for orthotropic materials. *International Journal for Numerical Methods in Engineering*, 40(21), 4033-4057.

Lourenço, P. B., & Rots, J. G. (1997). Multisurface interface model for analysis of masonry structures. *Journal of engineering mechanics*, 123(7), 660-668.

Lourenço, P. B., Rots, J. G., & Blaauwendraad, J. (1998). Continuum model for masonry: Parameter estimation and validation. *Journal of Structural Engineering*, 124(6), 642-652.

Lourenço, P. B., & Ramos, L. s. F. (2004). Characterization of cyclic behavior of dry masonry joints. *Journal of Structural Engineering*, 130(5), 779-786.

Lourenço, P. B., Almeida, J., & Barros, J. A. (2005). Experimental investigation of bricks under uniaxial tensile testing. *Journal of the British Masonry Society Masonry International*, 18.

Lourenço, P. B., & Pina-Henriques, J. (2006). Validation of analytical and continuum numerical methods for estimating the compressive strength of masonry. *Computers & structures*, 84(29-30), 1977-1989.

Lourenço, P. B., Roca, P., Modena, C., & Agrawal, S. (2006). Compressive strength of solid clay brick masonry: calibration of experimental tests and theoretical issues. *Structural Analysis of Historical Construction*, 2, 757.

Lumantarna, R. (2012). *Material Characterisation of New Zealand's Clay Brick Unreinforced Masonry Buildings*. (Doctor of Philosophy), The University of Auckland, New Zealand.

Lumantarna, R., Biggs, D. T., & Ingham, J. M. (2014a). Uniaxial compressive strength and stiffness of field-extracted and laboratory-constructed masonry prisms. *Journal of Materials in Civil Engineering*, 26(4), 567-575.

Lumantarna, R., Biggs, D. T., & Ingham, J. M. (2014b). Compressive, flexural bond, and shear bond strengths of in situ New Zealand unreinforced clay brick masonry constructed using lime mortar between the 1880s and 1940s. *Journal of Materials in Civil Engineering*, 26(4), 559-566.

Maalej, M., & Li, V. C. (1994). Flexural strength of fiber cementitious composites. *Journal of Materials in Civil Engineering*, 6(3), 390-406.

Magenes, G., & Calvi, G. M. (1997). In-plane seismic response of brick masonry walls. *Earthquake engineering & structural dynamics*, 26(11), 1091-1112.

Manning, E. C., Ramos, L. F., & Fernandes, F. (2016, 12-16 September). *Tube-jack testing: Semi-irregular masonry wall testing*. Paper presented at the 10<sup>th</sup> International Conference on Structural Analysis of Historical Constructions, Leuven, Belgium.

Marastoni, D., Pelà, L., Benedetti, A., & Roca, P. (2016). Combining Brazilian tests on masonry cores and double punch tests for the mechanical characterization of historical mortars. *Construction and Building Materials*, 112, 112-127.

Marfia, S., & Sacco, E. (2012). Multiscale damage contact-friction model for

- periodic masonry walls. *Computer Methods in Applied Mechanics and Engineering*, 205, 189-203.
- Massart, T., Peerlings, R., & Geers, M. (2007). An enhanced multi-scale approach for masonry wall computations with localization of damage. *International Journal for Numerical Methods in Engineering*, 69(5), 1022-1059.
- Mazzotti, C., Sassoni, E., & Pagliai, G. (2014). Determination of shear strength of historic masonries by moderately destructive testing of masonry cores. *Construction and Building Materials*, 54, 421-431.
- Messali, F., & Rots, J. (2018). In-plane drift capacity at near collapse of rocking unreinforced calcium silicate and clay masonry piers. *Engineering Structures*, 164, 183-194.
- Messali, F., Esposito, R., Ravenshorst, G., & Rots, J. (2020). Experimental investigation of the in-plane cyclic behaviour of calcium silicate brick masonry walls. *Bulletin of Earthquake Engineering*, 18(8), 3963-3994.
- Milani, G., Lourenço, P., & Tralli, A. (2006). Homogenization approach for the limit analysis of out-of-plane loaded masonry walls. *Journal of Structural Engineering*, 132(10), 1650-1663.
- Milani, G. (2008). 3D upper bound limit analysis of multi-leaf masonry walls. *International Journal of Mechanical Sciences*, 50(4), 817-836.
- Montazerolghaem, M., & Jaeger, W. (2014, 7-9 July). *A comparative numerical evaluation of masonry initial shear test methods and modifications proposed for EN 1052-3*. Paper presented at the 9<sup>th</sup> International Masonry Conference, Portugal, Guimarães.
- Moreno Regan, O., Colas, A.-S., Bourgeois, E., Chatellier, P., Desbordes, A., & Douroux, J.-F. (2018). Experimental characterisation of the constitutive materials composing an old masonry vaulted tunnel of the Paris subway system. *International Journal of Architectural Heritage*, 12(2), 195-215.
- Naraine, K., & Sinha, S. (1989). Behavior of brick masonry under cyclic compressive loading. *Journal of Structural Engineering*, 115(6), 1432-1445.
- Nazief, M. A. (2014). *Finite Element Characterisation of the Behaviour of Masonry Infill Shear Walls with and without Openings*. (Doctoral dissertation), University of Alberta, Edmonton.
- NEN-EN (1996), *Eurocode 6: Design of masonry structures- Part 1-1: General rules for reinforced and unreinforced masonry structures*, CEN 1996-1-1+A1:2013.
- NEN-EN (1998), *Methods of test for masonry - Part 1: Determination of compressive strength*, CEN 1052-1:1998.
- NEN-EN (1999), *Method of test for mortar for masonry – Part 11: Determination of flexural and compressive strength of hardened mortar*, CEN 1015-11:1999.
- NEN-EN (1999), *Methods of test for mortar for masonry - Part 3: Determination of*

- consistence of fresh mortar (by flow table)*, CEN 1015-3:1999.
- NEN-EN (2002), *Methods of test for masonry - Part 3: Determination of initial shear strength*, CEN 1052-3:2002.
- NEN-EN (2005), *Eurocode 8: Design of structures for earthquake resistance - Part 3: Assessment and retrofitting of buildings*, CEN 1998-3:2005.
- NEN-EN (2007), *Products and systems for the protection and repair of concrete structures. Test methods. Determination of modulus of elasticity in compression*, CEN 13412:2007.
- NEN-EN (2011), *Methods of test for masonry units - Part 1: Determination of compressive strength*, CEN 772-1:2011.
- NEN-EN (2013), *Methods of test for masonry - Part 5: Determination of bond strength by the bond wrench method*, CEN 1052-5:2005/C2:2013.
- NEN-EN (2015), *Specification for masonry units - Part 2: Calcium silicate masonry units*, CEN 771-2:2011+A1:2015.
- NEN-EN (2016), *Methods of test for masonry - Part 2: Determination of flexural strength*, CEN 1052-2:2016.
- NEN-EN (2018), *National Annex to NEN-EN 1996-1-1+A1: Eurocode 6: Design of masonry structures- Part 1-1: General rules for reinforced and unreinforced masonry structures*, NEN-EN 1996-1-1+A1/NB:2011.
- NEN-NPR (2020), *Assessment of structural safety of buildings in case of erection, reconstruction and disapproval- induced earthquake - Basis of design, actions and resistances*, NPR 9998:2020.
- NEN (2005), *Technical principles for building structures - TGB 1990 - Masonry structures - Basic requirements and calculation methods*, NEN 6790:2005.
- Nichols, J. M., & Holland, N. L. (2011, 5-8 June). *A comparative study of balanced bond wrench testing and unbalanced bond wrench testing*. Paper presented at the North American Masonry Conference, Minneapolis, USA.
- Noland, J., Kingsley, G., & Atkinson, R. (1988, 19-21 September). *Utilization of nondestructive techniques into the evaluation of masonry*. Paper presented at the 8<sup>th</sup> International Brick/Block Masonry Conference, Dublin, Ireland.
- Nonnekes, S. M. (2015a). *Masonry Research Report Location: Location: Molenweg 32, 9919 AJ, Loppersum*. Venlo, The Netherlands: B|A|S Research & Technology.
- Nonnekes, S. M. (2015b). *Masonry Research Report Location: Mr. A.T. Voslaan 11, 9902 LC, Appingedam*. Venlo, The Netherlands: B|A|S Research & Technology.
- Nonnekes, S. M. (2015c). *Masonry Research Report Location: Rengersweg 11, 9908 PL, Godlinze*. Venlo, The Netherlands: B|A|S Research & Technology.
- NZSEE (2017), *The seismic assessment of existing buildings, Technical guidelines for engineering assessments*, section C8-Seismic assessment of unreinforced masonry buildings, New Zealand Society for Earthquake Engineering, New Zealand; 2017.

- Olivito, R., & Stumpo, P. (2001). Fracture mechanics in the characterisation of brick masonry structures. *Materials and Structures*, 34(4), 217-223.
- Page, A. (1981). *The biaxial compressive strength of brick masonry*. Paper presented at the Proceedings of the Institution of Civil Engineers.
- Parisi, F., & Augenti, N. (2012). Uncertainty in seismic capacity of masonry buildings. *Buildings*, 2(3), 218-230.
- Peduto, D., Korff, M., Nicodemo, G., Marchese, A., & Ferlisi, S. (2019). Empirical fragility curves for settlement-affected buildings: Analysis of different intensity parameters for seven hundred masonry buildings in The Netherlands. *Soils and Foundations*, 59(2), 380-397.
- Pelà, L., Cervera, M., & Roca, P. (2011). Continuum damage model for orthotropic materials: Application to masonry. *Computer Methods in Applied Mechanics and Engineering*, 200(9-12), 917-930.
- Pelà, L., Canella, E., Aprile, A., & Roca, P. (2016a). Compression test of masonry core samples extracted from existing brickwork. *Construction and Building Materials*, 119, 230-240.
- Pelà, L., Roca, P., & Benedetti, A. (2016b). Mechanical characterization of historical masonry by core drilling and testing of cylindrical samples. *International Journal of Architectural Heritage*, 10(2-3), 360-374.
- Pelà, L., Kasioumi, K., & Roca, P. (2017). Experimental evaluation of the shear strength of aerial lime mortar brickwork by standard tests on triplets and non-standard tests on core samples. *Engineering Structures*, 136, 441-453.
- Pelà, L., Roca, P., & Aprile, A. (2018). Combined in-situ and laboratory minor destructive testing of historical mortars. *International Journal of Architectural Heritage*, 12(3), 334-349.
- Rahman, A., & Ueda, T. (2013). Experimental investigation and numerical modeling of peak shear stress of brick masonry mortar joint under compression. *Journal of Materials in Civil Engineering*, 26(9), 04014061.
- Raj, A., Borsaikia, A. C., & Dixit, U. S. (2020). Bond strength of autoclaved aerated concrete (AAC) masonry using various joint materials. *Journal of Building Engineering*, 28, 101039.
- Reddy, B. V., & Vyas, C. V. U. (2008). Influence of shear bond strength on compressive strength and stress-strain characteristics of masonry. *Materials and Structures*, 41(10), 1697-1712.
- Rota, M., Penna, A., & Magenes, G. (2010). A methodology for deriving analytical fragility curves for masonry buildings based on stochastic nonlinear analyses. *Engineering Structures*, 32(5), 1312-1323.
- Rots, J. G. (1991). Numerical simulation of cracking in structural masonry. *Heron*, 36(2), 49-63.

- Rots, J. G., van Der Pluijm, R., Vermeltoort, A. T., Janssen, H. J. M., & Lourenco, P. B. (Eds.). (1997). *Structural Masonry: An Experimental/Numerical Basis for Practical Design Rules (CUR Report 171)*: AA Balkema.
- Rots, J. G., Messali, F., Esposito, R., Jafari, S., & Mariani, V. (2016, 13-15 Sept). *Computational modeling of masonry with a view to Groningen induced seismicity*. Paper presented at the Structural Analysis of Historical Constructions (SAHC), Leuven, Belgium.
- Rots, J. G., Messali, F., Esposito, R., Mariani, V., & Jafari, S. (2017). *Multi-Scale Approach towards Groningen Masonry and Induced Seismicity*. Paper presented at the Key Engineering Materials.
- Russell, A. (2010). *Characterisation and Seismic Assessment of Unreinforced Masonry Buildings*. (Doctoral dissertation), The University of Auckland, Australia.
- Sacco, E. (2009). A nonlinear homogenization procedure for periodic masonry. *European Journal of Mechanics-A/Solids*, 28(2), 209-222.
- Sandoval, C., & Arnau, O. (2017). Experimental characterization and detailed micro-modeling of multi-perforated clay brick masonry structural response. *Materials and Structures*, 50(1), 34.
- Sarangapani, G., Venkatarama Reddy, B., & Jagadish, K. (2005). Brick-mortar bond and masonry compressive strength. *Journal of Materials in Civil Engineering*, 17(2), 229-237.
- Sassoni, E., & Mazzotti, C. (2013). The use of small diameter cores for assessing the compressive strength of clay brick masonries. *Journal of Cultural Heritage*, 14(3), e95-e101.
- Sassoni, E., Mazzotti, C., Boriani, M., Gabaglio, R., & Gulotta, D. (2013). Assessment of masonry mortar compressive strength by double punch test: The influence of mortar porosity. *Built Heritage*, 18-20.
- Sassoni, E., Mazzotti, C., & Pagliai, G. (2014). Comparison between experimental methods for evaluating the compressive strength of existing masonry buildings. *Construction and Building Materials*, 68, 206-219.
- Sassoni, E., Franzoni, E., & Mazzotti, C. (2015). Influence of sample thickness and capping on characterization of bedding mortars from historic masonries by double punch test (DPT). *Key Engineering Materials*, 624, 322-329.
- Sawko, F., & Rouf, M. (1984). On the stiffness properties of masonry. *Proceedings of the Institution of Civil Engineers*, 77(1), 1-12.
- Schmidt, A., Boersma, K., & Groenewegen, P. (2018). Management strategies in response to an institutional crisis: The case of earthquakes in the Netherlands. *Public Administration*, 96(3), 513-527.
- Schubert, P. (1994, 5-7 July). *Tensile and flexural strength of masonry—influences, test methods, test results*. Paper presented at the 10<sup>th</sup> International Brick and Block Masonry Conference, Calgary, Canada.

- Schuller, M. P. (2003). Nondestructive testing and damage assessment of masonry structures. *Progress in Structural Engineering and Materials*, 5(4), 239-251.
- Segura, J., Pelà, L., & Roca, P. (2018a). Monotonic and cyclic testing of clay brick and lime mortar masonry in compression. *Construction and Building Materials*, 193, 453-466.
- Segura, J., Pelà, L., & Roca, P. (2018b, 11-13 September). *Influence of geometry of cylindrical samples in the mechanical characterization of existing brickwork*. Paper presented at the 11<sup>th</sup> International Conference on Structural Analysis of Historical Constructions, Cusco, Perú.
- Silva, L. C., Lourenço, P. B., & Milani, G. (2017). Rigid block and spring homogenized model (HRBSM) for masonry subjected to impact and blast loading. *International Journal of Impact Engineering*, 109, 14-28.
- Silva, L. C., Lourenço, P. B., & Milani, G. (2020). Numerical homogenization-based seismic assessment of an English-bond masonry prototype: Structural level application. *Earthquake Engineering and Structural Dynamics*, 49(9), 841-862.
- Silvestri, S., Gasparini, G., Trombetti, T., & Ceccoli, C. (2008). *Statistical analysis towards the identification of accurate probability distribution models for the compressive strength of concrete*. Paper presented at the Proceedings of the 14<sup>th</sup> World Conference on Earthquake Engineering, Beijing, China.
- Simões, A., Bento, R., Gago, A., & Lopes, M. (2016). Mechanical characterization of masonry walls with flat-jack tests. *Experimental Techniques*, 40(3), 1163-1178.
- Singh, S., & Munjal, P. (2017). Bond strength and compressive stress-strain characteristics of brick masonry. *Journal of Building Engineering*, 9, 10-16.
- Stockl, S., Hofmann, P., & Mainz, J. (1990). A comparative finite element evaluation of mortar joint shear tests. *Masonry International*, 3(3), 101-104.
- Structural Response to Earthquakes. (2020). *Structural Response to Earthquakes*. Retrieved from <https://www.tudelft.nl/en/ceg/structural-response-to-earthquakes/publications>
- Sugo, H., Page, A. W., & Lawrence, S. (2007). Influence of age on masonry bond strength and mortar microstructure. *Canadian Journal of Civil Engineering*, 34(11), 1433-1442.
- Thaickavil, N. N., & Thomas, J. (2018). Behaviour and strength assessment of masonry prisms. *Case Studies in Construction Materials*, 8, 23-38.
- The MathWorks Inc. (2019). MATLAB and Statistics Toolbox Release. Massachusetts, United States: Natick.
- Tomažević, M., Lutman, M., & Petković, L. (1996). Seismic behavior of masonry walls: experimental simulation. *Journal of Structural Engineering*, 122(9), 1040-1047.
- Ugama, T., & Ejeh, S. (2014). Iron ore tailing as fine aggregate in mortar used for masonry. *International Journal of Advances in Engineering & Technology*, 7(4), 1170.



- Unanwa, C., & Mahan, M. (2014). Statistical analysis of concrete compressive strengths for California highway bridges. *Journal of Performance of Constructed Facilities*, 28(1), 157-167.
- Vaculik, J. (2012). *Unreinforced Masonry Walls Subjected To Out-of-Plane Seismic Actions*. (Doctor of Philosophy), The University of Adelaide, Australia.
- Vaculik, J., & Griffith, M. C. (2017). Probabilistic analysis of unreinforced brick masonry walls subjected to horizontal bending. *Journal of engineering mechanics*, 143(8), 04017056.
- van der Pluijm, R. (1993, 6-9 June). *Shear behaviour of bed joints*. Paper presented at the 6<sup>th</sup> Canadian Masonry Symposium, Pennsylvania, USA.
- van der Pluijm, R. (1999). *Out-of-Plane Bending of Masonry: Behaviour and Strength*. (Doctoral dissertation), Technische Universiteit Eindhoven, The Netherlands.
- van der Voort, N., & Vanclay, F. (2015). Social impacts of earthquakes caused by gas extraction in the Province of Groningen, The Netherlands. *Environmental Impact Assessment Review*, 50, 1-15.
- van Mier, J. G. M. (1984). *Strain-Softening of Concrete under Multiaxial Loading Conditions*. (Doctoral dissertation), Technische Hogeschool Eindhoven, The Netherlands.
- van Wees, J., Buijze, L., Van Thienen-Visser, K., Nepveu, M., Wassing, B., Orlic, B., & Fokker, P. (2014). Geomechanics response and induced seismicity during gas field depletion in the Netherlands. *Geothermics*, 52, 206-219.
- van Zijl, G. (1996). *Shear transfer across bed joints in masonry: A numerical study*. The Netherlands.
- van Zijl, G., Rots, J., & Vermeltoort, A. T. (2001). *Modelling shear-compression in masonry*. Paper presented at the Canadian Masonry Symposium.
- van Zijl, G. P. (2004). Modeling masonry shear-compression: Role of dilatancy highlighted. *Journal of engineering mechanics*, 130(11), 1289-1296.
- Vasanelli, E., Calia, A., Colangiuli, D., Micelli, F., & Aiello, M. A. (2016). Assessing the reliability of non-destructive and moderately invasive techniques for the evaluation of uniaxial compressive strength of stone masonry units. *Construction and Building Materials*, 124, 575-581.
- Vasconcelos, G., & Lourenço, P. (2009). Experimental characterization of stone masonry in shear and compression. *Construction and Building Materials*, 23(11), 3337-3345.
- Vermeltoort, A. T. (2005). *Brick-Mortar Interaction in Masonry under Compression*. (Doctoral dissertation), Technische Universiteit Eindhoven, The Netherlands.
- Vermeltoort, A. T., & van Schijndel, A. W. M. (2013). *Cmsol simulations of cracking in point loaded masonry with randomly distributed material properties*. Paper presented at the Cmsol Conference, Rotterdam.

- Vermeltoort, A. T. (2015). *Tests for the characterisation of original Groningen masonry under compression and shear loading*. Eindhoven University of Technology. The Netherlands.
- Vlek, C. (2018). Induced earthquakes from long-term gas extraction in Groningen, the Netherlands: Statistical analysis and prognosis for acceptable-risk regulation. *Risk analysis*, 38(7), 1455-1473.
- Vonk, R. A. (1992). *Softening of Concrete Loaded in Compression*. (Doctoral dissertation), Technische Universiteit Eindhoven, The Netherlands.
- Willis, C. R. (2004). *Design of Unreinforced Masonry Walls for Out-of-Plane Loading*. (Doctoral dissertation), The University of Adelaide, Australia.
- Zapico Blanco, B., Tondelli, M., Jafari, S., Graziotti, F., Rots, J., & Palmieri, M. (2018, 18-21 June). *A masonry catalogue for the Groningen region*. Paper presented at the 16<sup>th</sup> European Conference on Earthquake Engineering, Thessaloniki, Greece.
- Zhang, S., Richart, N., & Beyer, K. (2018). Numerical evaluation of test setups for determining the shear strength of masonry. *Materials and Structures*, 51(4), 1-12.
- Zhou, Z., Walker, P., & D'Ayala, D. (2008). Strength characteristics of hydraulic lime mortared brickwork. *Proceedings of the Institution of Civil Engineers-Construction Materials*, 161(4), 139-146.
- Zimmermann, T., Strauss, A., & Bergmeister, K. (2012). Structural behavior of low-and normal-strength interface mortar of masonry. *Materials and Structures*, 45(6), 829-839.

# LIST OF PUBLICATIONS

## JOURNAL ARTICLES

- Jafari, S., Rots, J., & Esposito, R. (2021). A correlation study in support of material characterisation of typical Dutch masonry structures, *Building Engineering* (2021), *Under Review*.
- Ferretti, F., Jafari, S., Esposito, R., Rots, J. G., & Mazzotti, C. (2021). Critical analyses on the use of the shove test for investigating the shear-sliding behaviour of brick masonry, *Submitted to Engineering Structures*.
- Jafari, S., Rots, J., & Esposito, R. (2020). Core testing method to assess nonlinear shear-sliding behaviour of brick-mortar interfaces: A comparative experimental study. *Construction and Building Material*, 244, [118236]. <https://doi.org/10.1016/j.conbuildmat.2020.118236>
- Jafari, S., Rots, J. G., & Esposito, R. (2019). Core testing method to assess nonlinear behaviour of brick masonry under compression: A comparative experimental study. *Construction and Building Materials*, 218, 193-205. <https://doi.org/10.1016/j.conbuildmat.2019.04.188>
- Jafari, S., Rots, J. G., Esposito, R., & Messali, F. (2017). Characterising the material properties of Dutch unreinforced masonry. *Procedia Engineering*, 193, 250-257. <https://doi.org/10.1016/j.proeng.2017.06.211>

## CONFERENCE PAPERS

- Jafari, S., Esposito, R., & Rots, J. G. (2019). From Brick to Element: Investigating the Mechanical Properties of Calcium Silicate Masonry. In R. Aguilar, D. Torrealva, S. Moreira, M. A. Pando, & L. F. Ramos (Eds.), *Structural Analysis of Historical Constructions: An Interdisciplinary Approach* (Vol. 18, pp. 596-604). (RILEM Bookseries; Vol. 18). Springer. [https://doi.org/10.1007/978-3-319-99441-3\\_64](https://doi.org/10.1007/978-3-319-99441-3_64)
- Ferretti, F., Jafari, S., Esposito, R., Rots, J. G., & Mazzotti, C. (2019). Investigation of the Shear-Sliding Behavior of Masonry Through Shove Test: Experimental and Numerical Studies. In R. Aguilar, D. Torrealva, S. Moreira, M. A. Pando, & L. F. Ramos (Eds.), *Structural Analysis of Historical Constructions: An Interdisciplinary Approach* (Vol. 18, pp. 523-531). (RILEM Bookseries; Vol. 18). Springer. [https://doi.org/10.1007/978-3-319-99441-3\\_56](https://doi.org/10.1007/978-3-319-99441-3_56)
- Jafari, S., Esposito, R., & Rots, J. (2018, July 9-11). A Comparative study on the evaluation of different testing techniques: Evaluating the mechanical properties of masonry. In G. Milani, A. Taliercio, & S. Garrity (Eds.), *10<sup>th</sup> International Masonry Conference*, Milan, Italy.
- Esposito, R., Jafari, S., Ravenshorst, G., Schipper, R., & Rots, J. (2018, 11 - 14 February). Influence of the behaviour of calcium silicate brick and element masonry on the lateral capacity of structures. *10<sup>th</sup> Australasian Masonry Conference*, Sydney, Australia.
- Messali, F., Esposito, R., Jafari, S., Ravenshorst, G., Korswagen Eguren, P., & Rots, J. (2018, June 18-21). A multiscale experimental characterisation of Dutch unreinforced masonry buildings. *16<sup>th</sup> European Conference on Earthquake Engineering*, Thessaloniki, Greece.
- Bonura V., Zapico Blanco B., Jafari S., Graziotti F. (2018, June 18-21). Interpretation of In-situ Shear Test for Brick Masonry: a Benchmark Study. *16<sup>th</sup> European Conference on Earthquake Engineering*, Thessaloniki, Greece.
- Zapico Blanco B., Tondelli M., Jafari S., Graziotti F., Millekamp H., Rots J., Palmieri M. (2018, June 18-21). A masonry catalogue for the Groningen region. *16<sup>th</sup> European Conference on Earthquake Engineering*, Thessaloniki, Greece.
- Pari, M., Jafari, S., Messali, F., Esposito, R., & Rots, J. (2017, September 13-16). Computational modeling of the cyclic pushover test on a calcium silicate element masonry assemblage. In W. J.

Quist, S. J. C. Granneman, & R. P. J. van Hees (Eds.), *4<sup>th</sup> WTA International PhD Symposium* (pp. 181 - 189). WTA Nederland - Vlaanderen.

- Jafari, S., Esposito, R., & Rots, J. (2017, September 13-16). Literature review on the assessment of masonry properties by tests on core samples. In W. J. Quist, S. J. C. Granneman, & R. P. J. van Hees (Eds.), *4<sup>th</sup> WTA International PhD Symposium* (pp. 173-180). WTA Nederland - Vlaanderen.
- Rots, J. G., Messali, F., Esposito, R., Mariani, V. & Jafari, S. (2017). Multi-scale approach towards Groningen masonry and induced seismicity. In: *Key Engineering Materials*. 747 KEM, p. 653-661 9 p.
- Rots, J. G., Messali, F., Esposito, R., Jafari, S. & Mariani, V. (2016, September 13-15). Computational modelling of masonry with a view to Groningen induced seismicity. *10<sup>th</sup> International Conference on Structural Analysis of Historical Constructions*, Leuven, Belgium.

## PROFESSIONAL REPORTS

- Jafari, S., Ferretti, F., & Esposito, R. (2018). *Flat-jack and shove tests: method validation and correlation (C31B67WP1-15)*. Delft University of Technology.
- Jafari, S., & Esposito, R. (2018). *Material characterisation of existing masonry for URM abacus (C31B67WP1-14)*. Delft University of Technology.
- Jafari, S., Licciardello, L., & Esposito, R. (2017). *Slightly-destructive tests on cores: method validation and correlations (C31B67WP1-13)*. Delft University of Technology.
- Jafari, S., & Esposito, R. (2017). *Material tests for the characterisation of replicated solid clay brick masonry (C31B67WP1-12)*. Delft University of Technology.
- Jafari, S., & Esposito, R. (2017). *Material characterisation of replicated calcium silicate element masonry (C31B67WP1-11)*. Delft University of Technology.
- Jafari, S., & Esposito, R. (2016). *Material tests for the characterisation of replicated calcium silicate brick masonry (C31B67WP1-9)*. Delft University of Technology.
- Jafari, S., Panoutsopoulou, L., & Rots, J. G. (2015). *Tests for the characterisation of original Groningen masonry (C31B60-3)*. Delft University of Technology.

# CURRICULUM VITAE

- 2004-2009 Bachelor of Science in Civil Engineering.  
Iran University of Science and Technology (IUST), Tehran, Iran.
- 2010-2012 Master of Science (MSc) in Civil Engineering.  
Specialisation: Earthquake Engineering  
Iran University of Science and Technology (IUST), Tehran, Iran.
- 2012-2013 Structural Engineer  
PAYBORZ  
Tehran, Iran.
- 2013-2014 Structural Engineer  
RAHSHAHR International Group  
Tehran, Iran.
- 2014-2016 Researcher in Computational Mechanics.  
Delft University of Technology (TU Delft), The Netherlands.
- 2016-2021 PhD in Computational Mechanics.  
Delft University of Technology (TU Delft), The Netherlands.  
Thesis: Material characterisation of existing masonry: A strategy to determine strength, stiffness and toughness properties for structural analysis
- Promotor: Prof. dr. ir. Jan G. Rots  
Copromotor: dr. Rita Esposito



# ACKNOWLEDGMENTS

My PhD journey could not have been possible without the presence of some people who served valuable roles in the development of this doctoral dissertation. First, a very special gratitude goes to Nederlandse Aardolie Maatschappij B.V (NAM) for providing the needed financial resources for this research.

I would like to express my sincere gratitude and great appreciation to my promotor Prof. Jan Rots whose support, knowledge, and encouragement helped me through these years. Further, I want to express my special thanks to my daily supervisor Dr. Rita Esposito, who was a main source of inspiration to me for self-reflection, gaining academic confidence, and critical thinking. I am also thankful to Dr. Rene Bram, Dr. Francesca Ferretti, Graziotti, Dr. Francesco Graziotti, Dr. Oguzhan Çopuroğlu, and Dr. Geert Ravenshorst for all simulating discussions. I extend my sincere gratitude to the doctoral committee for accepting to take part in the defense process.

During this work, experimental tests were performed in the Stevin II Laboratory of Delft University of Technology. This would have been not possible without the help of some master students and my colleges. In this regard, I am very grateful to Marina Damiola, Lucia Licciardello, Elena Casprini, Andrea Maioli, Irene Frana, and Edwin Meulman. I am certainty in debt to lab's people, in particular Kees van Beek, Georgios Stamoulis, Louis den Breejen, John Hermens, Fred Schilperoord, Tom Bloom, Maiko van Leeuwen, and Richard.

I was immensely lucky to have great officemates and fellows such as Marianthi Sousmali, Manimaran Pari, Marina Damiola, Monica Yolanda, Lucia Licciardello, and Somi who not only helped me to manage frustrations but also gave me a feeling of confidence and support. Moreover, I would like to thank a few inspiring colleagues such as Francesco Messali, Langzi Chang, Michele Longo, Paul Korswagen, Edwin Meulman, Maria Gaggero, Michele Palmiri, and Tao Lu.

I am also grateful to all my friends who made me feel at home and always had my back. A particular word goes to Amo Feri, Shahnaz, Saba, Maryam, Shirin, Ashkan, Sam, Kian, Rouzbeh, Safa, Bahar, Milad, Naghme, Babak, Peiman, Pouria, Roham, and Ali.

Above all, I am grateful to my adorable parents, Nahid and Asad, who always give me strength and perseverance to keep moving forward despite challenges. Moli, I also cannot thank you enough for being such a lovely sister and my best friend. I wish to thank Ghazal and Sanaz for being not only a sister but a mentor and role model. I am also grateful to Erfan, Radi, Mohamad, Shokoh, and Majid for your support.

Finally and most importantly, I would like to thank my beloved husband and friend. Mo you always embraced and encouraged me. Being with you taught me how a “true bond” can save a “slender wall” under “lateral loads”.

